N82 23109

EXPERIMENTAL STUDY OF HIGH DENSITY FOODS FOR THE SPACE OPERATIONS CENTER

Selina M. Ahmed, Ph.D.

Texas Southern University

1981 NASA ASEE Summer Faculty Fellow

Supervisor: Malcolm C. Smith, Jr., D.V.M.

Medical Research Branch

Medical Sciences Division

NATIONAL AERONAUTICS AND SPACE ADMINISTRATION

LYNDON B. JOHNSON SPACE CENTER

HOUSTON, TEXAS

AUGUST 20, 1981

TITLE: SYSTEMATIC STUDY TO DEVELOP AND EVALUATE CRITERIA FOR NUTRITIONAL SUPPORT OF PERSONS CONFINED TO CONTROLLED ECOLOGICAL LIFE SUPPORT SYSTEMS

This report will only provide the second part of a total research which consists of three projects which are shown as follows:

Project 1: Evaluation and progression of the space feeding concept from early missions to the present stage.

Project 2: Projected nutritional criteria for the Space Operations Center.

Project 3: Projected nutritional criteria for the Closed Ecological Life Support System.

TABLE OF CONTENTS

LIST OF TABLES

Based on experience from past missions, there are known physiological as well as psychological stresses existing in crew members as a result of space flight. It is also known that stress can contribute to the increased loss of calcium and nitrogen from the body. Since high density foods will be made with high calorie nutritionally complete liquid, it will be able to protect the body's loss of nitrogen (4, 5).

After considering all of these needs for the crew in an extended mission, the researcher looks for these projects to develop new high density foods.

OBJECTIVES

a. To achieve the nutritional need in LEO Space Station.

b. To bring varieties in the diet of crews for extended mission.

c. To provide highest calorie in concentrated form.

d. To provide complete nutrients.

e. To study the shelf-life of the products produced.

BACKGROUND AND REVIEW OF THE RELATED LITERATURE

The space flight missions are always supported with nutritious foods for the crews of the space flight. Research and technological developments in this field are going on as the man's desire to stay longer and longer in space is becoming increasingly inevitable. The dehydrated, frozen, irradiated and thermostabilized foods have played a very important role in space flights supplying necessary ingredients needed for supporting life in orbit and in space.

In this preview in mind, the researcher is interested in the preparation of high density food which will meet the criteria of space food. Following factors should be reviewed before applying any theoretical concepts foods into practice.

1. Nutritional Value. The Nutritional value of the food should be formulated to meet the need of the human in a relatively simple product. Nutritional availability must be fully supported by the food in quality and quantity.

2. Safety. The food intake should be safe in a given environment. Food consumed in a closed environment should take into account the special needs, if any, for safety as to its side effects, especially in regard to microbiological growth as well as its toxicity levels.

3. Convenience. Food items should be convenient to use by the crews with considerations as to their age, sex, health status and also to the personal preferences of the individual.

4. Food Acceptance. Very often food habits are very much of personal preferences given that variety of foods are available for consumption. Hence factors must be considered for their acceptability.

With these objectives in view, the researcher has tried to evaluate the high density liquid foods designed for enteral feeding by the Organon Food Company. Products evaluated were "Magnacal," "Sumacal" and "Microlipids." These products are used for hospital patients who may suffer from protein calories undernutrition, and of Cardiac Cachexia.

Magnacal is a lactose-free formula designed for both total and supplemental nutritional support in those clinical conditions that demand caloric and nutritional requirements which standard liquid feedings cannot satisfy. The exceptionally high caloric density (2.0 cal/ml) makes Magnacal especially suitable for patients who cannot tolerate high volume feedings but who require high caloric levels. Magnacal is useful in the dietary management of patients with a wide variety of hypermetabolic conditions resulting from such causes as:

1. Major Burns
2. Severe Trauma
3. Multiple Fractures
4. Major Sepsis
5. Major Surgery

6. Advanced or Metatastic Cancer
7. Severe Anorexia
8. Hyperactive States or Prolonged Muscular Hypertonicity

Magnacal is also effective as an oral supplement for patients requiring additional calories (15).

Microlipid is useful in the dietary management of patients requiring caloric supplementation. Microlipids high concentration of calories (4.5 cal/ml) is derived solely from fat and can provide energy for metabolism without an undue increase in the volume of the diet. Microlipids are rich in linoletic and other unsaturated fatty acids. Microlipids may be useful in the following conditions (16):

1. Fatty Acid Deficiencies
2. Uremia
3. Diseased and Debilitated States
4. Postoperative Convalescence
5. Preoperative Preparation of Malnourished Patients
6. Severe Burns
7. Major Sepsis

Sumacal is designed for nutritional support in those clinical conditions that demand a Supplemental Source of carbohydrate calories Unflavored Sumacal can provide additional carbohydrate calories in combination with other Organon nutritional products nutritionally complete formulas. Sumacal contains no fat or protein which makes it especially useful as a supplement for patients on fat and protein restricted diets. Sumacal may be beneficial in the dietary management of patients with the following condition (23):

1. Severe Burns
2. Major Sepsis
3. Severe Trauma
4. Acute or Chronic Renal Disease
5. Major Surgery
6. Cystic Fibrosis
7. Anorexia
8. Pre- and Postoperative Care

Dr. Steven B. Hemsfiled in his paper on Cardiac Cachexia has pointed out some of the uses of these HDL products (22).

The enteral route of refeeding is selected first unless severe intestinal problems limit intake. If the full dose of the prescribed diet cannot be orally ingested, then the balance is administered through a fine-bore naso-enteral cannula. The enteral formula selected for tube feeding should have the following properties: high caloric density (2.0 preferred over 1.0 Kcal/cc), low sodium (<2 g/day), and Kcal/gmN ratio of about 150:1. A commercially prepared solution is available which meets these criteria (i.e., MAGNACAL™, Organon Nutritional Products), or the formula can be prepared by the dietitian from readily available modules[8]. If only part of the daily requirements can be met by enteral feedings, the balance of daily requirements are supplied by peripheral vein fluids (i.e., P-900[9], Intralipid(R), etc. Recall that the undernourished cardiac patient is unduly susceptible to repletion heart failure, and therefore requires careful clinical monitoring and gradual increasing doses of nutrients. Dr. Horwitz, et. al, observed the use of these HDL foods in cases of Ascitises, Cirrhosis and Cachexia.

ACC patients with minimal elevations in serum bilirubin and plasma ammonia, often resistant to standard enteral formulae, can be effectively repleted using modular or fixed composition high density solutions (11).

Enteral and perenteral hyperalimentation can renourish the severely wasted malabsorbing diabetic as shown in a study conducted by Dr. T. Hersh, et al. (10).

Lean body mass can now be maintained or repleted by the enteral route in contrast to the parenteral route in patients with a wide variety of gastrointestinal and other diseases. The applicability of enteral hyperalimentation as a primary form of therapy in inflammatory bowel diseases, in reversing the cachexia of advanced cirrhosis, in protecting irradiated cancer patients from enteric and hemotologic toxicity and in the treatment of acute renal failure, hold promises but must await the outcome of carefully controlled clinical studies (21).

George L. Blackburn, et al., have pointed out in their study about the nutritional and metabolic assessment of the hospitalized patients that the nutritional and metabolic profile indicates the causes of malnutrition, namely insufficient protein and calories and establishes individual guidelines for the patient's nutritional therapy (2).

At present enteral hyperalimentation are used in hospital patients only. The researcher feels that these products can be used for the conventional diets with further study and modification to improve physical characteristics.

The Pillsbury Company also has made some remarkable contribution in the preparation of the high density bar to supplement the food supply for the Skylab 4 mission which was extended from the nominal mission of 56 days to a mission of 85 days in duration (18).

Jack R. Durst conducted research about stable food pieces, has pointed out that compact food units designed to provide a completely balanced diet provided by incorporating essential nutrients into a unitary, flexible food piece containing a continuous external phase of a hydrophilic film former, water and an

edible humectant. The external phase encapsulates an internal phase of minute fat globules. The food pieces are resistant to physical, chemical, and bacteriological degradation (13).

A protein fortified food bar of a controlled calorie content is composed of several crisp wafers stacked one above the other with a creamy filling between them. Each wafer is composed of 10 parts of flour, about 6 parts of added protein, e.g., calcium caseinate or a lactalbumin-casein coprecipitate, about 0.8 parts oil as a release agent and a small amount of chemical leavening. The filling layered between the wafers consists of 10 parts shortening, about 10 parts of a finely divided protein such as milk protein, about 6 parts sugar, a minor amount of flavor if desired and a vitamin and mineral moisture, if desired. A confectioners coating can be applied over the composite bar if desired.

Jay E. Morgan, in his research about high protein food bar, has discussed that (12). Betty L. Brooking conducted similar research as J. Durst about process for forming stable food pieces has found out that foods remain flexible during storage and do not lose oil when molded or otherwise formed into pieces (1).

Food bar and method for making, another research conducted by Jack R. Durst, showed that a compact, solid food unit characterized as possessing hardness, frangibility and water dispensible characteristics is imparted by utilization of a binder which provides a structural matrix for discrete edible food particles. The binder is comprised of a discontinuous phase of fat globules encapsulated by a continuous phase of water and a hydrophilic film former (14).

EXPERIMENTAL DESIGN AND PROCEDURES

The research activity was conducted in different phases to formulate high density foods. A standard recipe (#300) for Scones/Biscuits adapted from the recipe book of Culinary Arts Institute (7).

In the experimental phase, the researchers tried to make Scones/Biscuits changing variables such as replacing milk with various high density liquids produced by the Organon Food Company. Five different recipes were studied. In each recipe the milk component was replaced by the HDL product.

The first experimental high density Scones/Biscuits were made with Magnacal, a high density liquid product produced by Organon Food Company, replacing milk from the controlled recipe keeping all other ingredients intact as in the original recipe.

The second high density Scones/Biscuits were made by replacing milk with Sumacal, all other components unchanged from the controlled recipe.

The third high density Scones/Biscuits were made, replacing milk with Microlipids. Since microlipid is a fat emulsion product, shortening was also deleted from the experimental recipe.

The fourth high density Scones/Biscuits were made by replacing milk with Microlipids.

The fifth high density Scones/Biscuits were made by replacing milk with Magnacal and Microlipids by doubling the controlled recipe in every respect except baking powder.

#300 is the control recipe for Scones/Biscuits and #400 is the control recipe for muffins.

The researcher also made Muffins a standard recipe adapted from the book of Culinary Arts Institute. Muffins were also made in an experimental basis by replacing milk with Magnacal.

The recipes generated due to the experiments are appended in the appendix for further evaluation in order to produce and culture more about high density foods in the Space Program.

DISCUSSION

Sensory methods in which palatability is evaluated by a panel of judges are essential to most food experiments because they answer all the important questions of how a food should taste, smell, look, and feel. It is axiomatic that only a food which is prepared in a reproducible manner is worth the effort of scoring for it is only when the conditions of preparations are carefully controlled and defined that differences in quality can be a tribute to known variables. Careful sampling of the food is also necessary (20).

All of the food samples were judged by trained panelists (JSC Food Laboratory). All of the foods were labeled and coded carefully, and all foods were evaluated by the sensory method on the basis of the following characteristics:

a. Appearance

b. Color

c. Odor

d. Flavor

e. Texture

f. Overall

A nine-point hedonic scale was used to evaluate the products:

9-Like Extremely

8-Like Very Much

7-Like Moderately

6-Like Slightly

5-Neither Like or Dislike

4-Dislike Slightly

3-Dislike Moderately

2-Dislike Very Much

1-Dislike Extremely

Shelf-life of space food must be considerably longer than most conventional foods to allow for time to permit testing, evaluation and packaging of flight foods. These are time consuming operations and require that sufficient time be allocated before each mission.

The experimental Scones/Biscuits and Muffins required a shelf-life study, and stored at three different temperatures for three different time lengths. The products are stored at a temperature of 40^{0}, 70^{0} and 100^{0} Farenheit for 15, 30, and 90 days.

After shelf-life study, the high density Scones/Biscuits and Muffins will again be tested by the sensory evaluation panel. The products are also tested for any kind of visible changes, development of mold, etc.

Nutritional analysis of the high density foods are also in progress in the JSC Biomedical Laboratory. The results of the analyses will be completed within the next two months.

RESULTS

Table I. Scones/Biscuits with High Density Liquid

	Magnacal	Sumacal	Micro-lipid + Magnacal	Micro-lipid	Micro-lipid with Shortening	Control
Overall Rating	$7.0^{+}1.2$	$5.8^{+}1.3$	$6.2^{+}0.9$	$6.5^{+}1.1$	$5.2^{+}1.7$	$6.5^{+}1.3$
Range	4-8	3-8	5-8	5-9	2-8	4-9

Taole II. Muffins with High Density Liquid

	Control	Magnacal Muffin
Overall Rating	$6.7^{+}0.9$	$6.8^{+}1.2$
Range	5-8	4-8

A shelf-life study will be conducted only about the product which is rated above five in the nine-point hedonic scale.

SUMMARY AND CONCLUSION

Space flight poses special problems in food technology. Calorie-dense, nutritious and palatable, balanced diet in a suitable form are necessary for space flight. Food must influence with packaging, water supply, waste and residue disposal systems and with food preparation and serving equipment. Food must be adequately protected against deterioration, chemical, physical and biological. Also, all food must be adapted to consumption at Zero-gravity (3, 8, 9).

The conclusive report about high density foods -- particularly for Space Operations Center -- is yet to come.

REFERENCES

1. Brooking, Betty L.; W.F. Wright. Process for Forming Stable Food Pieces; Assigners to the Pillsbury Company, Minneapolis, November 26, 1974.
2. Blackburn, G., et al.: Nutritional Support in Cardiac Cachexia. *J. Thorac Cardiovasc Surg 73*:489, 1977.
3. Bourland, C.T.; R.M. Rapp; M.C. Smith, Jr.: Space Shuttle Food System. *Food Technol. 40*, 1977.
4. Chun, J.Y.; S. Margen; and F.M. Costa: Studies In Calcium Metabolism. II. Effects of Low Calcium and Variable Protein Intake on Human Calcium Metabolism. *Am. J. of Clin. Nutr.*, Vol. 28, 1975.
5. Clark, J.P.: Nutrition, Diet and Food Processing in Controlled Environment Life Support Systems. *Am. Inst. of Aeronautics and Astronautics, Inc.*, NY, 1979.
6. Cooper, H.S.F., Jr.: *A House in Space*. Banton Books, NY, 1978.
7. Culinary Arts Institute: 250 Breads, Biscuits and Rolls; 1975 North Hawthorne, Melrose Park, IL 60160.
8. Heidelbaugh, N.D.: Space Flight Feeding Systems: Characteristics, Concepts for Improvement and Public Health Implications. *J.A.M.A., 148*, 1966.
9. Heidelbaugh, N.D.; M.C. Smith, Jr.; P.C. Rambaut; L. Lutwak; C.S. Huber; C.R. Stadler; and B.M. Rouse: Clinical Nutrition Applications of Space Food Technology. *J. Am. Dietet. Assn. 62*:383-389, 1973.
10. Hersh, T.; S. Heyonsfield; C. Arteaga; D. Thomas: Nutritional Management of Protein Energy Malnutrition Secondary to Diabetic Autonomic Neuropathy. Paper Presented at Emory University School of Medicine, Atlanta, GA, 1981.
11. Horowitz, J.; J. Bleien; J. Smith; S. Heyonsfield: Repletion of the Cachectic Cirrhotic Using High Caloric Density Enteral Formulae. Paper Presented at The Fourth Clinical Congress of the American Society for Parenteral and Enteral Nutrition, Chicago, IL, January 31, 1980.

12. Morgan, Jay E.: High Protein Food Bar Assignor to the Pillsbury Company, Minneapolis, June 4, 1974.

13. Durst, Jack R.: Stable Food Pieces: Osseo, MN, Assignor to the Pillsbury Company, Minneapolis, March 25, 1969.

14. Durst, Jack R.: Food Bar and Method for Making; Osseo, MN, Assignor to the Pillsbury Company, Minneapolis, March 4, 1969.

15. Magnacal: High Caloric Density Formula, Nutritionally Complete for Oral and Tube Feedings. Organon Nutritional Products, Organon Inc., West Orange, NJ 07052.

16. Microlipid: A 50% Fat Emulsion for Special Dietary Use in Oral and Tube Feedings. Organon Nutritional Products. Organon Inc., West Orange, NJ 07052.

17. Glaser, Peter E.; Judith A. Mabel: Nutrition and Food Technology for a Controlled Ecological Life Support System. Report By: Arthur D. Little Inc., Cambridge, MA.

18. Rambaut, P.C., M.C. Smith, Jr., C.R. Stadler: Skylab Nutritional Studies, NASA/Johnson Space Center, Houston, TX and Technology Incorporated, Houston, TX, June 1976.

19. Rambaut, P.C.; M.C. Smith, Jr.; C.S. Leach; G.D. Whedon; J. Reid: Nutrition and Responses to Zero Gravity. *Federation Proceedings 36*, 1977.

20. Griswold, Ruth M.: *The Experimental Study of Foods*, Houghton Mifflin Company, Boston, 1962.

21. Heyonsfield, Steven B.; Jed Horowitz; David H. Lawson: Enteral Hyperalimentation: Courtesy of Organon Nutritional Products, 1980.

22. Heyonsfield, Steven B.: Cardiac Cachexia. Paper Presented at Harvard Medical School, Boston, MA, May 13, 1980.

23. Sumacal: A Liquid Carbohydrate Source of Calories for Special Dietary Use in Oral and Tube Feeding. Organon Nutritional Products. Organon Inc., West Orange, NJ 07052.

APPENDIX

MUFFINS

2 cups sifted flour

4 teaspoons baking powder

1/2 teaspoon salt

1/4 cup sugar

1 egg, beaten

1/4 cup melted shortening

1 cup milk

Method of Preparation

Sift dry ingredients together. Mix egg, shortening and milk together thoroughly. Combine mixtures, stirring just enough to dampen flour. Fill greased muffin pan 2/3 full. Bake at 400°F. 25 min. Makes 12-15 muffins.

MAGNACAL MUFFINS

2 cups Bisquick

1 cup Magnacal

1 egg

1/4 cup brown sugar

1 teaspoon cinnamon

1/2 cup apple (finely chopped)

1 tablespoon cooking oil

dash of salt

Method of Preparation

Heat oven to 400°F. Mix ingredients vigorously for 30 seconds. Fill muffin cups 2/3 full. Bake 15-18 min. (until golden brown).

NOTE: This is an experimental recipe. In this experiment milk component was substituted with high density fluid Magnacal.

SCONES/BISCUITS

2 cups sifted flour

1 tablespoon sugar

1/2 teaspoon salt

4 teaspoons baking powder

1/4 cup shortening

1/2 to 2/3 cup milk

1 egg well beaten

Melted butter

Sugar

Method of Preparation

Sift dry ingredients together; cut in shortening. Add milk to egg; add to flour mixture gradually, adding more milk if necessary. Knead lightly on a floured surface. Roll into a round 1/2" thick. Cut into wedges, place on baking sheet, brush with melted butter, dredge with sugar. Bake at 400°F 15-18 min. Makes 15 (4") Scones.

NOTE: This is a standard recipe for making Scones. In each experimental recipe, Scones were made by replacing milk with Microlipid, Sumacal and Magnacal.

CARDIOVASCULAR ADAPTATIONS IN WEIGHTLESSNESS:

The Influence of In-flight Exercise Programs on the Cardiovascular Adjustments during Weightlessness and Upon Returning to Earth

Charles H. Bennett, Ph.D.
Department of Biology
Kentucky State University

TABLE OF CONTENTS

LIST OF FIGURES

LIST OF TABLES

CARDIOVASCULAR ADAPTATIONS IN WEIGHTLESSNESS: The Influence of In-flight Exercise Programs on the Cardiovascular Adjustments during Weightlessness and Upon Returning to Earth

Charles H. Bennett, Ph.D.
Department of Biology
Kentucky State University

Introduction

The American Space Program has provided an environment for the biomedical investigation of physiological systems in the absence of gravity. Through use of the first long-term space station, the United States has acquired giant achievements in knowledge concerning the physiological effects of increasingly extended periods of exposure to the space flight environment and in determining how well man can function while performing tasks in space.

Space medicine studies using experimental animals were initiated prior to 1959. Limited medical studies and observations on men in space were initiated in the United States with the Project Mercury Program (1961-1963). This program served to dispel many basic concerns regarding the frailties of the human space explorer. It was shown that man could operate effectively during the acceleration periods of launch and entry, and that he could adapt to the weightless environment and perform useful

tasks. The biomedical studies conducted during the Gemini Program(1965-1966) were oriented toward evaluating the magnitude of flight-related changes first noted following the Mercury flights. Emphasis was placed upon evaluation of the cardiovascular system, since the principal changes observed during the Mercury flights involved alterations in cardiovascular reflexes that regulate blood flow in the presence of the Earth's gravitational field.

Several in-flight measurements or experiments were accomplished on the Gemini missions, as well as preflight and postflight studies. These investigations confirmed the postflight orthostatic intolerance observed in Mercury and extended the findings to include moderately decreased postflight exercise tolerance and red cell mass, minimal loss of bone calcium and muscle nitrogen, and the high metabolic cost of extravehicular activity. The few changes which occurred were moderate but reversible.

The Apollo Program(1968-1973) originally included the conduct of a series of medical studies for the early orbital missions. After the Apollo 204 accident, the decision was made to delete the medical studies and to dedicate all resources to the complex lunar landing program. Consequently, medical studies were primarily conducted with the Apollo crewmen before and after each flight. Generally, they confirmed the Gemini findings of postflight dehydration and weight loss, postflight decrease in orthostatic tolerance, and postflight reduction in exercise capacity. In addition, the decreased red cell mass and plasma volume noted in Gemini were confirmed, but were less pronounced in Apollo.

The three principal objectives of the Skylab Program(1973-1974) were

the study of man, his Earth, and his Sun. Skylab, at its inception called the Apollo Applications Program, was a natural and necessary follow-on to the Gemini and Apollo Programs. Development of medical experiments, initiated in the mid-1960's, included a decision to design the experimental program along classical lines of medical and physiological research. The results from the Gemini and Apollo flights influenced the planning and placement of emphasis for the new program. The experimental protocols developed to study the cardiovascular, musculoskeletal, hematologic, vestibular, metabolic and endocrine systems in the body, with few exceptions, remained unchanged throughout the Skylab Program.

Twelve Skylab medical experiments(Table I) were designed to provide an indepth study of individual body systems and at the same time provide an overlap to give comprehensive understanding of man's reaction to long-term weightless flight. The inclusion of major in-flight medical experiments provided the capability to study physiological responses during exposure to weightless flight as opposed to the pre- and postflight studies as carried out in the Apollo and Gemini flights. This paper will investigate the cardiovascular changes recorded during in-flight exercise and metabolic studies as well as during the application of lower body negative pressure and compare these responses with pre- and postflight values. Postflight cardiovascular responses following the extended duration flights of Skylab will also be examined in order to determine if the in-flight exercise programs selected by the Skylab crewmembers reduces the cardiovascular deconditioning observed during previous space flights.

TABLE I. SKYLAB MEDICAL EXPERIMENTS

Number	Experiment
M071	Mineral balance
M073	Bioassay of body fluids
M074	Specimen mass measurement
M078	Bone mineral measurement
M092	Lower body negative pressure
M093	Vectorcardiogram
M110	Hematology/immunology
M131	Human vestibular function
M133	Sleep monitoring
M151	Time and motion study
M171	Metabolic activity
M172	Body mass measurement

Medical evaluations after Gemini and Apollo flights demonstrated reduced orthostatic tolerance in virtually all crewmen specifically tested. Orthostatic tolerance describes the ability of the cardiovascular system to maintain an adequate level of arterial blood pressure, which provides the 'driving force' for maintaining organ system blood flow, during changes in body orientation in the earth's gravitational field. During changes in body position on earth, namely following movement from a supine to a vertical heads-up orientation, neurohumoral cardiovascular adjustments

occur to preserve arterial blood pressure through alteration in cardiac output(determined by the product of heart rate and stroke volume) and the peripheral resistance to blood flow. This 'short-term' regulation of cardiovascular homeostasis is further supplemented by the 'long-term' renal regulation of circulating fluids and electrolytes determined in part by the release of antidiuretic hormone(ADH), regulated by the Henry-Gauer reflex, as well as the renin-angiotensin-aldosterone regulatory system. The diminished ability of the cardiovascular system to function effectively against gravitational stress following exposure to weightlessness, while usually mild and not operationally significant during previous missions, sometimes resulted in pronounced increases in heart rate and decreases in pulse pressure during orthostatic testing. The magnitude of this postflight loss of orthostatic tolerance showed no clear correlation with flight durations ranging between 4 and 14 days. This caused concern for the potential postflight orthostatic intolerance in the crewmen of the extended Skylab missions, whose durations were planned for 28 days(Skylab 2), 59 days(Skylab 3), and 84 days(Skylab 4).

Statement of the problem

Postflight orthostatic intolerance and reduced physical work capacity have been reported following periods of weightlessness, bed rest, and water immersion. A quantitative assessment of the effects that in-flight, as well as preflight, exercise programs has on the cardiovascular responses

recorded during Skylab missions and following return to the earth's environment has not been performed. This report will attempt to determine if cardiovascular differences exist between Skylab astronauts following the application of physiological stress(e.g., lower body negative pressure, exercise, orthostatic stress) that can be related to the crewmembers pre- and in-flight training programs.

Methods

Cardiovascular evaluation during in-flight and postflight periods: Skylab M171 Experiment - Metabolic Activity

Twenty of the 27 Apollo crewmen tested following spaceflight exhibited a statistically significant decrease in their tolerance for exercise. Although this response was reversible within 1 to 2 days, it became obvious that man could not be committed to long-duration space flight until the magnitude and time course of these changes could be established and the underlying physiological mechanisms understood. The primary objective of the M171 Metabolic Activity experiment was to determine whether man's metabolic effectiveness while performing mechanical work was progressively altered by exposure to the space environment. The secondary objective was to evaluate the M171 bicycle ergometer as an in-flight crew personal exerciser.

A detailed description of the experimental hardware utilized for the M171 experiment has been reported elsewhere(ref. 1). The M171 Experiment

Protocol is shown in Table II, while the M171 Performance Summary is listed in Table III.

TABLE II. M171 EXPERIMENTAL PROTOCOL

Time	Exercise protocol
5 minutes	Rest
5 minutes	25 Percent of Maximun $\dot{V}_{O_2}$ (level 1)
5 minutes	50 Percent of Maximum $\dot{V}_{O_2}$ (level 2)
5 minutes	75 Percent of Maximum $\dot{V}_{O_2}$ (level 3)
5 minutes	Recovery

Performed by each of three crewmen: Five times in 28-day mission; Eight times in 59-day mission; Twelve times in 84-day mission.

TABLE III. M171 PERFORMANCE SUMMARY - THREE SKYLAB MISSIONS

Skylab mission		Preflight	In-flight	Postflight	Total
2	Commander	5	6	8	19
	Scientist Pilot	5	6	7	18
	Pilot	5	7	9	21
		15	19	24	58
3	Commander	7	9	8	24
	Scientist Pilot	7	9	8	24
	Pilot	7	9	8	24
		21	27	24	72
4	Commander	8	12	8	28
	Scientist Pilot	8	12	8	28
	Pilot	8	12	8	28
		24	36	24	84
	Total: 3 Missions	60	82	72	214

Results from this experiment, determined during pre-, in-, and post-flight periods, provided cardiovascular and pulmonary data(Table IV) which reflect adaptation as well as exercise-induced responses during weightlessness.

TABLE IV. M171 PHYSIOLOGICAL MEASUREMENTS

Raw data	Derived data
Ergometer Work Level(watts) Respiratory: Oxygen Consumption. Carbon Dioxide production. Minute volume. Cardiovascular: ECG/VCG. Systolic blood pressure. Diasystolic blood pressure. Cardiac output.* Vibrocardiogram.* Carotid pulse.*	Respiratory: Respiratory exchange ratio. Oxygen pulse. Pulmonary efficiency(V_E/V_{O_2}). Mechanical efficiency($\dot{V}_{O_2}$/watt). Cardiovascular: Mean arterial pressure. Total peripheral resistance. Arterial-Venous O_2 difference. Stroke volume.

*Preflight and postflight only.
ECG, Electrocardiograph.
VCG, Vectorcardiograph.

Skylab M092 Experiment - Lower Body Negative Pressure(LBNP)

The objective of the lower body negative pressure experiment, designated M092, was to determine the extent and the time course of changes in orthostatic tolerance during the weightlessness of space flight and to determine whether in-flight data from the experiment would be useful in predicting the postflight status of orthostatic tolerance. The equipment

design for supporting these studies has been described in detail(ref. 2). Preflight baseline data were acquired from the Skylab crewmen over a 4½ to 5 month period prior to launch, with three tests during the last 6 weeks prior to launch. In-flight tests were conducted usually at 3- or 4-day intervals while postflight tests were carried out daily at first and then at increasing intervals of time over a period of approximately 2 months. Table V lists the number of lower body negative pressure tests conducted for the three Skylab missions.

TABLE V. M092 PERFORMANCE SUMMARY - THREE SKYLAB MISSIONS

Skylab mission		Preflight	In-flight	Postflight	Total
2	Commander	6	7	8	21
	Scientist Pilot	6	7	8	21
	Pilot	6	8	8	22
		18	22	24	64
3	Commander	6	16	8	30
	Scientist Pilot	5	17	8	30
	Pilot	5	16	8	29
		16	49	24	89
4	Commander	6	22	9	37
	Scientist Pilot	7	22	9	38
	Pilot	7	23	9	39
		20	67	27	114
Total: 3 Missions		54	138	75	267

Basic measurements during all tests with the lower body negative pressure device included blood pressure at 30-second intervals, from an automatic system which detected and analyzed Korotkoff sounds, heart rate continuously from one component of a Frank lead vectorcardiogram, and

percentage change in calf volume continuously from capacitive plethysmographic bands encircling the legs. Prior to positioning these bands, a manual measurement was made of circumference of the largest portion of the calves, which also corresponded to the position where the left band was to be placed. The right band served to measure changes in capacitance due to alterations of temperature and humidity within the negative pressure device.

The lower body negative pressure protocol was identical to that adopted for Apollo studies. The first and last 5 minutes of the 25-minute test were at ambient atmospheric pressure to provide data from resting control and recovery periods, respectively. The 15-minute stress period consisted of five distinct levels of negative pressure applied sequentially: 8 and 16 mm Hg negative pressure for 1 minute each, 30 mm Hg for 3 minutes, and 40 and 50 mm Hg negative pressure for 5 minutes each. This profile is shown in fig. 1.

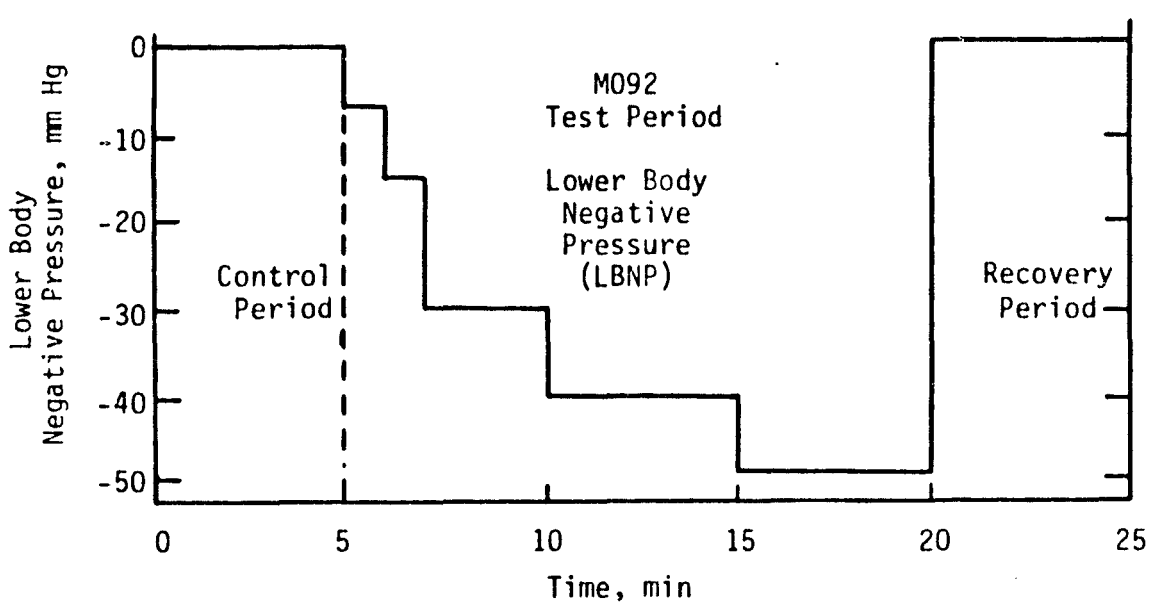

Figure 1. Levels of lower body negative pressure and time of individual phases of the lower body negative pressure protocol.

The hemodynamic changes induced by lower body negative pressure, like the orthostatic stress produced by tilting, depend upon the pooling of blood in the caudal part of the body. Depending upon the magnitude of the negative pressure and the time of exposure, 300 to over 800 ml of blood may be removed from the effective circulating blood volume. Central venous pressure is reduced, and the return of blood to the right heart (venous return) is diminished. Stroke volume and cardiac output, compensated by an increase in heart rate, is reduced. Lower body negative pressure has been reported to cause a smaller increase in heart rate than upright tilting for equivalent reductions in cardiac output. The absence of stimulation of carotid baroreceptors due to postural change has been offered as an explanation of this difference. A decrease in blood flow to the upper extremities and concomitant increase in venous tone of the upper-extremity veins has been reported in both situations to compensate for the contracted effective circulating volume.

A minor reduction in orthostatic tolerance, as observed following space flight, is accompanied by an excessive increase in heart rate, an excessive narrowing of pulse pressure, and a fall in systemic arterial blood pressure. The failure of cardiovascular compensation to gravity leads to the so-called vasodepressor reaction, the manifestations of which are presumably due to an overwhelming increase in parasympathetic nervous system activity(ref. 3). This reaction is characterized clinically by pallor, nausea, dimming of vision, sweating and eventually loss of consciousness, arising from a precipitous fall in arterial blood pressure

secondary to bradycardia(decreased heart rate) and a decrease in peripheral vascular resistance.

There is no doubt that the decrease of blood volume and reabsorption of fluid transudate from tissues of the lower extremities during exposure to weightlessness would diminish orthostatic tolerance, since a decrease of blood volume in a normal active individual from any cause, such as blood loss or dehydration, will result in a strain being placed on normal mechanisms required to maintain cardiovascular integrity during orthostatic stress. Orthostatic intolerance is still present in astronauts returning from space even after blood volume returned to preflight levels, suggesting that cardiovascular adaptation during weightlessness is influenced by more than one physiological regulatory system.

One important question addressed in this report is the effect of inflight exercise, as well as preflight conditioning, upon orthostatic tolerance, lower body negative pressure responses, and exercise capacity changes resulting from space travel. Since skeletal muscle loses tone, strength, work capacity, and mass during periods of inactivity such as weightlessness, inflight attempts to reduce these loses might assist in maintaining cardiovascular conditioning and therefore help reduce orthostatic intolerance during return to a 1-g environment. A quantitative assessment of Skylab data related to these points has not been performed.

Results

This section will evaluate the results from the Skylab missions in

the areas of crewmen pre- and in-flight training methods and exercise levels, and how training may have affected the cardiovascular responses observed following lower body negative pressure and exercise during and following spaceflight.

Skylab Crewmembers Preflight Exercise Training.

Preflight exercise methods among Skylab astronauts varied considerably, and the training effects are difficult to document. One can evaluate the state of cardiovascular conditioning, on a first order basis, by measuring preflight resting and stressed heart rates among the crewmembers. These are shown in Table VI, with the stressed heart rates determined following application of -50 mm Hg lower body negative pressure(54 preflight determinations among all Skylab astronauts).

TABLE VI. PREFLIGHT HEART RATES AMONG SKYLAB ASTRONAUTS

Skylab mission		Heart Rate(rest)	Heart Rate(stressed)
2	Commander	55	68
	Scientist Pilot	64	84
	Pilot	59	65
3	Commander	57	72
	Scientist Pilot	56	65
	Pilot	47	53
4	Commander	59	66
	Scientist Pilot	51	65
	Pilot	48	61
Average: 3 Missions		55	67

Heart rates measured in beats per minute.

Resting heart rates presented in Table VI were determined by averaging six to eight preflight measurements on each individual crewmember. Based on these data, one would predict that the Skylab crewmembers had undergone significant preflight conditioning, regardless of the method used.

The preflight exercise programs selected by individual crewmembers of the Skylab missions can be separated into one of three classes, although some overlap occurs. Class 1 includes a training program based primarily on distant running, Class 2 applies to crewmembers who primarily exercised by playing racquetball, and Class 3 included the crewmembers who combined the Class 1 and 2 programs, although at lower levels of intensity, with weights, swimming, gymnastics, etc. Again, there is considerable overlap among some crewmembers, but where possible, those who can be placed into one of the three clases will be identified.

Skylab Crewmembers In-flight Exercise Training.

Although in-flight exercise profiles and work levels varied among crewmembers, Table VII shows that following normalization of work data to the crewman's body weight, the Skylab 3 crewmembers exercised about 107 percent more than the Skylab 2 crew and the Skylab 4 crewmembers exercised 130 percent more than the Skylab 2 crew. The effects that the increased in-flight exercise load had on postflight recovery will be discussed later in this section. Special emphasis will be placed on measuring the rate of return of cardiovascular responses to preflight

recorded values.

TABLE VII. IN-FLIGHT QUANTITATIVE PERSONAL EXERCISE SUMMARY

Skylab mission	Crewman	(1)Total (watt min)	(2)Daily avg (watt min)	(3)Daily avg (watt min/kgm body weight)	Avg
2	Commander	62810	2855	47	
	Scientist Pilot	45307	1618	21	31.3
	Pilot	55795	1993	26	
3	Commander	228581	3874	58	
	Scientist Pilot	214645	3638	62	65.0
	Pilot	386193	6545	75	
4	Commander	349210	4108	62	
	Scientist Pilot	469420	5523	80	72.3
	Pilot	414760	4879	75	

(1) Includes M171 experiment tests and personal exercise
(2) Based on 28-day Skylab 2 mission, 59-day Skylab 3 mission, and 84-day Skylab 4 mission.
(3) Based on mean in-flight body weight.

Skylab 2 crewmembers primarily utilized the M171 bicycle ergometer(fig. 2) for in-flight exercise.

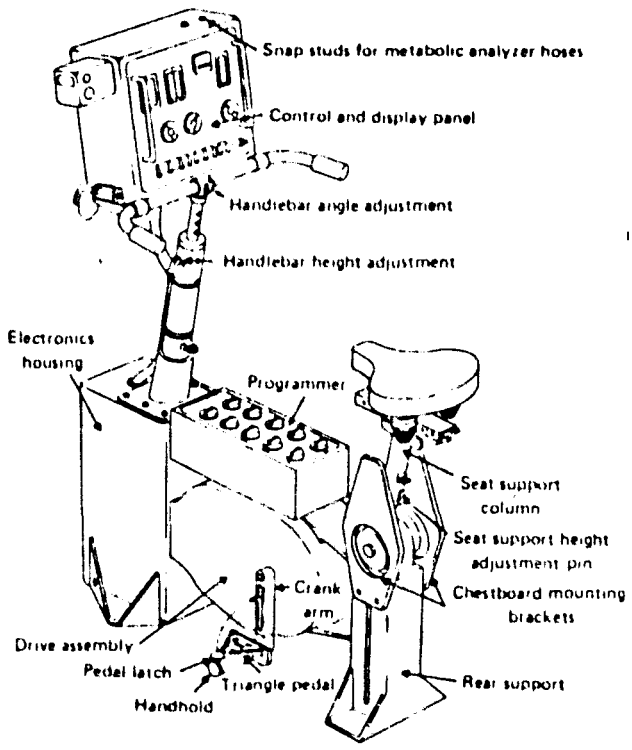

Fig. 2. Skylab Bicycle Ergometer

When their postflight return of exercise tolerance to preflight status exceeded the time for recovery observed in Apollo crewmen, it was decided to add a mass-produced commercial device, called Mini Gym, which was extensively modified and designed "MK-I"(fig. 3). This device was developed to provide adequate exercise to arms, trunk and legs. A series of exercises utilizing "MK-I" are presented in figure 3.

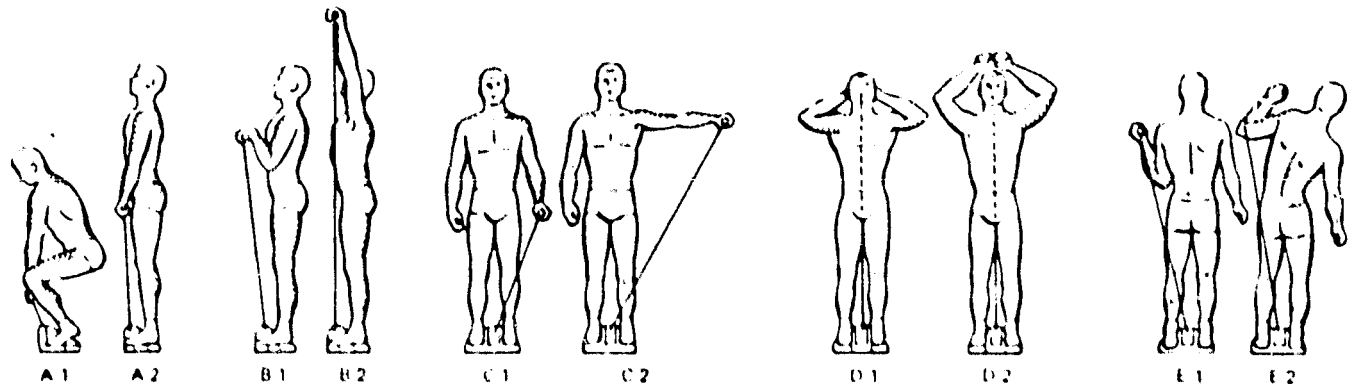

Fig. 3. Skylab "MK-I" Exerciser and Several Exercise Methods

A second device, designated "MK-II", consisted of a pair of handles between which up to five extension springs could be attached, allowing maximum forces of 25 pounds per foot of extension to be developed. These two devices were first flown on Skylab 3, and food and time for exercise was increased in-flight.

Although the bicycle ergometer is an excellent machine for aerobic exercise and cardiovascular conditioning, it could not develope either the type or level of forces to maintain strength for walking under 1-g. Because of the leg muscle strength and volume loses shown following Skylab

2, work was started to develope an in-flight treadmill exerciser(fig. 4).

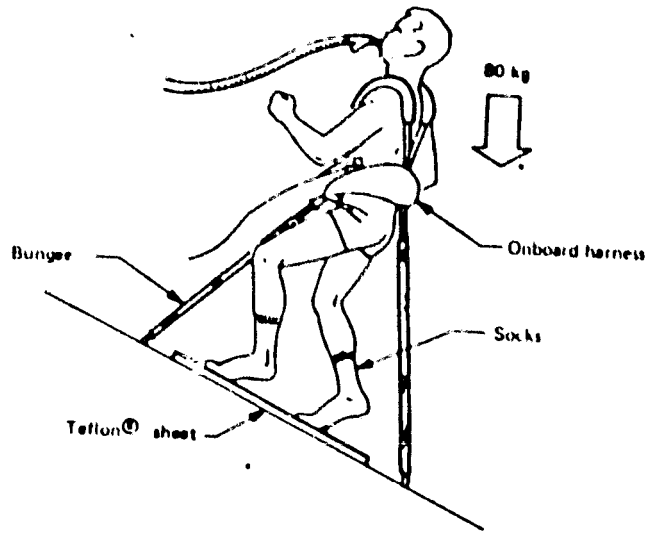

Fig. 4. Skylab Treadmill Exerciser

This device a lowed walking and running, plus other isotonic training, under forces equivalent to gravity(1-g). Four rubber bungees provided an equivalent weight of 80 kilograms and were attacned to a shoulder and waist harness. By angling the bungees, an equivalent to a slippery hill is presented to the subject who must climb it. High loads were placed on some leg muscles, especially the calf, and fatigue was rapid such that the device could not be used for significant aerobic work.

On Skylab 4, the crew used the bicycle ergometer at essentially the same rate as Skylab 3, and the "MK-I and II" exercisers. In addition, they typicaily performed 10 minutes per day of walking, jumping, and jogging on the treadmill. Food intake had again been increased. Daily exercise protocols

for the Skylab 4 crewmembers are shown in Table VIII.

TABLE VIII. DAILY PERSONAL EXERCISE - SKYLAB 4 CREWMEMBERS

Exercise	Commander	Scientist Pilot	Pilot
Leg Ergometry(watt min).	5000	8337	6000
Minigym(Total repetitions).	100	200	200
Springs(Total repetitions).	75	0	120
Torso Isometrics(Total repetitions)	20	0	20
Treadmill:			
Walk(min).	10	0	0
Run(min).	1	0	0
Springs(Repetitions).	300	1000	100
Toe Rises(Repetitions).	200	200	75

Physiological Changes in Muscle Strength and Volume During Weightlessness.

Figure 5 presents a summary of Skylab exercise levels as well as the changes in body weight, leg strength and leg volume following weightlessness.

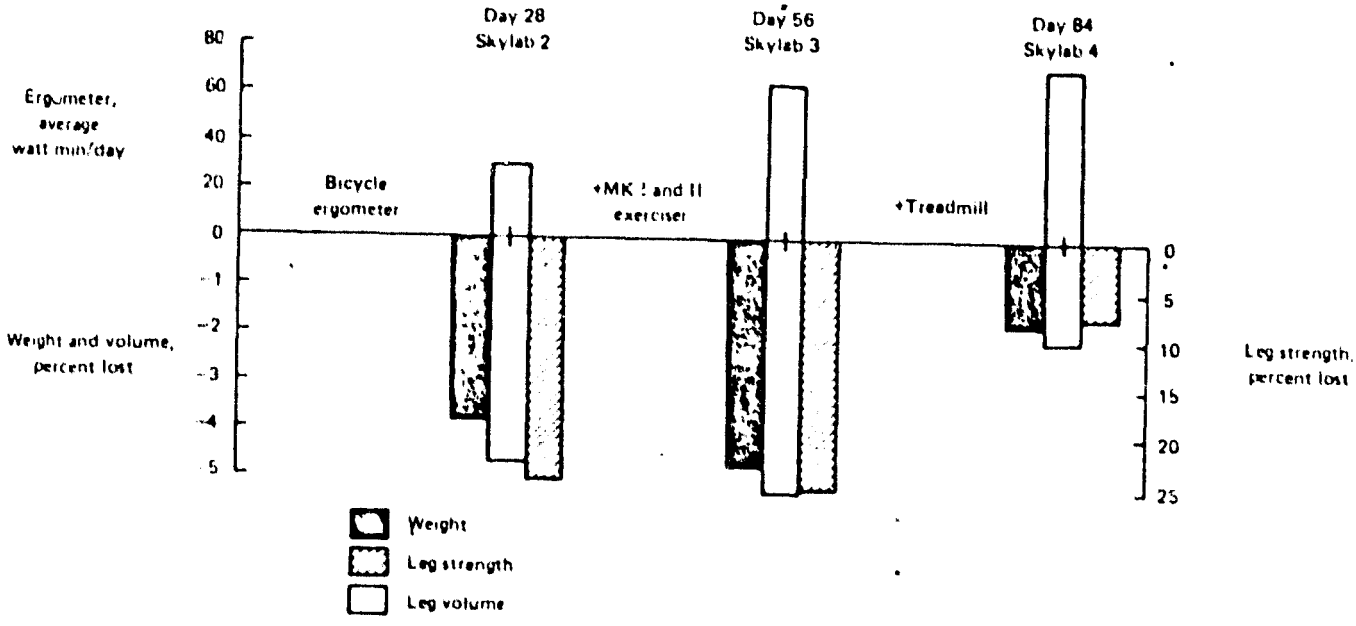

Fig. 5. Exercise related quantities on Skylab missions

From figure 5, it is apparant that the increased exercise loads, along with the increased caloric intake from dietary supplements, allowed the Skylab 4 crewmembers to undergo a significantly smaller decrease in body weight, leg volume and leg strength. One crewmember of Skylab 4, the commander, was only the second American astronaut to gain weight in space, even after a spaceflight of 84 days duration.

Even prior to muscle testing following re-entry from space, it was obvious that the Skylab 4 crew was in surprisingly good condition. They stood and walked for long periods without apparent difficulty on the day after recovery in contrast to the earlier missions. Results of the muscle testing, which will be presented later in this section, confirmed a surprisingly small loss in leg strength after almost three months in weightlessness(fig. 5). A summary of the exercise and strength testing shown in average values for the three missions is presented in figures 6 and 7.

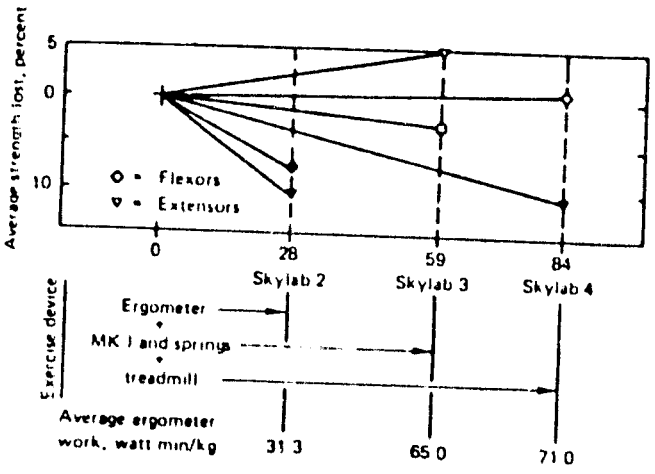

Fig. 6. Average strength changes, arms: all Skylab Missions.

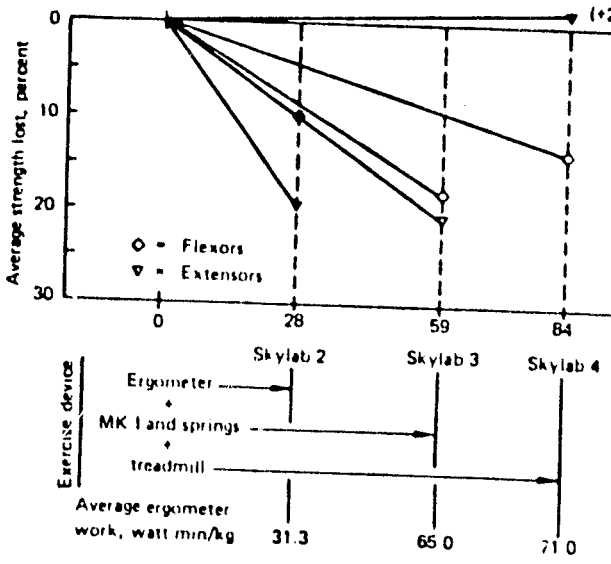

Fig. 7. Average strength changes legs: all Skylab Mission

Relatively small losses in arm strength(fig. 6), as compared to leg strength(fig. 7), is shown in all missions. This reflects the fact that in space ordinary work provides loads for the arms that are relatively much greater; the legs receive virtually no effective loading . The increase in leg extensor(antigravity) muscle strength observed on Skylab 4(fig. 7) undoubtedly contributed to their early postflight recovery.

A common measure of muscle condition is muscle size. Figure 5 shows that muscle size of the Skylab 4 astronauts was reduced only one-half the volume of the shorter flights. Recovery of leg volume to preflight status, shown in figure 8, illustrates that the Skylab 4 crewmembers displayed faster recovery rates than the Skylab 2 and 3 crewmen.

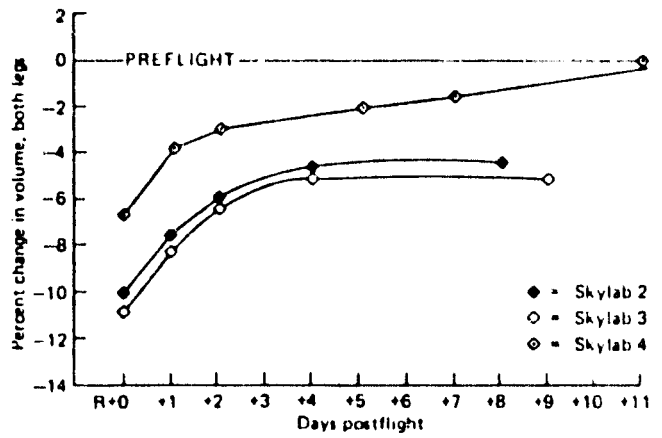

Fig. 8. Average leg volume change, postflight; all Skylab missions

It is interesting to note that the amount of exercise performed in-flight was inversely related to the length of time required postflight for return to preflight status. Except for some isolated individual responses

in cardiac output and stroke volume data, all other cardiopulmonary and work capacity parameters retunred to normal in approximately 18 - 21 days for the Skylab 2 crewmemebers, 7 days for the Skylab 3 crew, and 4 days for the Skylab 4 crew. Paradoxically, the Skylab 3 crewmen, who displayed leg volume and strength decrements equivalent to those recorded for the Skylab 2 crewmembers, returned to preflight status at a rate almost equal to the Skylab 4 crew.

Skylab Astronaut Cardiovascular Responses Recorded During Exercise Before, During, and Following Weightlessness: M171 Experiment.

Table IX presents the cardiovascular responses of the Skylab 4 crew collected from the M171 experiment. The measured parameters included heart rate, systolic blood pressure, and diastolic blood pressure collected at rest, during the final 3 minutes of 5-minute level 3 exercise, and the recovery values were those obtained for the second minute during the 5-minute recovery period.

All three crewmembers of the Skylab 4 mission experienced a significant decrease in in-flight recovery heart rate. It would appear that following exercise in weightlessness, heart rate values return toward resting values more rapidly, and to a lower level, than 1-g responses. In-flight heart rate increases during level 3 exercise were not significantly different from those recorded preflight. When the Skylab 4 crewmembers returned to e th, they all exhibited significantly elevated heart rate values in comparison to pre- and in-flight recorded resting heart rate values. This was a common observation among a majority of

Skylab astronauts following return to earth. The heart beats at a faster rate upon returning to earth in an attempt to maintain cardiovascular homeostasis induced by a reduction in cardiac output.

TABLE IX. SKYLAB 4 M171 DATA SUMMARY

	Variables								
	Heart Rate(BPM)			SBP(mm Hg)			DBP(mm Hg)		
	Rest	Level 3	Recovery	Rest	Level 3	Recovery	Rest	Level 3	Rec
CDR									
Preflight($\bar{X}$)	66	157	112	96	192	179	67	71	6
In-flight($\bar{X}$)	66	152	87*	97	195	181	59*	56*	6
Postflight($\bar{X}$)	76*	163	109	106	195	170	72	67	7
SPT									
Preflight($\bar{X}$)	64	164	104	127	204	186	84	55	6
In-flight($\bar{X}$)	62	166	92*	119*	200	174	74*	52	6
Postflight($\bar{X}$)	74*	167	102	123	198	189	78*	51	6
PT									
Preflight($\bar{X}$)	54	147	114	115	204	188	72	60	6
In-flight($\bar{X}$)	53	147	91*	115	200	186	64*	51*	6
Postflight($\bar{X}$)	65*	156*	118	125*	213	204	74	59	6

*Outside the preflight 95% confidence limit.
BPM, beats per minute; SBP, Systolic Blood Pressure; DBP, Diastolic Blood Pressure; CDR, Commander; SPT, Scientist Pilot; PT, Pilot.

Table IX also indicates that spaceflight significantly lowers diastolic blood pressure during resting conditions in all crewmembers. This parameter is also significantly reduced in two crewmen during level 3 exercise periods. Diastolic blood pressure changes will be discussed later in this section.

Generally, the in-flight and postflight responses to exercise by the crews of Skylab 2, 3 and 4 were similar. In-flight, some subtle, isolated

differences were seen. There were no trends observed which would indicate a degradation in the exercise responses of the crews. The Skylab 4 crew exhibited a significant in-flight decrease in recovery heart rate but not in resting(sitting position) heart rate. The Skylab 2 crew, on the other hand, exhibited decreases in both parameters while the Skylab 3 crew exhibited no changes in either. Figure 9 displays the heart rate responses of all Skylab crewmembers during pre-, in-, and postflight level 3 exercise.

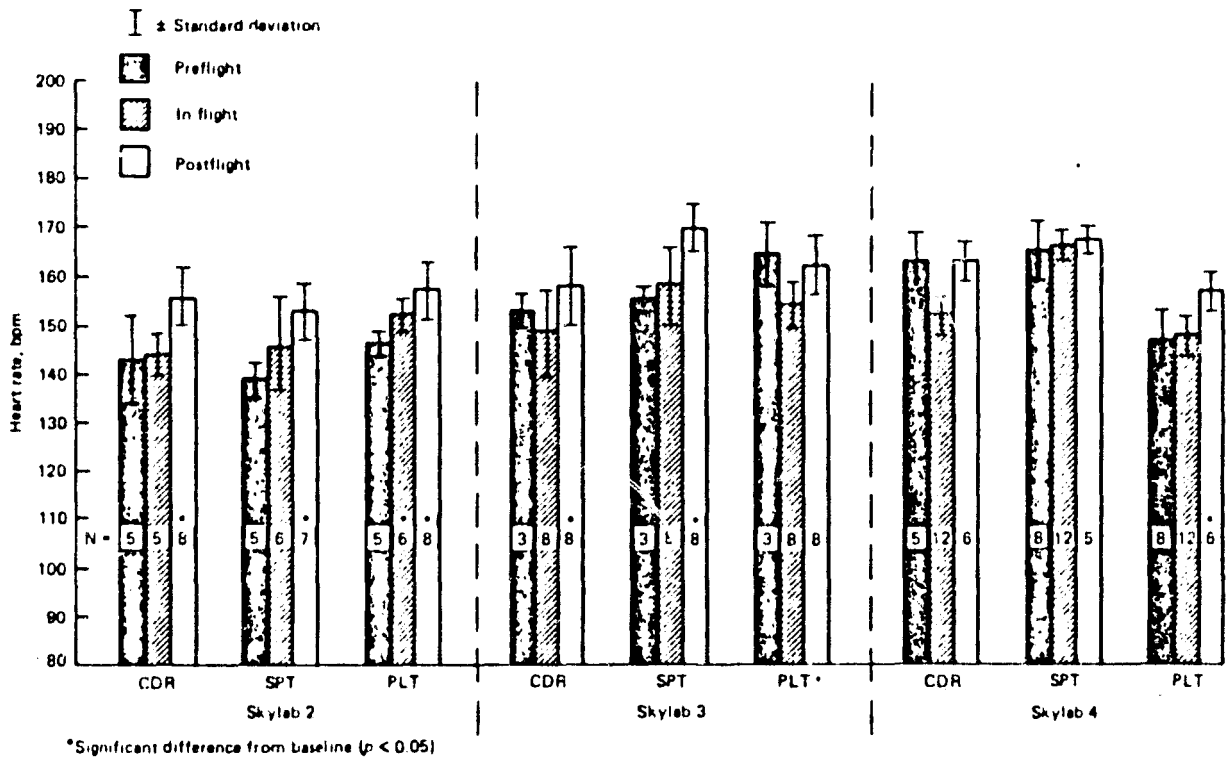

Fig. 9. Heart Rate Responses for Skylab Crews, Level 3 Exercise.

The data presented in figure 9 indicate that postflight recovery heart rates tend to return to preflight(and in-flight) values with longer duration flight

All Skylab 2 crewmembers had significantly higher heart rate values following postflight exercise, while two Skylab 3 and only one Skylab 4 crewmember displayed this response.

Figure 10 displays the diastolic blood pressure responses for all Skylab astronauts during level 3 exercise periods conducted pre-, in-, and postflight.

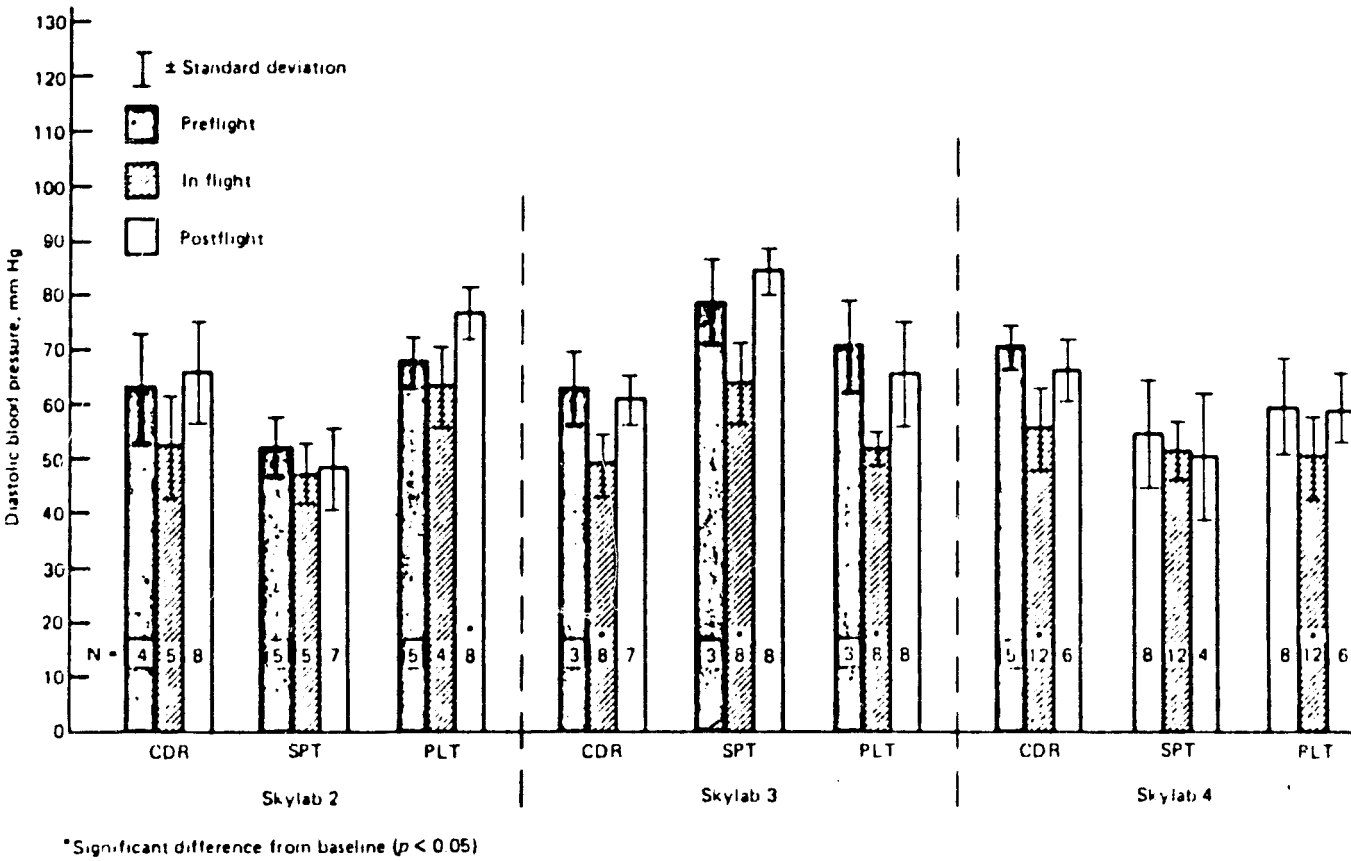

Fig. 10. Diastolic blood pressure, level 3 exercise: all Skylab missions.

Figure 10 shows an interesting trend in diastolic blood pressure among the

Skylab astronauts during spaceflight. Five of six Skylab astronauts from the longer duration missions(59- and 84-days) showed significantly lowered diastolic blood pressure during heavy exercise(level 3) while in the weightless condition.

One potentially dangerous cardiovascular adjustment noticed in all Skylab astronauts upon retunring to earth is a significant reduction in cardiac output and stroke volume(fig. 11). The exact explanation for this adjustment is not clear, but may reflect a reduced circulating blood volume (Table X) which therefore limits venous return of blood to the heart. Positive chronotropic(increases in heart rate) and inotropic(increases in myocardial contractility) responses of the heart may also be reduced following extended periods of weightlessness.

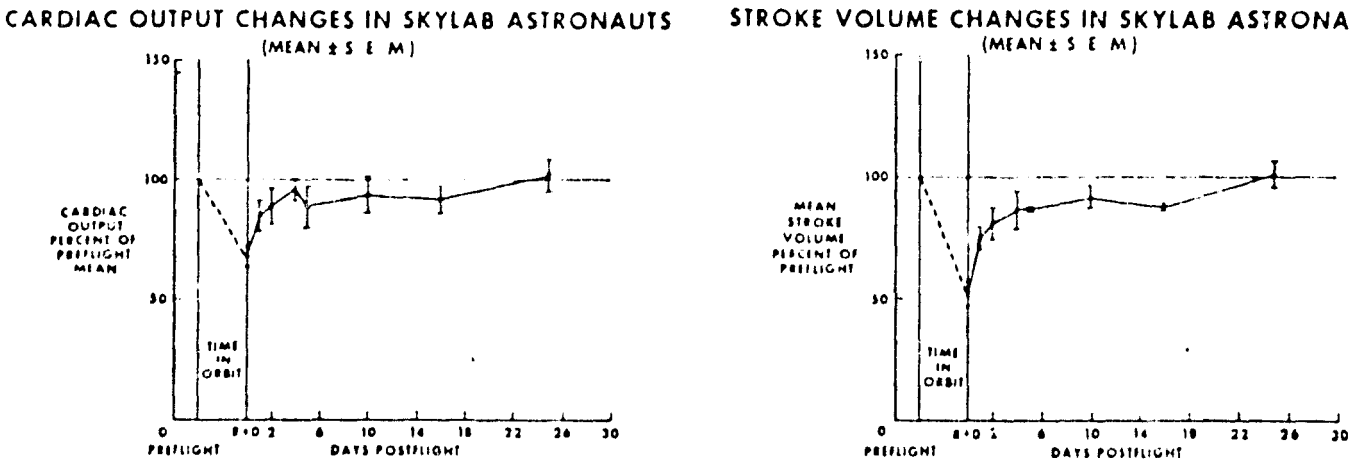

Figure 11. Changes in Cardiac Output and Stroke Volume in Skylab Astronauts Following Periods of Weightlessness.

One final observation in the area of cardiovascular adaptations during

weightlessness that awaits further study is the apparant loss of circulating plasma volume and what can be done to prevent this loss(Table X). This loss of circulating blood volume undoubtedly affects cardiovascular performance during spaceflight as well as following return to earth. As shown in Table X, longer duration missions produce greater losses in plasma volume. However, since the Skylab 4 astronauts were capable of retruning carviovascular parameters to preflight values at a rapid rate (4-days), their loss of plasma volume does not appear to limit cardiovascular performance following return to earth.

TABLE X. PLASMA VOLUME - PERCENT CHANGE FROM PREMISSION VALUE.

First Skylab Mission	Commander	Scientist Pilot	Pilot		Mean
Premission volume(ml)	3042	3506	3472		
	Percent	Percent	Percent	Percent	Percent
R + 0*	-2.5	-10.3	+2.6	(**-12.3)	-8.4
R + 13	-1.2	-5.6	+14.1	(**-2.5)	-3.1
R + 42	+8.5		+18.6	(**+1.4)	+4.9
R + 67	-5.7	-1.1	+17.0	(**0.0)	-2.3
Second Skylab Mission					
Premission volume(ml)	3157	2798	3885		
	Percent	Percent	Percent		Percent
R + 0*	-18.4	-9.1	-11.8		-13.1
R + 14	+0.1	+14.7	+2.0		+5.6
R + 45	+2.8	+11.7	+6.8		+7.1
Third Skylab Mission					
Premission value(ml)	3067	3620	3195		
	Percent	Percent	Percent		Percent
R + 0*	-15.7	-19.2	-12.9		-15.9
R + 14	+8.6	+7.4	+13.0		+9.7
R + 31	+6.4	+17.7	+5.9		+10.0

*R +, Recovery + day(s). **% change calculated using R + 67 day value.

Skylab Astronaut Cardiovascular Responses Recorded During the Application of Lower Body Negative Pressure(LBNP) - M092 Experiment.

An explanation of the changes in cardiovascular responses to lower body negative pressure in a weightless environment requires understanding of the manner in which the systems of the body and their functions adjust to the weightlessness of space flight. A more comprehensive understanding of these adjustments will, in turn, require the correlation of massive volumes of data from all the Skylab experiments, a task of monumental proportions which has barely been started.

Cardiovascular responses of the Skylab 4 Pilot during lower body negative pressure test 35 days prior to flight(fig. 12) and on mission day 10 (fig. 13) are shown for comparison. The mission day 10 test was terminated early due to presyncopal conditions developed by the Pilot.

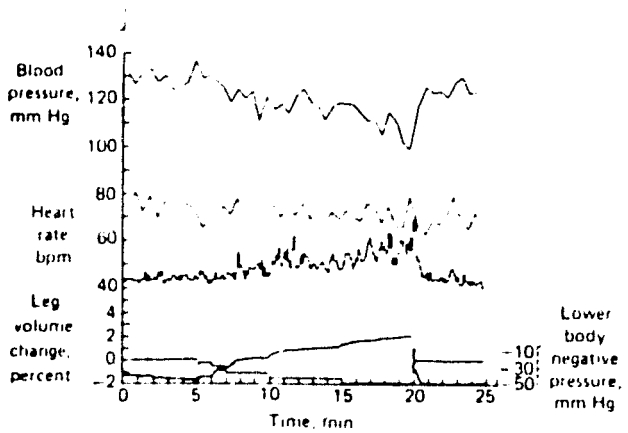

Fig. 12. Cardiovascular responses of the Skylab 4 Pilot during LBNP test 35 days prior to flight.

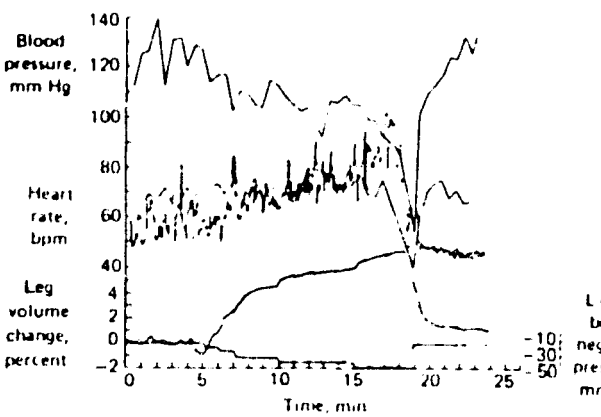

Fig. 13. Cardiovascular responses of the Skylab 4 Pilot during LBI test on mission day 10. Presync symptoms led to termination of test.

One area of interest that this report will not completely cover is the ability to predict the factors responsible for the presyncopal reactions demonstrated by Skylab crewmembers. No crewmen seemed immune to this response but some seemed more susceptible than others. One factor which awaits further analysis is the influence of physical training on the develoment of presyncopal conditions during lower body negative pressure. Recent studies have indicated that distant runners may be more susceptible to developing presyncopal responses during lower body negative pressure than individuals who train using other form of exercise, as weightlifting or swimming(ref. 4).

Other factors certainly influence the cardiovascular responses to lower body negative pressure. For example, none of the 13 instances of early termination of tests due to presyncopal symptoms occurred during tests conducted in the morning or within 7 hours of arising from sleep, although approximately one-third of all in-flight tests were conducted within that period. These 13 tests were associated with larger than usual calf volume increases(see e.g., fig. 13) during the lowest negative pressure phases of the tests. This suggests that the pooling of large volumes of blood during the first few minutes of the test may so alter the effectiveness of compensatory cardiovascular mechanisms as to render them incapable of adequate responsiveness to the greater stress later in the test.

Among the three astronauts, the Commander of Skylab 2, the Pilot of Skylab 3, and the Commander of Skylab 4, whose in-flight tests were nominally scheduled in the morning, only one presyncopal episode occurred and this was in the Commander during a test performed in the afternoon over 9 hours after arising. These crewmembers also could be grouped into class 2

based on their preflight exercise training.

The Pilot and Scientist Pilot of Skylab 4 exhibited a larger number of presyncopal responses during lower body negative pressure than a majority of the other Skylab astronauts. These two crewmembers, especially the Scientist Pilot, could be placed in Class 1 according to preflight exercise training. The Pilot had taken up distant running several years before flight and had experienced a significant weight loss during this period. When one examines the calf volume changes induced by lower body negative pressure, in-flight increases greatly exceeded those which occurred during preflight testing. Calf volume increases of the Skylab 4 Commander in preflight tests were relatively small in comparison to those of the Scientist Pilot and Pilot of that mission, which were larger than usually seen. This same pattern of difference continued throughout the mission. Whereas preflight calf volume increases at the end of the 50 mm Hg negative pressure phase averaged between 3 and 4 percent, during in-flight tests they reached values usually between 8 and 11 percent in the Scientist Pilot and Pilot. In the Commander, calf volume increases averaged 2.4 percent preflight but usually reached levels ranging between 5 and 7 percent in-flight.

The volume of blood pooled in the lower extremities during in-flight tests did not seem to correlate from test to test with the magnitude of heart rate or blood pressure change during lower body negative pressure. In general those of the nine Skylab astronauts with the greatest increase in calf volume during in-flight tests also showed the greatest increases in heart rate and changes in blood pressure. These data, for the Skylab 4 crewmembers, are shown

in Table XI. In addition, although correlation of heart rate increases with leg volume increases was not evident in preflight tests, the crewmen whose calf volume increases were greatest in preflight tests usually also showed the largest increases during the in-flight tests.

TABLE XI. DIFFERENCES BETWEEN MEAN IN-FLIGHT VALUES FOR HEART RATE AND BLOOD PRESSURE OF THE SKYLAB 4 CREWMEN DURING REST AND 50 mm HG PHASE OF LOWER BODY NEGATIVE PRESSURE FROM CORRESPONDING MEAN VALUES DURING PREFLIGHT TESTS.

	CDR	SPT	PT
Resting control:			
Heart rate(bpm)	+7.8*	+13.3*	+11.3*
Systolic blood pressure(mm Hg)	+1.8	+2.5	+1.0
Diastolic blood pressure(mm Hg)	-5.6*	-2.0	-2.5
Pulse pressure(mm Hg)	+7.4*	+4.5*	+3.4
Mean arterial pressure(mm Hg)	-3.2*	-0.5	-1.3
Stressed, -50 mm Hg:			
Heart rate(bpm)	+12.2*	+36.7*	+26.7*
Systolic blood pressure(mm Hg)	+6.2*	-10.9*	-1.6
Diastolic blood pressure(mm Hg)	-1.0	-4.8	+1.3
Pulse pressure(mm Hg)	+7.1*	-6.1	-2.8
Mean arterial pressure(mm Hg)	+1.5	-6.8*	+0.3

CDR, Commander; SPT, Scientist Pilot; PT, Pilot;
*Significant to 0.05 level by Student's paired t-test.

The in-flight mean increase in heart rate during 50 mm Hg lower body negative pressure over resting rates for all nine Skylab crewmen averaged 20.4 beats per minute, a highly significant difference. The increase in heart rate during orthostatic stress has generally proven to be the best single index in the assessment of orthostatic tolerance. The pattern of fluctuations of resting and stressed heart rates and blood pressure varied for each crewman, but their magnitude and frequency were greater during the first part of the mission than

later. Their nature and significance is unknown, but, in the case of the Skylab 4 crewmen, their prominence and duration appeared to decrease as cardiovascular responses to in-flight lower body negative pressure stabilized.

Conclusions

The Skylab Lower Body Negative Pressure experiment demonstrated that loss of orthostatic tolerance had already developed by the time of the first tests after 4 to 6 days of flight. Cardiovascular responses to lower body negative pressure showed the greatest instability and orthostatic tolerance the greatest decrement during the first three weeks of flight. After approximately 5 to 7 weeks, cardiovascular responses became more stable and evidence of improving orthostatic tolerance appeared.

In-flight data from the lower body negative pressure experiment proved to be useful not only in predicting the early postflight status of orthostatic tolerance, but also in the in-flight assessment of crew health status. In-flight lower body negative pressure presented a much greater stress to the cardiovascular system than the same levels of negative pressure during preflight tests.

At rest, in-flight mean resting heart rates, systolic blood pressures, and pulse pressures were typically increased while diastolic and mean arterial pressures decreased compared to preflight values in the majority of Skylab crewmembers. Differences in in-flight responses to lower body negative pressure stress from preflight responses included greater heart rate and leg volume increases in all crewmen and, in most, higher diastolic pressures and mean

arterial pressures and lower systolic blood pressures and pulse pressures.

The successful completion of the 28-, 59- and 84-day Skylab missions showed that man can perform submaximal and maximal aerobic exercise in the weightless environment without detrimental trends in any of the physiologic data. Exercise tolerance during flight was unaffected. It was only after return to Earth that a tolerance decrement was noted.

The rapid postflight recovery of orthostatic and exercise tolerance following two of the three Skylab missions appeared to be directly related to total in-flight exercise as well as to the graded, regular program of exercise performed during the postflight debriefing period.

The postflight orthostatic intolerance and diminished exercise capacity are both related etiologically to a decreased effective circulating blood volume at one-g, with consequent decreased venous return and cardiac output.

Acknowledgments

The author extends his sincere appreciation to many individuals who made this report possible, including Dr. F. S. Musgrave, a first-rate technical advisor and friend, Dr. C. J. Huang and Ms. Nancy Robertson, who patiently assisted and advised all the summer fellows, and the Hawks' and Mashburns' who 'put up' with my presence during the summer. Special thanks are also extended to NASA/ASEE for funding this study, and my strongest hopes are expressed that this program be continued in the future.

My thanks to the Skylab Astronauts and support personnel for making the data available for this study.

References

1. Michel, E. L., J. A. Rummel, C. F. Sawin, M. C. Buderer, and J. D. Lem. Results of Skylab Medical Experiment M171 - Metabolic Activity. In: Biomedical Results from Skylab, pp. 372-387. NASA SP-377, 1977.

2. Johnson, R. L., G. W. Hoffler, A. E. Nicogossian, S. A. Bergman, and M. M. Jackson. Lower Body Negative Pressure: Third Manned Mission. In: Biomedical Results from Skylab, pp. 284-312. NASA SP-377, 1977.

3. Stevens, P. M., and L. E. Lamb. Effects of lower body negative pressure on the cardiovascular system. Am. J. Cardiol. 16: 506, 1965.

4. Luft, U. C. Specialized Physiological Studies in Support of Manned Space Flight: Tolerance of lower body negative pressure(LBNP) in Endurance Runners, Weightlifters, Swimmers and Non-athletes. Report. NASA Contract NAS9-15483. 1980. pp. 1-104.

INTERNATIONAL AEROSPACE ENGINEERING: NASA SHUTTLE and EUROPEAN SPACELAB

Roger E. Bilstein, Ph. D.
University of Houston/Clear Lake City
1981 NASA-ASEE Summer Faculty Fellow

Supervisor:

Dr. Edward C. Ezell
History Office
Administration and Program Support Directorate

Abstract - For mutual benefit, NASA and European space research organizations agreed on European development of the Spacelab. Substantial diplomatic and technical collaboration preceded the official Memorandum of Understanding signed in 1973.

NATIONAL AERONAUTICS AND SPACE ADMINISTRATION
LYNDON B. JOHNSON SPACE CENTER
HOUSTON, TEXAS
AUGUST 12, 1981

INTERNATIONAL AEROSPACE ENGINEERING: NASA SHUTTLE and EUROPEAN SPACELAB

By

Roger E. Bilstein*

The successful mission of the shuttle Columbia in April 1981 brought a new sense of achievement to NASA and to America. The flight also sent an expectant tremor through the European Space Agency ESA, who plans to have a significant role in future shuttle flights. ESA designed and built the Spacelab, a major payload item for shuttle missions to come. Spacelab provides a shirt-sleeve environment for non-astronauts, or "mission-specialists," to conduct a host of laboratory research projects in space. It offers a flexibility never available to scientists before the Shuttle/Spacelab appeared on the scene. More importantly, Spacelab gives western Europe, for the time, a leading role in manned space flights, and represents a major turning-point for ESA and its contractors. A spokesman for ERNO, the European prime contractor, summarized the changed situation: "Award of the contract to build the space laboratory and its complex systems meant that ERNO and its partners would tread completely new paths," the European contractor observed. "Their space activities had so far been concentrated on the satellite and launch sector. Now new procedures and methods had to be established and tackled for the first manned space flight system. Spacelab exceeded all the familiar dimensions."[1]

*The opinions and conclusions are the author's only, and do not reflect official NASA policy. This paper is part of a longer study still in progress, and much of it is still tentative; contact the author for permission to cite or quote.

Shuttle/Spacelab operations also represent a major change for NASA. The American space agency traditionally managed its own contractors in the development of space hardware. Although NASA occasionally launched satellite payloads for foreign customers, including ESA, these were essentially discrete projects with minimal integration problems. Spacelab changed all that, requiring major collaboration on the design and operation of the Shuttle/Spacelab combination. Interaction between Europeans and Americans, against a background of long-established NASA procedures, demanded diplomatic give-and-take involving top-level administrators, program managers, and engineers--from chancellories all the way down to the shop floor. This paper emphasizes Shuttle/Spacelab developments through the Memorandum of Understanding in 1973.

IDEAS AND ORGANIZATIONS

At least a decade before Sputnik in 1957, the idea for a reusable space transportation system appeared in American popular and technical articles alike. The complexities of such schemes proved discouraging; in any case, the drive to perfect ICBM weapons offered a reasonable alternative to boost scientific payloads into space. Sputnik shocked the U.S. into a heavy investment in space research. The Russian-American space race that followed evolved in the spotlight of international attention and underscored space research as a measure of national prestige. In addition, an active space program seemed to generate considerable technological fall-out. Some leaders in Western Europe

began to worry about decline in both prestige and technical abilities unless they developed their own space program. France became particularly active in this respect and put its own Asterix satellite, aboard its own Diamant three-stage booster, in orbit by 1965. Britain became interested in the possibilities of using its Blue Streak rocket as a first-stage booster for a multi-staged European launch vehicle. These and other strands of European activity finally resulted in the creation of the European Launch Development Organization (ELDO) and the European Space Research Organization (ESRO) by the mid-60s.[2]

The European space organizations hoped to get into the space business in a way that would benefit Continental business and industry. ESRO, with 10 members, emphasized scientific payloads and satellite development. ELDO concentrated on a larger booster that would end dependence on NASA rockets launched from Cape Kennedy. ELDO's principals included Britain, France, Germany (builders, respectively, of first, second, and third stages of a launch vehicle), and Italy (coordinator of a satellite payload). By 1969, after eight years of effort, Europe's united bid for an independent space capability failed to coalesce.[3] The stage was set for European space research to move in different directions. Two lines of activity emerged: renewed attention to manned, earth-orbital vehicles that eventually led to the Spacelab concept; an "alliance of convenience" with NASA.

In the U.S., plans for a reusable Space Shuttle had already begun to finalize. Mercury, Gemini, and Apollo programs provided

increasing understanding of manned space vehicles. High-speed aerodynamics and thermal problems became better understood through the X-15 and other experimental aircraft programs. A series of "lifting bodies" yielded design information on high-speed descent and landing. By 1970, based on this experience, as well as prototype shuttle studies, the U.S. was committed to a shuttle transportation system. Plans called for a vehicle to ferry up to 12 passengers back and forth between Earth and a space station, itself built from modules carried in a shuttle cargo bay and assembled in orbit.[4] Through space transport studies similar to these, the idea for a European Spacelab began to emerge.

During the mid-1960s, European thinking about space exploration began to sharpen its focus through a 150-member industrial consortium called Eurospace. As early as September 1964 a Eurospace report summed up the group's thinking about a reusable spacecraft--an aerospace transporter--that had been under informal discussion for several years. The concept envisioned piloted booster and orbiter stages, the latter to have a two-man crew and to carry 2.5 tons into a 180-mile orbit. During a visit to the U.S. in the spring of 1965, Dr. Erhard Loewe, a vice-president of Telefunken, and Eurospace spokesman, discussed Europe's stake in the aerospace transporter. The U.S. and Russia had already committed themselves to a manned lunar landing, he observed. Europe did not have the technology for such lunar aspirations, but the aerospace transporter promised Europe a reasonable role

in the near-Earth space environment. More than that, the transporter would serve as a springboard for European survival in a technical world. "We are...influenced by the conviction that, should we be unable to go ahead with the realization of our objective, we should fall far behind in the technical field," Loewe empahsized. At the same time, he left the door open for discussing joint U.S.-Europe space ventures. Loewe stressed the importance of space stations for the true exploitation of space, and noted that space stations could offer a very useful option for joint efforts.[5]

Eurospace consideration of the aerospace transporter apparently included rather extensive paper studies and scale models of at least one proposed design. Junkers, the German aviation firm, fielded a design team including Boelkow-Entwicklungen KG, and another consortium known as ERNO. Eurospace sources insisted that the transporter idea was not too ambitious for them, and that they could develop the idea by 1975-80. Talk of a modest space station also continued. If all this was to be achieved, many European aerospace experts realized that the current organization for space exploration would have to be replaced by a different scheme. ESRO and ELDO continued to work independently. They shared laudable liaison connections, but still had no mechanism for joint planning. With no comprehensive policy, various European governments remained reluctant to fund programs. Christopher Ashton, an assistant technical director for ELDO, advocated more liaison at a high policy-making level, especially

a government-to-government basis, to establish a coherent European space program. Eurospace thinking tended to agree. . In short, ideas began coalescing for a single space agency--a European NASA.[6]

In retrospect, the activities and mood of European space interests in the Spring of 1965 assumed considerable significance in light of subsequent developments. Design studies for the aerospace transporter and space station started European aerospace thinking about the details involved in the launch, operation, and return of orbiting spacecraft; the life support systems and operational requirements for the manned transporter and manned space station in orbit; the need for a unified space organization to accomplish all of this. The eventual creation of ESA (the European Space Agency), and development of the Spacelab reflects a direct lineage to this period. Moreover, ERNO emerged as the principal Spacelab contractor.

Over the next few years, a series of developments drew Europe and the U.S. together as aerospace partners. Even though France put a number of modestly sized satellites into orbit, beginning in 1965, a vigorous European program failed t ter-ialize. Coordination of efforts remained indecisive, and substantial funds for extensive R&D never appeared. NASA spurned suggestions for joint research on the aerospace transporter as too much duplication of advanced U.S. work on the Shuttle. Instead, NASA opened a different door for cooperation. In February 1966, during a visit of West Germany's Chancellor, Ludwig Erhard, to the U.S., President Lyndon Johnson suggested collaborating in a major space exploration effort. The U.S. suggested

probes to the Sun and to Jupiter. Johnson possibly made the offer to side-step the issue of West German control of nuclear weapons, but Erhard, at least, appears to have encouraged the space venture. Shortly thereafter, NASA Administrator, James Webb, and a high-level NASA executive group left for Europe to pursue the issue.

The nature of subsequent talks seems to have shifted towards manned missions. NASA, during the late 1960s, began considering scientific modules to dock with space stations. By 1969, European interest in joint NASA ventures began to concentrate on the "Research and Applications Module" (RAM), an aspect of the American space station studies.[8] During the same period, ERNO became involved in studies to enhance Skylab operations,[9] thus adding to ERNO's growing understanding of manned missions. By the Autumn of 1969, a series of post-Apollo studies resulted in more positive steps for U.S.-Europe joint efforts. In September 1969, the Space Task Group advised President Nixon to pursue both manned and unmanned efforts. In the case of the former, STG recommended a reusable space transport system, and called specifically for international cooperation in U.S. space programs.[10] In October, NASA Administrator Paine and a select staff toured Europe (as well as Australia and Japan), describing NASA programs and officially inviting their participation. Europe quickly reacted to the possibilities, planning a permanent ELDO/ESRO liaison in Washington, D.C. The European representative would meet with NASA officials on a weekly basis and make periodic

trips to NASA centers and to contractors.[11]

By June 1970, ESRO earmarked funds for preliminary space station module studies, by September 1971, ELDO began collaborating with NASA on shuttle technical studies. In February 1972, a Joint Technical Experts Group of NASA and the European Space Conference endorsed emphasis on "Sortie Lab" studies. Urged by the U.S. to increase this aspect of investigation, the European Space Council eventually approved a comprehensive sortie lab study by ESRO on December 20, 1972.[12] Several considerations motivated American and European commitment to the sortie lab, eventually re-baptized as the Spacelab. The sortie lab idea, originating as a scientific module for space station operations, ran afoul of tight budgets. When NASA finally gave up its dreams for a permanent space station, the sortie lab became an attractive payload for the Shuttle, providing a flexible and resuable space station in miniature for near-Earth orbit.[13] But NASA found itself strapped for funds in 1972, having barely enough to continue the Shuttle project, let alone Spacelab. According to Werhher von Braun, former Director of Marshall Space Flight Center, and then Deputy Associate Administrator for planning at NASA Headquarters, this seemed a highly opportune time to invite European participation. Von Braun wrote that Europe seemed eager for an active space role, but continued to have major problems with ELDO's multi-stage booster, Europa. In any case, since Europa was a "throw-away" booster, and the U.S. Shuttle was reusable, Europe's large-thrust booster already seemed outmoded.[14]

Europe needed the means to establish a secure beachhead in manned spaceflight; NASA needed a moneyed partner; one might say it was a marriage made in heaven (or at least in near-Earth orbit).

As Europe gravitated towards acquisition of the Spacelab effort, the Continent's organization for space activities became realigned and consolidated. In 1968, a special advisory committee to the European Space Conference recommended more centralization of authority in order to facilitate coordinated plans and establish a cost-effective approach to European space efforts. The ESC would remain as the essential body at the ministerial level, with a standing committee to carry out decisions and set policies for both R&D and for commercial projects. The new organization would replace ESRO, ELDO, and CETS (European Council on Telecommunications by Satellite).[15] Four more years passed until the European Space Agency began to assume substantial outlines. During 1972, the Communications Satellite Corporation (Comsat), dominated by the U.S., continued to block European efforts to put up competing satellites. Growing European frustration prompted the ESC to take firm steps towards organizing the European Space Agency (ESA).[16] Even so, two more years passed before ESA's charter went permanently into force. At an ESRO meeting on 15 February 1973, representatives approved a new ESA charter, and planned to open it for signatures between March and September that year. Final details did not get ironed out until 15 April 1975, and ESA became a defacto entity on 31 May 1975.[17]

Against this background, the diplomatic and contractual details for Spacelab moved ahead. NASA and European representatives reached a series of agreements even before ESA became a reality. As noted earlier, the European Space Conference endorsed an ESRO study on the Sortie Lab late in 1972. During March, 1973, ESRO issued a statement "concerning execution for the Space Laboratory Program," signed by Belgium, Denmark, Federal Republic of Germany, France, Italy, Netherlands, Spain, Switzerland, United Kingdom, and later, Austria. This statement involved financial commitments and budgetary estimates. In many ways, it can be considered the beginning of the Spacelab program in Europe. During the Spring, contractor definition and cost studies proceeded; ESA began to form, and on 24 September 1973, European and American representatives signed a Memorandum of Understanding (MOU) that established the respective roles of Europe and the U.S. in the Spacelab program.[18]

Obviously, Europe did not plunge blindly into Spacelab development. Paper studies and negotiations with ESRO and ESC extended over many years prior to the MOU of 1973. In addition, European space firms had already received an impression of how NASA and its contractors approached complex manned space projects. The U.S. had its own sortie lab studies, and European firms were already involved in them.

TECHNICAL INTERCHANGES

Within NASA, Marshall Space Flight Center (MSFC) seized an early position in prototype "Spacelab" studies. In the early

days of Marshall's investigation, planners referred to the project as the "Sortie Can." J&C, with principal responsibilities for the Space Shuttle, received a major MSFC briefing on the Sortie Can (as a likely payload) in April 1972. "As most of you know," the JSC coordinator wrote to an invited audience, "the Sortie Can has received a considerable amount of attention by Marshall and NASA Headquarters, and this will be our first occasion to hear all the details directly."[19] The concept also used the acronym, RAM, meaning Research and Application Module. MSFC's activities included an extensive contract with General Dynamics/Astronautics for RAM studies, which "analyzed the Payload/Shuttle interface to a considerable depth."[20] General Dynamics submitted a lengthy document on 12 May 1972. The study itself holds interest as an early, comprehensive Spacelab prototype overview; as a clue to early European and U.S. contractor collaboration; and for description and illustration of early module studies.

Although General Dynamics led the contractor team, support came North American Rockwell Space Division (later called Rockwell International), Bendix, and TRW Systems Group. The latter eventually wound up as a sub-contractor to the European effort. In addition, General Dynamics had international assistance from SAAB-Scania, Messerschmitt-Bolkhow Blohm, and from ERNO.[21] The latter two both became competitors on the Spacelab project. In fact, ERNO's Spacelab studies, and its competition with MBB, predated its U.S. collaboration. In March of the same year, a

European consortium known as MESH launched a Spacelab feasibility study, with ERNO as the project leader. Competing proposals came from the "Cosmos" consortium (headed by MBB) and from "Star" (headed by British Aerospace Corporation.)[22] ERNO and MBB thus accumulated considerable capability concerning Spacelab uses and design details. The General Dynamics report in which they collaborated projected several RAM variants for different missions. There were two basic mission profiles: RAMS carried into orbit and still attached to the orbiter for seven-day missions; several RAMS delivered into orbit and joined together to create a modular space station. The individual RAM units could be varied for different missions. A pressurized sortie RAM, attached to the Shuttle Orbiter, provided a basic space laboratory with shirt-sleeve environment for mission specialists; a RAM support module provided more room for addition personnel; the RAM payload module was a "stripped-down" version. Although pressurized, it was basically a cargo space and had a minimum of autonomous subsystems, depending on the Orbiter or another RAM unit to function. The study also discussed RAM pallets, semi-circular structures with control and data hook-ups, mounted in the open section of the Orbiter's payload bay to expose experiments to the space environment.[23] This detailed review possessed striking similarities to eventual Spacelab modules and pallet configurations. European participation, including MBB as well as ERNO, represented an unusually early and extensive stage of collaboration, well before Europe

and America signed the formal MOU in the Autumn of 1973. It would also seem that the experience provided early opportunities for the eventual association between the European Spacelab contractors and U.S. firms like TRW and Rockwell.

MSFC, in the meantime, pursued work on the project, which received an official change in designation, from "Sortie Lab" to "Sortie Can." MSFC's effort included fairly detailed studies for laboratory equipment inside the Sortie Can, stressing off-the-shelf material as much as possible. Marshall technicians also established guidelines for identifying flammable and toxic materials, temperature and pressure environments, and the acoustic environment.[24] Planning intensified during the summer of 1972, as preparations for a NASA-wide "Shuttle Sortie Workshop" began to take shape. The workshop held at Goddard Space Flight Center from 31 July to 4 August engaged personnel from Headquarters and Centers alike, and the agenda convered a broad spectrum of management issues and technical questions.[25] The Shuttle Sortie Workshop also highlighted controversy about the size and utilization of modules. One camp advocated a well-equipped lab module, supporting two or more specialists for seven days. A second group argued for a minimum crew, filling the module with automated research equipment and allowing missions beyond seven days.[26] Some observors felt the whole meeting was too elaborate. "For me, the entire week was far too much time to spend, relative to the results," one JSC representative reported. "I believe

the equivalent could have been accomplished in about 2 days." The JSC correspondent also reported MSFC's desire to build the Sortie Can in-house to save money. "It sounded like the clock had been turned back several years when MSFC went from the wet workshop to the dry workshop," he wrote, referring to Skylab.[27]

Justified or not, the remark suggests a logical consequence of Spacelab's heritage. MSFC spent considerable time and effort on the Skylab program, and its expertise obviously provided reference points in Spacelab's evolution. European firms must have picked up useful information from their Skylab association, as well as firm participation in RAM investigations. At the same time, a succession of NASA activities strongly influenced Spacelab's basic configuration. Many of the preliminary design problems and technical issues became ironed out as a result of contract studies like the General Dynamics RAM study, continuing in-house work at MSFC, and agency-wide workshops such as the one at GSFC.

As Spacelab's outlines emerged into sharper focus and NASA's negotiations involving European participation neared formal agreement during 1973, exchanges at the technical levels were already well advanced. By the Spring of 1973, MSFC received the designation as "lead center" for the Sortie Lab. JSC questioned the decision, and Dale Myers, Associate Administrator for Manned Space Flight reiterated the decision in a letter to Christopher Kraft.[28] Even though Marshall remained the lead center, many

issues involved the Shuttle Orbiter, and correspondence often became a three-way affair, involving JSC, MSFC, and European space officials. As the technical discussions focussed on increasingly specific details, the first areas of technical differences began to crop up.

Constituted more as an international association, ESRO originally relied on contractors within its member states for technical contributions. But the organization recognized the usefulness of an indigenous and independent facility with technical expertise to perform certain in-house engineering projects and to enhance management of assorted contractors. For this reason, ESRO established the European Space Research and Technology Center (ESTEC) at Noordwijk, near Amsterdam, the Netherlands. With a staff of several hundred, ESTEC developed facilities for research, development, and testing of space hardware and space vehicles.[29] At this stage of Spacelab's evolution, ESTEC personnel became more enmeshed in technical issues. In May 1973, Heinz Stoewer of ESTEC voiced concerns to Bob Thompson of JSC, following a visit to Houston by a Spacelab team. Stoewer worried about the center of gravity and the landing weight of the Shuttle/Spacelab combination. After news of possible changes in center of gravity constraints popped up, "there has been considerable activity, as you know, on both sides of the Atlantic," Stoewer wrote, "and the results are far from encouraging." The arrangement preferred by ESTEC kept the Space-

lab snugged up to the Orbiter's forward bulkhead. Mounting the Spacelab further aft meant a longer access tunnel, more weight, more crew transfer problems, and less space for using pallets, Stoewer pointed out. He also suggested more flexibility for landing weight, targeted at 20,000 lbs. empty. If weight increased, it meant reducing payload or redesigning a smaller Spacelab.[30] Thompson wrote back, alluding to many issues already settled, and referring to documentation underway to enhance the Spacelab effort in Europe. As for the center of gravity issue, Thompson said that the first two Orbiters would have to stay at 2% envelopes; a modification kit for Orbiter #3 would give ESTEC the 3% they wanted. As for the landing weight, the payload limits had been raised, allowing for both Spacelab growth and payload capability as well.[31]

In addition to periodic visits and continuing correspondence, personnel assignments to European sites assisted ESRO/ESTEC in evaluating contractors and in negotiating the Memorandum of Understanding, pending in the Autumn of 1973. European design of the Spacelab made good progress, but they also recognized the wisdom in tapping accumulated experience of NASA experts. By the Spring of 1973, NASA already stationed two liaison officers at ESTEC, with additional people en route during June. As Myers explained the situation to the NASA Administrator: "In response to a specific ESRO request for technical assistance during the next 4-6 weeks, we are detailing to ESTEC from our Centers six technical experts in the fields of systems engineering, payload requirements, environmental control, safety, flight operations,

and ground operations." Their job called for working with the ESRO team looking at European contractors and evaluating their capabilities. ESTEC also placed liaison person in residence at MSFC.[32] NASA Headquarters evidently acquiesced in the dispatch of NASA experts to evaluate European contractors because the ESRO request appeared to be unique. As ESTEC built up its technical staff, there would be less demand for U.S. technical support over a lengthy period. On the other hand, NASA foresaw the need to send large observation teams to Europe as ESTEC reached certain milestones for systems and subsystems reviews, as well as for other key events.[33]

In fact, a major NASA deputation attended a "Phase B2" review during the Summer covering contractor definition and cost studies. Including personnel from Headquarters, JSC, MSFC, and KSC, 22 NASA executives and engineers assisted their ESTEC counterparts in evaluating the competing presentations for the Spacelab contract. MBB and ERNO each made their pitches at this time, backed by respective subcontractor teams from other nations. The NASA emissaries came away impressed by what they saw and heard. "Both contractor briefings were very professional and related the in-depth technical abilities of the entire team," a JSC delegate reported. Eventually, ESTEC and NASA teams both summarized their findings for ESRO management. The information from these deliberations became part of the information used by European negotiators for structuring the Memorandum of Understanding in September, and for the selection of the Spacelab contractor by Spring of the following year.[34] These events not

only underscored the collaboration in assessing many issues before signing the Memorandum of Understanding; NASA's action in sending experts from the various Centers to review the European contractors also revealed an unusual degree of participation in the process of selecting the eventual Spacelab builder. In addition, NASA participation gave the agency, an early look at the contractors, and presumably facilitated communications during subsequent phases of Spacelab development.

As this round of contractual arrangements neared conclusion, other international liaison efforts focussed on the probable scientific users of Spacelab and attempted to plan the lab's equipment and functional layout. At JSC, the Life Sciences Division played an important role in coordinating these activities receiving continuous data from within NASA and from potential customers outside the agency. The Life Sciences Division took a special look at such things as: dimensions; power; heat rejection; computer services; communications; rescue, EVA; crew size; operational modes and responsibilities. The Europeans had to consider customers from their side and work out appropriate arrangements with NASA, since Spacelab functions inevitably involved capabilities and systems aboard the Shuttle Orbiter. As a clearing house, both sides agreed on the need for a Joint NASA/ESRO Spacelab Users Requirements Group, which held its first meeting on 17 July 1973. And all the while, the minutiae of a major international manned space program, in which the European contribution rode as a passenger aboard a NASA vehicle, generated

a growing steam of information requests from the Continent. Queries ran the gamut, from miscellaneous interface issues (electrical, environmental, thermal, and computers) to routine information exchanges about the qualification status of electrical parts.[35]

Late in August 1973, the MOU draft began to circulate, officially entitled:

> Memorandum of Understanding Between the National Aeronautics and Space Administration and the European Space Research Organization for A Cooperative Program Concerning Development, Procurement, and Use of a Space Laboratory In Conjunction With the Space Shuttle System.

As the document spelled out responsibilities, ESRO agreed to develop "mannable laboratory modules and unpressurized instrument platforms (pallets)." For ESRO, this mean one flight unit, one engineering model, ground support equipment, spares, drawings, and so on. NASA, for its part, agreed to maintain liaison personnel in Europe, and to accomodate European personnel posted to the U.S. NASA further agreed to provide general technical and managerial consultation, and to "monitor ESRO technical progress in selected areas as defined in the Programme plan." In this regard, NASA made sure that crucial aspects of Spacelab development met its rigorous standards, which had, after all, become honed on successive generations of manned spaceflight operations, from Mercury to Gemini, Apollo, Skylab, and the Apollo-Soyuz Test Project. As partners in a new enterprise, the Europeans also picked up valuable engineering and management expertise from NASA.

In fact, potential European benefits were specifically singled out, permitting acquisition of U.S. aerospace technology, As phrased in the MOU, NASA would not infringe any U.S. proprietary rights, but did agree that "ESRO will have access to technology, including know-how, available to NASA and needed to accomplish successfully its tasks under this cooperative programme. . ." As a quid pro quo, NASA received the same prerogatives regarding ESRO activities. ESRO agreed to retain a capability to manufacture additional Spacelab units, and maintained a monopoly in this regard, since NASA agreed not to inaugurate any independent Spacelab development, unless ESRO failed to produce. Furthermore, Europe secured an additional position in manned space flights with the concurrence of NASA to include at least one European in the first Spacelab flight crew. The MOU also outlined an important mechanism to coordinate important managerial and technical issues through the Joint Spacelab Working Group (JSWG), co-chaired by U.S. and European Program heads, assisted by appropriate technical personnel. The JSWG exchanged essential information concerning the Orbiter and Spacelab; contended with interface problems and answers; identified potential problems for each other; made sure corrective action occurred.[36]

Formal signing of the Memorandum of Understanding occurred 24 September 1973 in Washington, D.C.; Dr. Alexander Hocker of Germany signed for ESRO, and James Fletcher, NASA Administrator signed for the U.S. The same day, Fletcher sent a NASA memorandum

officially re-christening the Sortie Lab as the Spacelab.[37] The Washington Post noted prior European failures to develop a reliable launcher; now the Europeans had embarked on a more complex manned space project costing $300-400 million. Since the European Spacelab constituted a major element in future U.S. space programs, the collaboration represented "a new dimension in the Atlantic partnership."[38] Other news commentators recalled Europe's failure in mounting a significant space program, and seemed dubious about the on-going relationship implicit in the MOU. The U.S. remained dependent on Europe for Spacelab units, and this did not necessarily seem to be a good thing. In any case Europe appeared to have a firm monopoly on Spacelab manufacturing as the only possible supplier in the near future.[39] If nothing else, Europe had definitely found a secure niche in manned space operations for many years ahead.

The contract award for Spacelab finally went to ERNO on 5 June 1974.[40] The European space reorganization begun during a meeting at Brussels on 31 July 1973, eventually resulted in the 11-member European Space Agency, which became official on 31 May 1975.[41] Members included Belgium, Denmark, Federal Republic of Germany, France, Ireland, Italy, The Netherlands, Spain, Sweden, Switzerland, and the United Kingdom. These events put Europe's manned space program on a firm basis. As Spacelab development moved ahead on a course parallel to NASA's Shuttle program, the "Atlantic partnership" looked forward to new dimensions in space exploration.

NOTES

(Memos, correspondence, and reports cited are in the files of the JSC History Office.)

1. VFW/ERNO, "Spacelab Report" (November, 1980), pg. 3

2. Howard Allaway, The Space Shuttle at Work (Washington, D.C.: NASA, 1979), pp. 29-30; Walter A. McDougall, "The Scramble for Space," The Wilson Quarterly (Autumn, 1980), pp. 71-74.

3. McDougall, "Scramble," pp. 76-77; Kenneth Gatland, Missiles and Rockets (New York, 1975); Reginald Turnill, The Observer's Spaceflight Directory (London, 1978).

4. Allaway, Space Shuttle, pp. 30-31.

5. "European Space Policy Group Urged," Aviation Week and Space Technology (June 14, 1965), p. 188; Erhard Loewe, "Eurospace Views Space Program Needs," Aviation Week and Space Technology (May 10, 1965), pp. 75,78,80. For an example of European technical development, see ERNO, "ERNO '75" (1975), p. 12.

6. "Space Transport Designed by Junkers," Aviation Week and Space Technology (June 14, 1965), pp. 219, 221; "European Space Policy," p. 188.

7. William S. Beller, "European Frustrated in Space Hopes," Missiles and Rockets (January 3, 1966), p. 34. European space research background covered in Gatland, Missiles and Rockets, and in Turnill, Spaceflight Directory.

8. David Baker, "Spacelab: Europe Prepares for Manned Flight," Spaceflight (November, 1975), p. 380.

9. VFW/ERNO, "Spacelab Report" (November, 1980), pp. 2-3.

10. NASA, News Release, "Europe to Build Spacelab for U.S. Reusable Space Shuttle" (September 24, 1973).

11. Arnold Frutkin to address list, 13 March 1970, with Congressional Testimony of Administrator Paine attached (11 March 1970).

12. NASA, "Europe to Build."

13. Baker, "Spacelab: Europe," p. 378

14. Wernher von Braun, "Spacelab," Popular Science (November, 1975), p. 73.

15. Richard van Osten, "Revamping of Europe Space Program Asked," Aerospace Technology (April 8, 1968), p. 20

16. McDougall, "Scramble," pp. 77-78.

17. Memo and agenda, "ESA Scientific Advisory Committee Visit," 16 October 1979; Memo, NASA Office of International Affairs, "Creation of the European Space Agency," 30 May 1975.

18. NASA, "Europe to Build"; NASA, "Spacelab Fact Sheet" (June, 1977), p. 12.

19. Memo, Jerome Hammack, "Sortie Can Presentation," 3 April 1972.

20. Memo, Douglas Lord, HQ, "Review of Research and Applications Modules (RAM) Study," 26 April 1972.

21. General Dynamics/Convair, "Research and Applications Modules (RAM) Phase B Study: Executive Summary," 12 May 1972.

22. VFW/FKNO, "Spacelab Report" (November, 1980), p. 3

23. General Dynamics, "RAM."

24. John Donnelly to Dale Myers, HQ, "Project Designation," 8 June 1972; Memo, John Aberg, MSFC, "Review of Experiment and General Laboratory Experiment Specification for Project Sortie Lab," 22 June 1972.

25. File folder, JSC, miscellaneous correspondence concerning "Sortie Lab Symposium at GSFC, July/August 1972," including May-June correspondence.

26. John E. Naugle, "Remarks," 31 July 1972, in folder cited above.

27. Glenn Smith to Manager, Earth Resources Program, "Shuttle Sortie Symposium Workshop," 10 August 1972.

28. Dale Myers to Christopher Kraft, "Sortie Lab Project Management," 4 June 1973.

29. Turnill, Spaceflight Directory, p. 31. A separate ESRO group, the European Space Operations Center, at Darmstadt, Germany, handled launch control, tracking, and data processing.

30. Heinz Stoewer to Bob Thompson, 11 May 1973.

31. Bob Thompson to Heinz Stoewer, 20 June 1973 (draft of letter not sent).

32. Myers to the Administrator, "Programmatic Status Report on Sortie Lab (Spacelab)" 4 June 1973.

33. Douglas Lord, HQ, to Associate Administrator, Manned Space Flight, "Spacelab Reviews in Europe," 2 August 1973.

34. Memo, Jack Heberlig, "Trip Report to ESTEC. . .", 22 July 1973.

35. On the Life Sciences Division, see, memo, Robert W. Dunning, "Life Science Sortie Lab Requirements," 18 July, 1973; memo, Charles Berry, HQ, "Sortie Lab Requirement Issues," 17 August 1973. On the NASA/ESRO Users Group,

see, L. L. Liccini, HQ, "Joint NASA/ESRO Spacelab Users Requirements Group," 17 July 1973. On other interface issues, see, L. S. Menear to T. J. Lee, 9 August 1973, referencing information requested by Dr. Hendrick H. Wessels at ESTEC.

36. Copy of the Memorandum of Understanding, dated 14 August 1973, in files of the JSC History Office.

37. Memo, James Fletcher, "Renaming of the Sortie Laboratory," 24 September 1973.

38. Dan Morgan, "Europeans to Use U.S. Space Shuttle," Washington Post (September 25, 1973)

39. Chris Bullock, "Europe's Spacelab Begins to Take Shape," Interavia, (April, 1978), pp. 312-13.

40. VFW/ERNO, "Spacelab Report" (November, 1980), p. 3

41. NASA, Astronautics and Aeronautics, 1973: Chronology of Science, Technology and Policy (Washington, 1975), p. 95. Ten nations signed in Paris; Ireland signed later.

WEATHERING OF IRON SULFIDES UNDER MARS SURFACE AMBIENT CONDITIONS

Thomas R. Blackburn
St. Andrews Presbyterian College
1981 NASA-ASEE Summer Faculty Fellow

Supervisor: Everett K. Gibson, Jr.
SN7, Geochemistry Branch
Planetary and Earth Sciences Division

Abstract: The study of iron sulfilde surface alternation reactions begun during 1980 was extended through improved irradiation design and experimental protocols, and to a wider range of humidities and more intense irradiation. X-ray photoelectron spectra of irradiated chips suggest formation of $FeSO_4$, $FeCO_3$, and an iron oxide on the iron sulfide substrate.

NATIONAL AERONAUTICS AND SPACE ADMINISTRATION

LYNDON B. JOHNSON SPACE CENTER

HOUSTON, TEXAS 77058

August 20, 1981

Gooding (1978) suggests that, in the oxidative weathering of primary iron sulfides (such as troilite, FeS, and pyrrhotite, $Fe_{(1-x)}S$) under Mars surface ambient conditions, the most stable product would be $FeSO_4$ or, given sufficient water vapor (2.5×10^{-7} atm at 240 K), its monohydrate szomolnokite, $FeSO_4 \cdot H_2O$:

$$FeS + 2O_2 \rightarrow FeSO_4; \Delta G^\circ_{298} = -174.08 \text{ kcal} \quad (1)$$

$$FeSO_4 + H_2O(g) \rightarrow FeSO_4 \cdot H_2O; \Delta G^\circ_{298} = -4.6 \text{ kcal} \quad (2)$$

but that the equilibrium O_2 pressure for the reaction

$$2FeS + 3/2O_2 \rightarrow Fe_2O_3 + 2S \quad (3)$$

is nearly the same as that for reaction (1), so that reaction (3) or the even more exoergic

$$2FeS + 7/2O_2 \rightarrow Fe_2O_3 + 2SO_2; \Delta G^\circ_{298} = -274.1 \text{ kcal} \quad (4)$$

might provide alternative product sets. The oxidation of iron sulfides would be an important provenance for sulfate in the Martian regolith, and therefore, hypothetically (Toulmin et al., 1977; Clark et al., 1976) for the cementing agent of duricrust. The assemblage ($Fe_2O_3 + 2S + 5/2O_2$) is about 220 kcal higher in Gibbs free energy than $2FeSO_4$ at 240 K and the ambient Martian oxygen fugacity of 1×10^{-5}, so that once $FeSO_4$ is formed there is no possibility of its conversion to hematite and elemental sulfur under these conditions. Finally, the combined oxidation and carbonation reaction

$$2FeS + 1/2O_2 + CO_2 \rightarrow FeCO_3 + + S; \Delta G^\circ_{298} = -20.1 \text{ kcal} \quad (5)$$

would lead to spontaneous formation of siderite.

However, in kinetically hindered reactions it is the relative rates of alternative pathways and not thermodynamics alone that determines the product set that is first produced, and if hematite and sulfur were once formed they could persist metastably for long times under a strictly gas-solid kinetic regime. The stabilities of $FeCO_3$ and $FeSO_4$ would depend on the availability of liquid (or other condensed, e.g., adsorbed) H_2O to serve as a medium for further reactions.

The present work was undertaken to investigate the surface oxidation of a set of primary iron sulfides (troilite, pyrrhotite, and pyrite, FeS_2) under Mars surface ambient conditions, and in the presence of a strong flux of ultraviolet light, in the assumption that attack by photochemically generated oxidants such as $O(^1D)$, O_3, and (in the presence of water vapor) HO_2 and H_2O_2 will dominate gas-solid oxidation kinetics. After irradiations under a variety of conditions of temperature and humidity, the surface chemical state of sample chips as measured by the X-ray photoelectron spectroscopy (XPS) of Fe, S, C, and O was compared to that of unexposed reference chips. Oxidation of sulfur from -2 (sulfide) to +6 (sulfate) states is accompanied by an easily detected positive shift of about 6 to 7 eV in its 2p electron binding energy. Relative iron and sulfur intensities give evidence of the extent to which sulfur anions are replaced by oxide or carbonate in the weathering of these minerals, while the presence of carbonate and iron oxides is detectable from characteristic shifts in the C(1s) and O(1s) electron binding energies.

EXPERIMENTAL

Samples were placed in Al containers on a Cu heat sink within a 3.7 liter stainless steel chamber (Fig. 1). Sample temperature and chamber humidity were controlled by the circulation of thermostatted coolant through a coil beneath the heat sink; temperature was measured by stainless steel jacketed thermocouples at three positions: (1) At the point on the heat sink where the coolant coil enters; 2) at the surface of a sample chip, in the UV beam; and (3) on the chamber baseplate, or immersed in the liquid water reservoir when present.

Light from a 50-watt deuterium lamp was admitted to the chamber through a 0.3 cm thick optical quartz window, after traversing an air path of 8 cm. The emission spectrum of this source at the quartz window is shown in Figure 2. The volume of the beam inside the chamber was 50 cm^3.

Polycrystalline bulk mineral samples (identity verified by powder X-ray diffraction) were sawn with a diamond blade, using purified isopropanol as lubricant, and cleaned by ultrasonication in high-purity trifluorotrichloroethane, followed by a 150° bakeout. The face to be irradiated was then polished in an Ar atmosphere with SiC paper to produce a fresh surface. Samples remained in an Ar or CO_2 atmosphere from the termination of irradiation until introduction into the sample chamber of the X-ray photoelectron spectrometer.

The irradiation atmosphere was "high-purity" carbon dioxide containing 350 ppm O_2, except in the lowest-humidity run, when CO_2 with certified H_2O and O_2 concentrations of 20 ppm was used. In all but this latter run, the $H_2O(g)$ composition of the gas phase present was controlled by varying the temperature of the heat sink, in the presence of a supply of H_2O (l or s). The variation of this parameter is summarized in Table I. The atmospheric leak rate of the assembled apparatus was about 8×10^{-3} torr/day, and thus the total atmospheric oxygen introduced through leaks during a 100-hour irradiation did not exceed the partial pressure of O_2 (0.13% of ambient pressure) at the surface of Mars.

X-ray photoelectron spectroxopy (XPS) was performed at Texas A&M University on a Hewlett-Packard 5950 photoelectron spectrometer using monochromatized AlK_α radiation. Data reduction employed the Surface Science Laboratories ESCA Data System, Revision E.

RESULTS

At the time of this report, the analysis of only one sample set (cold, humid; see Table I) has been completed. The wide-scan XPS spectra (Figure 2) show prominent peaks for carbon and oxygen in addition to those for iron and sulfur, indicating considerable alteration of the surface from the stoichiometric bulk compositions. High resolution scans of the sulfur (2p), carbon (1s), and oxygen (1s) indicate the presence of sulfur as S^{2-} and SO_4^{2-}; carbon as C(IV) (either CO_3^{2-}

or CO_2 (ads) and other compounds possibly including COS and CS_2 (Blackburn et al., 1980)) and, except in the case of FeS_2, oxygen as a metal (probably iron) oxide. Thus, an assemblage of $FeSO_4$, $FeCO_3$, and Fe_2O_3 on the original mineral substrate would account qualitatively for the appearance of the XPS spectra. The assumption that only these substances are present will permit calculation of the mole fractions of each present in the layer (about 2 nm deep) analyzed by XPS, and such calculations will be performed automatically as data sets are recorded. The results of these calculations will then be correlated with conditions during irradiation (Table It is emphasized that such a correlation will have only conjectural significance, since we have no firm evidence that the four components listed above are the only ones present in significant amounts at the irradiated surface; indeed, the XPS spectra not yet obtained may lead to a revision of the basis set of compounds assumed. (For example, there are unassigned peaks in the C(1s) spectra of most samples.)

Table I. Environmental Parameters During Irradiation.

Run	T_{H_2O} (a)	T_{Sample} (b)	P_{H_2O}, torr	P_{CO_2}, torr	Rubric (c)
1	246	249	1.6×10^{-4}	8	Cold, dry
2	249	256	0.53	8	Cold, humid
3	305	309	35.6	40	Warm, humid
4	300	297	26.7	38	Warm, wet
5	-	233		760	Cold, dry, dark (No UV irradiation)

Notes: (a) Temperature of the coolest point in the irradiation chamber.

(b) Temperature of in-beam thermocouple touching sample chip.

(c) As referenced in the text of this paper.

REFERENCES

Toulmin, P., III, A.K. Baird, B.C. Clark, K. Keil, H.J. Rose, Jr., R.P. Christian, P.H. Evans, and W.C. Kelliher, Geochemical and minerological interpretation of the Viking inorganic chemical results. J. Geophys. Res. 82, 4625-4634, 1977.

Gooding, J.L., Chemical weathering on Mars. Icarus 33, 483-513, 1978.

Clark, B.C., A.K. Baird, H.J. Rose, Jr., P. Toulmin, III, K. Keil, A.J. Castro, W.C. Kelliher, C.D. Rowe, and P.H. Evans. Science 194, 1283-1288, 1976.

Blackburn, T.R., E.K. Gibson, Jr., F.F. Andrawes, and V. Young, Sulfate production from photochemical oxidation of sulfides: Preliminary results. NASA TM 82385, 193-196, 1980.

CAPTIONS FOR FIGURES

Figure 1. Irradiation chamber. All construction is of stainless steel except for the Cu gasket and heat sink (S) and quartz window.
B: UV beam volume.
TC: Thermocouple leads.

Figure 2. Emission spectrum of deuterium arc lamp.

Figure 3. Typical post-irradiation XPS spectra, $Fe_{(1-x)}S$, out-of-beam sample.
A: Wide-scan spectrum showing peaks for Fe (2p), O (1s), C (1s), and S (2s and 2p) electrons.
B: High-resolution O (1s) spectrum. The low-binding energy shoulder at 530 eV indicates iron oxide(s) present.
C: High-resolution C (1s) spectrum. The peaks at 288 and 284.4 eV are assigned to CO_3^{2-} and hydrocarbon, respectively; the 286 eV component is not identified.
D: High-resolution S (2p) spectrum. All peaks are doubled because of the multiplicity of the $^2P_{3/2,\ 1/2}$ state produced by photoelectron emission. The doublet at about 169 eV indicates sulfur as SO_4^{2-}; the lower-binding energy doublets indicate two chemical states of sulfur, probably S^{2-} and S_2^{2-}.

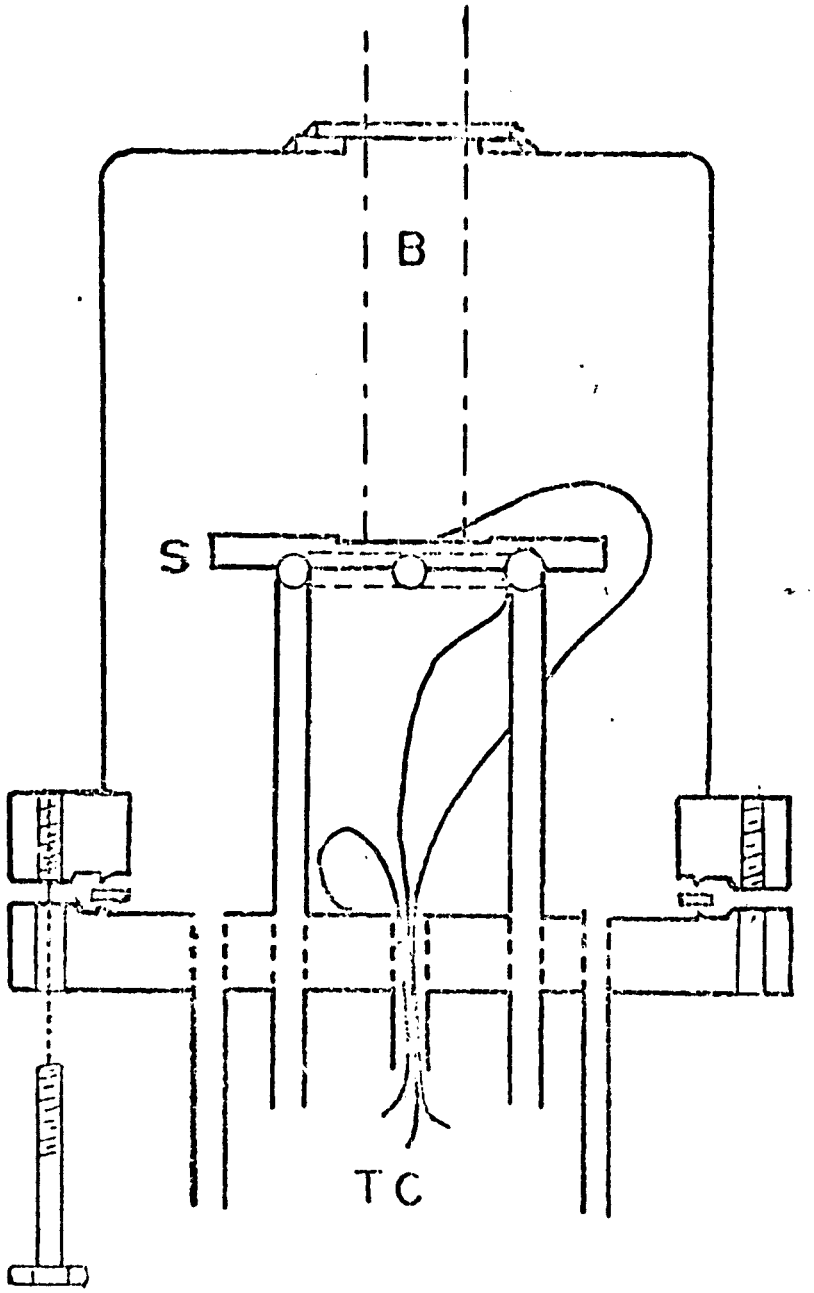

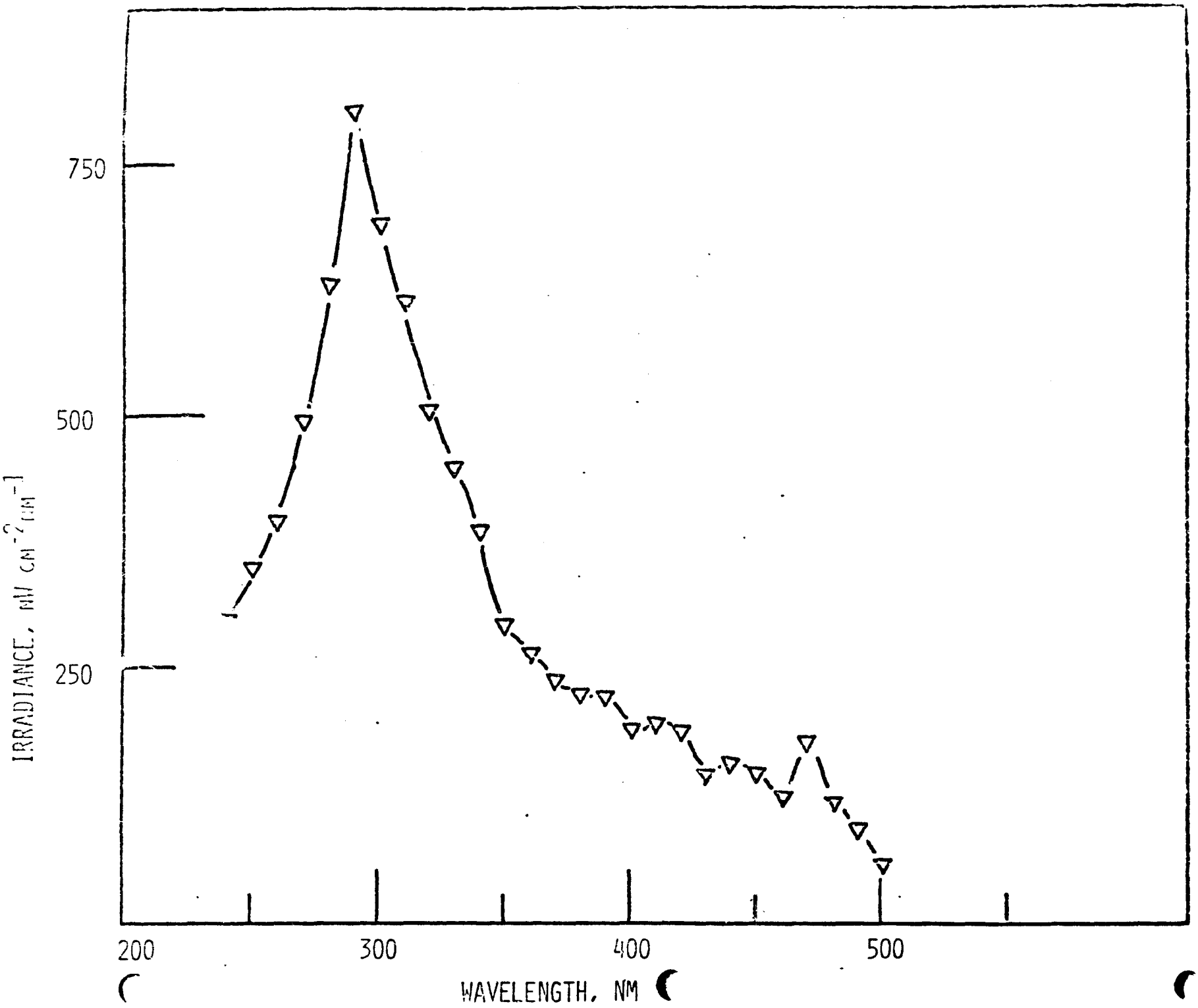

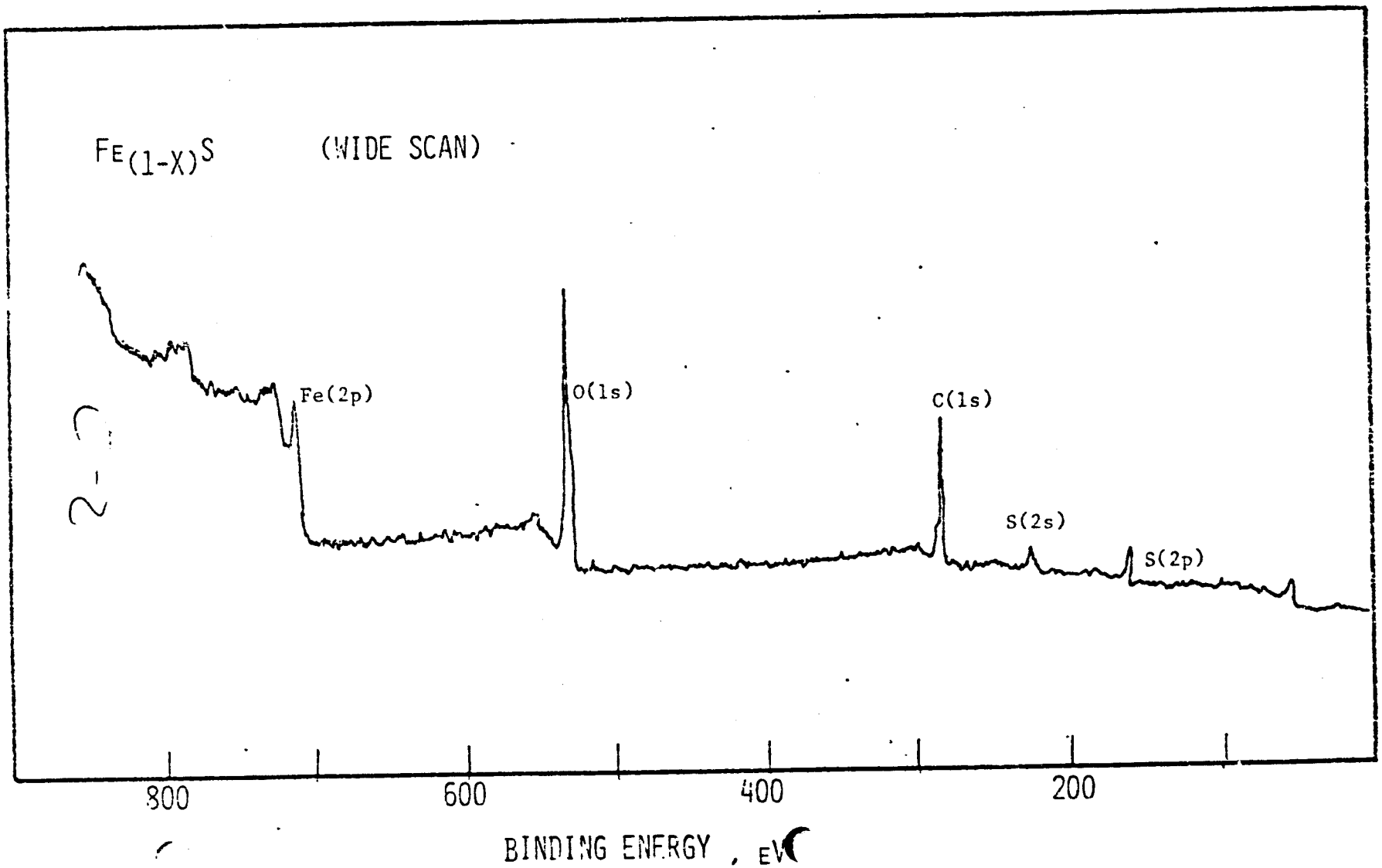

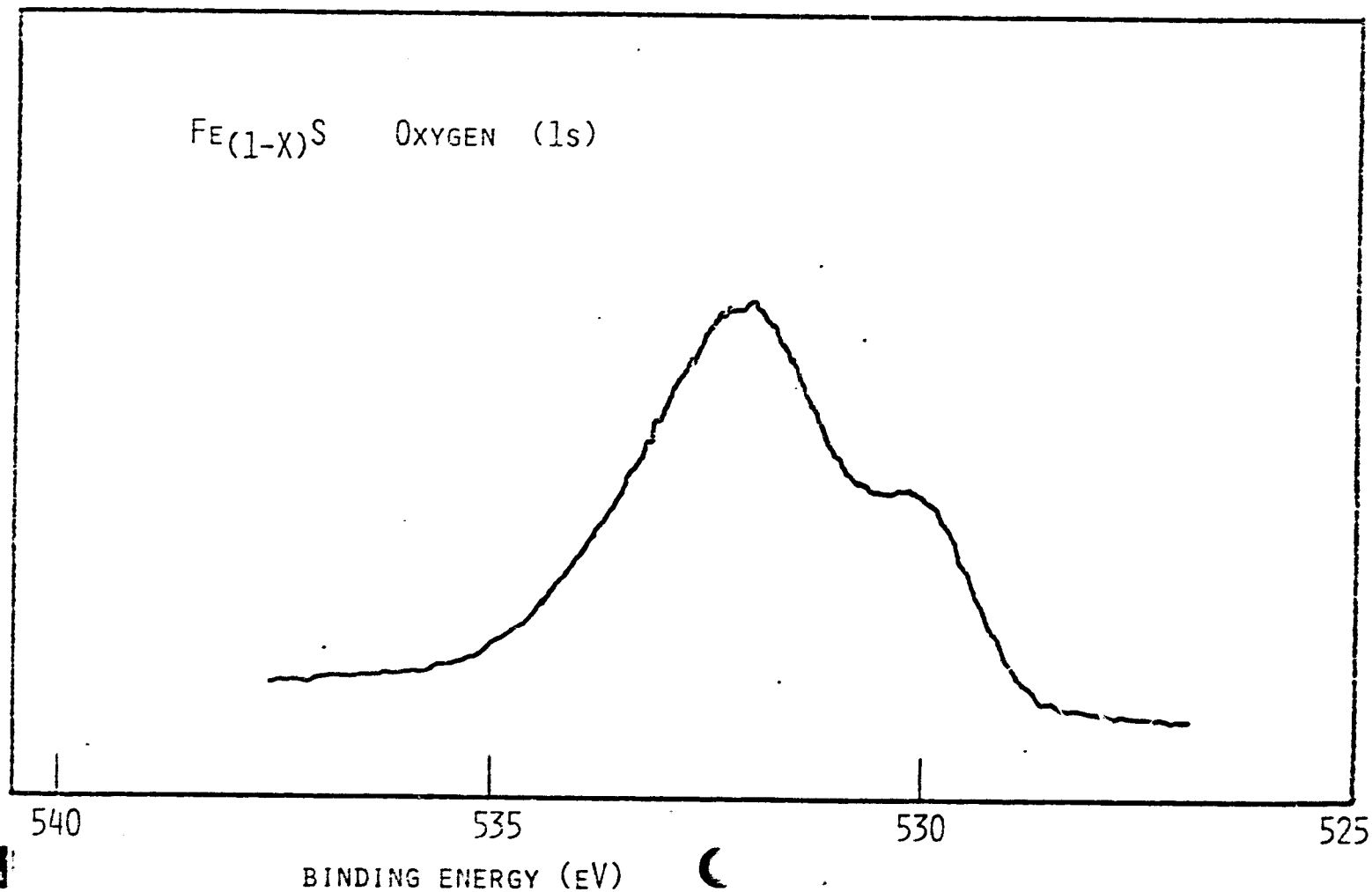

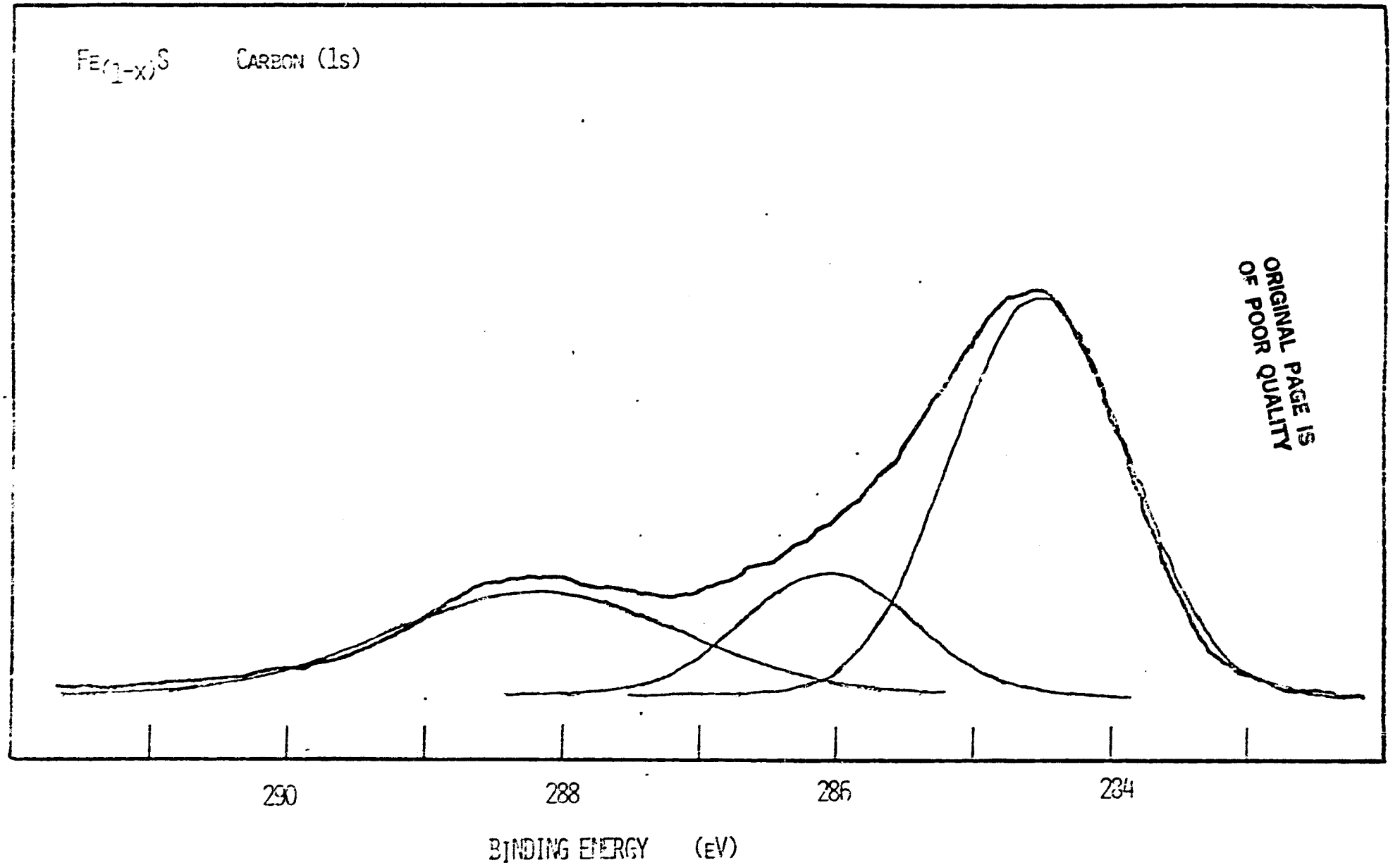
$Fe_{(1-x)}S$ Carbon (1s)
ORIGINAL PAGE IS OF POOR QUALITY
290
288
286
284
Binding Energy (eV)

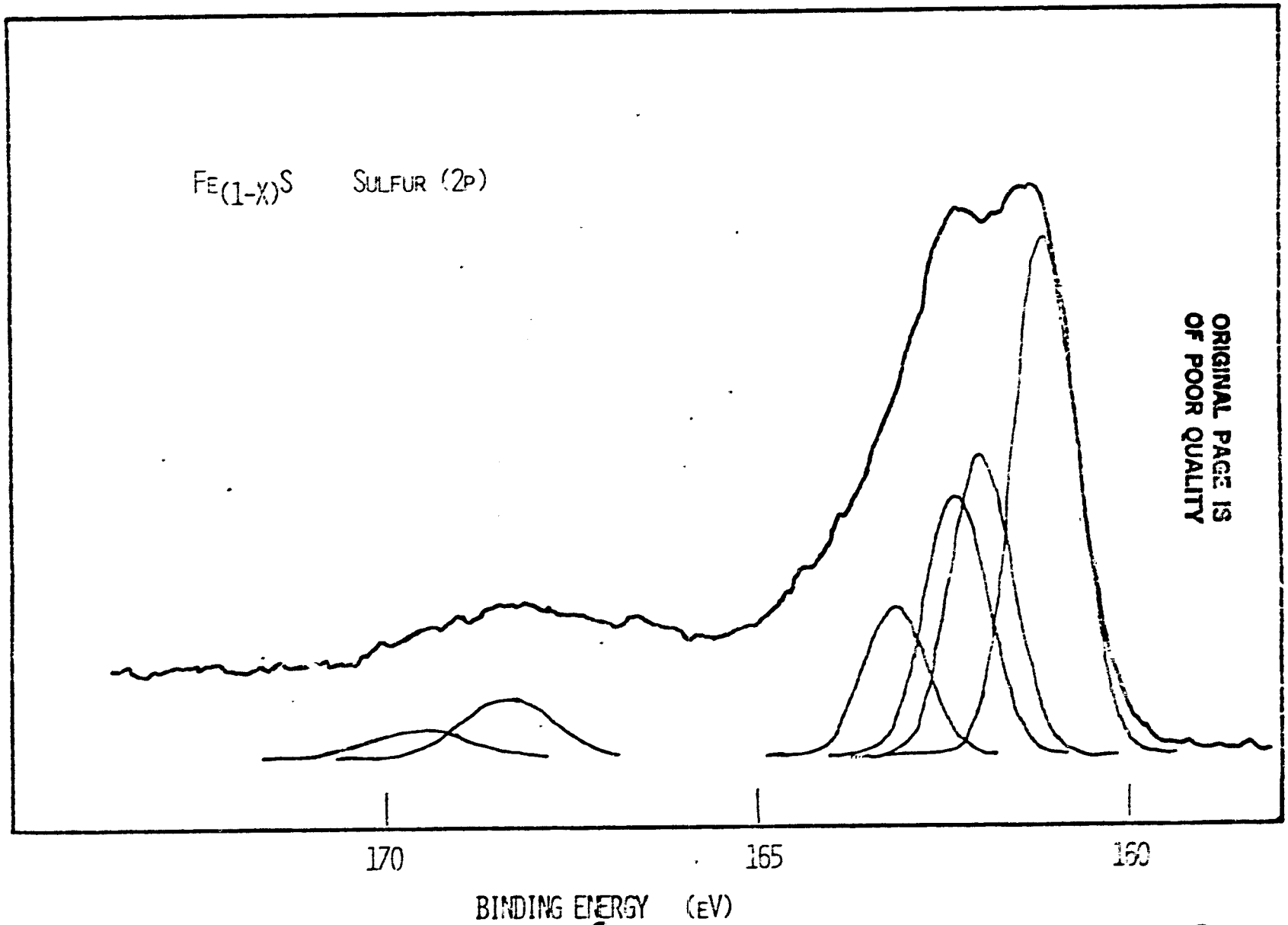
$Fe_{(1-x)}S$ Sulfur (2p)
ORIGINAL PAGE IS
OF POOR QUALITY
170
165
160
BINDING ENERGY (eV)

DETERMINATION OF WATER-SOLUBLE IONS IN SOILS FROM THE DRY VALLEYS OF ANTARCTICA

Roberta Bustin
Arkansas College
Batesville, Arkansas

Supervisor: Dr. Everett K. Gibson, Jr.
Geochemistry Branch
Planetary and Earth Sciences Division
NASA Johnson Space Center
Houston, Texas

Abstract:

Several Antarctic soils were studied. Water extracts were analyzed for sodium, potassium, magnesium, calcium, chloride, and nitrate ions using flame photometry, atomic absorption spectroscopy, and ion selective electrodes. Significant differences were noted in soils from different regions. Upward ionic transport above the permafrost layer with almost no evidence of migration below this line was observed in core samples. Very high ionic concentrations of sodium and chloride were observed in the Prospect Mesa Formation of Wright Balley. Calcium chloride was the most predominant species in soils from the Don Juan Pond. The high concentrations of salts reflects the aridity of the dry valley system.

The dry valleys of Antarctica provide an excellent terrestrial analog of the surface of Mars. Studies such as this one provide important information to aid in understanding the processes operating within the Martian regolith.

DETERMINATION OF WATER-SOLUBLE IONS IN SOILS FROM THE DRY VALLEYS OF ANTARCTICA

The dry valleys of Antarctica furnish one of the best terrestrial analogs for the surface of Mars. In many places surface features are similar. Both Antarctica and Mars have low humidities, desiccating winds, and an oxidizing environment. Even though the air temperatures of both are seldom above freezing even in summer, the soil experiences a diurnal cycle of freezing and thawing (1). It is possible to increase our understanding of changes occurring within the Martian regolith by studying processes operating in the cold, dry environment of Antarctica.

During the austral summer of 1979-80, a group of Antarctic soils was collected. The primary purpose of the project described here was to determine the abundances of the water-soluble ions magnesium, calcium, potassium, sodium, chloride, and nitrate in soils from different regions and at various locations and depths within a given region. These data not only give soil composition but also provide information which is useful in studying processes such as weathering and ionic transport. When combined with additional studies of the soils, they provide a detailed picture of the soil chemistry in a cold, dry environment.

To retard ionic migration, soil cores were stored below -10°C. The cores were cut into individual samples which were then air dried, weighed, and extracted with water. After filtration, the samples were analyzed.

An Orion Research Ionalyzer 901 and the appropriate ion selective electrodes were used for determining calcium, chloride, and nitrate in all samples. Sodium and potassium were determined by ion selective electrodes for all samples except those in the four detailed core studies (DJ 33, DJ 2074, WV 52, and DQ 35). For

those samples, sodium and potassium were determined by flame photometry using an Instrumentation Laboratory 643 flame photometer. A Perkin-Elmer 373 atomic absorption spectrophotometer was used for all the magnesium determinations.

Because of the aridity of the Antarctic environment, water-soluble salts have not been leached out of the soils and are often present in high concentrations. Salts accumulate within rocks by natural desert processes, are transferred from rocks to the soil during weathering, and by the action of wind and by slow partial leaching eventually accumulate in low-lying areas such as basins and lakes.

Most of the samples for this study were obtained from Taylor Valley and Wright Valley, two ice-free valleys in Victoria Land (see Figure 1). Taylor Valley runs east-west and is bounded on the west by the Taylor Glacier and on the east by McMurdo Sound. Hills and mountains on the north and south separate Taylor Valley from the rest of Victoria Land. Taylor Valley serves as a basin for a much smaller region than that around Wright Valley. This was reflected in the data which showed much lower ionic abundances in Taylor Valley soils than in the other soils.

The salt layer in Lake Hoare, a dry lake bed in Taylor Valley, was very thin, and concentrations were low. The permafrost level was near the surface. Even greater ionic depletion was observed in surface soil from an island in the lake. Figure 2 shows variations with depth in a core from Taylor Valley. Note from the scale of the graph that all concentrations were low.

Patterned ground consisting of a system of polygons is common in many areas of Antarctica, including Taylor Valley. These features apparently result from seasonal expansion and contraction. During the winter, fractures occur as the permafrost contracts due to the cold temperatures. By summer these cracks may become filled as wind and melting ice carry surface material into the fracture. When the soil expands during the summer, the weaker zone at the fracture is pushed

upward. Repetition of this process through the years causes the observed patterns (3). Several areas of Mars show similar patterns except that the scale is very different (4). A sample of Taylor Valley soil taken between the polygons was low in all ions checked. If Martian polygons were formed by the same mechanism responsible for the patterned ground in Antarctica, it is likely that the Martian surface soil between the polygons would show similar ionic depletion.

Wright Valley is one of the major valleys in Victoria Land. It reaches from the Polar Plateau to the Wilson Piedmont Glacier where it is filled by the Wright Lower Glacier. It is bounded on both north and south by mountain ranges. The western section of the valley is separated by the Dais Plateau into the upper and lower forks. Concentrations of ions in soils from Wright Valley were much higher than those in Taylor Valley soils but varied dramatically with depth and from one location to another. Figure 3 is a comparison of chloride ion concentrations in four different cores from Wright Valley.

Two Wright Valley ponds gave widely divergent results. The Don Quixote Pond in the North Fork had relatively high concentrations of most ions near the surface, with sodium and chloride ions predominating (see Figure 4). Concentrations decreased dramatically to a depth of approximately 3 to 4 centimeters, where they started to level off to low values changing very little throughout the rest of the core. Upon visual examination, the core appeared homogeneous below approximately 3 centimeters. Analysis of the white crystalline encrustations on the surface of the pond gave results which were very similar to those from the top of the core. All ions checked, except potassium, were present in relatively high amounts, indicating the presence of several different minerals. The data showed that salts from upper-lying areas were transported into lower areas such as ponds and lakes. As an illustration, ionic concentrations near the surface of Don Quixote Pond were more than tenfold greater than the corresponding concentrations at a point 20 meters above the pond.

The Don Juan Pond in the South Fork remains unfrozen because of its high salt content (2). Two core samples were obtained from the soil of the Don Juan Pond. Sample DJ 2074 was taken from the center of the pond, and sample DJ 33 was obtained near the periphery. In the two core samples, ionic concentrations varied in a similar manner with depth. However, concentrations in the central core were much higher, indicating a movement of the salts to the lowest part of the pond. The increased abundance of sodium ions near the surface of the central core shows that sodium salts are transported more easily than other salts. In both cores the preponderance of the sodium ions was near the surface, whereas calcium ion concentration fluctuated considerably down the core. Figures 5 and 6 illustrate that both sodium chloride and calcium chloride are present in the Don Juan samples with calcium chloride significantly predominating below the surface layer. The data verify that upward ionic migration occurred. As surface water evaporated or sublimed, the salts were left behind. From these results, it appears that sodium chloride has a greater upward mobility than does calcium chloride.

Core 52 was obtained from the southeastern end of Wright Valley. Ionic concentrations were generally much lower than those of the Don Juan samples. As shown in Figure 7, the molar concentration of calcium ions did not correspond to any of the other species, predicting the presence of an additional calcium salt. Visual examination indicated the likelihood of a small amount of calcium carbonate and a much larger amount of calcium sulfate. The broad maximum in calcium ion concentration occurring at the 8 centimeter level indicates that the upward migration of calcium ions is hindered, probably because the calcium salts present in this sample are only slightly soluble in water and are not transported upward as readily as more soluble salts.

Samples were obtained from a large, 1 meter deep pit in the Prospect Mesa Formation in Wright Valley. Figure 8 shows the ionic abundances. The molar ratio of sodium and chloride ions is very close to 1:1, indicating the presence of sodium chloride (see Figure 9). A salt layer occurred just below the surface again indicating an upward mobility of sodium and chloride ions. Concentrations of these ions decreased down to the permafrost level at a depth of 35 to 40 centimeters. Below this level, concentrations of all ions remained essentially constant, indicating that little or no ionic transport occurred in the permafrost zone. The depletion of ions in the surface layer is indicative of weathering action, probably due to wind.

In summary, all samples examined contained water-soluble salts, reflecting the aridity of the region. Calcium chloride was most abundant in samples from the Don Juan Pond, whereas sodium chloride was present in very high concentrations in the Prospect Mesa Formation of Wright Valley. Considering all ions checked, the soil pit in the Prospect Mesa Formation was the richest area examined. Abundances of both potassium and nitrate ions were low in most areas but were significant in some of the samples from the Prospect Mesa pit. Magnesium ion concentrations were generally low throughout the dry valleys. A few samples were checked for fluoride ions; the results were so low that further determinations seemed impractical.

Movement of salts into low-lying areas was verified. Upward ionic migration was evident in all core samples. Of all cations observed, sodium showed the greatest degree of migration.

The chemistry of soils from the dry valleys of Antarctica is both interesting and unusual. A detailed knowledge of these soils may prove to be quite valuable in planetary studies.

REFERENCES

(1) Gibson, E.K., Jr., and Ransom, B. (1981) Twelfth Lunar and Planetary Science Conference, Houston, Texas.

(2) Harris, H.J.H. (1981) Ph.D. Dissertation, University of Illinois.

(3) Berg, T.E. and Black, R.F. (1966) American Geophysical Union, Antarctic Research Series, No. 8, 61-108.

(4) Carr, M.H. and Schaber, G.G. (1977) Journal of Geophysical Research 82(28), 4039-4054.

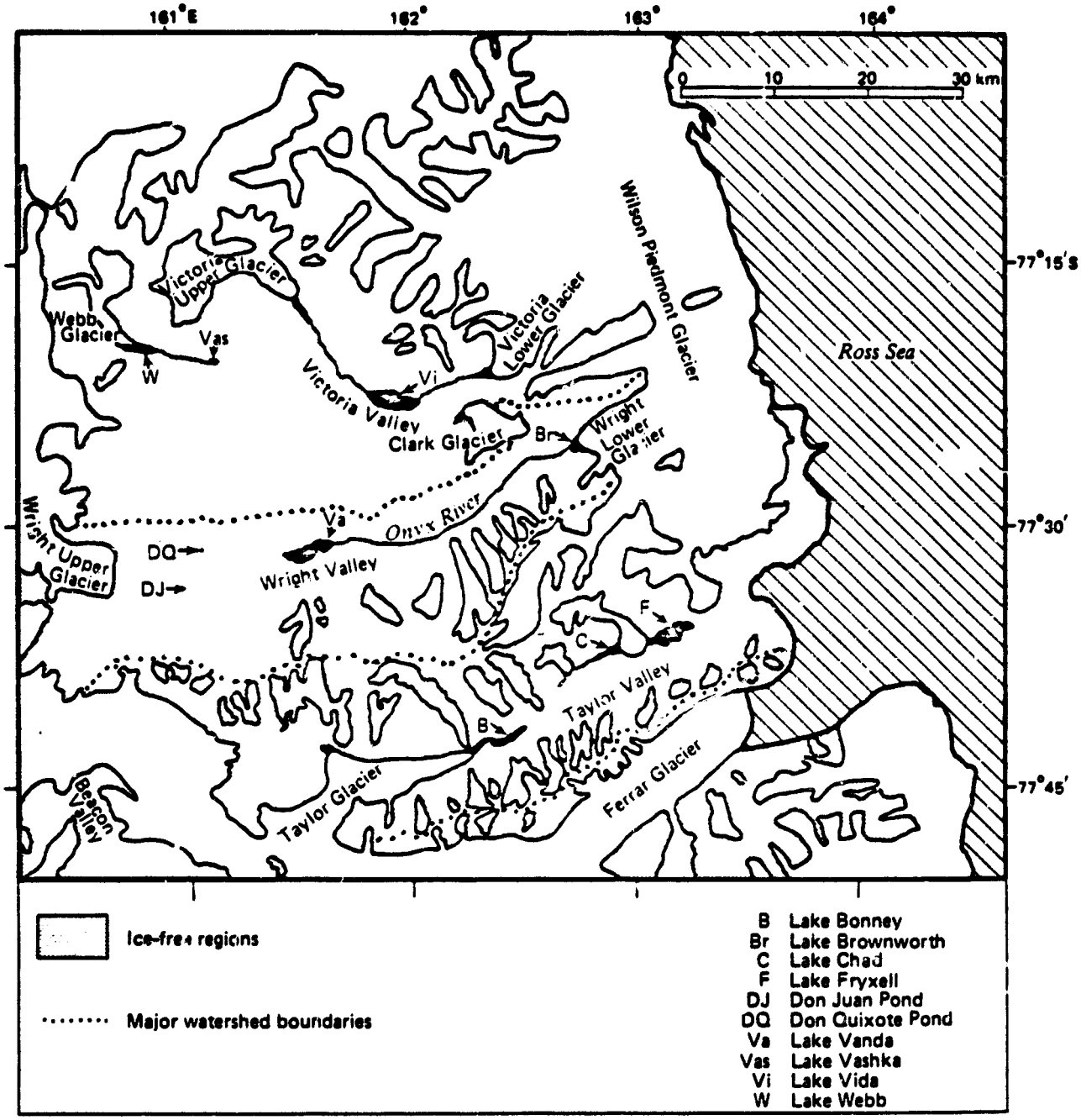

Figure 1 The Dry Valley Region in detail (2)

FIGURE 2

TAYLOR VALLEY CORE 50

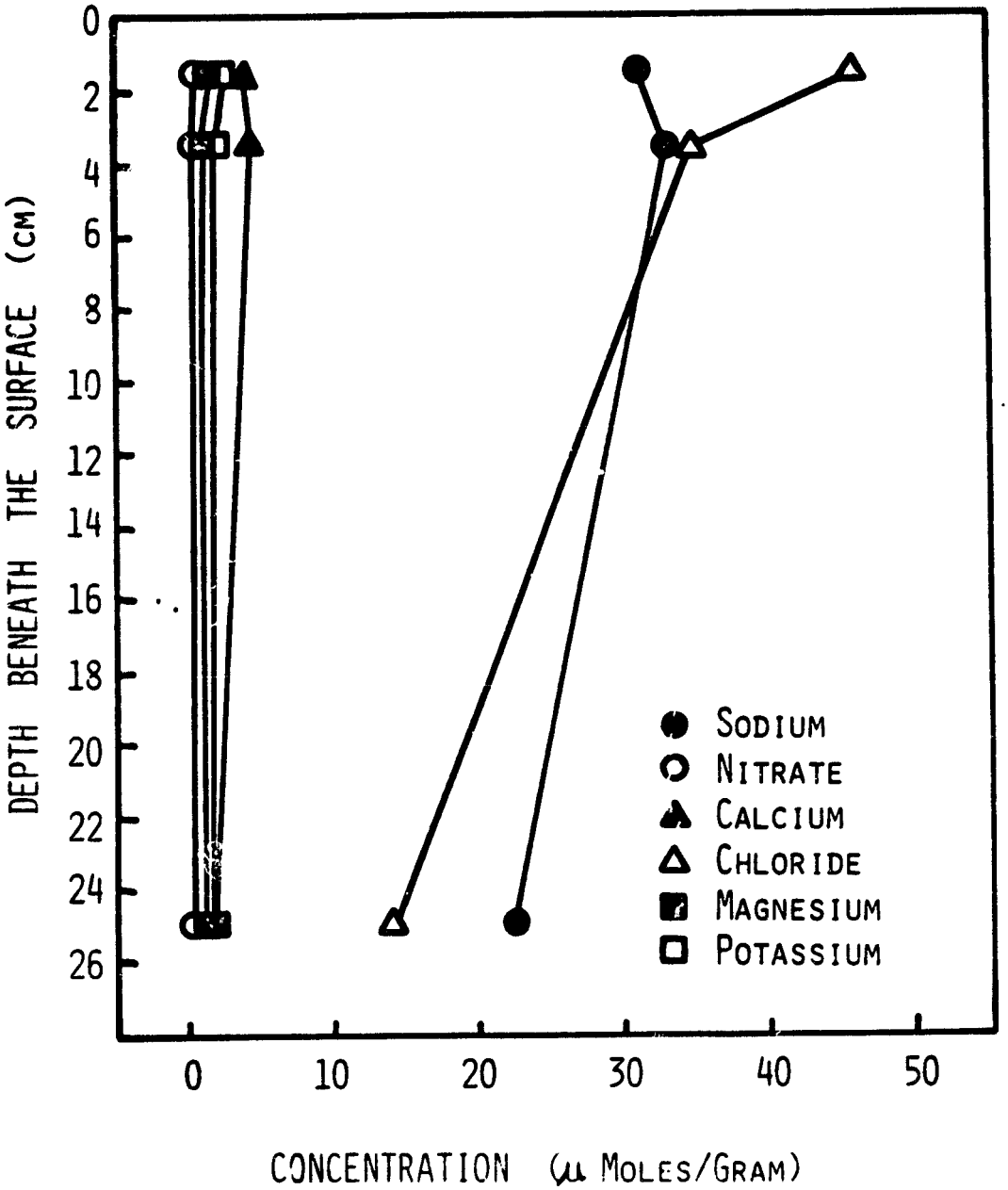

FIGURE 3

COMPARISON OF Cl^- CONCENTRATIONS IN DIFFERENT CORES

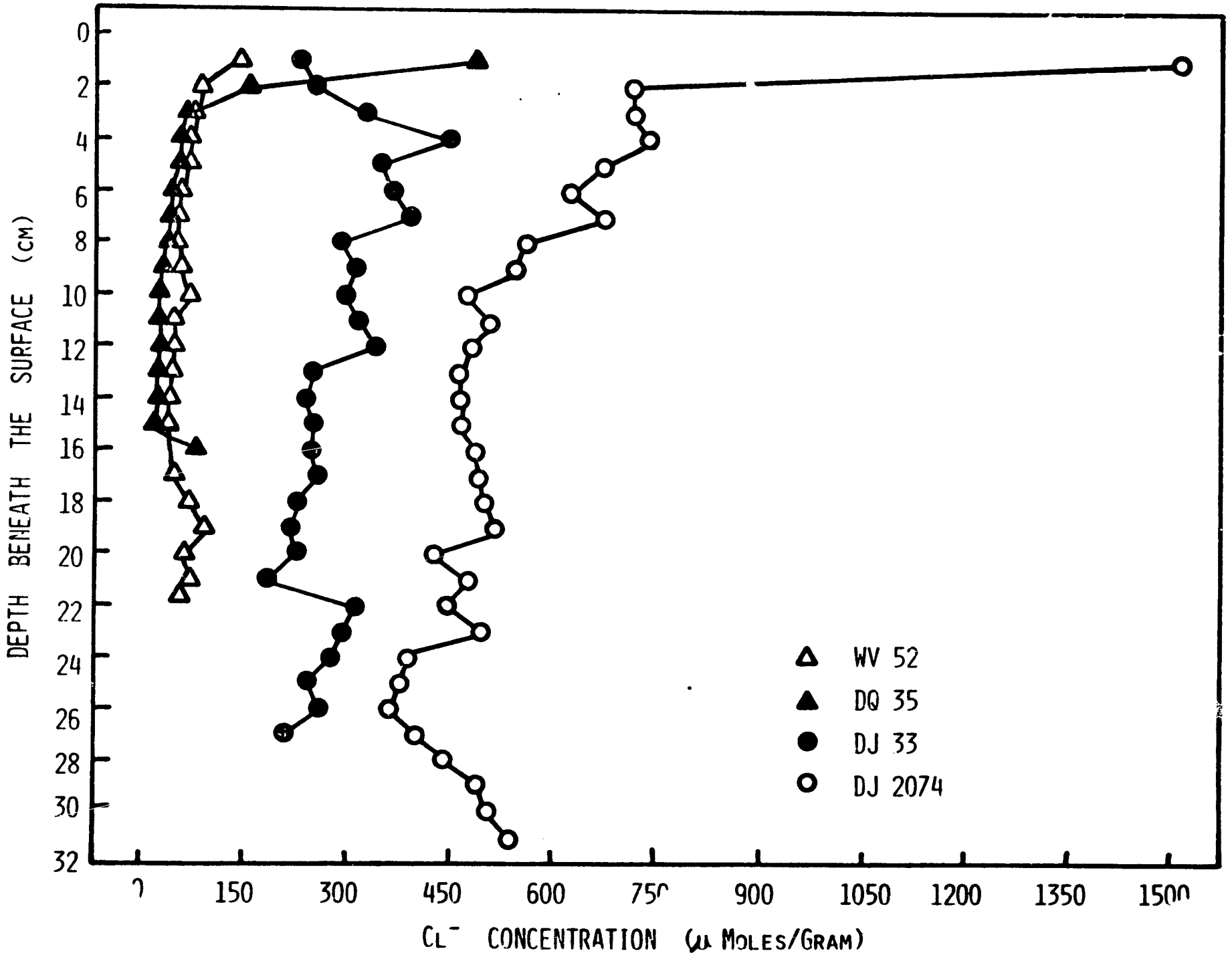

FIGURE 4

DON QUIXOTE CORE 35

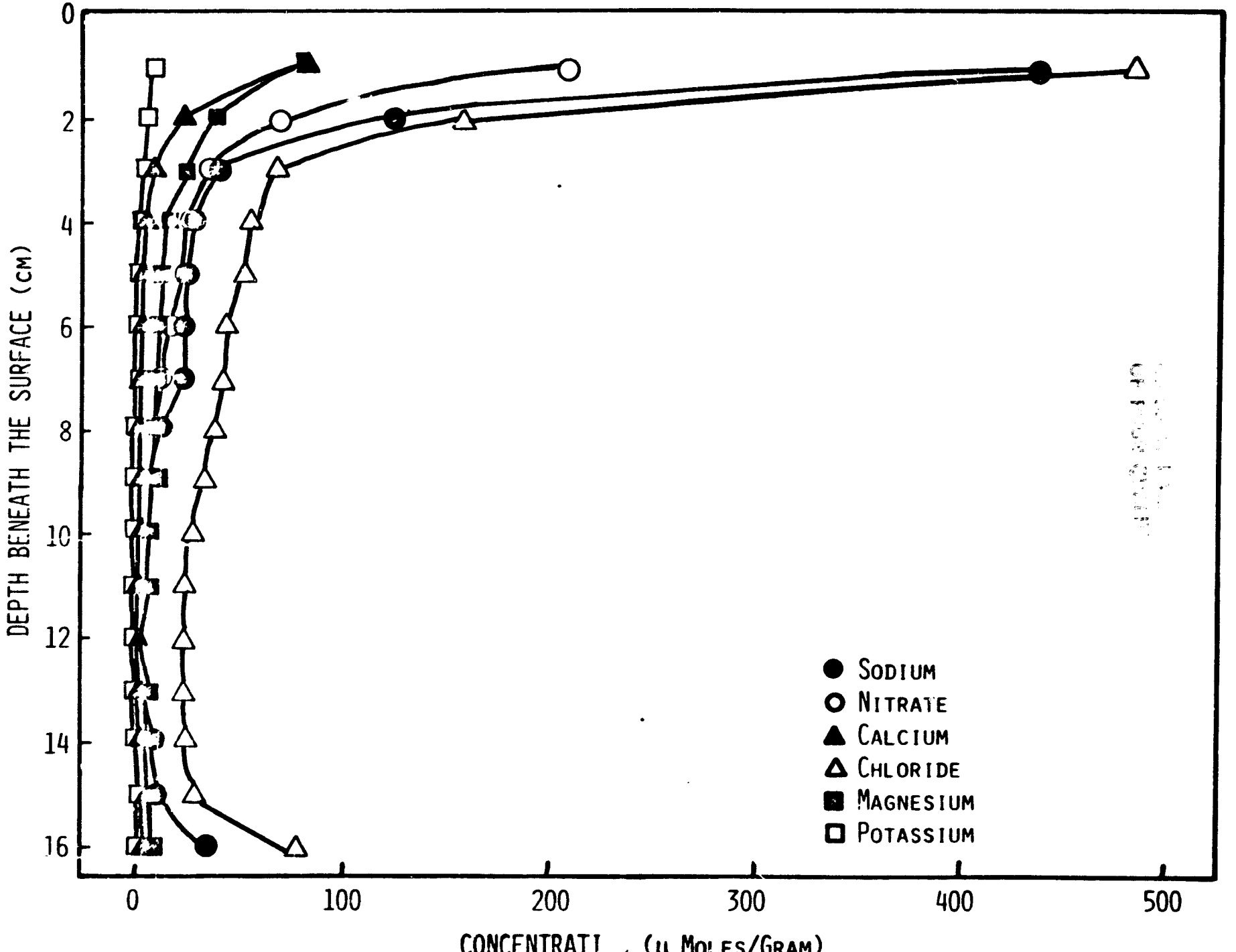

FIGURE 5

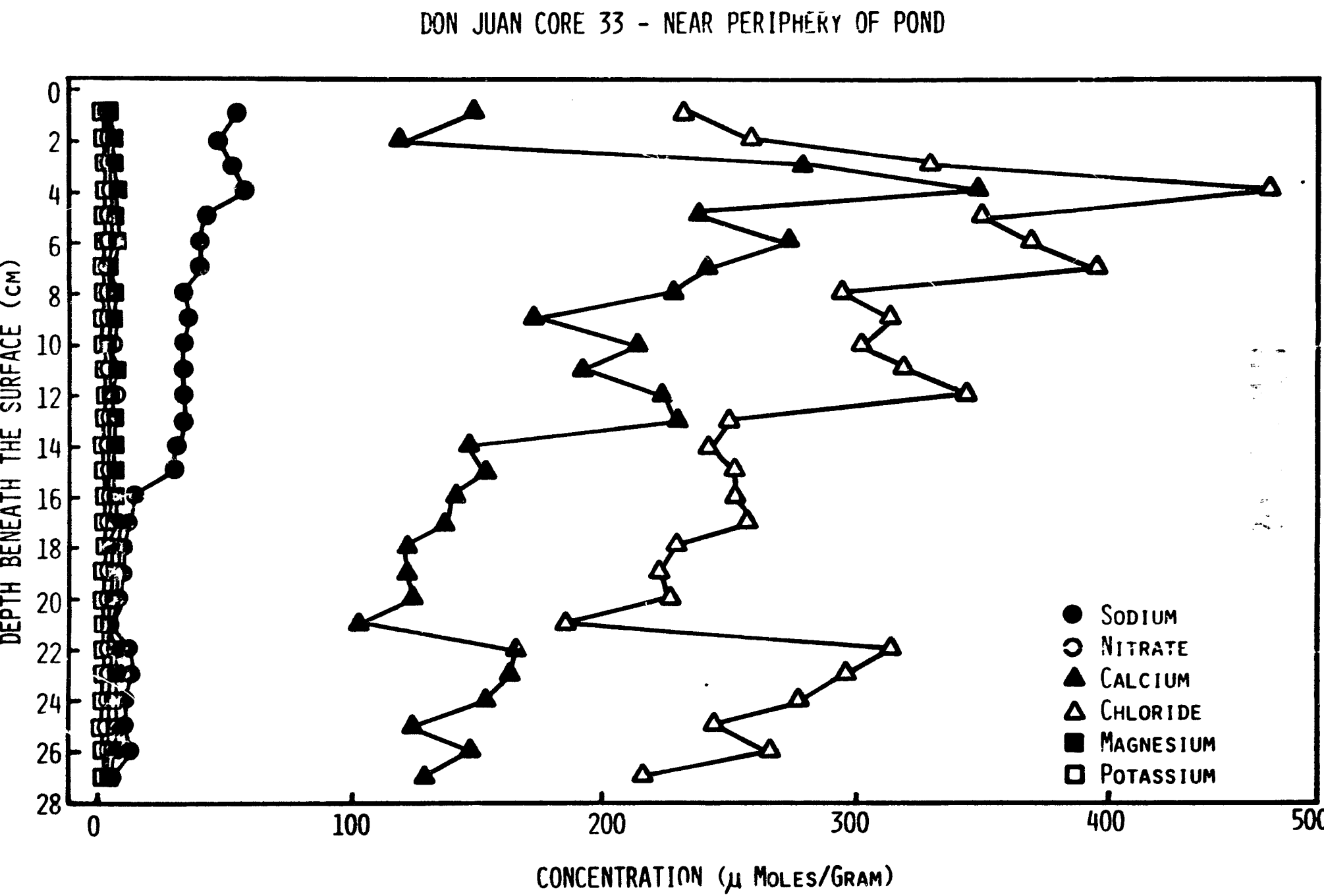
DON JUAN CORE 33 - NEAR PERIPHERY OF POND
DEPTH BENEATH THE SURFACE (CM)
0
2
4
6
8
10
12
14
16
18
20
22
24
26
28
0
100
200
300
400
500
CONCENTRATION (μ MOLES/GRAM)
SODIUM
NITRATE
CALCIUM
CHLORIDE
MAGNESIUM
POTASSIUM

FIGURE 8

DON JUAN CORE 2074 - CENTER OF POND

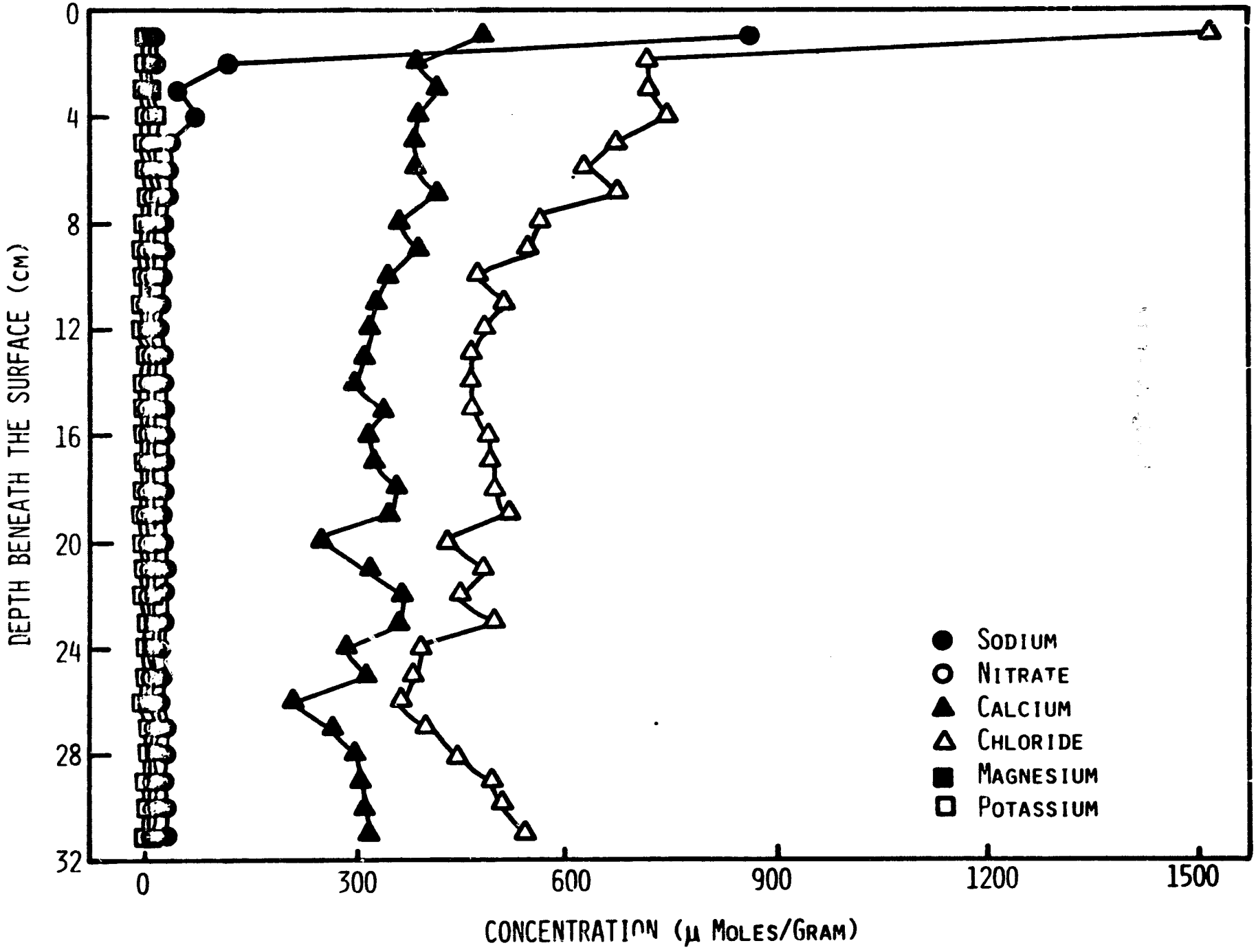

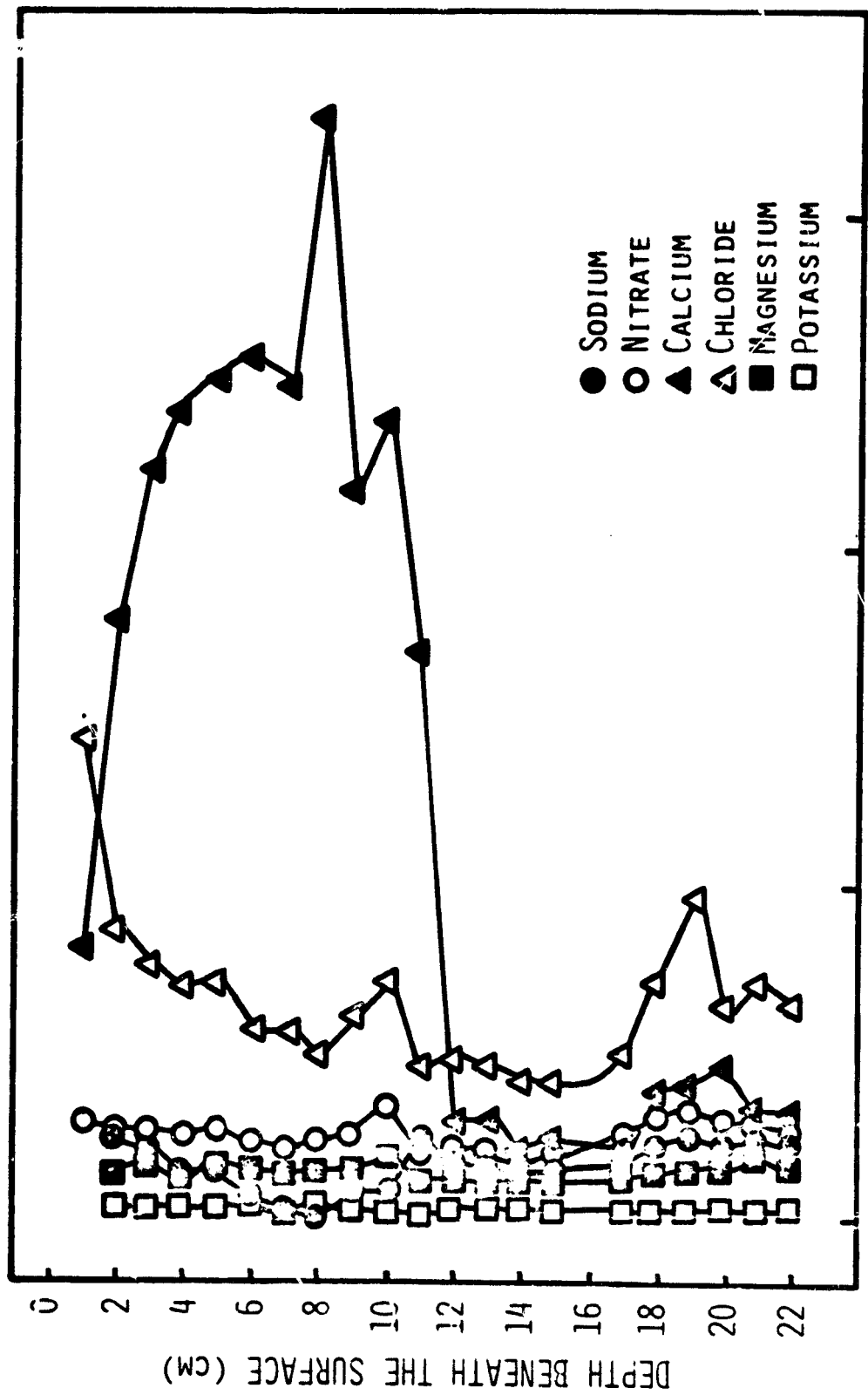

FIGURE 7

FIGURE 8

SOIL PIT, PROSPECT MESA FORMATION, WRIGHT VALLEY

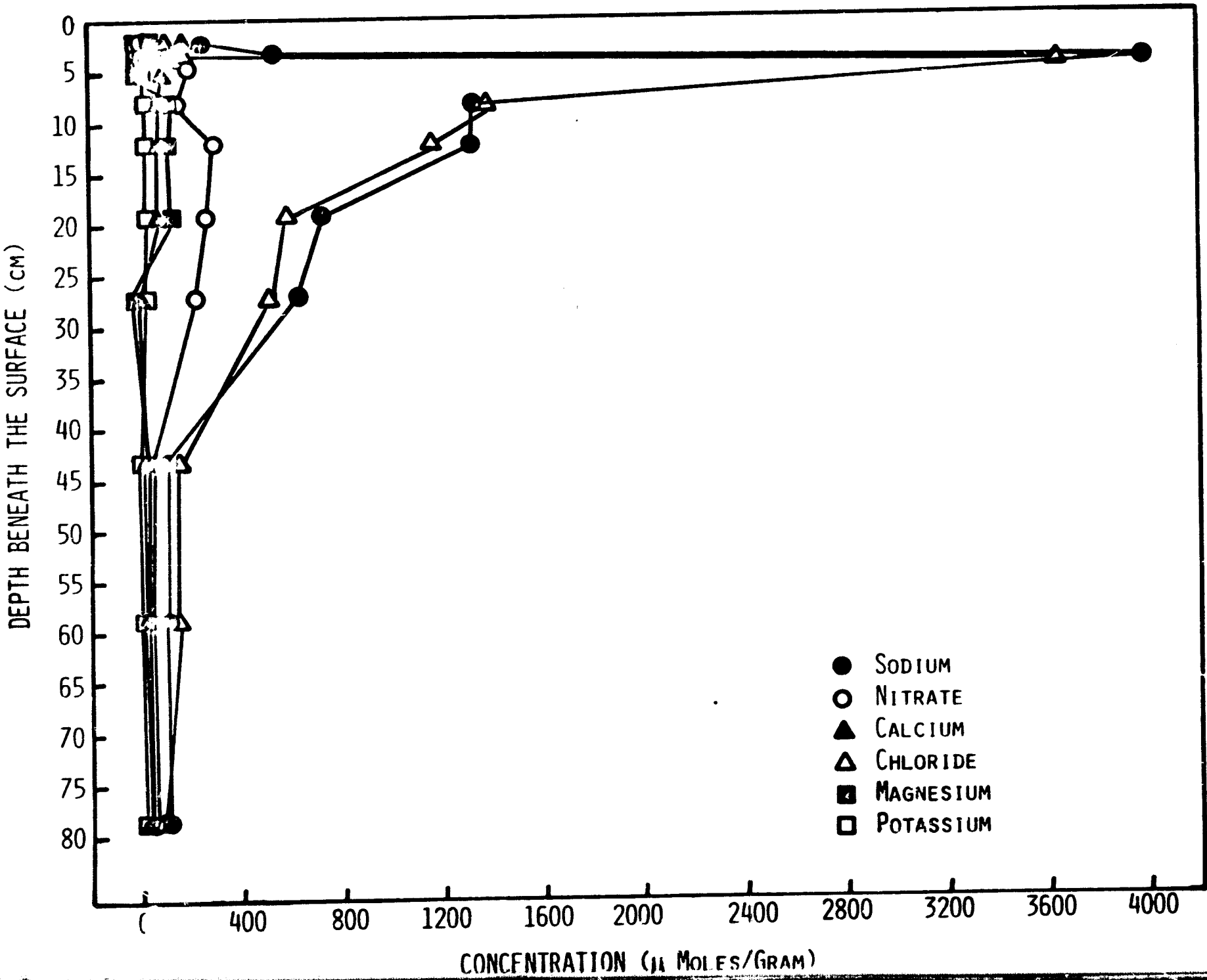

FIGURE 9

SOIL PIT, PROSPECT MESA FORMATION
WRIGHT VALLEY

NA/CL MOLAR RELATIONSHIP

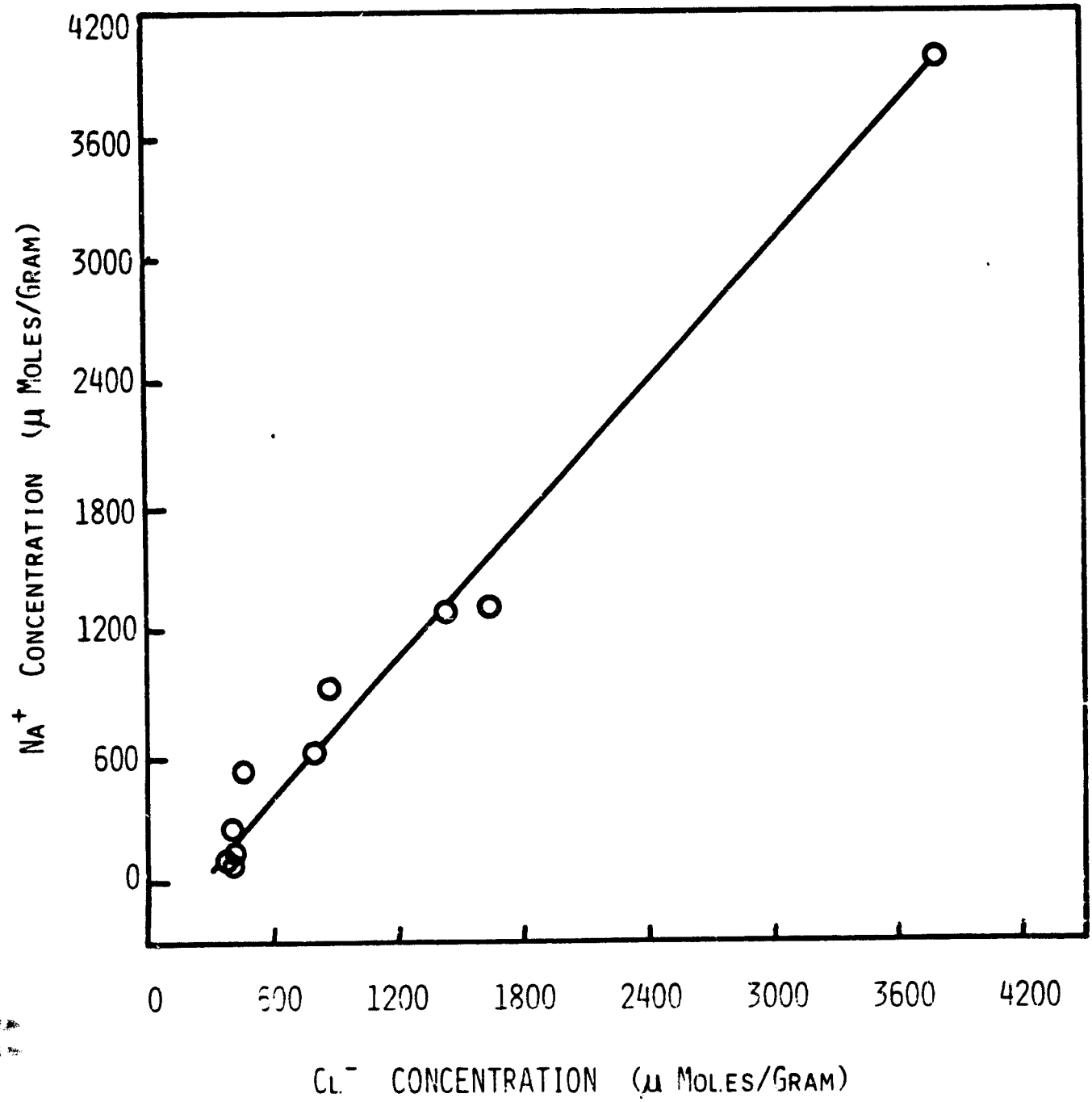

Tracking and Communications

Development Division

Internal Note

Effects of Rain and Fog on the Shuttle Ku-band Microwave Scanning Beam Landing System Range and Accuracy Performance

Dennis Butler

NASA/ASEE Summer Fellow

August, 1981

I. Introduction

The Microwave Scanning Beam Landing System (MSBLS) is a navigation system which provides distance, azimuth, and elevation coordinates to the Shuttle orbiter during final approach and landing (Harton 1979). Azimuth information is transmitted to the orbiter via a pulse-encoded, vertically polarized, planar vertical beam sweeping through a 30° transmission sector centered on the runway centerline extension; vertical coverage of the azimuth beam extends to 23°. Similarly, elevation data are transmitted to the orbiter via a pulse-encoded, vertically polarized, planar horizontal beam sweeping trhough a 30° transmission sector; usable azimuth coverage of the elevation beam extends to approximately 50°. For range determination, the orbiter, after detecting a solicit signal from the ground station, returns an interrogation signal. Upon receiving the interrogation signal, the ground station sends a reply signal to the orbiter. The orbiter then determines its range by measuring the time spacing between interrogation and reply. The entire sequence, range-azimuth-elevation, is repeated every 200 milliseconds, and at a frequency near 15.5 GHz. (wavelength $\sim$ 1.94 cm).

At a fixed tracking level of about -4 dB, the azimuth full beam width is $\sim$ 2.4°. Since the ground station changes the pulse encoding (pulse-pair spacing) every 0.125°, as the beam sweeps past the orbiter, a distribution of pulse pairs is received. In computing azimuth, the orbiter averages the pulse-pair spacings of all pulse-pairs in the received distribution. Elevation signal reception and decoding is similar to that for azimuth, except that the -4dB beam width is 1.4°, and the received pulse distribution contains fewer pulse-pairs.

The MSBLS is expected to be particularly useful during periods of decreased optical visibility such as at night or those resulting from the presence of rain, fog, or clouds in the line-of-sight between the ground station and orbiter. Certainly, there will be times when meteorological conditions are sufficiently poor that an orbiter landing would be unacceptably risky. Consequently, it is important to be able to predict the signal attenuation, beam distortion, and coordinate errors which result from operation of the system in poor weather conditions.

Radar literature abounds with studies of microwave attenuation due to rain and fog. Robel (1978, and references therein; 1981) has appealed to those studies in estimating the most adverse meteorological conditions under which the MSBLS will function reliably. He deals with the problem of attenuation exclusively. One can anticipate, however, rain and fog conditions that will lead to systematic elevation and azimuth error as well as the random error expected from a weakened signal at the orbiter. The systematic, or bias error results from beam distortion as it traverses asymmetrical weather configurations such as those which could occur in fog, rain or cloud conditions.

The main physical processes giving rise to attenuation of MSBLS signals are absorption and scattering of microwaves from distributions of water droplets. In scattering, the frequency of radiation after encounter with a drop is the same as the frequency before the encounter; only the direction of propagation changes. In absorption, the microwave energy goes into heating the drop, which later radiates isotropically with a blackbody (Plankian) distribution of

frequencies. Since scattering is a markedly directional phenomenon, one expects beam shape distortion in scanning beam systems like the MSBLS to depend on the relative importance of scattering and absorption. These two effects must be evaluated if one is to determine whether or not beam distortion is an important source of error.

In proceding, we utilize a fully general theory of scattering and absorption (Mie 1908; Debye 1909), valid for all drop sizes from fine mist to heavy rain. Availability of high speed, high capacity computing machines renders this approach preferable to those involving various limiting approximations for drops of different sizes. Since the general theory lends itself quite readily to attenuation calculations, we use them as much as possible as a check to ensure that the programming is correct. Necessary formulae are collected in Section II. Attenuation, scattering and absorption efficiencies are discussed in Section III, and finally, a general discussion and recommendations appear in Section IV. A listing of the computer program appears in the appendix.

II. Formulae

Mie theory gives, among other things, the far-field solution to the problem of scattering and absorption of plane-polarized E&M waves of sinusoidal time variation. Within the Mie formalism, one can determine intensity and polarization of microwaves scattered from a single spheroidal drop; the generalization to drop-size distributions is straightforward We do not wish to reproduce the theory herein; interested readers are referred to Van der Hulst (1957). Our preference is to extract only those

formulae necessary for our computations:

a: radius of sphere

λ: wavelength of microwaves

l: real part of complex refraction index, m

k: imaginary part of complex refractive index, m

$$x = 2\pi a/\lambda, \tag{1}$$

$$m = l - ik. \tag{2}$$

C_{sca}: cross section for scattering (units of area)

C_{abs}: cross section for absorption

C_{bk} : cross section for back-scattering

Q_{sca}: efficiency factor for scattering (dimensionless)

Q_{abs}: efficiency factor for absorption

Q_{bk} : efficiency factor for back-scattering

Q_{ext}: efficiency factor for extinction (attenuation)

$$C_{sca} = \pi a^2 Q_{sca}, \tag{3}$$

$$C_{abs} = \pi a^2 Q_{abs}, \tag{4}$$

$$C_{bk} = \pi a^2 Q_{bk}, \tag{5}$$

$$Q_{ext} = Q_{sca} + Q_{abs}, \tag{6}$$

$$y = mx, \tag{7}$$

$$A_0(y) = \cos y / \sin y, \tag{8}$$

$$A_n(y) = -\frac{n}{y} + \left(\frac{n}{y} - A_{n-1}(y)\right)^{-1}, \tag{9}$$

$$\xi_{-1}(x) = \cos x - i \sin x, \tag{10}$$

$$\xi_0(x) = \sin x + i \cos x, \tag{11}$$

$$\xi_n(x) = \frac{2n-1}{x}\xi_{n-1}(x) - \xi_{n-2}(x), \tag{12}$$

$$a_n = \frac{\left[\frac{A_n(y)}{m} + \frac{n}{x}\right] \mathrm{Re}[\xi_n(x)] - \mathrm{Re}[\xi_{n-1}(x)]}{\left[\frac{A_n(y)}{m} + \frac{n}{x}\right]\xi_n(x) - \xi_{n-1}(x)}, \tag{13}$$

$$b_n = \frac{\left[m A_n(y) + \frac{n}{x}\right] \mathrm{Re}[\xi_n(x)] - \mathrm{Re}[\xi_{n-1}(x)]}{\left[m A_n(y) + \frac{n}{x}\right]\xi_n(x) - \xi_{n-1}(x)}, \tag{14}$$

$$Q_{sca} = \frac{2}{x^2}\sum_{n=1}^{\infty}(2n+1)\left[|a_n|^2 + |b_n|^2\right], \tag{15}$$

$$Q_{ext} = \frac{2}{x^2}\sum_{n=1}^{\infty}(2n+1)\,\mathrm{Re}(a_n + b_n), \tag{16}$$

$$Q_{bk} = \frac{4}{x^2}\left|\sum_{n=1}^{\infty}(n+\tfrac{1}{2})(-1)^n(a_n - b_n)\right|^2, \tag{17}$$

$$\begin{aligned} \pi_0(\cos\theta) &= 0, \\ \pi_1(\cos\theta) &= 1, \\ \pi_2(\cos\theta) &= 3\cos\theta, \end{aligned} \tag{18}$$

$$\pi_n(\cos\theta) = \cos\theta\left(\frac{2n-1}{n-1}\right)\pi_{n-1}(\cos\theta) - \frac{n}{n-1}\pi_{n-2}(\cos\theta), \tag{19}$$

$$\tau_0(\cos\theta) = 0,$$

$$\tau_1(\cos\theta) = 1, \tag{20}$$

$$\tau_2(\cos\theta) = 3\cos 2\theta,$$

$$\tau_n(\cos\theta) = \cos\theta\left[\pi_n(\cos\theta) - \pi_{n-2}(\cos\theta)\right] - (2n-1)\sin^2\theta\left[\pi_{n-1}(\cos\theta)\right] + \tau_{n-2}(\cos\theta), \tag{21}$$

where θ is the scattering angle, measured from the direction of the forward beam.

$$S_1(\theta) = \sum_{n=1}^{\infty} \frac{2n+1}{n(n+1)}\left[a_n\pi_n(\cos\theta) + b_n\tau_n(\cos\theta)\right], \tag{22}$$

$$S_2(\theta) = \sum_{n=1}^{\infty} \frac{2n+1}{n(n+1)}\left[b_n\pi_n(\cos\theta) + a_n\tau_n(\cos\theta)\right], \tag{23}$$

$$S(\theta) = \frac{1}{2}\left(\frac{\lambda}{2\pi}\right)^2\left[|S_1(\theta)|^2 + |S_2(\theta)|^2\right], \tag{24}$$

$$\langle\cos\theta\rangle = \frac{4}{\chi^2 Q_{sca}}\sum_{n=1}^{\infty}\frac{n(n+2)}{n+1}\mathrm{Re}\left[a_n a_{n+1}^* + b_n b_{n+1}^*\right] + \frac{2n+1}{n(n+1)}\mathrm{Re}\left[a_n b_n^*\right], \tag{25}$$

where the asterisks indicate complex conjugate.

For the case of ∥ polarization, i.e., the electric field vectors are parallel to the plane defined by the incident, and scattered wave propagation vectors,

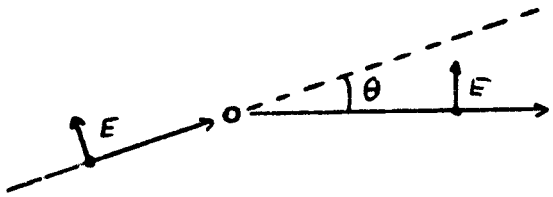

$$\frac{I}{I_0} = \frac{|S_1(\theta)|^2}{k^2 r^2} \quad , \tag{26}$$

where $$k = \frac{2\pi}{\lambda} \quad . \tag{27}$$

r: distance from scattering drop to observer

I_0: incident intersity

I: intersity at r

$S_2(\theta)$: complex amplitude function (equation 23)

And for the case of ⊥ polarization, i.e., the electric field vectors are perpendicular to the plane defined by the incident, and scattered wave propagation vectors,

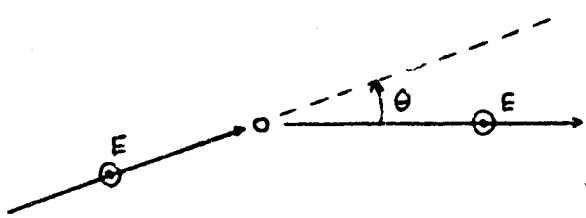

$$\frac{I}{I_0} = \frac{|S_1(\theta)|^2}{k^2 r^2} . \tag{28}$$

For unpolarized incident radiation,

$$\frac{I}{I_0} = \frac{\frac{1}{2}\left[|S_1(\theta)|^2 + |S_2(\theta)|^2\right]}{k^2 r^2} . \tag{29}$$

The standard attenuation formula for the case of single scattering of N_V drops, each having (the same) radius, a, is

$$I(r) = I(0)\, e^{-N_V g \pi a^2 Q_{ext}} , \tag{30}$$

N_V: number of drops per unit volume,

g: attenuation path length .

Rain

We must relate N_V to the measurable quantity p.

p: rainfall rate (mm/hr)

D: drop diameter (cm)

v: terminal velocity of drop (m/sec)

$$p = \frac{\pi}{6} D^3 N_v v \qquad (m/sec), \tag{31}$$

$$= 6\pi \times 10^5 \nu N_v D^3 \qquad (mm/hr). \tag{32}$$

v can be expressed as a function of D via a polynomial fit to the data collected by Medhurst (1965). The specific fit is

$$v(D) = \sum_{n=0}^{5} C_n D^n, \tag{33}$$

where

N	C_n
0	-0.02366
1	47.38010
2	-81.56769
3	38.93966
4	26.05586
5	-21.69620

Combining equations 30, 32, we find

$$I(h) = I(o)\, e^{-\frac{p g Q_{ext}}{24 \nu D}}, \tag{34}$$

where g is in km.

Generalization to Size Distributions

Equation 34 becomes

$$I = I_o\, e^{-\frac{100 g p}{24} \sum_i \frac{Q_i^{ext} t_i}{\nu_i D_i}}, \tag{35}$$

where f_i = percent of total volume containing drops of diameter between D_i and $D_i + \Delta D$.

Specific drop-size distributions used are those of Laws and Parsons (1943) as tabulated by Medhurst (1965). In general, rain drop-size distributions depend on rain rate (p) in such a way that as p increases, the distribution becomes wider and is shifted toward larger drop size. Figures 1-7 are the distributions and our truncated polynomial representations of them. For rain rates within the range 2.5 $\leq$ p (mm/hr) $\leq$ 150, linear interpolation between the two distributions which bracket the rain rate of interest is done; for values outside of this range, the extrema alone are used.

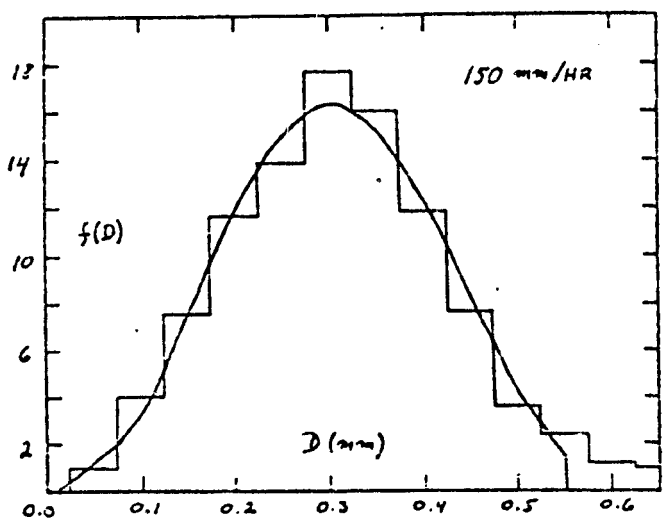

Figures 1-7:

Truncated polynomial representation of rain drop-size distributions for rain rates ranging from 150 mm/hr to 2.5 mm/hr. See text for details.

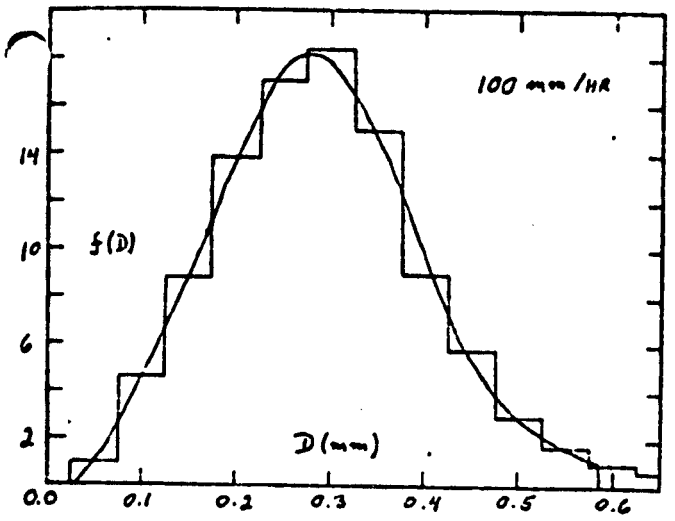

Figure 2

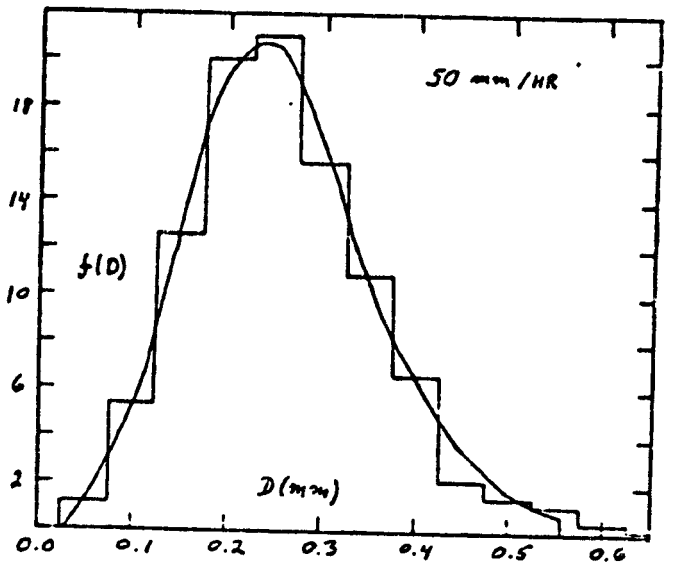

Figure 3

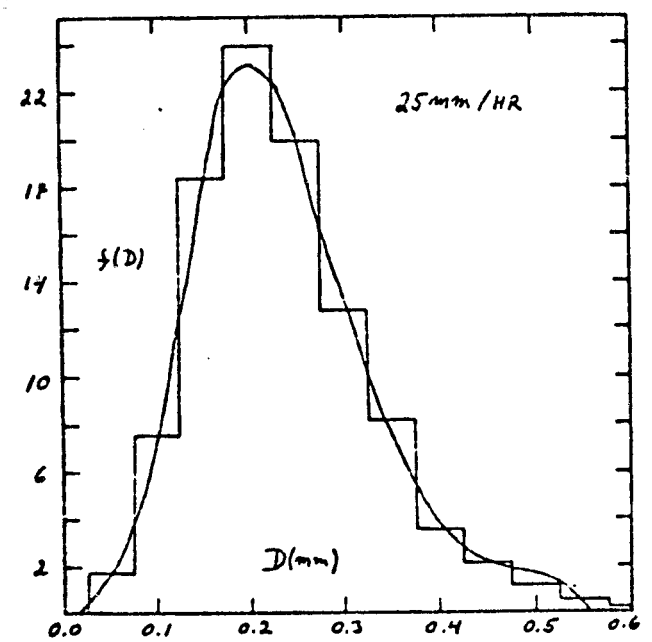

Figure 4

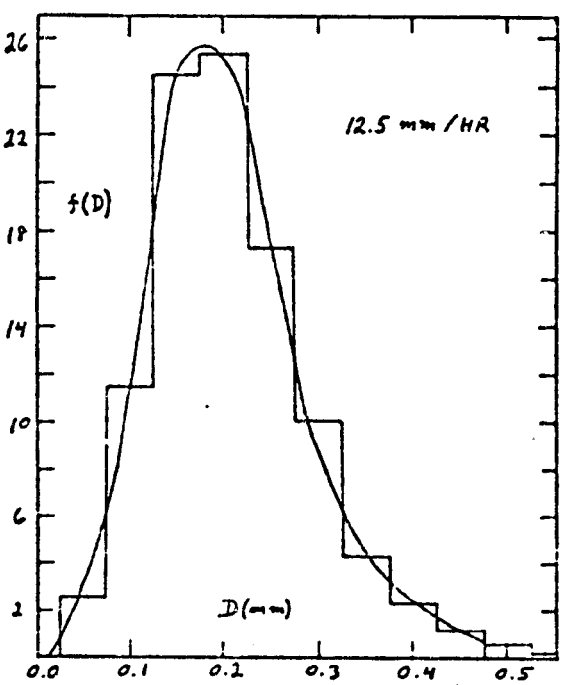

Figure 5

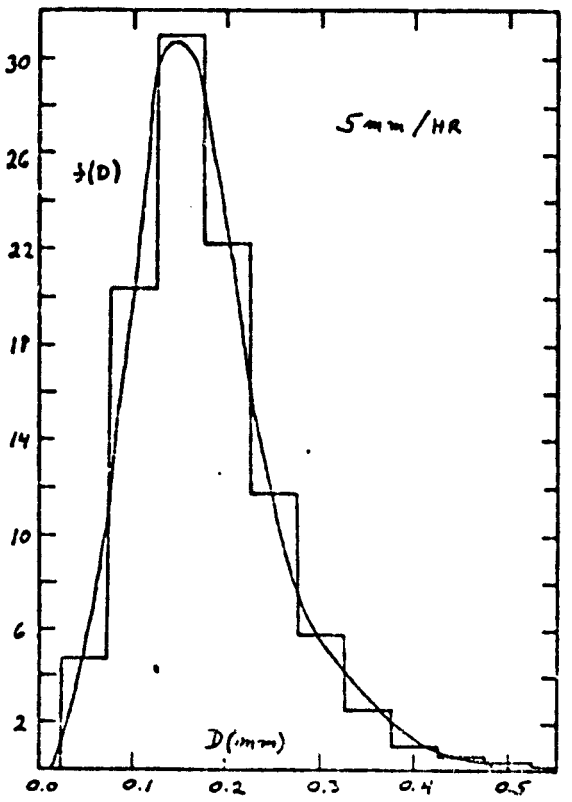

Figure 6

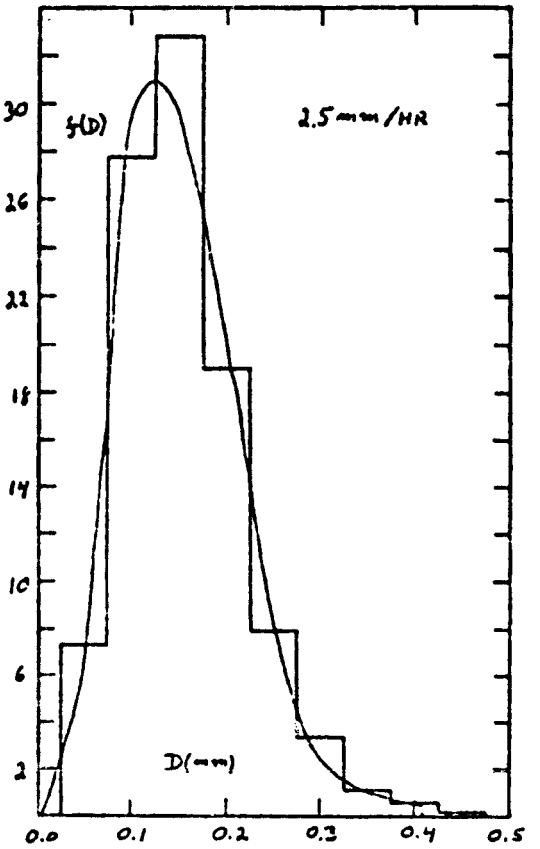

Figure 7

Land Fog (Radiation Fog)

Again, $$I(r) = I_0 e^{-N_v \pi a^2 Q_{ext}}, \quad (30)$$

but now the measureable quantity which N_v is related to is the optical visibility, V. For landfog,

$$M = 0.00332\ V^{-1.538} \quad (36)$$

(Koester and Kosowsky 1970), where M is the total water content (gm/m^3). Converting water content to N_v, we find

$$I(r) = I(0)\, e^{\frac{-4.98\times10^{-4}\, g\, Q_{ext}\, V^{-1.53}}{D}}, \qquad (37)$$

where D = 1.0 X 10^{-3} cm = average droplet diameter, and V is given in km.

Note that equation 37 has a "canonical" size distribution built into it.

Sea Fog (Advection Fog)

Formalism is the same as for landfog, but with

$$M = 0.0156V^{-1.43} \qquad (38)$$

(Koester and Kosowsky 1970). Equation 38 is valid for V ≳ 100 m. For lower visibility, one must use equation 36. Equation 30, 38 combine to give

$$I(r) = I(0)\, e^{\frac{-2.34\times10^{-3}\, g\, Q_{ext}\, V^{-1.43}}{D}}, \qquad (39)$$

where D is now 2 X 10^{-3} cm.

One expects true fogs to have properties intermediate between radiation and advection fogs.

Clouds

The simplest cloud can be viewed as high-level radiation fog. For the present, we adopt Equation 37 to describe the attenuation of all clouds, but not without realizing and appreciating the general complexity of true clouds. These systems can contain rain, fog, hail, partially melting hail, snow, and partially melting snow. In the future, our "cloud" subroutines could be modified to take account of these possibilities.

III. Attenuation

a) Program Verification

As a check that major parts of the computer program are working properly, sample calculations (at a MSBLS frequency of 15.5 GHz) for attenuation due to rain and two types of fog were made. Temperature - dependent complex refraction indices of Robel (1981) were used in all computations. In Figure 8, our results for attenuation vs. rain rate are plotted for a range of temperature.

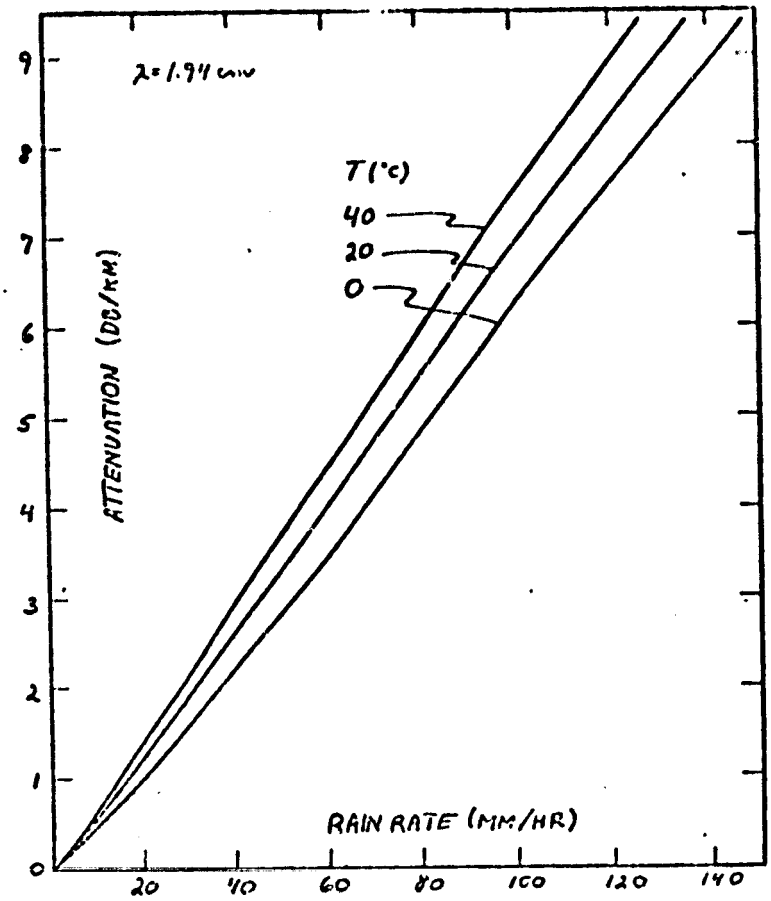

Figure 8: Attenuation as a function of rain rate.

These results are in excellent agreement with those of Robel (1978), especially since different drop-size distributions and different theoretical formalisms were used. Our attenuation - rain rate relationships show a slight curvature. This results from the convolution of extinction efficiency factors with rain-rate dependent drop-size distributions in the full theory.

In Figure 9, we plot attenuation vs. optical visibility for two kinds of fogs at three temperatures.

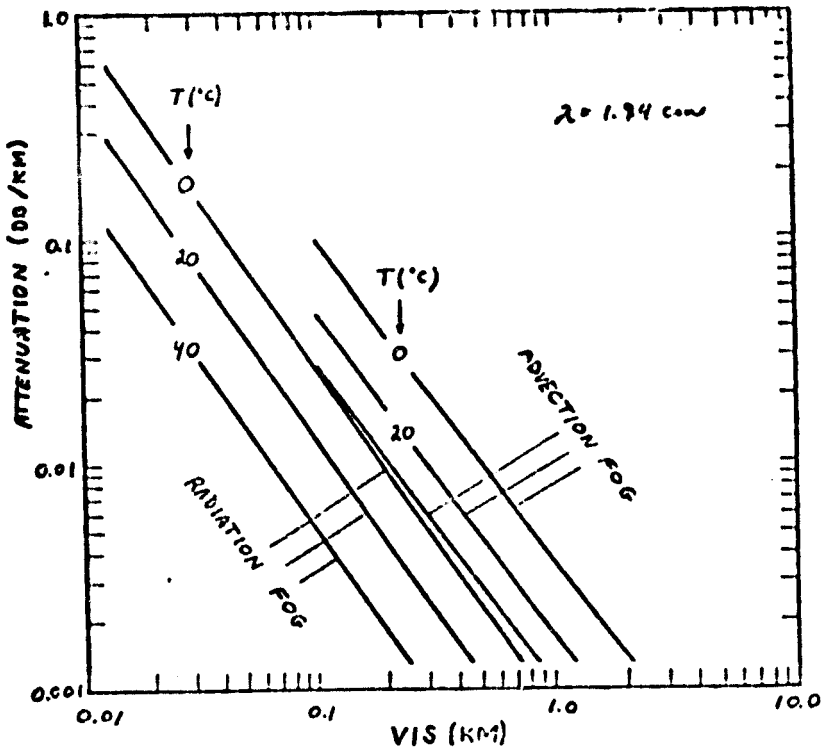

Figure 9: Attenuation as a function of fog visibility for two types of fogs.

Agreement between results from the full theory and the Rayleigh scattering approximation of Robel (1981) is fine.

Finally, we compare our full-theory result for rain attenuation with data obtained during static tests of MSBLS performance in rain (Harton and Robel 1980 a; 1980 b). The data have been normalized to units of decibel/kilometer, and are plotted in Figure 10 against rain-rate.

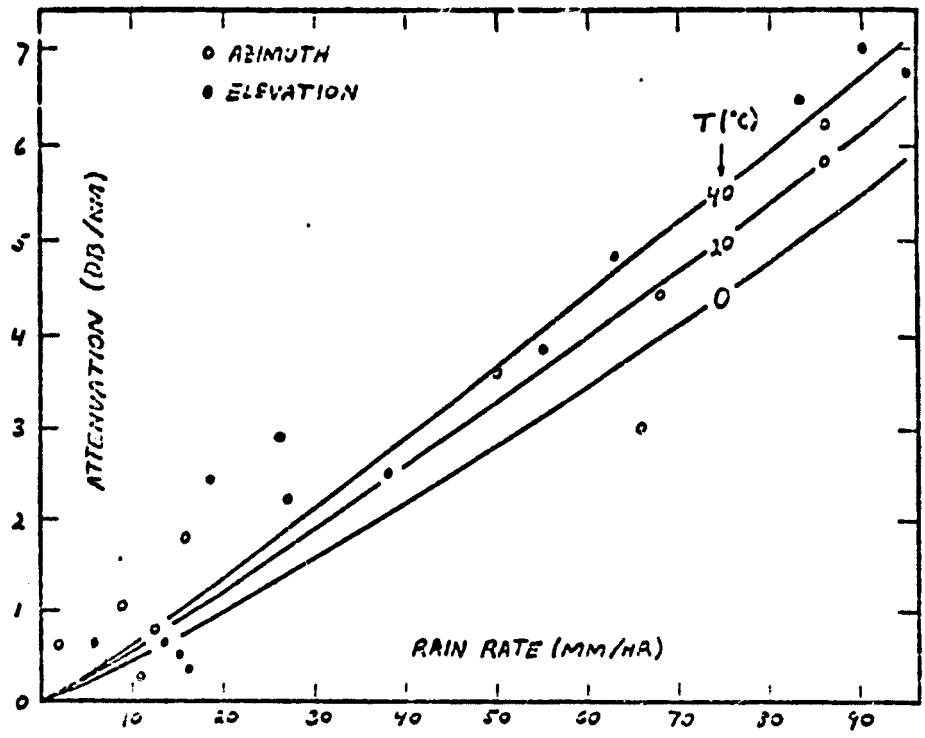

Figure 10: Static MSBLS test data.

Open circles correspond to azimuth beam (4.97 km path length), while filled circles denote elevation (1.03 km path length). Superimposed on the data are the theoretical curves of Figure 8. Considering that the data were taken in July at KSC, where temperature usually ranges between 25°C and 35°C, agreement is quite good.

b) Breakdown into Scattering and Absorption Components.

Q-values (see Equation 30) for absorption, scattering, and extinction ($Q_{ext} = Q_{abs} + Q_{sca}$) are plotted against drop diameter in Figures 11-15.

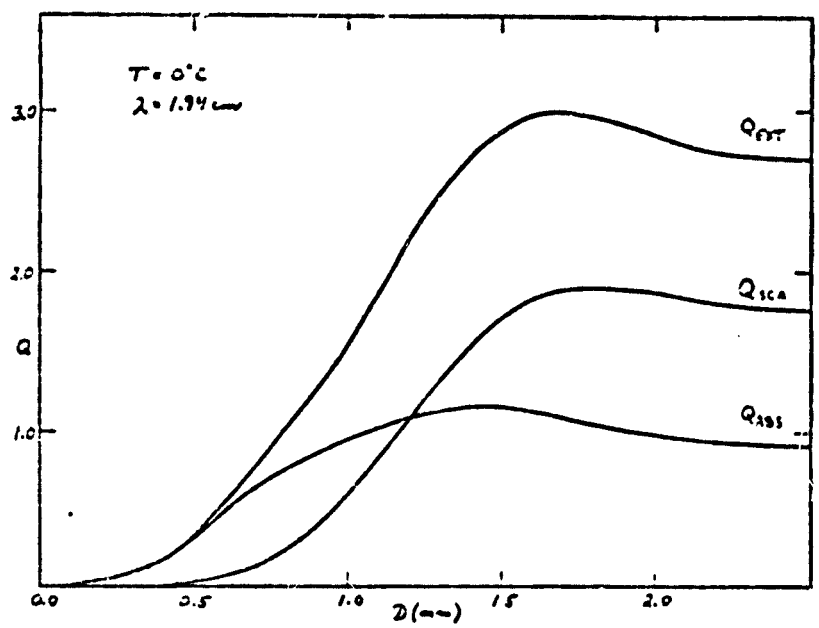

Figures 11-15: Theoretical efficiency factors plotted as a function of particle diameter for a range of temperature.

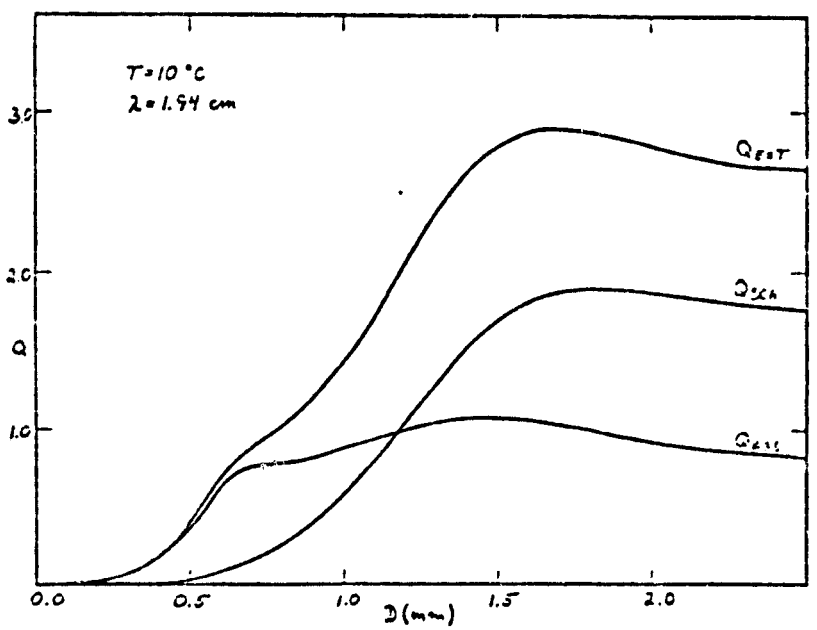

Figure 12:

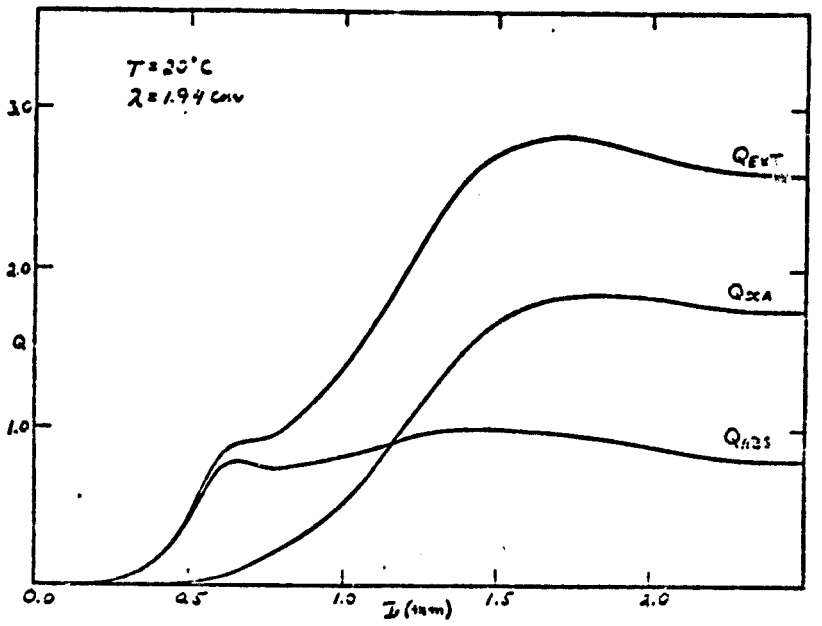

Figure 13:

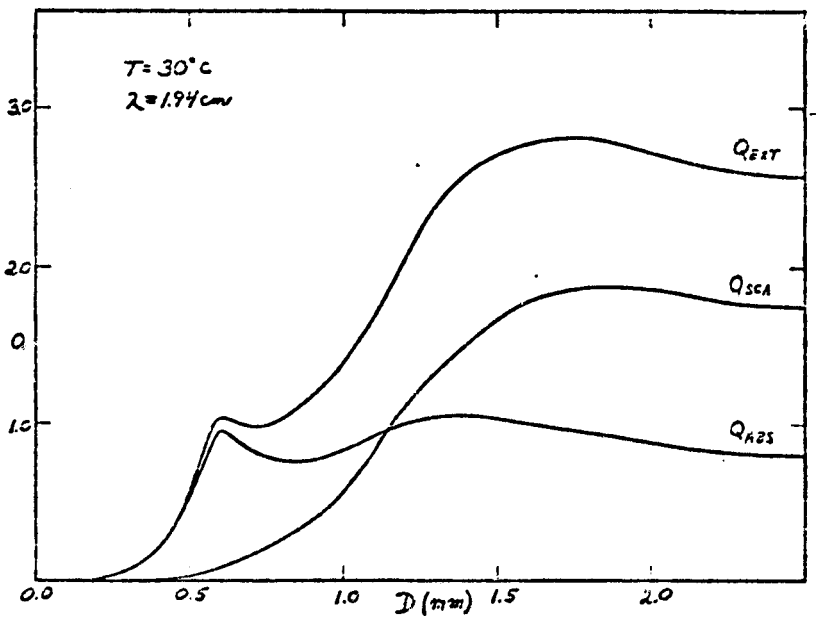

Figure 14:

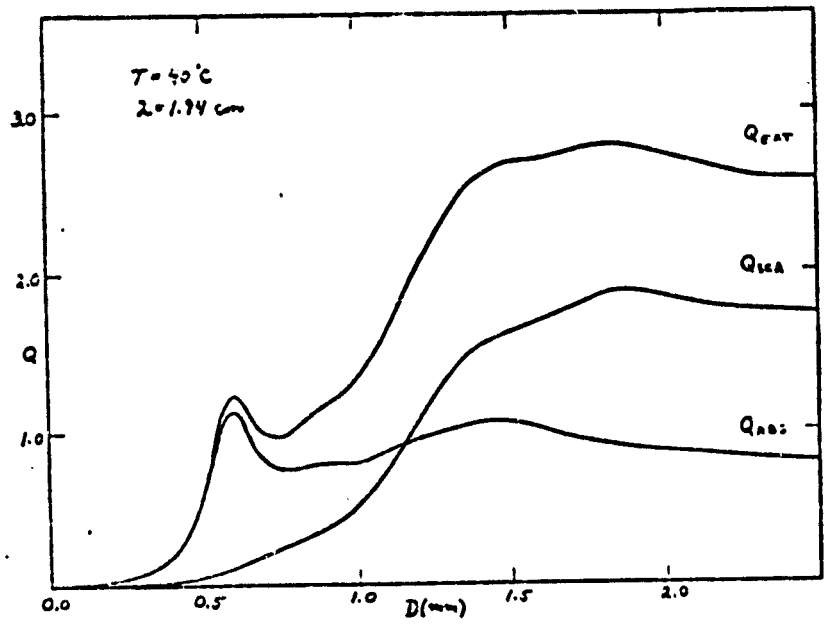

Figure 15:

One can see that absorption dominates the total attenuation for D ≤ 1 mm. For the drop size range $5 < D\ (\mu) < 65$ of a typical fog (Koester and Kosowsky 1970), the ratio Q_{sca}/Q_{abs} is never greater than $\sim 2.3 \times 10^{-2}$. For rain which follows the drop-size distribution of Figures 1-7, the corresponding maximum value is ~ 1.6. Table 1 gives the values of Q_{sca}/Q_{abs} (at T = 30°C) for the sizes corresponding to f_{max} in Figures 1-7.

Table 1

Rain Rate	$D(f_{max})$	Q_{sca}/Q_{abs} (T=30°c)
150 mm/hr	0.30 mm	0.28
100	0.27	0.21
50	0.23	0.08
25	0.20	0.06
12.5	0.17	0.06
5	0.14	0.06
2.5	0.12	0.06

Since for fog, Q_{sca}/Q_{abs} is always less than about 2%, it is probably unlikely that scattering of MSBLS microwave radiation from fog will result in serious beam distortion. For rain, the situation is quite different, and scattering-induced beam distortion could be a significant source of error.

IV. Discussion and Recommendations

a) Fog

For a given visibility, advection fog is ~ 3.5 times more effective than radiation fog in attenuation of 15.5 GHz microwaves. Except for brief afternoon periods, heavy fog is the rule and not the exception during summer months at VAFB (Robel 1981). At VAFB, this author has experienced fog with optical visibility $\lesssim$ 20 m. A 40 km path length through radiation fog of 20 m visibility at T=0°C results in 12 dB of MSBLS microwave attenuation for radiation fog. The 12 dB figure is only a rough lower limit to the true attenuation, since it is likely that the fog contains an advection component. A priori, there is no way to know what the particular composition of VAFB fog is. One can only set limits to attenuation at fixed temperature and

visibility. Depending on (1) the specific nature of VAFB fog, and (2) the applicability of complex refractive indices for pure water, microwave attenuation could approach or exceed 40 dB over a 40 km path length. One would like to be able to predict signal attenuation and link margins more precisely than indicated by our 28 dB range (factor of 630). Consequently, it is recommended that simultaneous measurements of optical visibility and MSBLS microwave attenuation be made for VAFB summer fogs of differing visibility and temperatures. These data would be used in setting realistic zero-points in Figure 9.

b) Rain

We have determined that microwave scattering is non-negligible for intermediate and heavy rains (Section III). Under these conditions, coordinate errors due to scattering-induced beam distortion could contribute significantly to the total error budget. It is recommended that the formalism of Section II, and the computer program listed in the appendix be used to evaluate the specific magnitude of this source of error. The additional work is straightforward, and involves the inclusion of beam profile and weather system geometry. The scattering phase functions are already included in the program. Even though we expect relatively unimportant scattering effects of light rain, fog, and clouds, the specific magnitudes of the errors could be calculated with the same beam geometry developed for rain.

c) Closing Note

This author expects to make considerable progress in beam profile inclusion during the remaining two weeks of his summer fellowship. Informal notes kept during this time will be made available to anyone requesting them.

References

Debye, P. 1909, Ann. Physik, 30, 59

Harton, P.L. 1979, MSBLS Handbook, 3rd ED., LEC-6872.

Harton, P. L. and Robel, M. C. 1980a "Effects of July Rains at KSC on MSBLS Azimuth Accuracy and Signal Level", Report No. JSC-89.

Harton, P. L., and Robel, M. C. 1980b, "Effects of July Rain at KSC on MSBLS Elevation Accuracy and Signal Level", Report No. JSC-91.

Koester, K. L., and Kosowsky, L. H. 1970, in American Meteorology Society, Radar Meteorology Conference, 14th, Tucson, Arizona A71 10-580(Norden).

Laws, J. O., and Parsons, D. A. 1943, TRANS. AM. GEOPHYS. UNION, 24, 432.

Medhurst, R. G. 1965, I.E.E.E. TRANS., AP-13, 550

MIE, G. 1908, Ann. Physik., 25, 377.

Robel, M. C. 1978, "Updated Attenuation - Rainfall (A-R) Relationships for MSBLS Performance Predictions", LEC-12295.

Robel, M. C. 1981, "Effects of Fog and Clouds on the Shuttle MSBLS Signal Level with Emphasis on the Occurence of Fog at VAFB", LEMSCO - 16973.

Van De Hulst, H. C. 1957, "Light Scattering by Small Particles" (New York: Wiley).

Appendix

Following is a listing of the FORTRAN computer program used for our attenuation and scattering calculations.

```
      IMPLICIT COMPLEX(Y,Z)
      DIMENSION ZA(30),ZB(30),ZAN(30),ZBN(30)
      DIMENSION P(30),T(30),D(36),ANG(36)
      DIMENSION ZS1(36,12),ZS2(36,12),S(36,12),S1AS(36,12)
      DIMENSION S2AS(36,12),ANGL(12)
      DIMENSION DL(12),XN(12),QSCA(12),QEXT(12),QBK(12),QABS(12)
      DATA DL/.05,.1,.15,.2,.25,.3,.35,.4,.45,.5,.55,.6/
      I=1
      MM=36
      PI=3.14159265
      TP360=2.*PI/360.
      DO 1 M=1,MM
      ANG(M)=10.*(M-1)
      D(M)=ANG(M)*TP360
    1 CONTINUE
  800 CONTINUE
      WRITE(6,110)
  110 FORMAT('   ENTER NUMBER OF TERMS (NN)')
      READ(5,120)NN
  120 FORMAT()
      WRITE(6,130)
  130 FORMAT('   RAIN, LANDFOG, SEAFOG, OR CLOUDS? (0,1,2,3)')
      READ(5,120)NRFC
      WRITE(6,140)
  140 FORMAT('   ENTER WAVELENGTH (CM)')
      READ(5,120)W
      WRITE(6,150)
  150 FORMAT('   ENTER COMPLEX REFRACTIVE INDEX (A,B)')
      READ(5,120)Z1
      WRITE(6,210)
  210 FORMAT('   ENTER PATH LENGTH (KM)')
      READ(5,120)PL
      IF(NRFC.EQ.1)GO TO 20
      IF(NRFC.EQ.2)GO TO 30
      IF(NRFC.EQ.3)GO TO 40
      WRITE(6,160)
  160 FORMAT('   ENTER RAINFALL RATE (MM/HR)')
      READ(5,120)RR
      WRITE(6,230)
  230 FORMAT('   SINGLE SIZE OR DISTRIBUTION? (0,1)')
      READ(5,120)NS
      IF(NS.EQ.1)GO TO 820
      WRITE(6,170)
  170 FORMAT('   ENTER PARTICLE DIAMETER (MM)')
      READ(5,120)DM
      DM=DM/10.
      DIAM=DM
      GO TO 820
   20 WRITE(6,180)
  180 FORMAT('   ENTER VISIBILITY OF LANDFOG (KM)')
      READ(5,120)VIS
      GO TO 820
```

```
 30   WRITE(6,190)
190   FORMAT('   ENTER VISIBILITY OF SEAFOG (KM)')
      READ(5,120)VIS
      IF(VIS.LT.0.1)GO TO 20
      GO TO 820
 40   WRITE(6,200)
200   FORMAT('   ENTER VISIBILITY OF CLOUDS (KM)')
      READ(5,120)VIS
820   CONTINUE
      DO 70 I=1,12
      DM=DL(I)
      CALL SIZE(RR,DM,XN,I)
      IF(NS.EQ.0)DM=DIAM
      IF(NREC.EQ.1)DM=1.E-03
      IF(NREC.EQ.2)DM=2.E-03
      IF(NREC.EQ.3)DM=1.E-03
      X=PI*DM/W
      Y=Z1*X
      CALL ZACALC(Y,ZA,NN)
      CALL ZBCALC(X,ZB,ZBO,NN)
      CALL ABCALC(ZA,ZB,ZBO,Z1,X,ZAN,ZBN,NN)
      CALL QCALC(X,ZAN,ZBN,QSCA,QEXT,QBK,QABS,NN,I)
      CALL ANGCAL(X,ZAN,ZBN,QSCA,ANGL,NN,I)
      DO 2 M=1,MM
      CALL PTCALC(D,P,T,M,NN)
      CALL SCOMP(W,ZAN,ZBN,P,T,ZS1,ZS2,S,PI,M,NN,S1AS,S2AS,I)
 2    CONTINUE
 70   CONTINUE
      IF(NREC.EQ.1)GO TO 4
      IF(NREC.EQ.2)GO TO 5
      IF(NREC.EQ.3)GO TO 6
      IF(NS.EQ.1)GO TO 71
      CALL RAIN(RR,PL,QEXT,DM,ATN,ATNDB,I)
      GO TO 7
 71   CONTINUE
      CALL RAINXN(RR,PL,QEXT,DL,ATN,ATNDB,XN)
      GO TO 7
 4    CALL LNDFOG(DM,VIS,PL,QEXT,ATN,ATNDB,I)
      GO TO 7
 5    IF(VIS.LT.0.1)GO TO 4
      CALL SEAFOG(DM,VIS,PL,QEXT,ATN,ATNDB,I)
      GO TO 7
 6    CALL CLOUDS(DM,VIS,PL,QEXT,ATN,ATNDB,I)
 7    CONTINUE
      WRITE(6,120)PL,ATN,ATNDB
      WRITE(6,220)
220   FORMAT('   REPEAT? (1=YES,0=NO)',/)
      READ(5,120)NREP
      IF(NREP.EQ.1)GO TO 800
999   CONTINUE
      CALL EXIT
      END
```

```
      SUBROUTINE SIZE(RR,DM,XN,I)
      DIMENSION X1(10),X2(10),X3(10),X4(10),X5(10),X6(10),X7(10)
      DIMENSION XA(10),XB(10),R(7),CUT(7),XN(12)
      DATA X1/3.90906,-1.2236E02,1.6357E03,-5.13497E03,
     15.4409E03,-1.463E03,0.,0.,0.,0./
      DATA X2/-1.5255E01,6.38345E02,-9.14623E03,6.9662E04,
     1-2.69783E05,5.42977E05,-5.45427E05,2.16777E05,0.,0./
      DATA X3/-9.9461,5.81251E02,-1.2434E04,1.38727E05,
     1-7.68E05,2.29E06,-3.7841E06,3.27524E06,-1.161E06,0./
      DATA X4/2.3709E01,-9.8352E02,1.42472E04,-7.68455E04,
     11.91541E05,-2.25279E05,1.01277E05,0.,0.,0./
      DATA X5/6.5918E01,-2.8817E03,4.53181E04,-3.10239E05,
     11.10129E06,-2.13855E06,2.16497E06,-8.9636E05,0.,0./
      DATA X6/1.E02,-4.8157E03,8.63391E04,-6.93122E05,
     12.90943E06,-6.68496E06,7.98558E06,-3.88423E06,0.,0./
      DATA X7/-5.4314E01,1.72908E03,-1.14533E04,2.79273E04,
     1-2.29091E04,0.,0.,0.,0.,0./
      DATA R/150.,100.,50.,25.,12.5,5.,2.5/
      DATA CUT/.53,.58,.53,.53,.48,.48,.38/
      IF(RR.GE.150.)GO TO 1
      IF(RR.LE.2.5)GO TO 4
      IF(RR.LT.150..AND.RR.GE.100.)GO TO 7
      IF(RR.LT.100..AND.RR.GE.50.)GO TO 11
      IF(RR.LT.50..AND.RR.GE.25.)GO TO 14
      IF(RR.LT.25..AND.RR.GE.12.5)GO TO 17
      IF(RR.LT.12.5.AND.RR.GE.5.)GO TO 20
      IF(RR.LT.5..AND.RR.GT.2.5)GO TO 23
1     DO 2 K=1,10
      XA(K)=X1(K)
2     CONTINUE
      CT=CUT(1)
6     XN(I)=0.
      DO 3 K=1,10
      XN(I)=XN(I)+XA(K)*DM**(K-1)
      IF(DM.GE.CT)XN(I)=0.
3     CONTINUE
      GO TO 999
4     DO 5 K=1,10
      XA(K)=X7(K)
5     CONTINUE
      CT=CUT(7)
      GO TO 6
7     A=150.
      B=100.
      DO 8 K=1,10
      XA(K)=X1(K)
      XB(K)=X2(K)
8     CONTINUE
      GO TO 50
11    A=100.
      B=50.
      CT=CUT(2)
```

```
53:        DO 9 K=1,10
54:        XA(K)=X2(K)
55:        XB(K)=X3(K)
56:  9     CONTINUE
57:        GO TO 50
58:  14    A=50.
59:        B=25.
60:        CT=CUT(3)
61:        DO 15 K=1,10
62:        XA(K)=X3(K)
63:        XB(K)=X4(K)
64:  15    CONTINUE
65:        GO TO 50
66:  17    A=25.
67:        B=12.5
68:        CT=CUT(4)
69:        DO 18 K=1,10
70:        XA(K)=X4(K)
71:        XB(K)=X5(K)
72:  18    CONTINUE
73:        GO TO 50
74:  20    A=12.5
75:        B=5.
76:        CT=CUT(5)
77:        DO 21 K=1,10
78:        XA(K)=X5(K)
79:        XB(K)=X6(K)
80:  21    CONTINUE
81:        GO TO 50
82:  23    A=5.
83:        B=2.5
84:        CT=CUT(6)
85:        DO 24 K=1,10
86:        XA(K)=X6(K)
87:        XB(K)=X7(K)
88:  24    CONTINUE
89:  50    CONTINUE
90:        XN1=0.
91:        XN2=0.
92:        DO 51 K=1,10
93:        XN1=XN1+XA(K)*DM**(K-1)
94:        XN2=XN2+XB(K)*DM**(K-1)
95:        IF(DM.GE.CT)XN1=0.
96:        IF(DM.GE.CT)XN2=0.
97:  51    CONTINUE
98:        S=(XN1-XN2)/(A-B)
99:        XN(I)=XN2+S*(RR-B)
100:  999  CONTINUE
101:       RETURN
102:       END
```

```
      SUBROUTINE ABCALC(ZA,ZB,ZBO,Z1,X,ZAN,ZBN,NN)
      IMPLICIT COMPLEX(Y,Z)
      DIMENSION ZA(30),ZB(30),ZAN(30),ZBN(30),ZXA(30),ZXB(30)
      DO 1 N=1,NN
      ZXA(N)=ZA(N)/Z1+N/X
      ZXB(N)=Z1*ZA(N)+N/X
1     CONTINUE
      ZAN(1)=(ZXA(1)*REAL(ZB(1))-REAL(ZBO))/(ZXA(1)*ZB(1)-ZBO)
      ZBN(1)=(ZXB(1)*REAL(ZB(1))-REAL(ZBO))/(ZXB(1)*ZB(1)-ZBO)
      DO 2 N=2,NN
      ZAN(N)=(ZXA(N)*REAL(ZB(N))-REAL(ZB(N-1)))/(ZXA(N)*ZB(N)-ZB(N-1)
      ZBN(N)=(ZXB(N)*REAL(ZB(N))-REAL(ZB(N-1)))/(ZXB(N)*ZB(N)-ZB(N-1
2     CONTINUE
      RETURN
      END
```

```
      SUBROUTINE ZACALC(Y,ZA,NN)
      IMPLICIT COMPLEX(Y,Z)
      DIMENSION ZA(30)
      ZA0=CCOS(Y)/CSIN(Y)
      ZA(1)=-1/Y+1/(1/Y-ZA0)
      DO 1 N=2,NN
      ZA(N)=-N/Y+1/(N/Y-ZA(N-1))
1     CONTINUE
      RETURN
      END
```

```
      SUBROUTINE ZBCALC(X,ZB,ZBO,NN)
      IMPLICIT COMPLEX(Y,Z)
      DIMENSION ZB(30)
      ZBO=CMPLX(SIN(X),COS(X))
      ZBM=CMPLX(COS(X),-SIN(X))
      ZB(1)=ZBO/X-ZBM
      ZB(2)=ZB(1)*3/X-ZBO
      DO 1 N=3,NN
      ZB(N)=(2*N-1)*ZB(N-1)/X-ZB(N-2)
1     CONTINUE
      RETURN
      END
```

```
      SUBROUTINE SCOMP(U,ZAN,ZBN,P,T,ZS1,ZS2,S,PI,M,NN,S1AS,S2AS,I)
      IMPLICIT COMPLEX(V,Z)
      DIMENSION ZAN(30),ZBN(30),P(30),T(30),ZS1(36,12),ZS2(36,12)
      DIMENSION S(36,12),S1AS(36,12),S2AS(36,12)
      ZS1(M,I)=0.
      ZS2(M,I)=0.
      DO 1 N=1,NN
      ZS1(M,I)=ZS1(M,I)+(2*N+1)*(ZAN(N)*P(N)+ZBN(N)*T(N))/(N*(N+1))
      ZS2(M,I)=ZS2(M,I)+(2*N+1)*(ZBN(N)*P(N)+ZAN(N)*T(N))/(N*(N+1))
    1 CONTINUE
      S(M,I)=.5*(.5*U/PI)**2*(CABS(ZS1(M,I))**2+CABS(ZS2(M,I))**2)
      S1AS(M,I)=CABS(ZS1(M,I))**2
      S2AS(M,I)=CABS(ZS2(M,I))**2
      RETURN
      END
```

```
      SUBROUTINE RAIN(RR,PL,QEXT,DM,ATN,ATNDB,I)
      DIMENSION VA(6),QEXT(12)
      DATA VA/-.02366,47.38,-81.568,38.94,26.056,-21.696/
      V=0.
      DO 1 K=1,6
      V=V+VA(K)*DM**(K-1)
    1 CONTINUE
      ATN=EXP(-RR*PL*QEXT(I)/(24.*V*DM))
      ATNDB=10.*ALOG10(ATN)
      RETURN
      END
```

```
      SUBROUTINE RAINXN(RR,PL,QEXT,DL,ATN,ATNDB,XN)
      DIMENSION DL(12),QEXT(12),V(12),XN(12),QNVD(12)
      DIMENSION VA(6)
      DATA VA/-.02366,47.38,-81.568,38.94,26.056,-21.696/
      SUM=0.
      DO 2 J=1,12
      V(J)=0.
      DO 1 K=1,6
      V(J)=V(J)+VA(K)*DL(J)**(K-1)
    1 CONTINUE
    2 CONTINUE
      DO 6 J=1,12
      XN(J)=XN(J)/100.
    6 CONTINUE
      DO 3 J=1,12
      QNVD(J)=QEXT(J)*XN(J)/(V(J)*DL(J))
    3 CONTINUE
      DO 4 J=1,12
      SUM=SUM+QNVD(J)
    4 CONTINUE
      POW=PL*RR*SUM/24.
      ATN=EXP(-POW)
      ATNDB=10.*ALOG10(ATN)
  120 FORMAT()
      RETURN
      END
```

```
      SUBROUTINE QCALC(X,ZAN,ZBN,QSCA,QEXT,QBK,QABS,NN,I)
      IMPLICIT COMPLEX(Y,Z)
      DIMENSION ZAN(30),ZBN(30)
      DIMENSION QSCA(12),QEXT(12),QBK(12),QABS(12)
      SUM1=0.
      SUM2=0.
      ZSUM3=0.
      DO 1 N=1,NN
      SUM1=SUM1+(2*N+1)*(CABS(ZAN(N))**2+CABS(ZBN(N))**2)
      SUM2=SUM2+(2*N+1)*REAL(ZAN(N)+ZBN(N))
      ZSUM3=ZSUM3+(N+.5)*(-1)**N*(ZAN(N)-ZBN(N))
    1 CONTINUE
      QSCA(I)=2.*SUM1/X**2
      QEXT(I)=2.*SUM2/X**2
      QBK(I)=4.*CABS(ZSUM3)**2/X**2
      QABS(I)=QEXT(I)-QSCA(I)
      RETURN
      END
```

```
      SUBROUTINE ANGCAL(X,ZAN,ZBN,QSCA,ANGL,NN,I)
      IMPLICIT COMPLEX(Y,Z)
      DIMENSION ZAN(30),ANGL(12),QSCA(12),ZBN(30)
      ANGL=0.
      DO 1 N=1,NN
      ANGL(I)=ANGL(I)+N*(N+2)/(N+1)*REAL(CONJG(ZAN(N))*ZAN(N+1)+
     1CONJG(ZBN(N))*ZBN(N+1))+(2*N+1)/(N*(N+1))*
     2REAL(CONJG(ZAN(N))*ZBN(N))
    1 CONTINUE
      ANGL(I)=ANGL(I)*4./X**2
      ANGL(I)=ANGL(I)/QSCA(I)
      RETURN
      END
```

```
      SUBROUTINE PTCALC(D,P,T,M,NN)
      DIMENSION P(30),T(30),D(36)
      E=COS(D(M))
      G=SIN(D(M))*SIN(D(M))
      P0=0.
      T0=0.
      P(1)=1.
      T(1)=E
      P(2)=3.*E
      T(2)=3.*COS(2.*D(M))
      DO 1 N=3,NN
      P(N)=P(N-1)*E*(2*N-1)/(N-1)-N*P(N-2)/(N-1)
      T(N)=E*(P(N)-P(N-2))-(2*N-1)*G*P(N-1)+T(N-2)
    1 CONTINUE
      RETURN
      END
```

```
1:      SUBROUTINE LNDFOG(DM,VIS,PL,QEXT,ATN,ATNDB,I)
2:      DIMENSION QEXT(12)
3:      C=4.98E-04
4:      ATN=EXP(-C*PL*QEXT(I)*VIS**(-1.538)/DM)
5:      ATNDB=10.*ALOG10(ATN)
6:      RETURN
7:      END
```

```
1:      SUBROUTINE SEAFOG(DM,VIS,PL,QEXT,ATN,ATNDB,I)
2:      DIMENSION QEXT(12)
3:      C=2.34E-03
4:      ATN=EXP(-C*PL*QEXT(I)*VIS**(-1.43)/DM)
5:      ATNDB=10.*ALOG10(ATN)
6:      RETURN
7:      END
```

```
1:      SUBROUTINE CLOUDS(DM,VIS,PL,QEXT,ATN,ATNDB,I)
2:      DIMENSION QEXT(12)
3:      C=4.98E-04
4:      ATN=EXP(-C*PL*QEXT(I)*VIS**(-1.538)/DM)
5:      ATNDB=10.*ALOG10(ATN)
6:      RETURN
7:      END
```

1981 NASA-ASEE SUMMER FACULTY RESEARCH FELLOWSHIP PROGRAM

AT

NASA JOHNSON SPACE CENTER

ANTHROPOMETRIC DATA ERROR DETECTION AND CORRECTION WITH A COMPUTER

FACULTY FELLOW: David D. Chesak, Ph.D.,P.E.
St. Joseph's College

SUPERVISORS: James L. Lewis, Jr., Ph.D.
Head, Crew Station Design Section

Michael M. Thomas
Manager, Design Performance Laboratory

Barbara J. Woolford
Manager, Anthropometric Measurements Laboratory

Crew Station Branch
Spacecraft Design Division

ACKNOWLEDGMENT

I would like to extend my thanks to my research colleagues, Barbara Woolford, Michael Thomas and James Lewis for the many considerations and kindnesses that they extended to me throughout the summer. In addition, I am grateful for the friendly cooperation of all the people at Johnson Space Center. However, my greatest affection is for two fine men and their families: Marion Hix and John Jackson. They went far beyond ordinary courtesy to make me feel comfortable and a part of the community. I will forever be in their debt.

DDC

ABSTRACT

Data obtained with automated anthropometric data acquisition equipment is subject to short term errors. These errors are due to random reflections of light, masking of the light rays and other types of interference, optical and electrical. These signals are impossible to eliminate from the initial data produced by the television cameras. There is a need to ascertain which data values are erroneous and to replace them with corrected values, if possible. This is primarily a software problem and requires a digital computer to refine the data off line. This paper discusses the use of the least squares method for this purpose.

Anthropometry has been defined as the practice of measuring the parts and proportions of the human body. In particular, NASA's interest in anthropometry arises from the need to know, quantitatively, the limits of physical performance imposed on an astronaut by a space suit at a spacecraft work station. The specific interest of this paper is the arm reach envelope of an individual as shown in Figure 1. From a simplistic standpoint, all that one would need to determine the arm reach of a subject would be a tape measure, a pad of paper for recording data and the subject in an environment of interest. As a practical matter, the time required to measure and tabulate this information becomes a significant value if a detailed picture is needed. Further, the data would need to be entered into computer files for use in work station studies.

There are techniques that involve high speed motion pictures which are projected so that the data can be extracted manually, frame by frame. This minimizes the time required of the subject but still requires extensive time for technician to collect data.

Electronic means are now available to expedite this work. An automatic anthropometric data acquisition system is in use at Johnson Space Center. The system, developed by Southwest Research Institute of San Antonio, TX. utilizes three modified television cameras in conjunction with a microprocessor controlled interface unit and a Digital Equipment Corporation (DEC) MINC-11 minicomputer. (See figure 2.) The interface unit is synchronized with the television cameras and determines the coordinates of a bright light source as it appears in the televised picture. The minicomputer stores the coordinate data on a floppy disk in a format that is acceptable to the mainframe computer in the Data Processing Laboratory. The large computer, using the PLAID program,

generates the human subject's arm reach envelope and displays it on a video monitor or draws it on a sheet of paper on a plotter. (See figure 3.) The reach data files are also available for work station design studies.

One of the difficulties with the television aided system is that errors occur in the data acquisition process. A small light bulb is attached to the arm of the person on whom reach data is desired. In the darkened room, the television cameras can easily pick up the bright point of light. The two principal sources of error are due to reflections of the light from surrounding objects and due to the subject inadvertantly blocking the camera's view of the light. In the latter case, the computer enters zeros into the data set when a particular camera fails to receive an image of the light. A third type of error, much less in evidence, can be most reasonably ascribed to electrical interference coming from sources external to the system. This type of disturbance, in so far as data correction is concerned, is treated in the same fashion as are unwanted light reflections.

Each television camera sees only a two dimensional view of the subject. Thus a minimum of two cameras would be required to gain the information needed for determining a three dimensional reach envelope. Three cameras, viewing the back, side and front of the subject, provide some data redundancy so that even though one unit may not provide correct data, another may supply it. All three cameras shown in figure 2 are capable of indicating the vertical displacement of the light. The front and back cameras both can provide side to side motion data. However, only the side viewing camera can determine back and forth motion. Thus while some positional errors can be detected by comparing similar data points, this has limited potential. Other measures must be taken.

The approach that seems to hold the greatest promise is based on the fact that the subject cannot move his arms or any other part of his body at an infinite rate. That is, true motion is continuous in time and space without any sudden excursions. The type of errors that appear in the data from this system have this characteristic. They render values for position changes that are not physically possible in the short interval between sampling times.

The system is calibrated so that the horizontal and vertical coordinates are set at 256 points for each axis. Thus the actual distance represented by a unit distance either vertically or horizontally will depend on the focal length of the camera lens and the subject to camera distance. In the system used at the Johnson Space Center Anthropometric Measurements Laboratory, the height and width of the field viewed is about 2 meters. Thus one unit change in a data value represents .78 cm in actual displacement. Since a camera is polled 20 times per second, the time between two consecutive data values is 50 milliseconds. Thus if two consecutive data values show a change of 50 units, this represents a speed of 8 m/sec. Since most measurements are made with slow subject motion, a 50 unit change reflects an error and not actual displacement. If, to further belabor the point, the actual speed during the previous interval had been 1 m/sec. and the data indicated a speed of 8 m/sec. in the following interval, this sudden velocity increase would require an approximate acceleration of 140 m/sec. ^{2}. The force required to move one's hand with this acceleration is quite beyond human capability.

Having established the point that a subject will move in a continuous, uniform manner, how do we not only detect abrupt changes in data values with the computer but also make good approximations of what the values actually were? The approach

used here fits an equation to a limited number of data points adjacent to the value in question. A predicted value is determined and compared to the suspect value. If the difference is greater than a predetermined tolerance, the original value is replaced with the predicted value. The program then advances to the next new data point and repeats the above testing procedure.

Using the least squares curve fitting technique, straight line and parabolic approximations have been used for the predictive equation. Ostensibly, the parabolic curve should provide a better fit than the straight line. However, computational instability has been found to occur more frequently with a second degree polynomial equation where the gaps due to erroneous data are large and the adjacent valid data points are subject to moderate, random error or "noise". Thus the straight line approximation based on a few data points is felt to be the better choice.

An additional constraint that has been placed on this development of an algorithm for error correction is that it is to be eventually used with a microcomputer of limited speed and memory. Thus the method should be straight forward and amenable to machine language coding.

The development of the least squares error method of curve fitting will not be discussed here since it is found in most texts on elementary numerical analysis. The interested reader may find an article by F. R. Ruckdeschel helpful.(1) A more thorough treatment is offered by C. Daniel and F.S. Wood.(2)

A modification to the measuring technique is suggested. All three cameras are physically situated in a plane parallel to the floor. This means that the vertical displacement is measured by all three cameras. One horizontal axis is monitored by two of the cameras and the other horizontal axis is seen by only one. Thus when the latter camera has its view blocked by subject motion, then the information from the other two cameras is not useful. All three measurements are required.

The recommendation is that two of the cameras be kept in the present position viewing the front and side of the subject but the third camera should be placed so that it has an overhead view. This would mean that each of the three coordinates would have double redundancy. Loss of view of the light by the cameras is one of the major problems in using the system. Since ceiling height is not great in the laboratory, either a wide angle lens could be fitted to the overhead camera or else a large mirror could be positioned overhead and the third camera could be placed in a more convenient position.

An alternative scheme would be to use a fourth camera that could be under the control of the microprocessor and its output could be used in place of that of the camera that has its view blocked.

BIBLIOGRAPHY

(1) Ruckdeschel, Fred R., "Curve Fitting with Your Computer," BYTE magazine, October 1979

(2) Daniel, Cuthbert and Wood, Fred S., "Fitting Equations to Data," John Wiley, 1971

Anthropometric Measurement System

Orthogonal Reach Planes

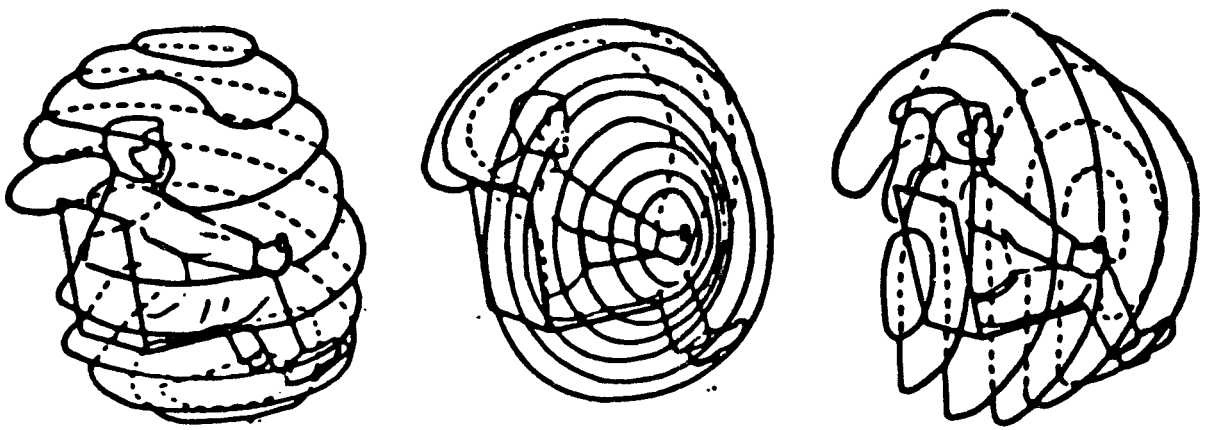

FIGURE 1

HIGH SPEED AI D SYSTEM

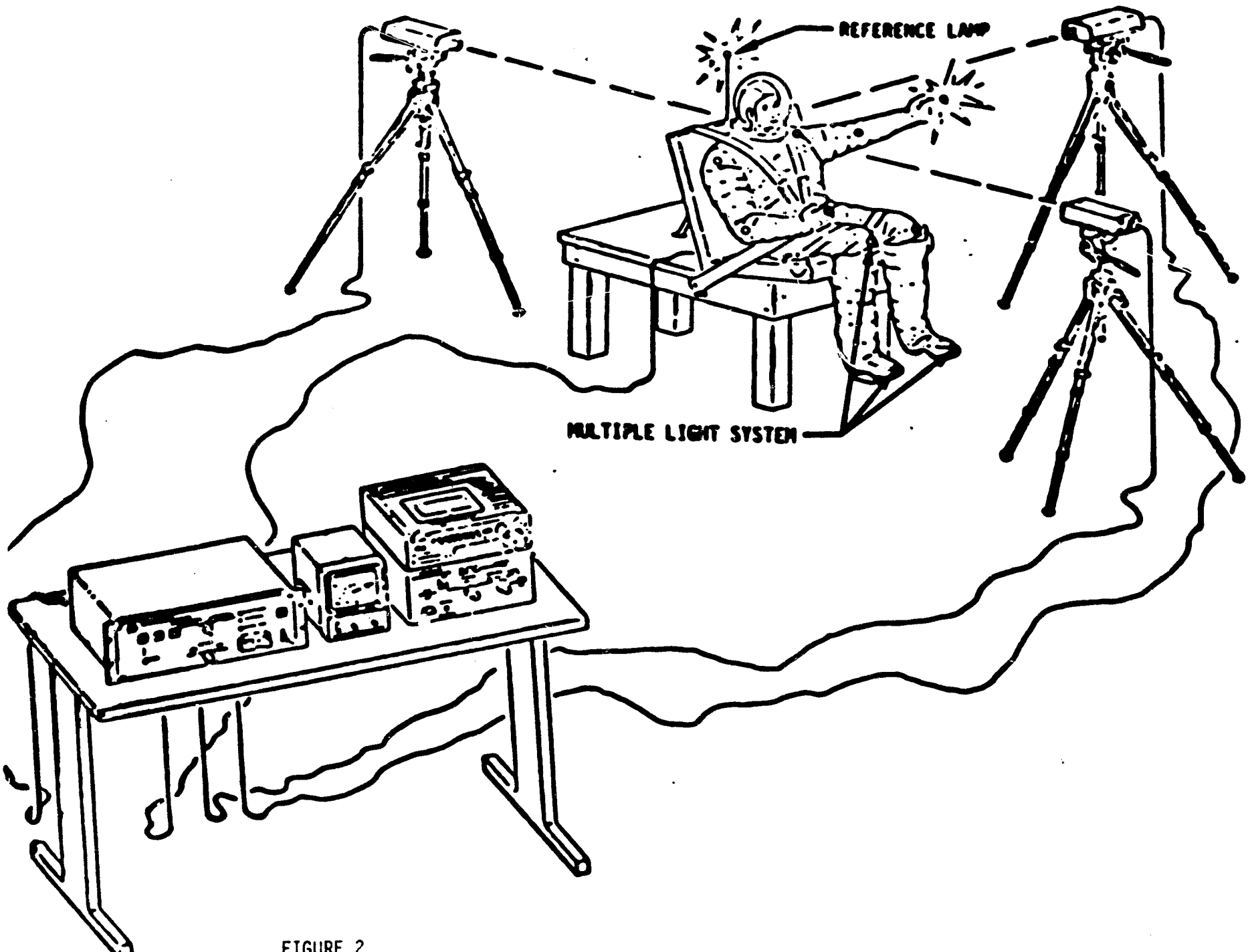

FIGURE 2

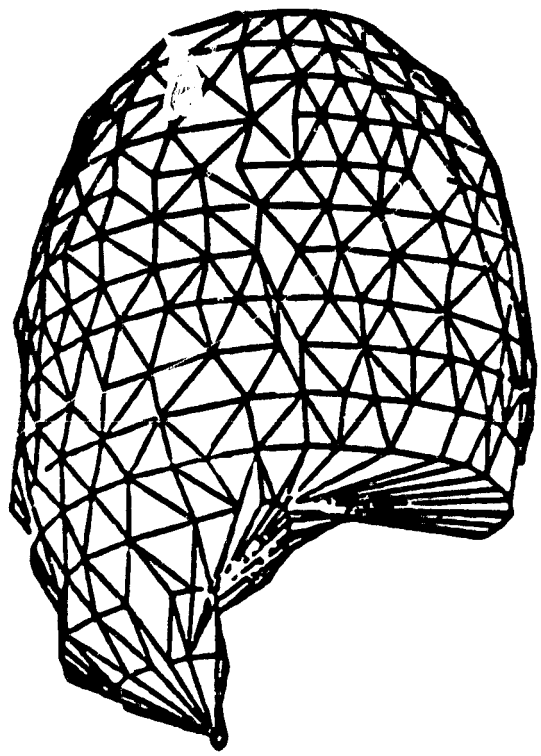

RIGHT ARM REACH STEREOSPHERE FROM NASA PLAID SOFTWARE

FIGURE 3

USE OF LANDSAT DATA TO DEFINE SOIL BOUNDARIES IN CARROLL COUNTY, MISSOURI

Steve E. Davidson, Ph. D.
Evangel College, Springfield, MO
1981 NASA-ASEE Summer Faculty Fellow

Supervisor: Dr. David R. Thompson
Scene Analysis Branch
Earth Resources Research Division

Abstract:

Bands 4,5 and 7 false color composite photographs were prepared using multitemporal data from LANDSAT scenes acquired during April 1977 and April 1981 on computer compatible tapes, and these color composites were compared with band 7 black and white photographs prepared for the entire county. Delineations of soil boundaries at the soil association level were achieved using LANDSAT spectral reflectance data and slope maps for a portion of Carroll County, Missouri. Forty two spectral reflectance classes from April 1977 LANDSAT data were overlaid on digitized slope maps of nine USGS 7.5 minute series topographic quadrangle slope maps to achieve boundary delineations of the soil associations.

ACKNOWLEDGEMENTS

Appreciation is expressed to the following for their support and encouragement during this project.

(i) Dr. William McFarland of the Geographic Resources Center in Columbia, Missouri who suggested the project and provided technical support with the PDP 11/50 computer system.

(ii) Dr. David R. Thompson at Johnson Space Center, National Aeronautics and Space Administration who served as research supervisor and arranged for access to the G.E. Image 100 computer system.

(iii) Bruce Thompson, Missouri state soil scientist in the state SCS office at Columbia, Missouri who assisted in field study of the soils in Carroll County, Missouri.

(iiii) John Baker, SCS party leader for Carroll County who assisted in field study of the soils in Carroll County and helped in decisions concerning the placement of soil association boundaries.

INTRODUCTION

A need exists in the state of Missouri to use LANDSAT data to aid in Soil Survey mapping. The Missouri Department of Natural Resources has responsibility for conservation programs in the state and is committed to accelerating the National Cooperative Soil Survey Program. Research to date has shown strong correlation between the spectral reflectance characteristics of soils and some of the soil properties such as texture, organic matter content, drainage, color, etc. While LANDSAT classification of soils will not alone distinguish between different soils which exhibit similar spectral signatures, it is possible to prepare a product which will aid the soil mapping process by delineating patterns, and possible divisions of soil associations.

A party leader has been assigned by the state soil scientist of Missouri to begin mapping this summer a progressive soil survey of Carroll County, Missouri and Saline county, Missouri next year. The state soil scientist has indicated that it would be of considerable value to the party leader if he could be provided maps based on LANDSAT analysis to help in the progressive soil surveys of Carroll and Saline counties, Missouri. Approximately two thirds of Missouri still needs a detailed county soil survey to assist land managers in their decisions. A recent letter from the state conservationist of Indiana to the state conservationist of Missouri indicated that the detailed County Soil Survey of Jasper County, Indiana was completed with a savings of 1½ man-years time. Since the Missouri Department of Natural Resources would like to complete in the 1980-1990 time frame modern

detailed county soil survey reports for the entire state it appears that LANDSAT analysis to aid in soil survey mapping would help them to acheive this worthwhile goal.

Study Area

Carroll County, Missouri was selected as the study site because (i) preparations are underway to procure 7.5 minute USGS orthophotoquads for use as a base for conducting a detailed soil survey of this county by the party leader, (ii) this county contains more Missouri River bottomland than any county in the state (4), (iii) and the large tracts of farmland in the bottomlands are more likely to show relationships with the LANDSAT spectral reflectance data than land subdivided into smaller units.

Carroll County, Missouri is situated in the northwestern part of the state, 66 miles east of Kansas City and 211 miles northwest of St. Louis. It is bounded on the north by Livingston County, on the west by Caldwell and Ray Counties, and is separated from Saline and Lafayette Counties on the south by the Missouri River and from Chariton County on the east by the Grand River. It has an area of 703 square miles with 449,920 acres in the county. The last Carroll County soil survey published was in 1912 (4). A soil survey of Livingston County was published in 1956 (3), one for Caldwell County was published in 1974 (1), one for Lafayette County was published in 1975 (2), and a soil inventory of Chariton County from digital analysis of satellite and scanner data was published in the Soil Science Society of America Journal in 1977 (5). These publications were useful as indicators of the soil series to be expected in Carroll County. The soils of the

area formed in deep loess and glacial till in the uplands and in alluvial sediments in the floodplains.

Data Set Formulation

LANDSAT-2 MSS data collected on 26 April 1977 were utilized as the main data source for this study and LANDSAT-2 MSS data collected 23 April 1981 were utilized to prepare band 7 Polaroid photographs of Carroll County. These scenes were selected because the data were (i) of high quality, (ii) acquired when most row crop cropland is in a bare soil state, and (iii) free of interfering atmospheric and surface conditions (i.e., clouds, haze, saturated soils, and standing water.)

The LANDSAT MSS data were geometrically corrected (i.e., rotated, deskewed, and rescaled to an approximate scale of 1:24,000.) That portion of the scene containing the eastern part of Carroll County (Big Creek and Hurricane Creek Watersheds) were selected for further preprocessing. These data were registered to ground control points selected from USGS 7.5 minute topographic quadrangles. This procedure produced a data set of an exact scale of 1:24,000 and registered geographic points in the data to their exact ground position. Using these same quadrangles slope maps produced by USGS were digitized and subsequently overlaid and registered to the LANDSAT data. Six physiographic position boundaries (water, Bottomlands, 0-5% slopes, 5-9% slopes, 9-14% slopes, and greater than 14% slopes) were digitized and overlaid on the LANDSAT-2 data for the April 1977 scene. Forty two spectral reflectance values were obtained as an overlay and a computer

printout obtained for each of the six physiographic boundaries.

Methods

Topographic data (e.g., physiographic position) were used to delineate boundaries at the soil association level, and was helpful in separating soils which were spectrally similar but genetically different. Alphanumeric 1:24,000 spectral maps representing the 42 classes inventoried were produced for the following 9 quadrangles: Coloma, Tina, Hale, Bogard, Standish, Bosworth, Brunswick West, Carrollton East, Miami Station. Comparisons were made between the maps produced by this technique and the soil association boundaries observed for the adjacent counties of Lafayette and Caldwell.

Color infrared photographs were obtained from the photographic services laboratory of JSC/NASA at Houston, Texas for mission 213 which included the portion of the Missouri River basin that forms the southern boundary of Carroll County. Attempts were made to relate colors and tonal differences in the photographs to the published soil survey of Lafayette County which contains an aerial photographic base and compare these tones with similar features across the River in Carroll County. A portion of the bottomland was enlarged to an approximate scale of 1:24,000 using LANDSAT-2 data and the General Electric Image 100 system in the Scene Analysis Branch of the Earth Resources Research Division at JSC/NASA. This enlargement was subsequently photographed with the Color Polaroid Camera device so that individual pixels were readily visible and could be compared to tonal differences seen in the Color Infrared Photographs of Mission 213

which was filmed 11 September 1972.

Results and Discussion

The 42 spectral reflectance classes contained within the inventory of Carroll County are shown in Table 1 for bands 5 and 7 with the character that was printed on a line printer for the 6 physiographic boundaries. Table 2 shows the soil association that were predicted using these data. Table 3 provides information about the taxonomic characteristics of these soil series, and the parent materials of the soils.

The Haynie-Leta-Waldron soil association is found only in the Missouri River bottomlands. The Kennebec-Nodaway-Colo-Zook soils are found in the bottomlands along upland streams along with the associated Blackoar, Bremer, Booker, Moniteau, and Otter soil series. It is a relatively easy task to define the soil boundaries for these two associations using the computer line printer products, but it is more difficult to attempt separations of the upland soil associations.

The Grundy-Lagonda, the Marshall-Higginsville-Macksburg, and the Knox-Marshall-Kennebec are upland soil associations. These associations could not be delineated using the computer printouts because there is an overlap of slopes on the landscapes where these soils are found.

Digital mapping of soils using LANDSAT data is based primarily upon the surface reflectance properties of the various soils. Such distinguishing soil characteristics as parent material, profile development, and landscape position are not observable with current satellite systems.

Often widely different soils exhibit similar spectral responses and cannot be differentiated from one another using satellite data alone. However, appropriate ancillary data used in conjunction with the LANDSAT data can greatly increase the informational content of a spectral soils map.

TABLE 1

MEAN VALUE OF SPECTRAL REFLECTANCE ASSOCIATED WITH EACH CHARACTER FOR BANDS 5 and 7 FOR THE 42 CLASSES

CHARACTER	BAND 5	BAND 7
A	29	29
B	24	30
C	23	44
D	25	24
E	29	46
F	33	32
G	25	48
H	23	21
I	26	42
J	19	50
K	28	23
L	20	57
M	41	42
N	36	38
O	29	35
P	22	26
Q	45	44
R	34	46
S	26	15
T	17	13
U	25	37
V	22	50
W	21	18
X	13	2
Y	32	39
Z	32	27
1	50	47
2	56	52
3	17	16
4	19	3
5	17	67
6	18	40
7	20	22
8	19	15
9	17	55
@	18	18
#	25	11
*	24	5
¢	24	56
$	22	38
&	40	48
+	34	22

TABLE 2

PREDICTED SOIL ASSOCIATIONS IN THE QUADRANGLES OF CARROLL COUNTY

QUADRANGLE	SOIL ASSOCIATIONS
BOGARD	GRUNDY-LAGONDA* MARSHALL-HIGGINSVILLE-MACKSBURG** KENNEBEC-NODAWAY-COLO-ZOOK***
BOSWORTH	KNOX-MARSHALL-KENNEBEC**** GRUNDY-LAGONDA MARSHALL-HIGGINSVILLE-MACKSBURG KENNEBEC-NODAWAY-COLO-ZOOK
BRUNSWICK WEST	HAYNIE-LETA-WALDRON***** KNOX-MARSHALL-KENNEBEC
CARROLLTON EAST	HAYNIE-LETA-WALDRON KNOX-MARSHALL-KENNEBEC KENNEBEC-NODAWAY-COLO-ZOOK
COLOMA	GRUNDY-LAGONDA MARSHALL-HIGGINSVILLE-MACKSBURG KENNEBEC-NODAWAY-COLO-ZOOK
HALE	GRUNDY-LAGONDA MARSHALL-HIGGINSVILLE-MACKSBURG KENNEBEC-NODAWAY-COLO-ZOOK
MIAMI STATION	HAYNIE-LETA-WALDRON KNOX-MARSHALL-KENNEBEC KENNEBEC-NODAWAY-COLO-ZOOK
STANDISH	KNOX-MARSHALL-KENNEBEC GRUNDY-LAGONDA MARSHALL-HIGGINSVILLE-MACKSBURG KENNEBEC-NODAWAY-COLO-ZOOK
TINA	GRUNDY-LAGONDA MARSHALL-HIGGINSVILLE-MACKSBURG KENNEBEC-NODAWAY-COLO-ZOOK

* Other possible series: ADAIR, ARMSTER, LAMONI, LINEVILLE, SEYMOUR

** Other possible series: LESLIE, MCGIRK, MINDEN

*** Other possible series: BLACKOAR, BREMER, BOOKER, MONITEAU, OTTER

**** Other possible series: HIGGINSVILLE, MINDEN

***** Other possible series: DOCKERY, HODGE, MODALE, MYRICK, RAY, SARPY, WAUBONSIE

TABLE 3

PARENT MATERIAL AND TAXONOMIC GROUPS OF THE MAJOR SOIL SERIES FOR THE PREDICTED SOIL ASSOCIATIONS IN CARROLL COUNTY

SOIL SERIES	SOIL ORDER	SUBGROUP	PARENT MATERIALS
COLO	MOLLISOLS	CUMULIC HAPLAQUOLLS	ALLUVIUM
GRUNDY	MOLLISOLS	AQUIC ARGIUDOLLS	LOESS
HAYNIE	ENTISOLS	TYPIC UDIFLUVENTS	VERY RECENT ALLUVI
HIGGINSVILLE	MOLLISOLS	AQUIC ARGIUDOLLS	LOESS
KENNEBEC	MOLLISOLS	CUMULIC HAPLUDOLLS	ALLUVIUM
KNOX	ALFISOLS	MOLLIC HAPLUDALFS	LOESS
LAGONDA	MOLLISOLS	AQUIC ARGIUDOLLS	LOESS, GLACIAL DRI
LETA	MOLLISOLS	AQUIC FLUVENTIC HAPLUDOLLS	ALLUVIUM
MACKSBURG	MOLLISOLS	AQUIC ARGIUDOLLS	LOESS
MARSHALL	MOLLISOLS	TYPIC HAPLUDOLLS	LOESS
NODAWAY	ENTISOLS	TYPIC UDIFLUVENTS	ALLUVIUM
WALDRON	MOLLISOLS	AQUIC FLUVENTIC HAPLUDOLLS	RECENT ALLUVIUM
ZOOK	MOLLISOLS	CUMULIC HAPLAQUOLLS	CLAYEY ALLUVIUM

REFERENCES

1. Soil Survey of Caldwell County, Missouri. USDA/SCS and Missouri Agricultural Experiment Station. April 1974.

2. Soil Survey of Lafayette County, Missouri. USDA/SCS and Missouri Agricultural Experiment Station. February 1975.

3. Soil Survey of Livingston County, Missouri. USDA/SCS and Missouri Agricultural Experiment Station. December 1956.

4. Vanatta, E. S. and Davis, L. V. Soil Survey of Carroll County, Missouri. USDA and University of Missouri. 1912.

5. Weismiller, R. A., Persinger, I. D. and Montgomery, O. L. Soil inventory from digital analysis of satellite scanner and topographic data. Soil Sci. Soc. Am. J. 41:11661170. 1977.

INVESTIGATION OF A SOLID STATE POWER COMBINING ANTENNA PROPOSED FOR USE IN THE SOLAR POWER SATELLITE

Larry A. Farmer
Kansas Technical Institute
1981 NASA-ASEE Summer Faculty Fellow

Supervisor:

Dr. G. Dickey Arndt
Guidance, Navigation and
Control Analysis Branch

Abstract - An analysis of certain performance test performed on a four feed microstrip antenna and feed network. Includes frequency response with and without amplifiers, an investigation of noise threshold, phase tracking and jitter. Also, recommendations for further development of SPS power conversion modules.

NATIONAL AERONAUTICS AND SPACE ADMINISTRATION
LYNDON B. JOHNSON SPACE CENTER
HOUSTON, TEXAS
August 19, 1981

Introduction:

The purpose of this investigation is to verify certain performance criteria for a solid state power combining antenna proposed for use on the solar power satellite.

Background:

The reference system solar power satellite concept (1) was developed around the use of the Klystron as the device utilized to convert DC power produced by solar cells into microwave energy for transmission to ground based receiving antennas. The improvement in performance and reliability of modern microwave transistors offers the potential for the development of a solid state microwave power transmission system. The obvious benefits of longer life, smaller size and ease of manufacture provides adequate incentive to pursue the development of a solid state system. Under NASA sponsorship several studies have been performed to explore the potential for solid state microwave power transmission (2), (3), (4), (5). While the power handling capabilities of microwave solid state devices have improved significantly, it is generally agreed that some form of power combining will be required to attain practical levels of power in a solid state system.

The realization of efficient transmission of microwave power dictates that a low loss power combining technique be

utilized. A prototype system has been designed, fabricated and delivered to JSC under contract by the Boeing Corporation. The system incorporates a four feed microstrip antenna, a stripline antenna phasing network and provides for the integration of four transistor amplifiers. The antenna and feed network have been designed to operate in S-Band at 2.45 GHZ

The power combining technique utilized is considered to be somewhat unique in that the power combining and radiating functions occur in a single cavity (2). Each amplifier is directly coupled to the cavity via four microstrip feedlines which are mounted on a ceramic type dielectric substrate. The substrate is backed by a light weight aluminum cavity which sums the power of the four sources. On the opposite side of the substrate is mounted two radiating slots which are each fed on the ends by two narrow slot-lines. The antenna behaves like two one-half wavelength slots coupled via a common cavity, thus the radiated energy is summed to yield a single radiated phase.

The original concept is illustrated in figure 1. The foil pattern for the unit delivered to JSC contains certain design improvements and is shown in figure 2. Proper feed of the antenna requires that two of the RF inputs be 180° out of phase with the remaining two. Therefore, an important component of the antenna system is a balanced feed network that provides four 0° - 180° equal amplitude outputs. The stripline feed network consist of two 0° - 180° rat-race type hybrid circuits connected to the output of a two-way in

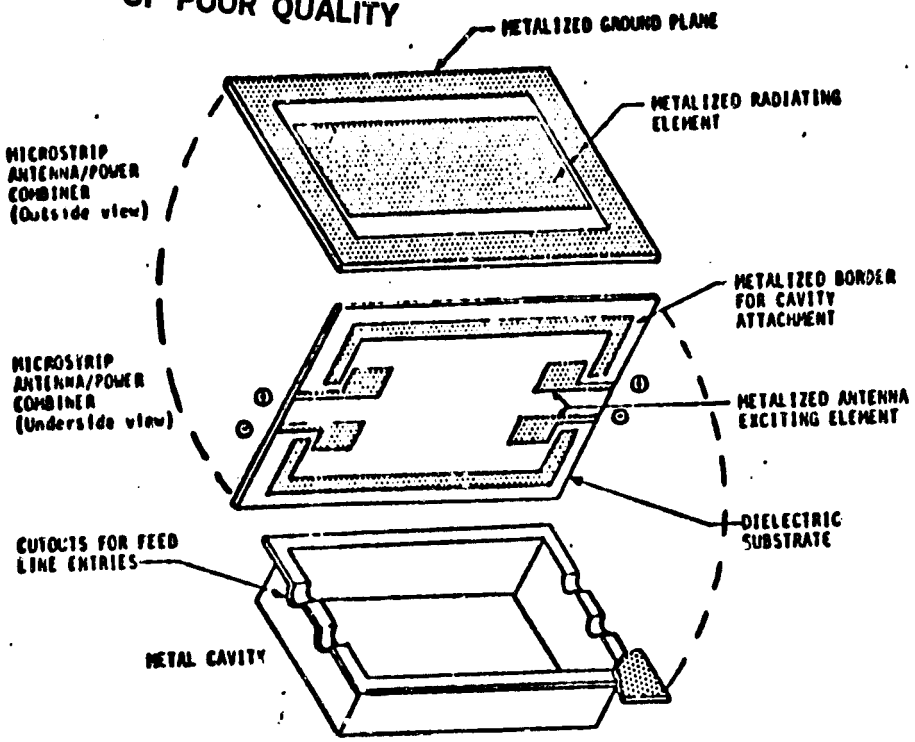

(a) BREAK-A-WAY VIEW

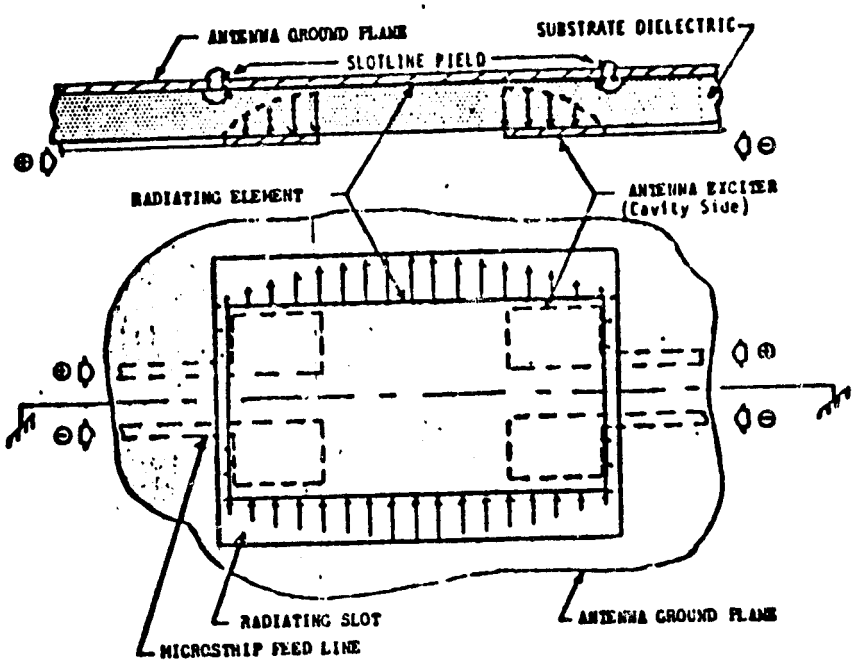

(b) "E" FIELD PROFILE

FIGURE 1 POWER COMBINING MICROSTRIP SLOTLINE ANTENNA

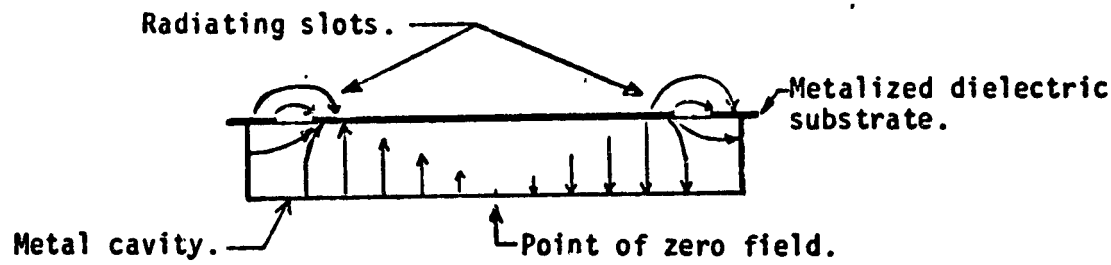

CAVITY "E" FIELD PROFILE

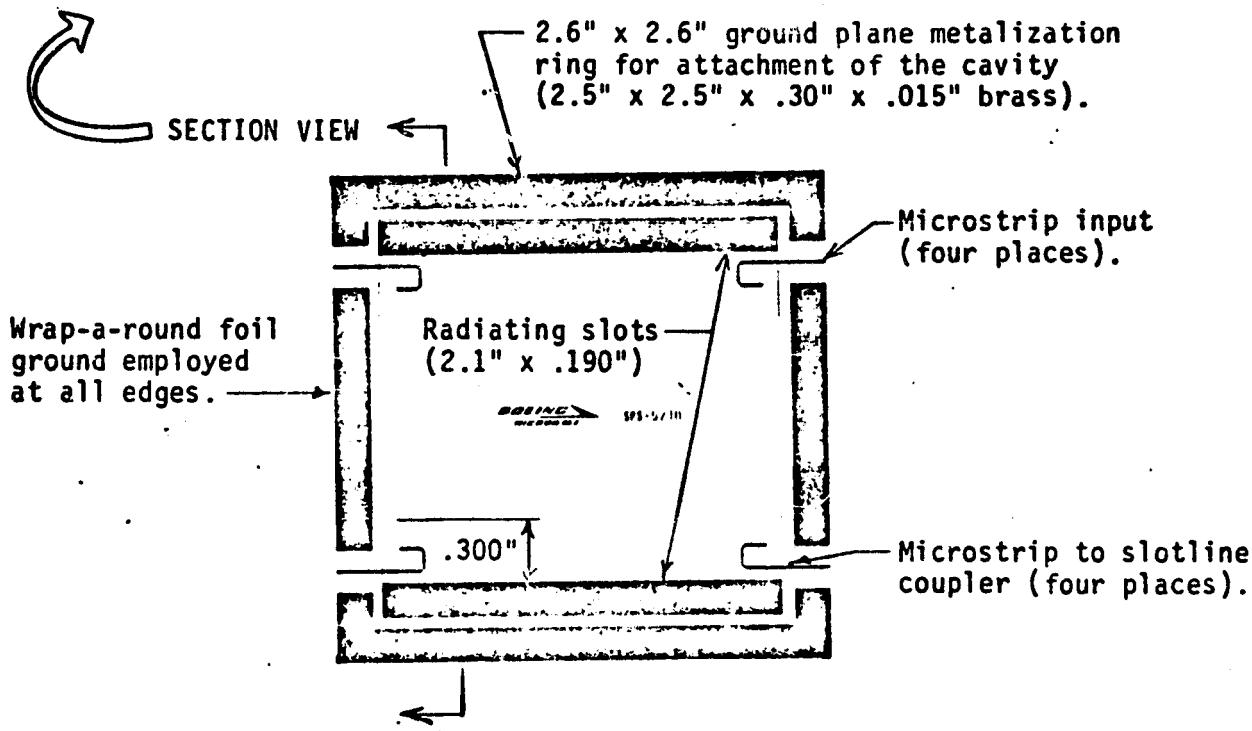

FIGURE 2. COPPER METALIZATION PATTERN FOR FOUR FEED MICROSTRIP ANTENNA (Two patterns superimposed)

phase power divider all integrated into a single stripline circuit.

The remaining elements of the test system consist of four silicon bipolar type transistor amplifiers each capable of producing 1/8 watt for a combined total of 1/2 watt.

The silicon devices were supplied as a means of testing the power combining technique. Other studies are concentrating on the development of satisfactory amplifying techniques for SPS usage (1), (3), (4), (5). The interconnection of the antenna, amplifiers and feed network is illustrated in figure 3.

The solid state antenna module has been evaluated for gain, pattern and efficiency on the antenna range with and without amplifiers by the builder. However, it was desired to obtain additional information concerning the performance of the power combining prototype. The following test were accomplished:

(1) Frequency response of the antenna and feed network with and without amplifiers over a band of frequencies ranging from 2.2 GHZ - 2.7 GHZ.

(2) SWR was determined for several frequencies.

(3) Output power of the antenna was measured with one feedline disconnected.

(4) An investigation of the noise "threshold" of the antenna and amplifier system was attempted.

(5) Phase tracking and phase jitter of the antenna feed network and amplifier system was measured.

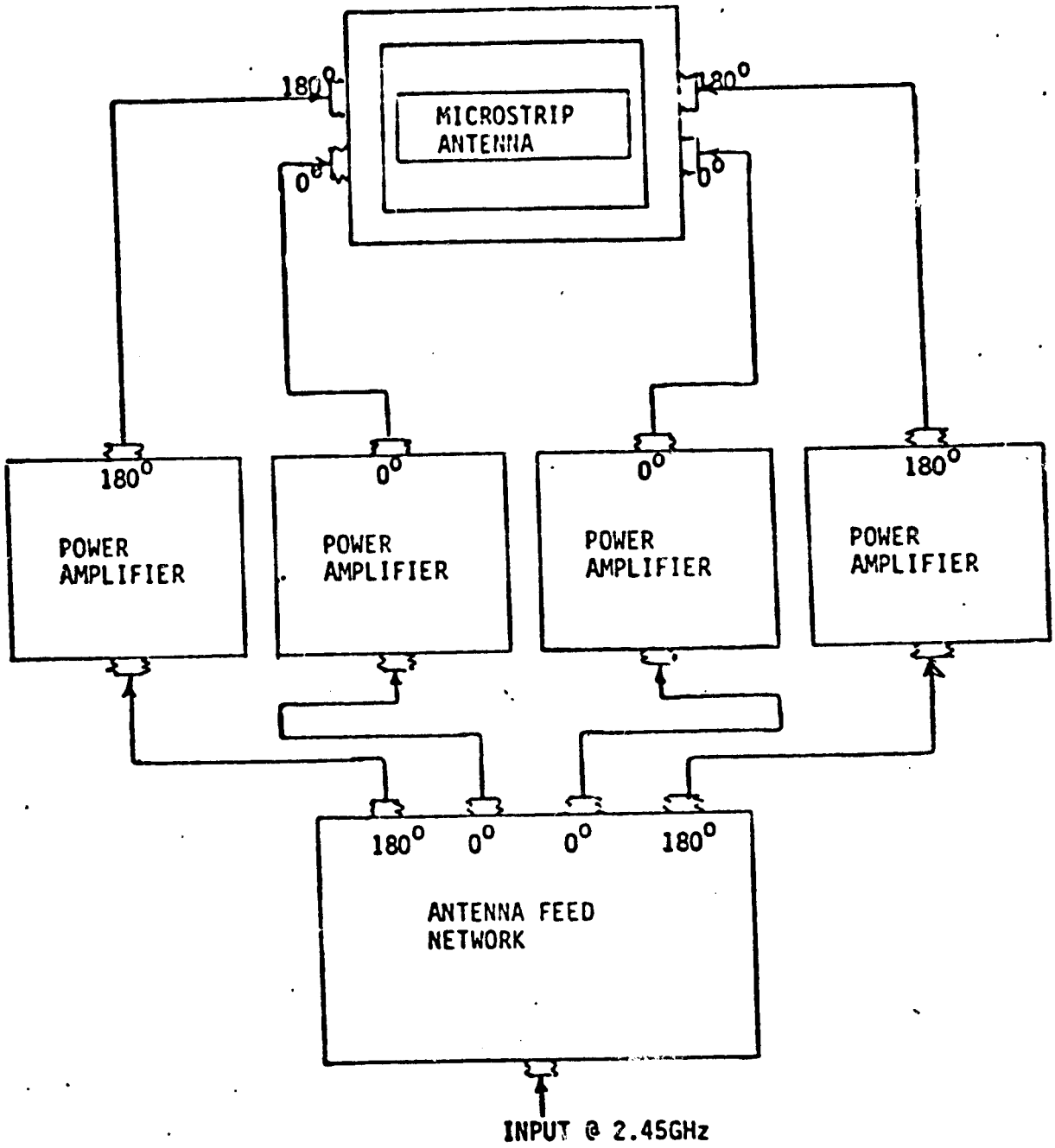

FIGURE 3 POWER COMBINING ANTENNA, FEED NETWORK AND POWER AMPLIFIER BLOCK DIAGRAM

Procedure and Results:

The majority of the testing was accomplished in the small anechoic chamber located in the JSC antenna test facility. The phase tracking and jitter test were accomplished utilizing the LINCOM statistical loop analyzer system located in the ESTL facility at JSC.

The test configuration for all of the measurements other than the SWR and phase jitter test is shown in figure 4. The separation of the two antennas is approximately three meters which should provide adequate near field correction(2). The input power was maintained at a constant level, while the signal generator was varied over the desired frequency range.

The output signal was measured with the microwave power meter and recorded. Since the gain of the receiving antenna varies with frequency it was necessary to correct the raw data for the effects of the receiving antenna before plotting the results. Table I and figure 5 depicts the data for the antenna and feed network alone while Table II and figure 6 shows the results with the amplifiers installed.

In reviewing these results, it would appear that the cavity associated with the power combining and radiating circuits is not a particularly good filter.

The half power points (-3 db) occur approximately at 2.3 GHZ and 2.6 GHZ. These points are somewhat difficult to determine because of the erratic nature of this data. This would indicate

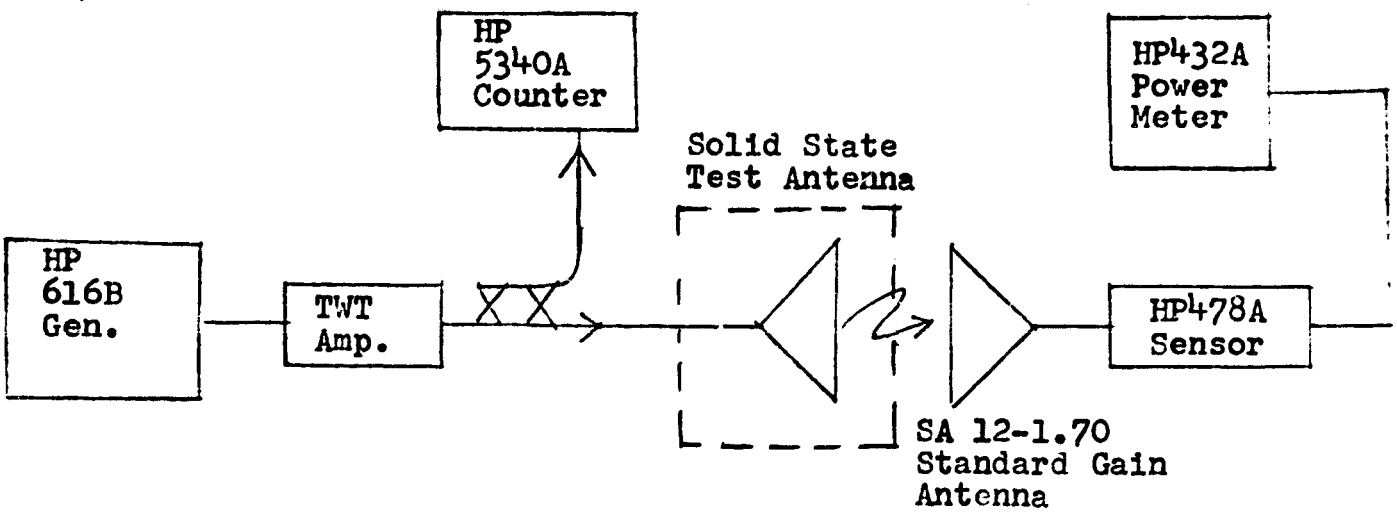

Figure 4 Test Configuration For
Frequency Response Measurements

TABLE I
(Antenna and Feed Network Only)

Frequency	PO dbm	Receiving Antenna Gain	Gain Normalized to 2.45 GHZ	SPS Antenna Response (dbm)
2225	-7.2	16.2	+0.7	-6.50
2250	-5.1	16.35	+0.55	-4.55
2275	-5.8	16.44	+0.46	-5.34
2300	-5.8	16.50	+0.40	-5.40
2325	-3.5	16.55	+0.35	-3.15
2350	-4.6	16.65	+0.25	-4.35
2375	-3.0	16.70	+0.20	-2.80
2400	-2.95	16.80	+0.10	-2.85
2425	-2.7	16.82	+0.08	-2.62
2450	-2.5	16.90	-0	-2.50
2475	-3.1	16.95	-0.05	-3.15
2500	-2.4	17.05	-0.15	-2.55
2525	-4.0	17.10	-0.20	-4.2
2550	-3.7	17.15	-0.25	-3.95
2575	-5.3	17.20	-0.30	-5.6
2600	-6.5	17.25	-0.35	-6.85
2625	-5.6	17.30	-0.40	-6.00
2650	-7.0	17.35	-0.45	-7.45
2675	-6.7	17.40	-0.5	-7.20

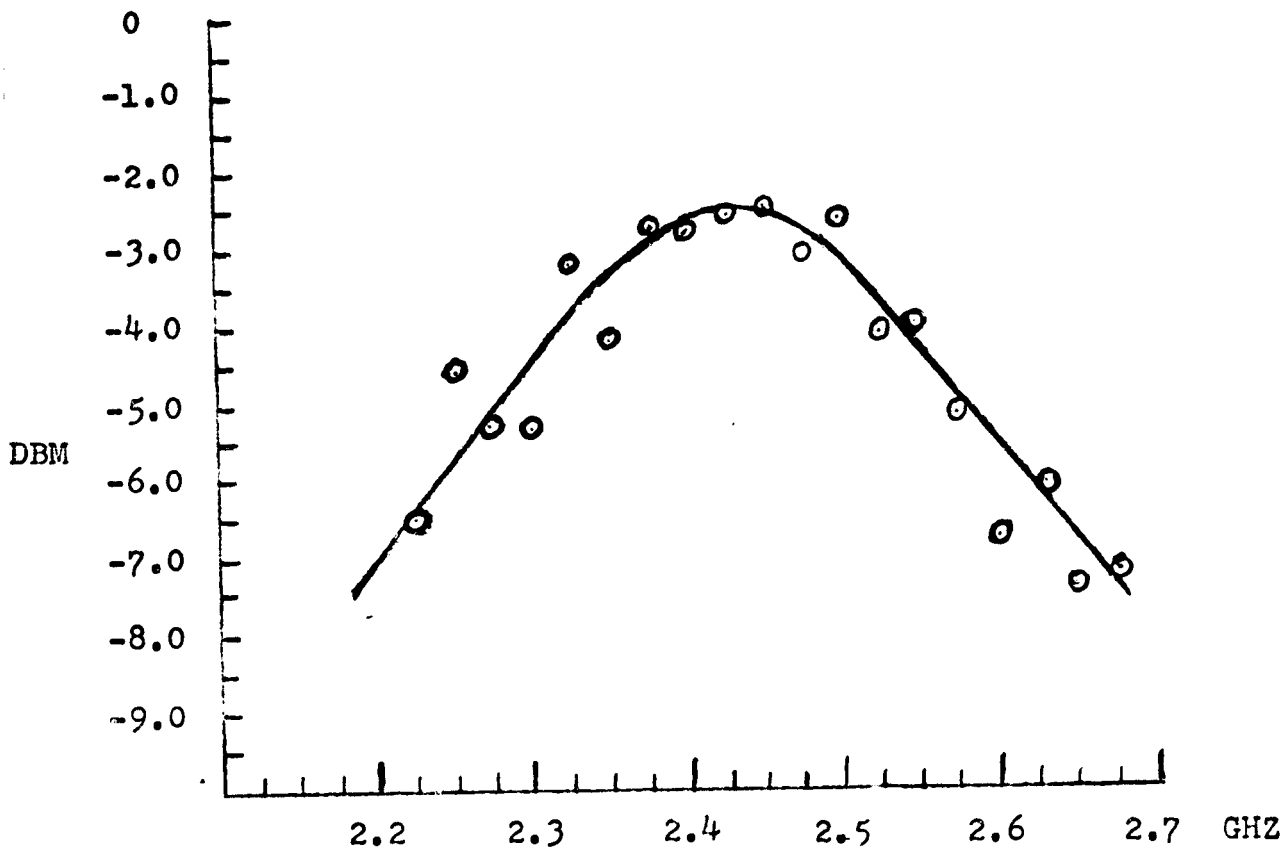

Figure 5 Frequency Response of the Antenna and Feed Network.

TABLE II
(Antenna and Feed Network with Amplifiers connected)

Frequency	PO dbm	Receiving Antenna Gain	Gain Normalized to 2.45 GHZ	SPS Antenna Response (dbm)
2200	<-30	16.2	+0.70	
2225	-21.3	16.25	+0.65	-20.65
2250	-18	16.35	+0.55	-17.45
2275	-13.8	16.44	+0.46	-13.34
2300	-13.3	16.50	+0.40	-12.90
2325	-11.7	16.55	+0.35	-11.35
2350	-13.8	16.65	+0.25	-13.55
2375	-12.4	16.70	+0.20	-12.20
2400	- 7.5	16.80	+0.10	- 7.40
2425	- 4.0	16.82	+0.08	- 3.92
2450	- 1.5	16.90	±0	- 1.5
2475	- 3.6	16.95	-0.05	- 3.65
2500	- 7.2	17.05	-0.15	- 7.35
2525	-11.5	17.10	-0.20	-11.70
2550	-13.0	17.15	-0.25	-12.75
2575	-17.2	17.20	-0.30	-16.90
2600	-18.3	17.25	-0.35	-17.95
2625	-19.7	17.30	-0.40	-19.30
2650	-26.3	17.35	-0.45	-25.85
2675	<-30	17.40	-0.5	

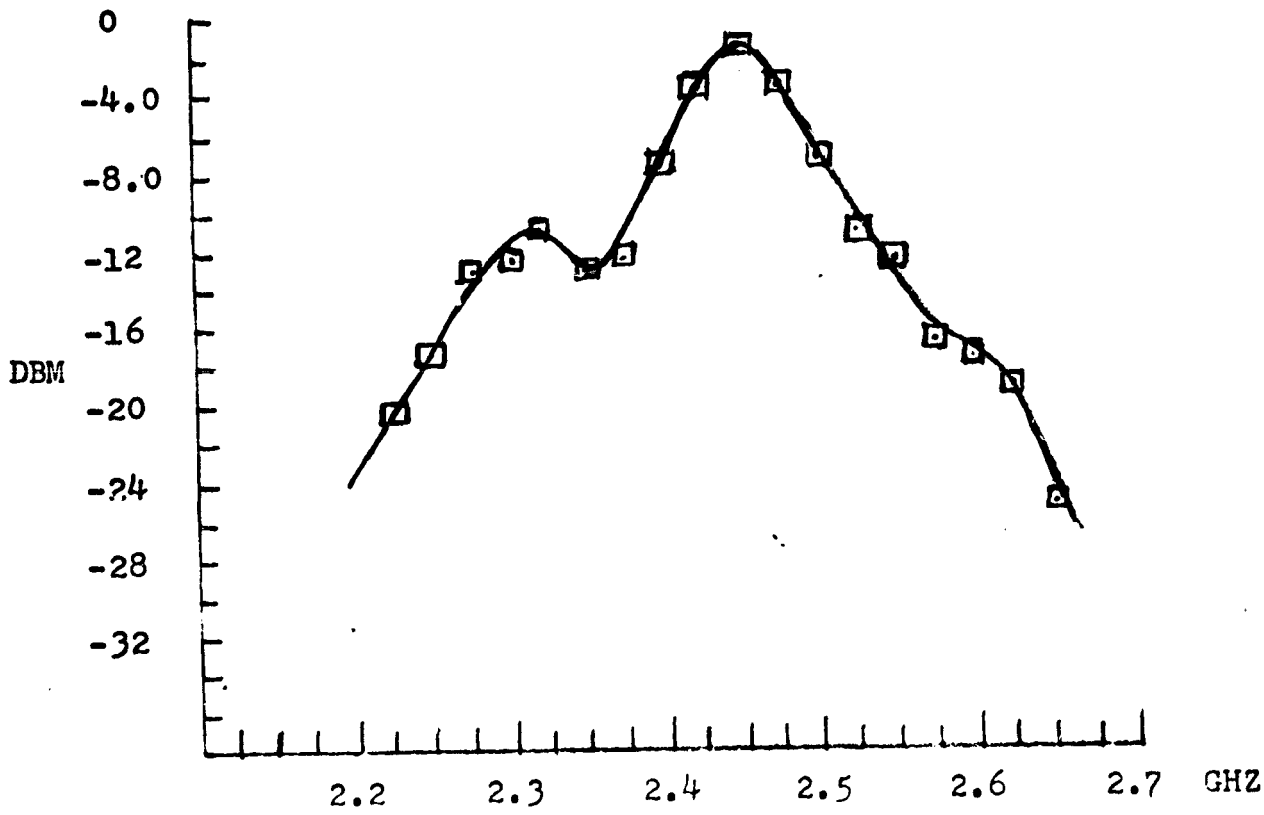

Figure 6 Frequency Response with Amplifiers Installed.

a bandwidth of roughly 275-350 MHZ, yielding a low Q for the cavity. Since the IMS band where the SPS will likely operate is only 100 MHZ wide, it would appear that some form of filter would be required if an antenna similar to this one is used. The results for the antenna with the transistors installed was improved considerably. The approximate half power points occur at 2.420 GHZ and 2.485 GHZ yielding a bandwidth of 65 MHZ. The improved performance with the amplifiers is attributed to the fact that each of the four amplifiers were gain and phase matched to operate at 2.45 GHZ by the builder, thus some filtering is supplied by amplifier action.

Additional questions concerning the filtering capabilities of the power combining cavity were raised by swept frequency measurements performed on the solid state module utilizing the Hewlett Packard network analyzer. The results were obtained in the form of Smith chart plots. These plots indicate a number of frequencies outside of the IMS band where the VSWR at the input to the module is 1.5 or less indicating that energy is being absorbed into the antenna system and would possibly be transmitted by the antenna. Figures 7 and 8 are examples of the plots obtained, while Table III is a list of some of the out of band low VSWR points.

During the testing of the antenna and feed network, prior to the insertion of the amplifiers, one leg of the feed network was disconnected from the antenna and the effected parts left in an open circuit condition to simulate the effect of the failure of

TABLE III

Frequencies with VSWR less than 1.5

2.45 GHZ

3.32 - 3.37 GHZ

3.75 GHZ

3.88 - 3.98 MHZ

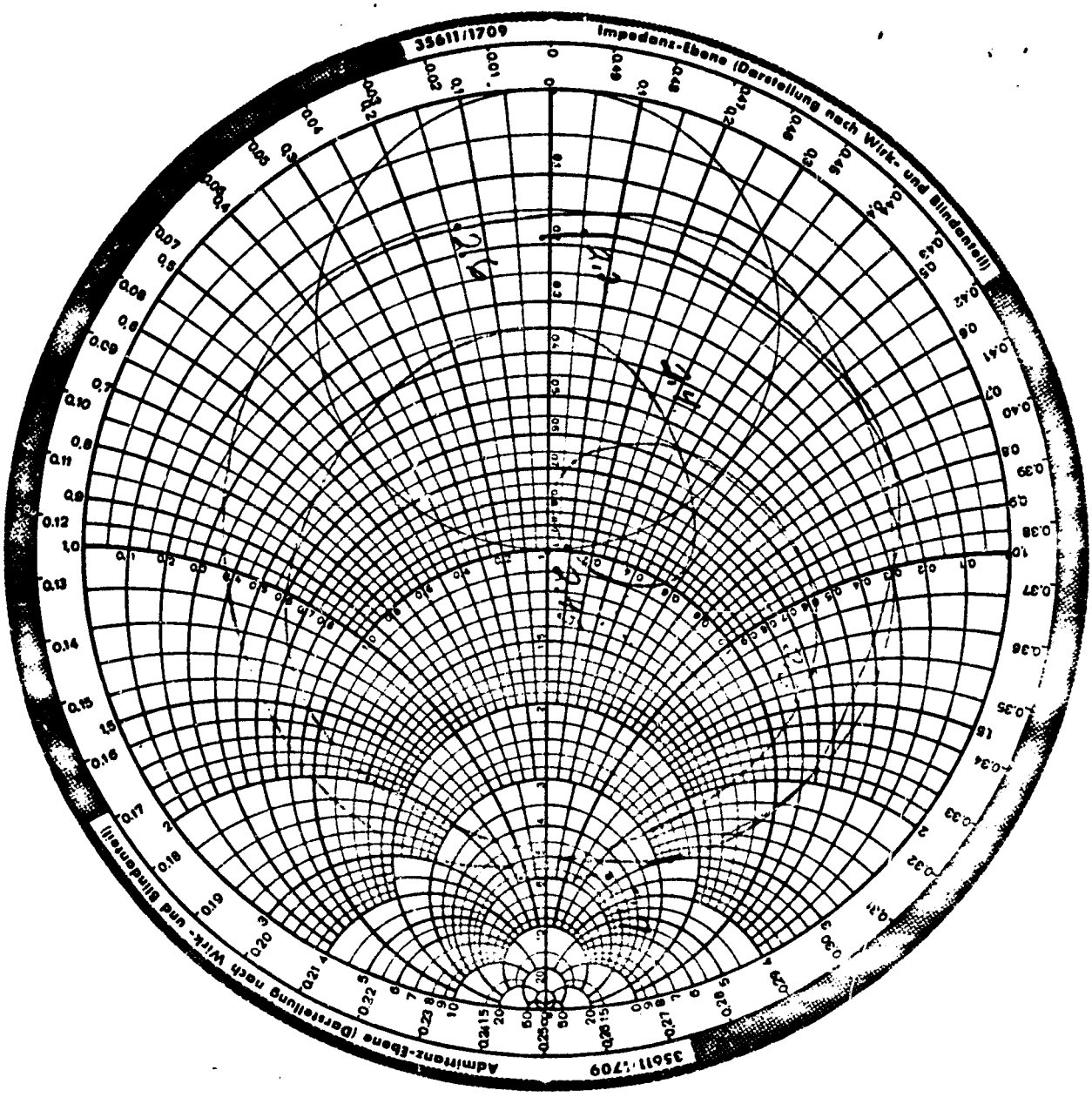

Figure 7 VSWR Measurements between 2.2 and 2.7 GHZ

C-3

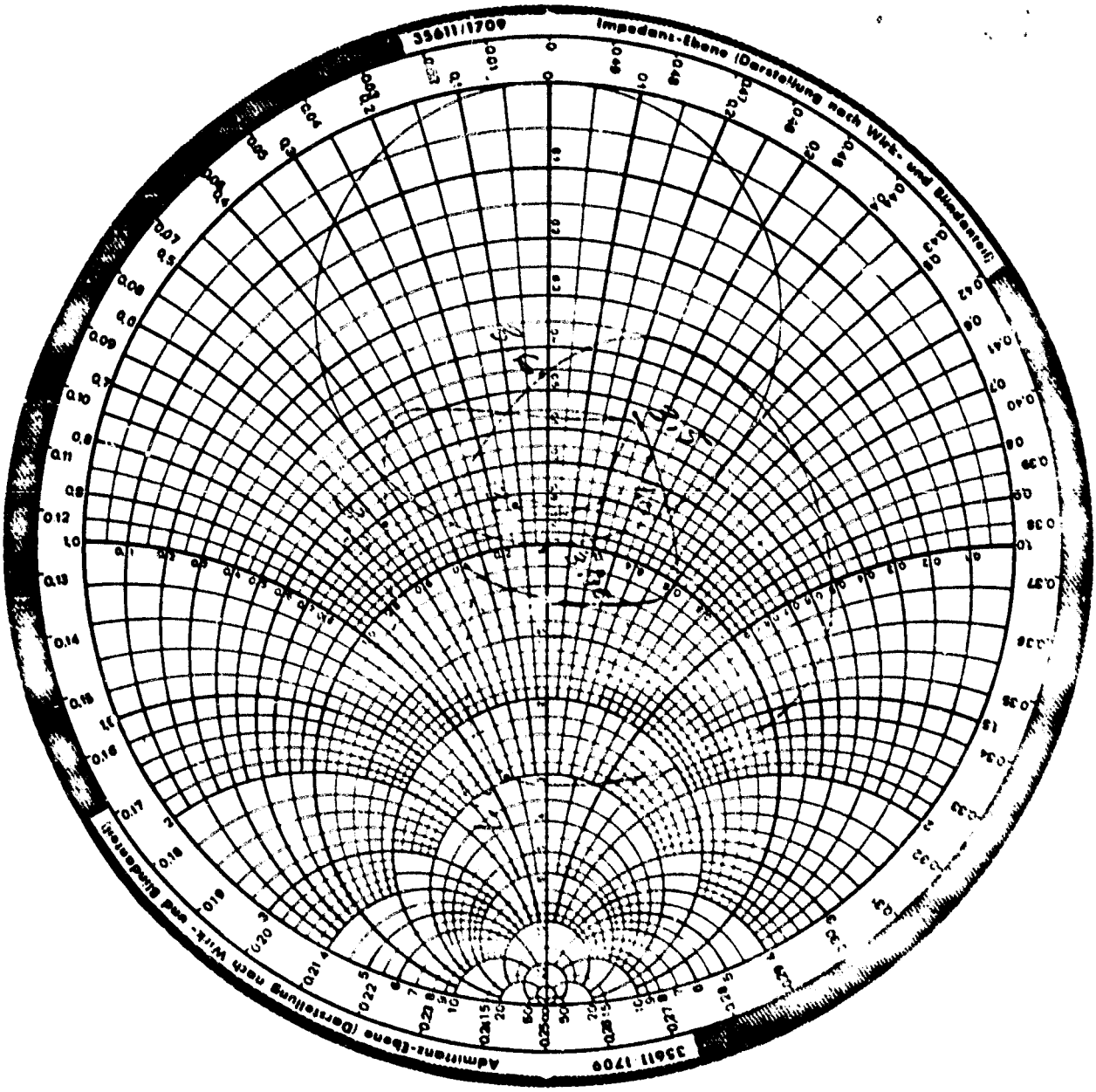

Figure 8 VSWR Measurements between 3.5 and 3.9 GHZ

one transistor. The output power was measured at the center frequency of 2.45 HIZ. The observed power loss was -2.3 db compared to the results with all feedlines connected. The expected result when there is a 25% loss of power is about -1.25 db. This observation was discussed with the builder of the antenna (6) and it was concluded that the reflection coefficient introduced into the cavity from the open feedline probably would account for the additional reduction in output power.

The final test conducted in the anechoic chamber involved an attempt to check the "noise threshold" of the power combining module. In this test the SPS antenna with amplifiers was placed directly in front of the receiving antenna while the signal source was attenuated by a 0 - 99 db step attenuator. On the detector side, the HP 432A power meter was replaced first with an HP 435A power meter equipped with the HP 8484A diode type sensor and later with a Stoddard sensitive RFI communications receiver. The minimum sensitivity of the HP 8484A sensor is -65 dbm while the Stoddard receiver and its connecting cable was calibrated to a noise level of -83 dbm. Neither instrument was able to detect a measurable level of thermal noise. It has been determined that the addition of a high gain amplifier of known noise performance was needed to accomplish this testing function.

The phase tracking and jitter test on the antenna feed network and the silicon transistors was conducted utilizing the LINCOM statistical loop analyzer (SLA).

The SLA provides for automatic acquistion and tracking of two signals. In the tracking mode it can be programmed to acquire up to 1000 samples over a period of one minute. The signals are analyzed for a variety of information including phase difference and phase jitter. The test configuration utilized is shown in Figure 9.

Since the SLA requires an 8.5 MHZ input signal on each of its inputs; it was necessary to mix the SPS output of 2.45 GHZ with the output of a 2.4415 GHZ reference oscillator to obtain the desired 8.5 MHZ SLA input signals. The mixers are followed with 8.5 MHZ bandpass filters. As noted on the diagram, the unused amplifiers were connected to 50 ohm terminations.

The signal sources are synthesized type signal generators with stable phase tracking and jitter characteristics. This is indicated by a measured mean jitter of 0.827° for the two oscillator mixer combinations.

The SPS antenna feed network and amplifier system was connected to the SLA and the two 180° ports (1 - 4) were selected for comparison. Later the cables were rotated and the 0° ports (2 - 3) were tested. Following this, port one was selected as a reference and was sequentially compared with each of the remaining ports. The data for these measurements are plotted in figure 10. The data that are plotted represents a mean of all data runs.

The RMS phase jitter plot has been corrected by subtracting the RMS value of the oscillator-mixer phase jitter. As noted by

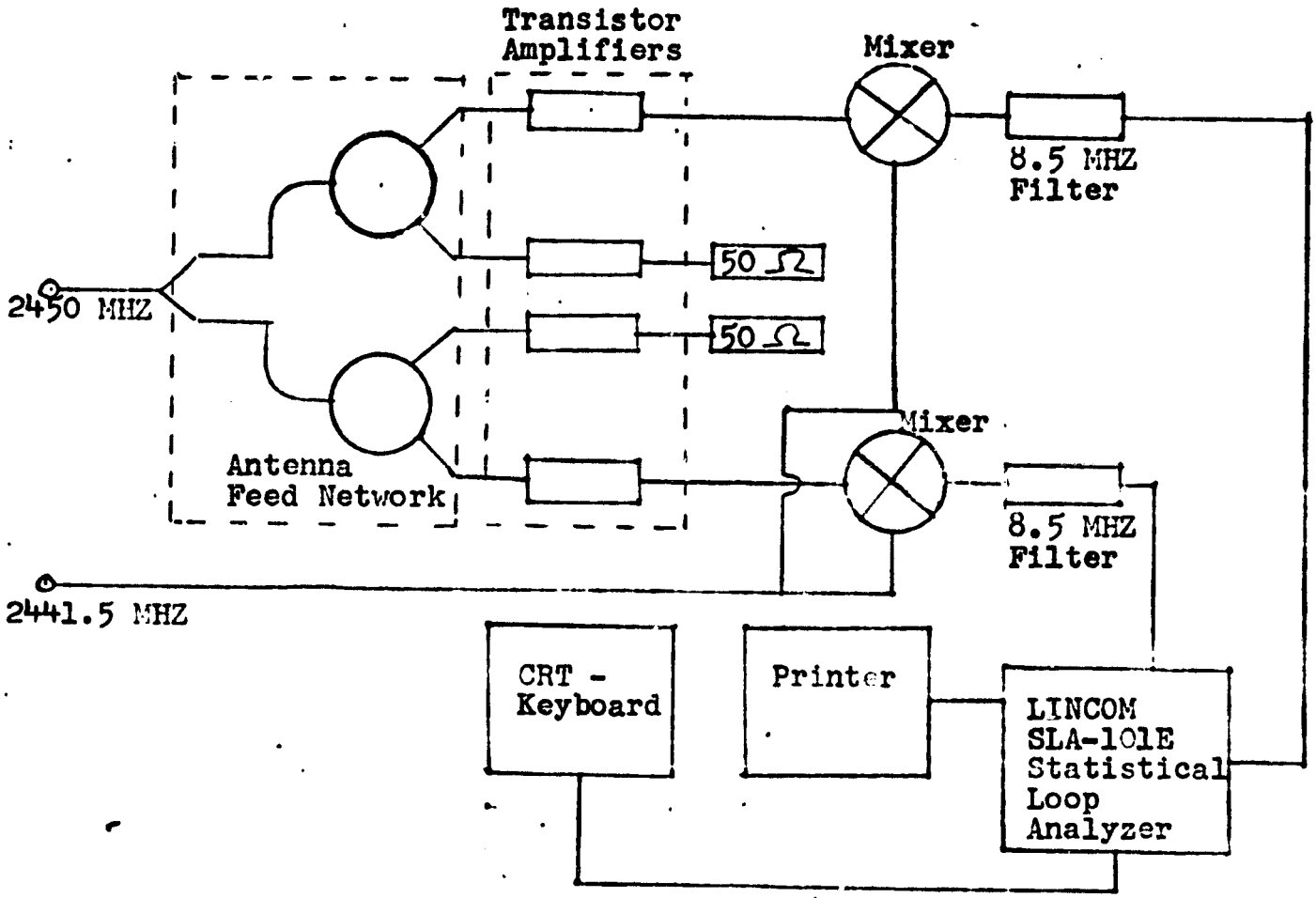

Figure 9 Test Configuration
For Phase Jitter Measurement

MEAN VALUE OF AMPLIFIER JITTER

Amplifier Pair	Mean Jitter Amplifier with Oscillator Mixer Noise Included	RMS Value of Amplifier Jitter
1 & 4	1.72°	1.51°
2 & 3	1.17°	0.82°
1 & 2	1.87°	1.68°
1 & 3	1.07°	0.68°
Oscillator-Mixer	0.827°	

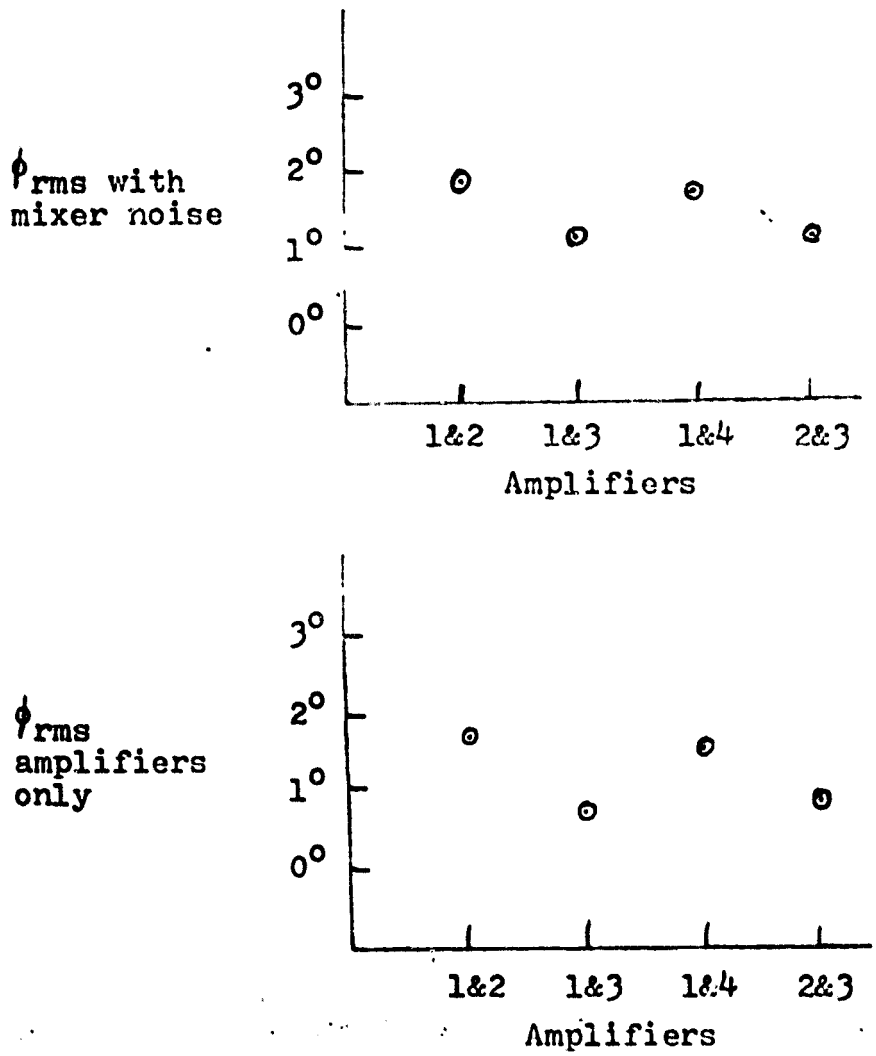

Figure 10 Amplifier Phase Jitter

SLA MODEL 101-E

PHASE ERROR JITTER AND SLIP RATE

-- TEST CONDITIONS --

THE LOOP TYPE UNDER TEST IS CW CARRIER
THE TRACKING BANDWIDTH = 200.00 HZ
TEST PARAMETER = 1 TO 4 Amplifiers
SIGNAL POWER TO NOISE DENSITY RATIO = 0.00 DB-HZ
DOPPLER OFFSET = 1.0 KHZ
SYMBOL RATE = 1.0 KSPS
ACCURACY OF TEST RESULTS = 95.52 %

-- TEST RESULTS --

DIFFERENTIAL PHASE MEASUREMENT = 57.75 DEG
STANDARD DEVIATION OF THE PHASE ERROR JITTER = 1.14 DEG
AVERAGE CLOCK-WISE SLIP RATE = 0.00000000 SLIPS PER SEC
AVERAGE COUNTER CLOCK-WISE SLIP RATE = 0.00000000 SLIPS PER SEC
AL AVERAGE SLIP RATE = 0.00000000 SLIPS PER SEC

Figure 11 Sample printout from the Statistical Loop Analyzer (SLA)

the graphs, the amplifier feed network appears to stable in terms of phase jitter. The mean variation noted for the 180° ports (1 - 4) was 1.51°. These data were taken from 12 data runs, which includes 12,000 samples.

The mean variation noted for the 0° ports (2 - 3) involving 2000 samples was 0.82°. Figure 11 indicates a sample of the SLA data output format.

Conclusions and Recommendations:

This exercise involved a series of test on a prototype power combining antenna proposed for use on the solar power satellite. The primary purpose was to investigate the filtering capabilities of the antenna along with the phase jitter of the antenna feed network. The effect of transistor failure was briefly examined. In addition, an attempt was made to determine the noise threshold of the system.

A summary of the findings follow:

1. The frequency response test indicate that some filtering will be needed to achieve the bandwidth necessary for operation in the IMS band.
2. The limited swept frequency testing that was accomplished indicated several frequencies outside of the proposed band of operation where the VSWR of the antenna feed system was less than 1.5. This testing included only a few data runs and did not include any harmonic

frequencies. The implication is that energy would be absorbed into the antenna system at these frequencies and probably transmitted.

3. With one feedline disconnected the observed power drop was -2.3 db. The normal loss expected when the input is reduced by 25% is roughly -1.25 db. This would indicate that the one open feedline causes enough mismatch to degrade the performance of the power combining cavity beyond a 25% loss. The assumption is that the normal failure mode for a transistor is an open circuit and that its geometry with respect to the input port introduces the necessary reflection coefficients to further degrade the signal.
4. The phase tracking and jitter measurements indicate that the feed network is quite stable with a low level of phase jitter. The use of the statistical loop analyzer greatly enhanced the acquistion of this data. No effort was made to correlate the absolute phase difference between the ports because of the difference in the lengths of the interconnecting transmission lines.
5. The attempt to measure the noise threshold of

the SPS module was inconclusive due to a failure to devise a suitable testing procedure. The no signal noise power level is apparantly less than the -83 dbm sensitivity of the Stoddard RFI receiver available in the antenna testing facility.

Recommendations for further development include:

1. Gallium arsenide MESFETS suitable for use in the SPS application need to be designed and developed. Most researchers propose a switching mode of operation (class D or E) (5). However, the current generation of MESFETS are not well suited for operation in this mode (4).
2. "Off the shelf" gallium arsenide devices capable of operation at 2 - 5 watts have been recently adapted to operation at the proposed SPS frequency (4). It is recommended that these devices be incorporated into the prototype antenna system. This would provide for a realistic module power of 8 - 20 watts. While these devices operate in class AB and are somewhat short of the desired efficiency, they represent a reasonable increment of improvement.
3. It is recommended that the full power prototype

be tested for the following:

a. Gain, directivity and pattern at full power.

b. Harmonics, out of band frequencies, and noise levels to determine the level of filtering required.

4. Improvements be made to the microstrip antenna and cavity as noted by its builder (2). Improvements in the Q of the cavity system could greatly reduce the need for filtering

5. Since class E and other switching modes of operation require the use of matching networks to optimize the performance of the transistor (7) it is recommended that suitable designs be developed and built. Further, it is recommended that these be implemented in microstrip with an eye toward the ability to mass produce. Ideally any filtering requirements set forth in step 3 could be implemented in the matching network.

6. Additional analysis is needed concerning the effect of amplifier failure on the power output. The geometry and design of filtering, phase matching and impedance matching networks possibly could be used to minimize the effects of mismatches caused by the failure of an amplifier.

REFERENCES

(1) E. F. Belohoubek, M. Ettenburg, H. C. Huang, M. Nowogrodzki, and F. N. Sechi, Analysis of S-Band Solid State Transmitters for the Solar Power Satellite, Final Report, RCA Laboratories, David Sarnoff Research Center, Princeton, NJ 08540, June 1, 1979, Prepared for NASA, Lyndon B. Johnson Space Center, Houston, TX 77058, Contract Number NAS9-15755.

(2) G. W. Fitzsimmons, SPS Solid-State Antenna Power Combiner, Final Report, Boeing Aerospace Company, Post Office Box 3999, Seattle, WA 98124, February 29, 1980, Prepared for NASA, Lyndon B. Johnson Space Center, Houston, TX 77058, Contract Number NAS9-15636A.

(3) Solar Power Satellite System Definition Study, Phase III, Final Report, Vol. 4 - Solid State SPS Analysis, Boeing Aerospace Company, Post Office Box 3999, Seattle, WA 98124, June, 1980, Prepared for NASA, Lyndon B. Johnson Space Center, Houston, TX 77058, Contract Number NAS9-16536.

(4) F. N. Sechi and J. E. Brown, SPS Solid State Amplifier, Final Report, RCA Laboratories, David Sarnoff Research Center, Princeton, NJ 08540, August, 1980, Prepared for Rockwell International, Anaheim, CA 92803, Contract Number A9EA-766939- 10.

(5) Owen E. Maynard, Solid State SPS Microwave Generation and Transmission Study, Vol. I - Phase II, Final Report, Raytheon Company, Wayland, Massachusetts, November, 1980, Prepared for Marshall Space Flight Center, Huntsville, AL, Contract Number NAS8-33157.

(6) L. A. Farmer, Telephone Conversation with G. W. Fitzsimmons, Boeing Aerospace Company, Post Office Box 3999, Seattle, WA 98124, August 14, 1981.

(7) N. O. Sokal and A. D. Sokal, Class E - A New Class of High-Efficiency Tuned Single-Ended Switching Power Amplifier, IEEE Journal of Solid-State Circuits, Vol. SC10, No. 3, June 1975, pp. 168-76.

NONLINEAR COUPLING BETWEEN THE IN-PLANE AND OUT-OF-PLANE MOTION ABOUT A STATIONARY POINT IN GEOSYNCHRONOUS ORBIT

By Bruce R. Feiring
Software Development Branch
Mission Planning and Analysis Division

1.0 INTRODUCTION

The equations of motion of a satellite in a coordinate system rotating with the Earth were recently given in reference 1. In this system when the oblateness (J_2) coefficient and ellipticity coefficient (J_{22}) of the geopotential are given, it is a relatively simple matter to obtain the equilibrium points of the problem. This is done in a manner quite analagous to that of finding the equilibrium points of the restricted three body problem (ref.2). There are four equilibrium points which are found to occur in the equatorial plane. Two of the points are located over the ends of the minor axis of the elliptical figure of the Earth's equator and two of the points are located over the major axis. The radii to there points are very nearly the same or the radius of a satellite orbit in a 24-hour period about the Earth.

The stability of our orbit in the neighborhood of these four points is found by linearizing the equations of motion about the points. This linearization by definition results in solutions which are valid in our infinitesimal region about an equilibrium point. This type of stability analysis follows that done in reference 2 for the restricted three body problem.

In this note the range of validity of the solutions in the vicinity of the libration points will be extended to included significant out-of-plane oscillations by the satellite. This will permit study of the stability of inclined geosynchronous satellites.

2.0 THE DIFFERENTIAL EQUATIONS

Following Band (1), the differential equations of motion of a satellite in a gravitational field with J_2 (oblateness) and J_{22} (ellipticity) perturbation forms included in the potential function in a coordinate system rotating with the Earth are

$$\ddot{x} - 2w\dot{y} = \Phi x$$

$$\ddot{y} + 2w\dot{x} = \Phi y \qquad (2.1)$$

$$\ddot{z} = \Phi z \ ,$$

where the force function, Φ , is defined as

$$\Phi = 1/2\ w^2\ (x^2 + y^2) - u\ , \qquad (2.2)$$

and

$$U = -\frac{\mu}{r} + \frac{\epsilon_2}{r^3}\ (3 \sin^2 \phi - 1)$$

$$-\frac{\epsilon_{22}}{r^3}\ .\ \cos_2 \Phi\ \cos^2 (\lambda - \lambda_{22})\ , \qquad (2.3)$$

is the geopotential function,

where

μ = the gravitational constant of the Earth,

$\epsilon_2 = 1/2\ \mu\ J_2 (R_e)^2$,

$\epsilon_{22} = 3\mu\ J_{22}\ (R_e)^2 > 0$ ($\sin u\ J_{22} < 0$),

J_2 is the oblateness coefficient,

J_{22} is the ellipticity (of the Earth at the equator) coefficient,

R_E is the Earth's radius,

$r = (x^2 + y^2 + z^2)^{1/2}$, (the radius to the satellite),

ϕ is the geographic latitude of the satellite measured from the equator of the Earth,

λ is the geographic longitude of the satellite measure from the Greenwich meridian, and

λ_{22} is the longitude of the major axis equatorial ellipse of the Earth (a constant)

The quantities ϕ and λ are related to the rotating coordinates by

$$\sin \phi = \frac{z}{r}, \quad \cos \phi = \frac{(x^2 + y^2)^{1/2}}{r} \tag{2.4}$$

and

$$\sin \lambda = \frac{y}{(x^2 + y^2)^{1/2}}, \quad \cos \lambda = \frac{x}{(x^2 + y^2)^{1/2}} \tag{2.5}$$

The values of J_2, J_{22}, and λ_{22} are numbers that have been determined experimentally. If turns out that J_2 is of order 10^{-3}, J_{22} is of order 10^{-6}, ε_2 is of order 10^{-3}, ε_{22} is of order 10^{-6} (by non-dimensionalizing), and λ_{22} is approximately $-25.^{o}3$. By equation (2.5), the orientation of the coordinate system is such that x is in the equatorial plane and passes through the Greenwich meridian.

By equations (2.2) and (2.3),

$$\Phi = 1/2\ \omega^2 (x^2 + y^2) + \frac{\mu}{r} - \frac{\varepsilon_2}{r^3} (3 \sin^2 \phi - 1)$$

$$+ \frac{\varepsilon_{22}}{r^3} \cos 2\phi \cos 2 (\lambda - \lambda_{22}) \tag{2.6}$$

Then

$$\Phi = 1/2\ \omega^2\ (x^2 + y^2) + \frac{\mu}{r} + \frac{1}{r^3}\ (\varepsilon_2 + \varepsilon_{22} \cos 2\ (\lambda - \lambda_{22}))$$

$$- \frac{z^2}{r^5}(3\ \varepsilon_2 + \varepsilon_{22} \cos 2\ (\lambda - \lambda_{22})) \qquad (2.7)$$

The point(s) $(x,y,z) = (a,b,c)$, where ε,b,c are constant are called equilibrium (stationary) points, and may be computed by noting that, since

$$x = a,$$

$$y = b,$$

$$Z = c,$$

$$\dot{x} = \dot{y} = \dot{z} = x = y = z = 0,$$

so that equation (2.1) becomes

$$\Phi_x\ (a,b,c) = 0,$$

$$\Phi_y\ (a,b,c) = 0, \qquad (2.8)$$

$$\Phi_z\ (a,b,c) = 0,$$

By taking partial derivatives of Φ in equation (2.7) with respect to x,y, and z, respectively, and using the abbreviations

$$W\ (x,y,z) = \omega^2 - \frac{\mu}{r^3} - \frac{3}{r^5}\ (\varepsilon_2 + \varepsilon_{22} \cos 2\ (\lambda - \lambda_{22})),$$

$$Z\ (x,y,z) = \frac{2\varepsilon_{22}}{r^5} \sin 2\ (\lambda - \lambda_{22}), \qquad (2.9)$$

$$Y\ (x,y,z) = \frac{\xi}{r^5}\ (3\ e_2 + \varepsilon_{22} \cos 2\ (\lambda - \lambda_{22})),$$

in light of equations (2.8), it turns out that

$$\phi^{o}_{x} \equiv \phi_x\,(a,b,c) = xW + yZ\left(1 - \frac{z^2}{r^2}\right) + \frac{z^2}{r^2}\,Y\ (a,b,c) = 0,$$

$$\phi^{o}_{y} \equiv \phi_y\,(a,b,c) = yW - xZ\left(1 - \frac{z^2}{r^2}\right) + \frac{z^2 y}{r^2}\,Y\ (a,b,c) = 0, \qquad (2.10)$$

$$\phi^{o}_{z} \equiv \phi_z\,(a,b,c) = -Z\ (\omega^2 - W) + \frac{1}{5}\left(2 - 5\frac{z^2}{r^2}\right) Y\ (a,b,c) = 0,$$

which is satisfied if all of

$$W\,(a,b,c) = 0$$

$$Z\,(a,b,c) = 0 \qquad (2.11)$$

and

$$Z = c = 0$$

are satisfied.

By equation (2.9),

$$Z\,(a,b,c) = 0$$

gives

$$\sin 2\,(\lambda - \lambda_{22}) = 0$$

so that

$$\lambda - \lambda_{22} = 0, -\frac{\pi}{2},\ \pi,\ \frac{3\pi}{2}, \qquad (2.12)$$

and thus

$$\cos 2 (\lambda - \lambda_{22}) = \pm 1.$$

Note that a and b may be computed from equation (2.5).

Also, by equation (2.10)

$$W (a,b,c) = 0$$

through equation (2.9) gives

$$\omega^2\rho = \mu/\rho^2 + (3/\rho^4)(\epsilon_2 \pm \epsilon_{22}), \tag{2.13}$$

where

$$\rho = r = (a^2 + b^2 + c^2)^{1/2},$$

thus enabling ρ to be computed. (It turns out that ρ = 42,400 Km.)

3.0 LINEARIZATION

Motion in a neighborhood of the four libration (stationary) points may be investigated by introducing displacements ξ, η, ζ from a libration point a,b,c by

$$\begin{aligned} x &= a + \xi, \\ y &= b + \eta, \\ z &= c + \zeta. \end{aligned} \tag{3.1}$$

Consider the Taylor series expansion of the force function, Φ, about (a,b,c),

$$\begin{aligned} \Phi(x,y,z) = \Phi^{\circ} + (\Phi^{\circ}_{x}\xi + \Phi^{\circ}_{y}\eta + \Phi^{\circ}_{z}\zeta) + (\tfrac{1}{2}\Phi^{\circ}_{xx}\xi^2 \\ + \tfrac{1}{2}\Phi^{\circ}_{yy}\eta^2)2 + \tfrac{1}{2}\Phi^{\circ}_{zz}\zeta^2 + \Phi^{\circ}_{xy}\xi\eta + \Phi^{\circ}_{xz}\xi\zeta + \Phi^{\circ}_{yz}\eta\zeta) + \cdots . \end{aligned} \tag{3.2}$$

By equation (2.1), if a second order Taylor series approximation is used, the following equations are obtained

$$\begin{aligned} \dot{\xi} - 2\omega\dot{\eta} = \Phi_x &= \Phi^{\circ}_{x} + (\Phi^{\circ}_{xx}\xi + \Phi^{\circ}_{xy}\eta + \Phi^{\circ}_{xz}\zeta) = \Phi^{\circ}_{x} + \nabla\Phi^{\circ}_{x}(\xi,\eta,\zeta)^T \\ \dot{\eta} + 2\omega\dot{\xi} = \Phi_y &= \Phi^{\circ}_{y} + (\Phi^{\circ}_{yx}\xi + \Phi^{\circ}_{yy}\eta + \Phi^{\circ}_{yz}\zeta) \\ &= \Phi^{\circ}_{y} + \nabla\Phi^{\circ}_{y}(\xi,\eta,\zeta)^T \\ \ddot{\zeta} = \Phi_z &= \Phi^{\circ}_{z} + (\Phi^{\circ}_{zx}\xi + \Phi^{\circ}_{zy}\eta + \Phi^{\circ}_{zz}\zeta) = \Phi^{\circ}_{z} + \nabla\Phi^{\circ}_{z}(\xi,\eta,\zeta)^T . \end{aligned} \tag{3.3}$$

Since $\Phi^{\circ}_{x} = \Phi^{\circ}_{y} = \Phi^{\circ}_{z} = 0$,

equation (3.3) reduce to

$$\begin{aligned}
\xi - 2\omega\dot{\eta} &= \Phi^{o}_{xx}\xi + \Phi^{o}_{xy}\eta + \Phi^{o}_{xz}\zeta = \nabla\Phi^{o}_{x}\,(\xi,\eta,\zeta)^{T} \\
\eta + 2\omega\dot{\xi} &= \Phi^{o}_{yx}\xi + \Phi^{o}_{yy}\eta + \Phi^{o}_{yz}\zeta = \nabla\Phi^{o}_{y}\,(\xi,\eta,\zeta)^{T} \qquad (3.4) \\
\zeta &= \Phi^{o}_{zx}\xi + \Phi^{o}_{zy}\eta + \Phi^{o}_{zz}\zeta = \nabla\Phi^{o}_{z}\,(\xi,\eta,\zeta)^{T},
\end{aligned}$$

or

$$(\xi - 2\omega\dot{\eta},\ \eta + 2\omega\dot{\xi},\ \dot{\zeta}) = H^{o}(\xi,\eta,\zeta)^{T}\ ,\ \text{a linear equation in } \xi,\eta,\zeta,$$

where

$$H^{o} = \begin{pmatrix} \Phi^{o}_{xx} & \Phi^{o}_{xy} & \Phi^{o}_{xz} \\ \Phi^{o}_{yx} & \Phi^{o}_{yy} & \Phi^{o}_{yz} \\ \Phi^{o}_{zx} & \Phi^{o}_{zy} & \Phi^{o}_{zz} \end{pmatrix}$$

is the mission matrix of Φ at (a,b,c), the stationary point.

By using equations (2.2) and (2.9), the clements of H^{o} are shown in appendix A to be

$$\begin{aligned}
\Phi^{o}_{xx} &= \alpha a^{2} - \beta b^{2}\ , \\
\Phi^{o}_{yy} &= \alpha b^{2} - \beta a^{2}, \qquad (3.5) \\
\Phi^{o}_{zz} &= -\omega^{2} - \gamma \\
\Phi^{o}_{xy} &= ab\,(\alpha + \beta) = \Phi^{o}_{yx}, \\
\Phi^{o}_{xz} &= 0 = \Phi^{o}_{zx}, \\
\Phi^{o}_{yz} &= 0 = \Phi^{o}_{zy}.
\end{aligned}$$

where

$$\alpha = 3\mu/\rho^5 + (15/\rho^7)(\epsilon_2 \pm \epsilon_{22}),$$
$$\beta = \pm 4\epsilon_{22}/\rho^7, \qquad (3.6)$$
$$\gamma = (2/\rho^5)(3\epsilon_2 \pm \epsilon_{22}).$$

Thus, by equations (3.4) and (3.6),

$$\dot{\xi} - 2\omega\dot{\eta} = \alpha a^2 - \beta b^2)\xi + ab(\alpha + \beta)\eta$$
$$\dot{\eta} + 2\omega\dot{\xi} = ab(\alpha + \beta)\xi + (\alpha b^2 - \beta a^2)\eta \qquad (3.7)$$
$$\ddot{\zeta} = (\omega^2 - \gamma)\zeta.$$

Note that equation (3.7) states that the out-of-plane motion (z-direction) is completely uncoupled from the in-plane motion (x-y plane, or equatorial plane). Bond (,pp. 12-17) discusses the stability of this motion which allows a solution to the differential equation (3.7).

4.0 QUADRATIE EFFECTS

As in section 3.0, consider a third-order Taylor series approximation to the force function given by equation (3.2), i.e.,

$$\begin{aligned}\Phi(x,y,z) = \Phi^{o} &+ (\Phi^{o}_{x}\xi + \Phi^{o}_{y}\eta + \Phi^{o}_{z}\zeta) + \frac{1}{2!}(\Phi^{o}_{xx}\xi^2 + \Phi^{o}_{yy}\eta^2 + \Phi^{o}_{zz}\zeta^2 \\ &+ 2\Phi^{o}_{xy}\xi\eta + 2\Phi^{o}_{xz}\xi\zeta + 2\Phi^{o}_{yz}\eta\zeta) + \frac{1}{3!}(\Phi^{o}_{xxx}\xi^3 + \Phi^{o}_{yyy}\eta^3 \\ &+ \Phi^{o}_{zzz}\zeta^3 + 3\Phi^{o}_{xxy}\xi^2\eta + 3\Phi^{o}_{xxz}\xi^2\zeta + 3\Phi^{o}_{xyy}\xi\eta^2 \\ &+ 3\Phi^{o}_{yyz}\eta^2\zeta + 3\Phi^{o}_{xzz}\xi\zeta^2 + 3\Phi^{o}_{yzz}\eta\zeta^2 \\ &+ 6\Phi^{o}_{xyz}\xi\eta\zeta) + \cdots .\end{aligned} \tag{4.1}$$

Since $\Phi^{o}_{x} = \Phi^{o}_{y} = \Phi^{o}_{z} = 0$, by using equation (4.1) and substituting into equation (2.1), the following equations are obtained:

$$\begin{aligned}\ddot{\xi} - 2\omega\dot{\eta} = \Phi_x &= (\Phi^{o}_{xx}\xi + \Phi^{o}_{xy}\eta + \Phi^{o}_{xz}\zeta) + \frac{1}{2!}(\Phi^{o}_{xxx}\xi^2 + \Phi^{o}_{xyy}\eta^2 \\ &+ \Phi^{o}_{xzz}\zeta^2 + 2\Phi^{o}_{xxy}\xi\eta + 2\Phi^{o}_{xxz}\xi\zeta + 2\Phi^{o}_{xyz}\eta\zeta) \\ &= \nabla\Phi^{o}_{x}(\xi,\eta,\zeta)^T + \frac{1}{2!}(\xi,\eta,\zeta)\,H^{o}_{x}(\xi,\eta,\zeta)^T, \\ \ddot{\eta} + 2\omega\dot{\xi} = \Phi_y &= (\Phi^{o}_{yx}\xi + \Phi^{o}_{yy}\eta + \Phi^{o}_{yz}\zeta) + \frac{1}{2!}(\Phi^{o}_{yxx}\xi^2 + \Phi^{o}_{yyy}\eta^2 \\ &+ \Phi^{o}_{yzz}\zeta^2 + 2\Phi^{o}_{yxy}\xi\eta + 2\Phi^{o}_{yxz}\xi\zeta + 2\Phi^{o}_{yyz}\eta\zeta \\ &= \nabla\Phi^{o}_{y}(\xi,\eta,\zeta)^T + \frac{1}{2!}(\xi,\eta,\zeta)\,H^{o}_{y}(\xi,\eta,\zeta)^T, \\ \ddot{\zeta} = \Phi_z &= (\Phi^{o}_{zx}\xi + \Phi^{o}_{zy}\eta + \Phi^{o}_{zz}\zeta) + \frac{1}{2!}(\Phi^{o}_{zxx}\xi^2 + \Phi^{o}_{zyy}\eta^2 \\ &+ \Phi^{o}_{zzz}\zeta^2 + 2\Phi^{o}_{zxy}\xi\eta + 2\Phi^{o}_{zxz}\xi\zeta + 2\Phi^{o}_{zyz}\eta\zeta) \\ &= \nabla\Phi^{o}_{z}(\xi,\eta,\zeta)^T + \frac{1}{2!}(\xi,\eta,\zeta)\,H^{o}_{z}(\xi,\eta,\zeta)^T,\end{aligned} \tag{4.2}$$

where

$$H_w^o = \begin{matrix} \phi^o_{wxx} & \phi^o_{wxy} & \phi^o_{wxz} \\ \phi^o_{wyx} & \phi^o_{wyy} & \phi^o_{wyz} \\ \phi^o_{wzx} & \phi^o_{wzy} & \phi^o_{wzz} \end{matrix}$$

where the index variable $w = x,y,z$.

Note that equation (4.2) pass on a quadratic form not found in equation (3.4).

By using equations (2.2) and (2.9) (see the appendix), the following equations are obtained (this is similar to the analysis performed in equations (3.4) through (3.7)).

$$\begin{aligned} \ddot{\xi} - 2\omega\dot{\eta} = {} & (\alpha a^2 - \beta b^2)\,\xi + ab\,(\alpha + \beta)\eta + \left(-\frac{3}{2}a\,\alpha + \frac{5}{\rho^2}(b^2\beta - \alpha^2)\right)\xi^2 \\ & + \left(\frac{1}{2}a\,\alpha + \frac{3}{\rho^2}(a^2 - 4b^2)\,\beta - 5b^2\nu + 2\beta\right)\eta^2 \\ & + \left(\frac{1}{2}a\,(\alpha + \frac{5}{\rho^2}\gamma)\zeta^2 + b\left(\alpha + \frac{3}{\rho^2}(b^2 - 4a^2)\,\beta\right.\right. \\ & \left.\left. - 5a^2\nu + 2\beta\right)\xi\eta, \end{aligned} \tag{4.3}$$

$$\begin{aligned} \ddot{\eta} + 2\omega\dot{\xi} = {} & ab\,(\alpha + \beta)\xi + (\alpha b^2 - \beta a^2)\eta + \left(\frac{1}{2}b\,\alpha + \frac{3}{\rho^2}(b^2 + 4a^2)\beta\right. \\ & \left. - 5a^2\nu + 2\beta\right)\xi^2 + \left(\frac{3}{2}b\,\alpha + \frac{5}{\rho^2}(a^2\beta - b^2\nu)\right)\eta^2 \\ & + \left(\frac{1}{2}b\,(\alpha + \frac{5}{\rho^2}\gamma)\zeta^2 + a\left(\alpha + \frac{3}{\rho^2}(a^2 - 4b^2)\beta - 5b^2\nu\right.\right. \\ & \left.\left. + 2\beta\right)\xi\eta, \end{aligned} \tag{4.4}$$

$$\zeta = (-\omega^2 - \gamma)\zeta + (\alpha + \frac{5}{\rho^2}\gamma)(a\xi + b\eta)\zeta, \tag{4.5}$$

where

$$\nu = \frac{\mu}{\rho^5} + \frac{7}{\rho^7}(\epsilon_2 + \epsilon_{22}).$$

5.0 SUMMARY

In 1 , by using a second-order Taylor series expanded about a stationary point, Bond found the following linear second-order differential equations governing motion about the stationary point (see eq.(3.7)):

$$\xi - 2\omega\dot{\eta} = (\alpha a^2 - \beta b^2)\xi + ab\,(\alpha + \beta)\eta,$$

$$\eta - 2\omega\dot{\eta} = ab\,(\alpha + \beta)\xi + (\alpha b^2 - \beta a^2)\eta,$$

$$\zeta = (-\omega^2 - \gamma)\zeta.$$

By using a third-order Taylor series expanded about a stationary point, it has been shown here that the following quadratic second-order differential equations governing motion about the stationary point (see eq.(4.3), (4.4), and (4.5)):

$$\begin{aligned}\xi - 2\omega\dot{\eta} = {} & (\alpha a^2 - \beta b^2)\xi + ab\,(\alpha + \beta)\eta + \frac{3}{2}a\left(\alpha + \frac{5}{\rho^2}(b^2\beta - a^2\nu)\right)\xi^2 + \frac{1}{2}a\left(\alpha + \frac{3}{\rho^2}(a^2 - 4b^2)\beta + 2\beta\right)\eta^2 \\ & + \frac{1}{2}a\left(\alpha + \frac{5}{\rho^2}\gamma\right)\zeta^2 + b\left(\alpha + \frac{3}{\rho^2}(b^2 - 4a^2)\beta - 5a^2\nu\right) + 2\beta\,\xi\eta,\end{aligned}$$

$$\begin{aligned}\eta + 2\omega\dot{\xi} = {} & ab\,(\alpha + \beta)\xi + (\alpha b^2 - \beta a^2)\eta + \frac{1}{2}b\left(\alpha + \frac{3}{\rho^2}(b^2 - 4a^2)\beta - 5a^2\nu + 2\beta\right)\xi^2 \\ & + \frac{3}{2}b\left(\alpha + \frac{5}{\rho^2}(a^2\beta - b^2\nu)\right)\eta^2 + \frac{1}{2}b\left(\alpha + \frac{5}{\rho^2}\gamma\right)\zeta^2 \\ & + a\left(\alpha + \frac{3}{\rho^2}(a^2 - 4b^2)\beta - 5b^2\nu + 2\beta\right)\xi\eta,\end{aligned}$$

$$\zeta = (-\omega^2 - \gamma)\zeta + \left(\alpha + \frac{5}{\rho^2}\gamma\right)(a\xi + b\eta)\zeta.$$

6.0 CONCLUSIONS

Note that the first two terms of the in-plane equations (eqs. (4.3) and (4.4)) are the same as in the linear case (the first two equations of equation (3.7)). Also, the first term in the out-of-plane equation (equation (4.5)) is the same as in linear case (the last equation of equation (3.7)). The remaining terms in equations (4.3) through (4.5) are quadratic terms. Then, it is necessary to go to a third-order expansion of the force function ϕ to observe coupling between the in-plane and out-of-plane motion, i.e., so that the in-plane and out-of-plane motion do not seem to be independent of one another.

The next phase of study will be to consider only the coupling effects of the in-plane motion in the out-of-plane equation (equation (4.5)). Note that the out-of-plane equation has a perturbation from the nonlinear terms which is of the order of the frequency, ω.

7.0 REFERENCES

1. Bond, V. R.: "Satellite Theory in a Coordinate System Rotating With The Earth," NASA Internal Note, January, 1981.

2. Szebehely, V.: Theory of Onbits. Academic Press, 1967.

3. Alfriend, K. T.: "A Non Linear Stability Problem in the Three Dimensional Restricted Three Body Problem". Celestial Medianics. Vol. 5 (1972) pp 502-511.

x,y are in Earth equatorial plane

x is through the Greenwich Meridian

z is rotational axis of Earth

op is inertial direction in Earth equatorial plane

$\underline{\omega}$ is angular velocity of Earth and the x,y,z frame

α_g is the right asrcension of Greenwich

Figure 1.- The geometry of the rotating system.

Figure 2. The geometry of the elliptical equator with respect to rotating system.

TEMPORAL CHANGES OF THE GLOBAL REFLECTANCE OF A WHEAT FIELD AS A FUNCTION OF DAILY SOLAR IRRADIANCE

Prof. Guy A. Franceschini, Ph.D.
Department of Meteorology
Texas A&M University

Supervisor: Dr. David E. Pitts
Supporting Research Branch
Earth Observations Division

Abstract: Based on in situ measurements of incident and reflected solar irradiation over a wheat field, daily values of the surface reflectance, a scene signature, were determined for a crop year. Diagnoses of these data reveal the character of the signature, and its changes with time, crop stage, and the magnitude of incident irradiance. The latter varies inversely with cloud cover.

1. Introduction

This is a diagnostic study of the characteristics of thermal-IR signatures of a field planted in spring wheat during the 1978 crop year. To date, and to my knowledge, the greater effort in dealing with crops and satellite-derived data has involved shortwave radiation, i.e., solar radiation, of which 99% is in wavelengths shorter than 4.0 μm. This concentration of effort is primarily a consequence of the large variations in optical properties, viz., reflectance, associated with soil and crops. Such variations are wavelength dependent, and are a function of crop geometry, stage of maturity, and stressing which is associated with atmospheric and edaphic conditions. In addition, the nature, condition,and moisture of the exposed soil also influence the surface reflectance to a great degree. Hence, spectral measurements of surface-reflected shortwave radiation make it possible to characterize soil moisture, and crop extent and conditions, as well as to estimate ultimate possible crop yield.

In considerations of thermal infrared radiation, i.e., that within the terrestrial waveband which extends from 3.0 to 80 μm, we essentially are dealing with a thermodynamic coordinate, temperature, of the target. Ideally, most terrestrial surfaces behave nearly as 'black bodies' in this longwave spectral domain. However, except for limited wavebands, the atmosphere also behaves as a black body primarily because of carbon dioxide, water vapor, methane, nitrogen-oxygen molecules, and clouds. Consequently, to view the surface with satellite-mounted sensors on essentially cloud-free days, we must select a spectral region over which the atmosphere is nearly transparent, e.g., 8-13 μm. Unfortunately, the atmosphere, even in this waveband, behaves as a somewhat 'dirty window' having a transmittance less than one. Nonetheless, meteorological satellites effectively and routinely use this waveband to delineate surface (land and ocean) and cloud top temperatures, i.e., corditions associated with well defined horizontal temperature gradients.

A question which should be asked is: Can such infrared spectral information be used tc characterize croplands? In this study, we have examined spectral radiance data obtained with sensors mounted on an aircraft flying at a low altitude over an area planted in spring wheat.

Because atmospheric interference is minimized due to the low altitude, the data may be considered a ground truth for satellite measurements.

2. Theoretical considerations

a. The nature of radiation

According to Planck's law, the monochromatic radiance, R_λ, from a blackbody may be expressed as a function of wavelength, λ μm, and the temperature, T °K. For the units chosen,

$$R_\lambda = (c_1/\lambda^5)\left(\exp(c_2/\lambda T) - 1\right)^{-1} \quad (\mu W/cm^2\ sr\ \mu m), \qquad (1)$$

where $c_1 = 1.19096 \times 10^{10}$; and $c_2 = 1.43879 \times 10^4$. For given values of R_λ and λ, the effective or radiation temperature of a target may be computed using (1). The Planck curve, as given by (1), for a blackbody at a temperature of 300°K is shown below.

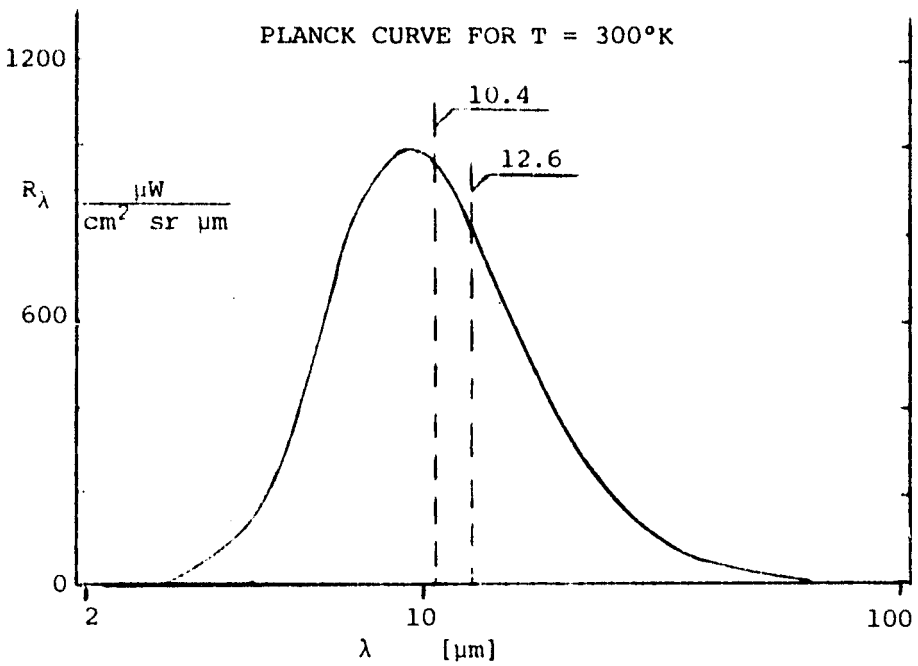

As seen in the figure, the modal wavelength, i.e., the wavelength of maximum radiance, is near 9.66 μm. The total waveband of interest in this study, 10.4 - 12.6 μm as indicated in the figure, involves nearly 14% of the total radiance. In addition, within this spectral band, the value of R_λ varies inversely with wavelength. Observed values in this band range from 750 to 1130 SU (1 SU = 1 Standard Unit = 1 $\mu W/cm^2 sr\ \mu m$) with associated effective temperatures from 290°K to 310°K, respectively, over the limits of the total waveband.

b. The energy budget

Changes in temperature of a target depend upon its net gains and losses of energy. A physically sound approach to the problem is given by the energy equation which is a statement of the boundary condition at the interface between the atmosphere and its subjacent volume. The condition states that the energy flux is continuous across the interface, i.e., the net flux on both sides of the boundary are equal. In terms of energy fluxes, and with the convention that fluxes toward the interface, on both sides, are positive, the energy equation may be symbolically expressed as

$$N + Q + L + H = 0. \qquad (2)$$

In (2), the first three terms refer to fluxes on the air side of the interface, and the last term, H, refers to the flux on the opposite side, i.e., the side of the subjacent volume, e.g., soil and/or plants. Individual terms are: N, the net radiation, both short- and longwave; Q, the sensible heat flux; L, the latent heat flux associated with the phase change of water; and H, essentially the sensible heat flux below the interface.

Individual terms of (2) may qualitatively be expresses as:

net radiation,

$$N = (1 - r)I + (F_a - F),$$

where I is the solar irradiance, r is the associated surface reflectance, and the longwave fluxes, F_a and F, are

$$F_a \propto T_a^4 \quad \text{(downward from the atmosphere)}$$

$$F \propto T^4 \quad \text{(upward from the surface target);}$$

the sensible heat flux,

$$Q \propto (T_a - T)v^n,$$

in which v is the wind speed, and n is an empirically derived exponent often taken as $n = 2$;

the latent heat flux which may produce surface evaporative cooling,

$$L \propto (e_a - e)v^n,$$

where e_a is the vapor pressure of the air, and e is the vapor tension of the target surface; and finally,

the sub-interface flux,

$$H \propto (T - T_z),$$

in which T_z is a near-surface temperature of the interior of the target. Consequently, the energy equation shows the interrelations and feedback mechanisms between the transfer processes. More importantly, for our purpose, it indicates the dependence of target temperature, T, on the atmospheric elements, i.e., temperature, wind speed, and moisture, as well as the moisture state of the target, both soil and crop.

In particular, the heat transfer, H, within crop and soil, which must balance all the other in-air fluxes, represents the energy which enters the surface, and is consequently responsible for target temperature changes. For a thin near-surface layer of the target, extending to a distance z_1 from the interface,

$$(\partial T/\partial t) \propto (H_1 - H), \tag{3}$$

where H_1 represents the flux across the level z_1, and depends on the temperature gradient at that interior level. In (3), a prognostic equation, we see the dependence of the rate of surface temperature change on the atmospheric fluxes, since, from (2), $H = -(N + Q + L)$.

c. Areal averaging

In principle, (2) applies to each different element of the surface,

crop and soil, separately. However, for this study, we will treat the target area, u, as a collective system with representative temperature T, as an area average defined by the mean-value theorem:

$$T = (1/u)\int_u \tau du \simeq (1/u)\sum_{i=1}^{m} \tau_i u_i . \qquad (4)$$

In (4), τ represents the variable temperature of m target elements, i. Since a target area usually consists of soil and crop, a differentiation of the contribution of each to the upward flux of longwave radiation, F, is important. If c represents the fractional area of the target which is covered by the crop, i.e., ground cover, then in a manner analogous to (4), area-weighting each contribution leads to

$$F = cF_c + (1 - c)F_s, \qquad (5)$$

where subscripts c and s refer to crop and soil, respectively, and

$$F \propto T^4 \propto R_\lambda$$

$$F_c \propto T_c^4$$

$$F_s \propto T_s^4,$$

where R_λ is the measured monochromatic radiance of the collective target, as given by (1).

Since airborne sensor measurements slur the successive readings over different wavelength intervals, a further area-weighting of the individual readings is possible. For example, if A_i represents the fractional target-area overlap successive readings, a different space-average value of target temperature, $\langle T_t \rangle$, at time t, may be defined as

$$\langle T_t \rangle = (A_{t-j}T_{t-j} + T_t + A_{t+k}T_{t+k})/(A_{t-j} + 1 + A_{t+k}), \qquad (6)$$

where: the T values are obtained from radiance data assigned to the central wavelength of the interval; and j and k represent the interval of time, respectively, between values preceding and following that at time t. The values of A_i in (6), pertinent to this study, are treated

in the section on target geometry. However, due to time limitations, such area-averages of target temperatures were not calculated.

3. Observations

There were five observation periods, each on different days of the 1978 crop year. Measurements were made of: spectral radiance over a time interval of 48 - 56 s, once each day; atmospheric elements; soil field moisture; and certain agronomic information. Each is discussed below.

a. Ancillary data

Supporting simultaneous atmospheric measurements of wind, pressure, temperature, relative humidity, and cloud cover were made during each observation period. Agronomic data included: ground cover (including weed coverage), maturity stage, plant height, and dates of planting and harvesting. Field moisture information consisted of qualitive estimates, e.g., dry, damp, and wet. The latter condition, although not reported, was assumed after viewing photographs taken during the observation periods. Information on soil type was not available.

b. Radiance data

The radiance sensor of the airborne Field Spectrometer System, FSS, has a field of view of 20.00°, and a scan rate of 1 s, i.e., all channels were slur-scanned sequentially every second. In all, there are 42 channels from 10.4 to 12.6 μm, and each covers an interval of 0.05 μm. Average values of monochromatic radiance were available for five wavebands involving different numbers of channels, hence, different time intervals, and different areas viewed. Details are tabulated below, where $\Delta\lambda$ is the wavelength interval, and $\bar{\lambda}$ is the median or central wavelength of the interval.

Band	$\Delta\lambda$ (μm)	No. Channels	$\bar{\lambda}$ (μm)	Scan Time (s)
1	10.40 - 10.80	8	10.60	0.191
2	10.80 - 11.30	10	11.05	0.238
3	11.30 - 11.80	10	11.55	0.238
4	11.80 - 12.30	10	12.05	0.238
5	12.30 - 12.50	4	12.40	0.095

4. Target geometry

Flight altitude was 60.96 m (200 ft). Consequently, with a 20.00° field of view, the target diameter was 21.5 m. At a flight speed of 96.52 km/h (60 mi/h), the distance between initiation of successive 1-s scans was 26.82 m, and the average length of the area scanned was approximately 1.6 km. Hence, the area scanned was approximately 3 ha.

Since the distance between successive scans of any specific wavelength band is greater than the target diameter, there is no overlap of related targets. However, target areas of sequential but different wavebands do overlap. In general, if we assign the average radiance value of a waveband to the central time, hence, position, of that waveband, the overlap area A_l of two successive and related targets may be expressed as

$$A_l = \{\pi d^2 - 2L_l\sqrt{d^2 - L_l^2} - (2d^2)\sin^{-1}(L_l/d)\}/4, \qquad (7)$$

where d is the target diameter, and L_l is the variable distance between successive target centers. Values of L_l and the related fractional target overlap, A_l associated with successive average radiance readings are given below. Fractional target areas from (7) may be used in (6) to evaluate $\langle T_l \rangle$. Again, due to time constraints, it was not possible to complete the evaluations.

Bands	L_l (m)	A_l (%)
1 to 2	5.747	74.58
2 to 3	6.386	71.77
3 to 4	6.386	71.77
4 to 5	4.470	80.19
5 to 1	3.832	83.01

5. The site

The observation site is located in the wheat drylands of Hand Co., SD, in field No. 281, having an area of 128 ha (316 acres). Specific location is: 44° 30' N, and 99° 0' W. The field was planted in spring wheat, variety Fortuna HRS, on 26 April 1978, using the R-and-R method with 7 in. between rows. The crop was harvested before the last period of observation on 16 August 1978. Plants had attained a height of .81m at which time the ground cover was 30%.

6. Source of data

Data were obtained from the Laboratory for Applications of Remote Sensing (LARS) of Purdue University, West Lafayette, ID. LARS was responsible for taking the observations, as well as determining the average radiance values.

7. Discussion

Data are presented on the following five figures, one for each observation period. Each contains a time reference, all available ancillary data, and graphs of average monochromatic radiance values for each of the five wavebands. The latter are plotted versus time

and approximate travel distance. Included in the graphs are scales for temperature, one for each waveband. These effective temperatures were calculated using the Planck relation as given by (1). Local mean solar time for the site is approximately 6.6 h earlier in the day than the indicated GMT.

a. Observation number 014, 780515, 17:13 GMT

On this day, 19 days after planting, the crop had not emerged, but there was a reported ground cover of 10% due to weeds. The wind was strong from the SSE during this late morning period, and the relative humidity was only 40%. Both conditions would have tended to enhance the sensible and latent heat fluxes, but the latter must have been minimal since the soil was reported as being dry.

Variations of radiance values for all bands were in phase, and showed a range of 61 to 87 SU with B-5 (Band 5, 12.40 μm) and B-1 (Band 1, 10.60 μm), respectively, which correspond to ranges of T, the effective temperature, of 5.1° and 5.5°K. The average range, ΔT, for all bands was 5.3°K.

In considering the average values of T, i.e., $\bar{T}$, for all bands, shown by horizontal lines in the figure, the maximum difference, $d\bar{T}$, between values was 2.5°K, and was found between data for B-1 and B-5. B-1 had the highest, B-5 the lowest, viz., 307.9°K and 305.4°K, respectively. A similar result appeared in all the periods, and may be due to the method of determining the average radiances. For bands 2,3,and 4, $d\bar{T} \leq 0.2$°K. Of the three, B-2 had the highest temperature, 306.5°K.

For all bands, the values of $\bar{T}$ were higher than air temperature, 295.1°K. Differences ranged from 10.3°K to 12.8°K. Although excessive, such vertical differences are not surprising for the following reasons: the 1% cloud coverage permitted maximum insolational heating; the soil was dry and essentially bare, thus, evaporative cooling was a minimum; the time was during the upswing of the diurnal temperature cycle when air temperature lags that of the surface; and the strong winds induced sufficient turbulence to concentrate the vertical temperature gradient, as shown by the large differences, in the near-surface layer of the atmosphere.

MONOCHROMATIC RADIANCE, R_λ, AND EFFECTIVE TEMPERATURE, T

Date/Time: 780515/17:13 GMT Observation No. 014

Air Temperature, 295.1°K; Wind, 155° 32 km/h; Relative Humidity, 40%

Ground Cover, 10 % (weeds); Maturity Stage, no emergence; PLHT, 0 dm

Field Moisture, dry.

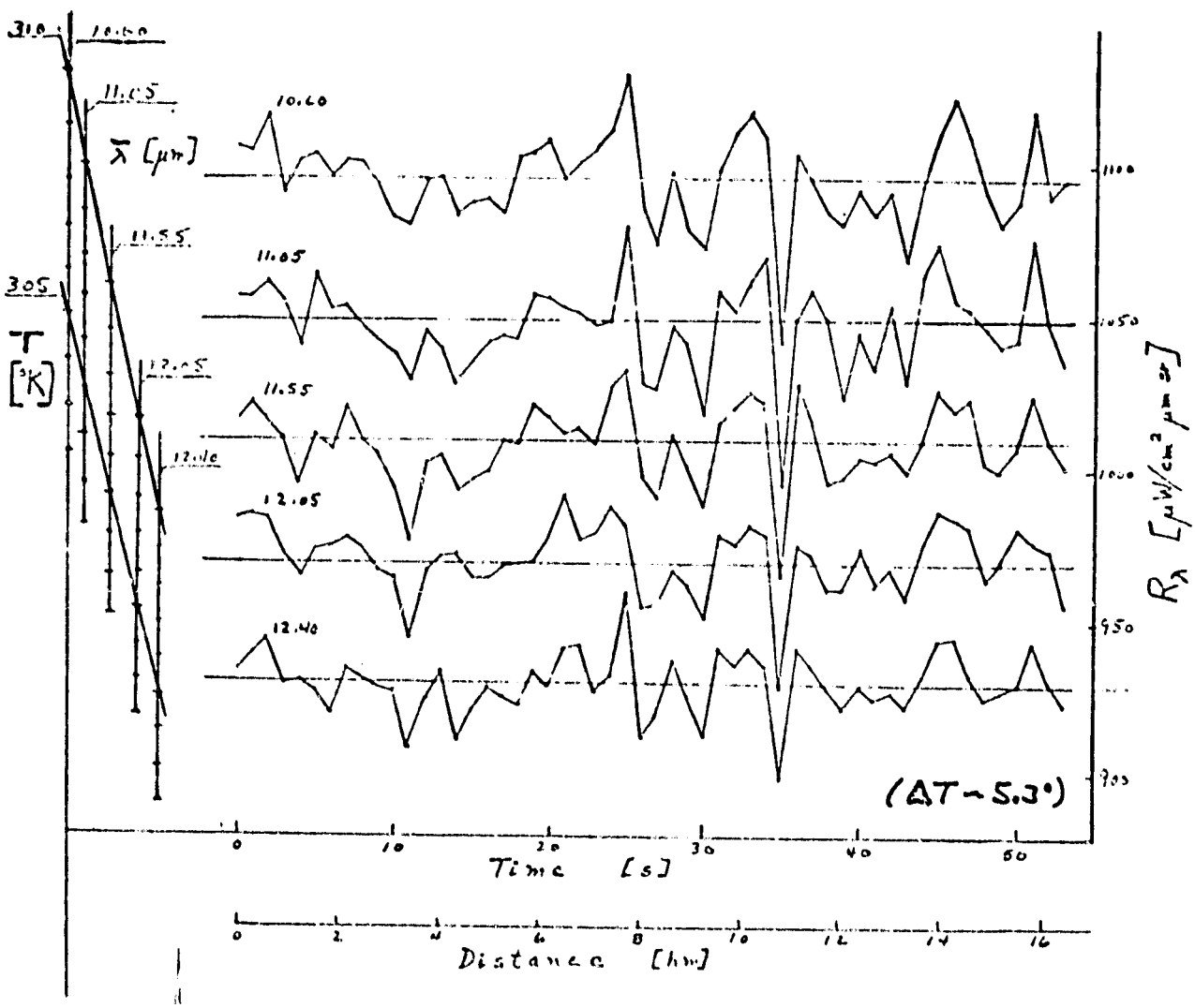

b. Observation number 094, 780602, 15:55 GMT

The maturity stage of the crop, on this 37th day after planting, was reported as tillering prebud. Plant height was 0.1 m, and ground cover was 10% with no weeds present. Although the field moisture was reported as dry, antecedent precipitation and field photographs taken during the period indicated a possible wet condition. The wind was light to moderate from the west; and relative humidity was 60% which was more in keeping with a non-dry surface. Cloud coverage was only 5%.

As with OBNO 014, radiance variations were in phase, and all minimum values corresponded to the wet and dark areas that were seen in the photographs. Ranges were excessive, the largest encountered in this study, and varied from 80 to 110 SU for B-5 and B-1, respectively. The associated ranges in T were 7.3°K and 7.7°K, with an average for all bands of $\Delta T = 7.6°K$.

Values of $d\overline{T}$, the interband maximum difference in average values of temperature, was only 1.8°K, and was found between data for B-1 ($\overline{T} = 295.1°K$) and B-5 ($\overline{T} = 293.3°K$). For the central bands, 2,3,and 4, $d\overline{T} \leq 0.6°K$; and for B-2, $\overline{T} = 294.6°K$, which was highest of the three.

Although all values of $\overline{T}$ were higher than air temperature, 290.9°K, the differences were much smaller than in OBNO 014, and ranged from a minimum of 2.4°K to a maximum of 4.2°K. The lower temperatures were presumably a consequence, in part, of evaporative cooling of the wet surface. Also, advection associated with the westerly wind may have contributed. The latter two comments are speculative, since the true situation was not investigated.

MONOCHROMATIC RADIANCE, R_λ, AND EFFECTIVE TEMPERATURE, T

Date/Time: 780602/15:55 GMT Observation No. 094

Air Temperature, 290.9°K; Wind, 267° 14 km/h; Relative Humidity, 60%

Ground Cover, 10%; Maturity Stage, tillering prebud; PLHT, 1.0 dm

Field Moisture, wet.

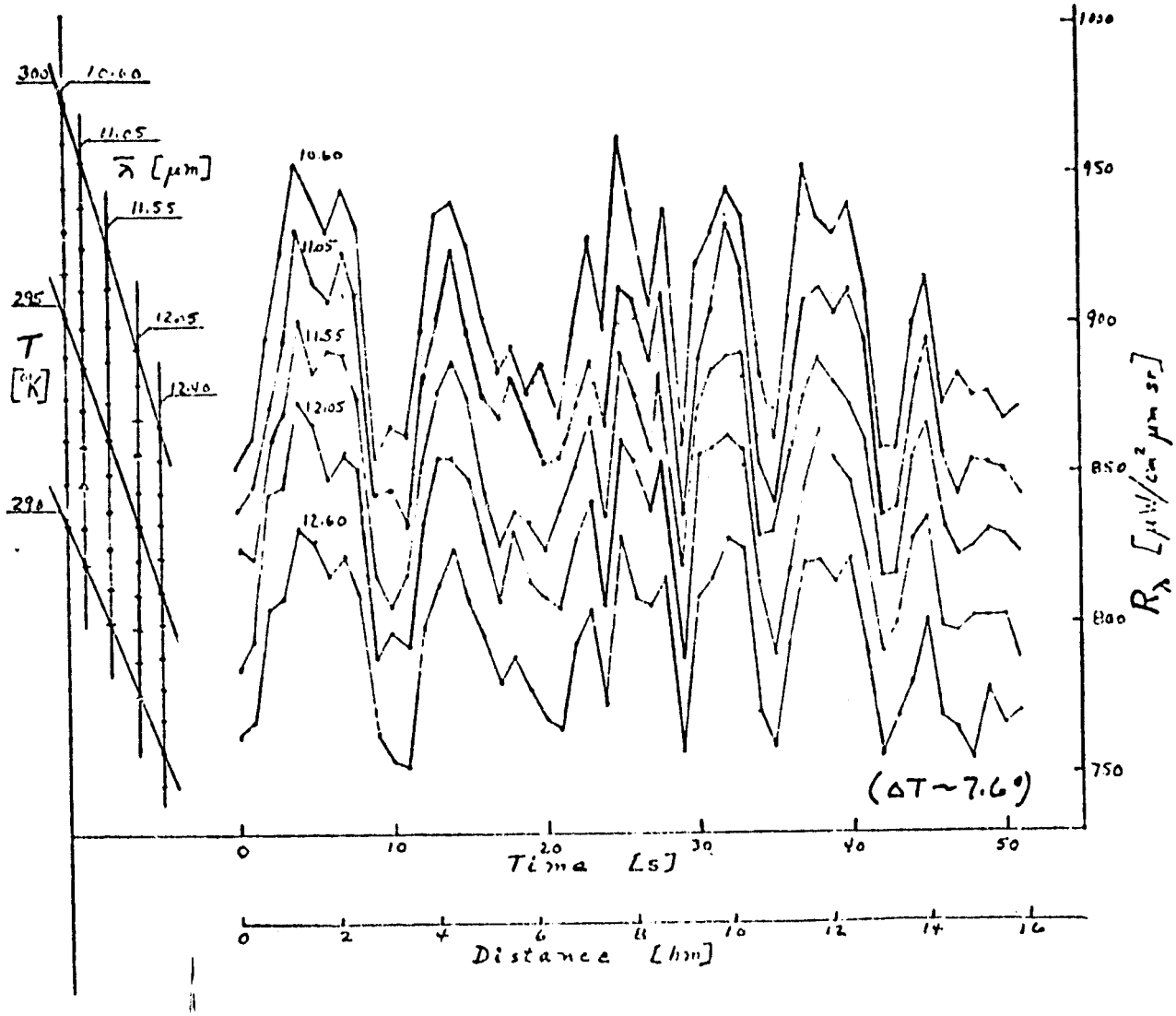

c. Observation number 243, 780709, 19:01 GMT

This period was shortly after local mean solar noon on the 74th day after planting. The crop was fully headed; plant height was 0.76 m; and the ground cover was 30% with no weeds present on the dry field. The wind was light to moderate from the north; and the atmospheric relative humidity was 50%. Sky cover was 10%, but should not have interfered appreciably with solar heating.

As with the two preceding periods, the radiance variations were in phase, but showed smaller ranges. These were from 38 to 73 SU, again associated with B-5 and B-1, respectively. Corresponding ranges of temperature, ΔT, were 3.4°K and 4.8°K, respectively. However, the minimum range, viz., ΔT = 3.2°K, was with B-2, not B-5 as in the two preceding observation periods. The average range of temperature for all bands was 3.9°K.

The interband maximum difference between average temperatures, $d\overline{T}$, was 2.3°K between B-1 with $\overline{T}$ = 300.1°K, and B-5 with $\overline{T}$ = 297.8°K. As in the other periods, minimum differences were found between bands 2,3, and 4, viz., $d\overline{T} \leq 0.5$°K; and of the three, B-2 had the highest $\overline{T}$, viz., 299.4°K, as in OBNO 014.

The average effective temperature, $\overline{T}$, associated with each of the bands was again higher than the air temperature, 296.5°K; and the range of differences was from 1.3°K to 3.6°K. These differences were smaller than those found in the preceding two periods.

MONOCHROMATIC RADIANCE, R_λ, AND EFFECTIVE TEMPERATURE, T

Date/Time: 780709/19:01 GMT Observation No. 243

Air Temperature, 296.5°K; Wind, 005° 16 km/h; Relative Humidity, 50%

Ground Cover, 30%; Maturity Stage, fully headed; Plant Height, 7.6dm

Field Moisture, dry.

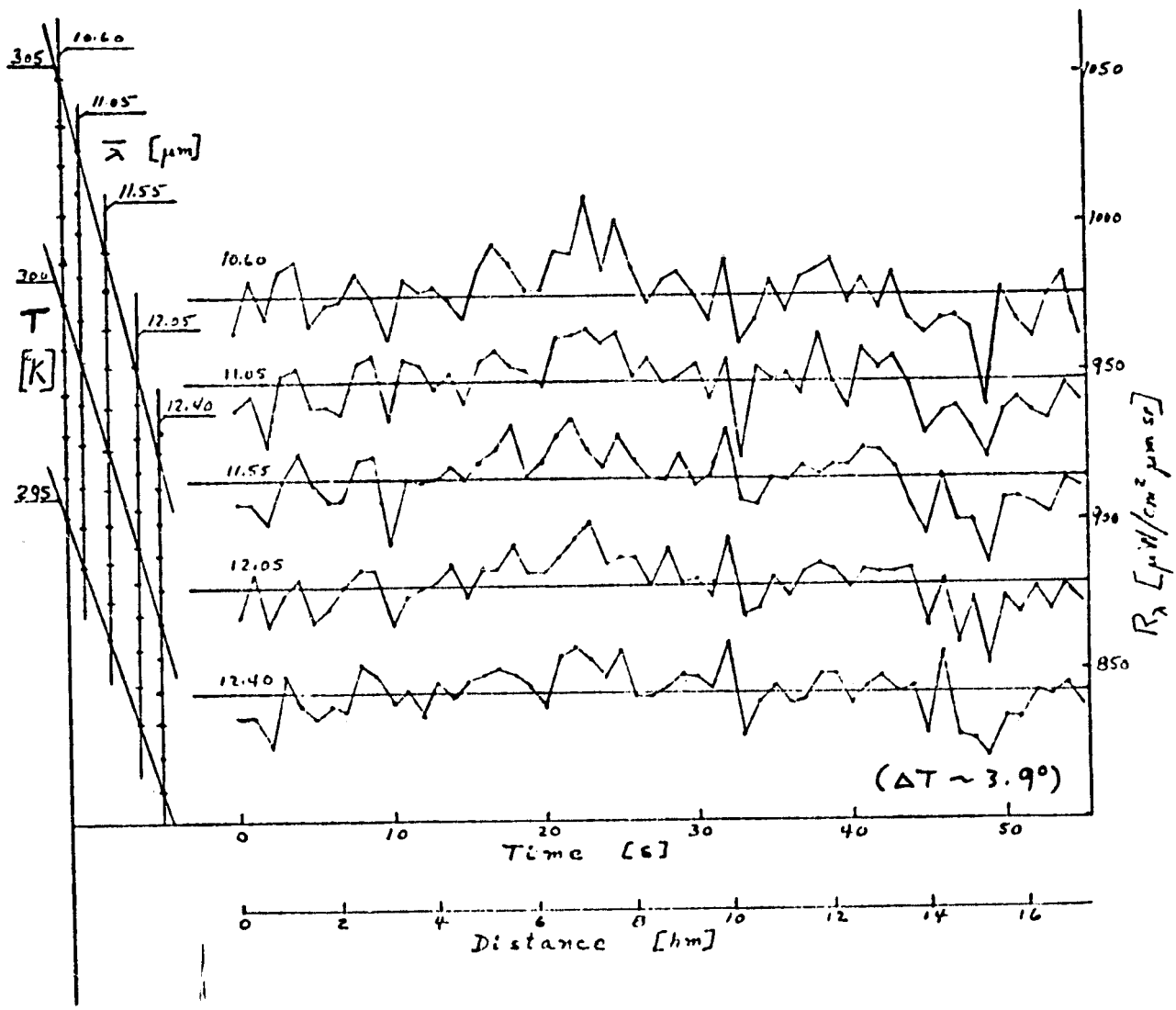

d. Observation number 332, 780726, 15:10 GMT

On this day, the 91st after planting, the crop, at a height of 0.81 m, was beginning to ripen, and covered 30% of the ground. The field was dry and weedless. A very light westerly wind, relative humidity of 54%, and a clear sky characterized the atmosphere.

Radiance variations for all bands were again in phase; and ranges varied from 55 to 84 SU, with associated ΔT values of 4.4°K to 5.5°K, respectively. However, although the maxima were found with B-1, the minima were in the B-4 data. Nevertheless, values for B-5 were quite close, viz., 57 SU and 5.0°K. The average temperature range values for all bands was 5.0°K. The light wind, with a minimum of turbulent mixing, may have been responsible for these larger values, i.e., as compared with those of OBNO 243 which had the same percentage value of ground cover.

Between B-1 and B-5, the interband maximum difference in average temperature, $d\overline{T}$, was 2.3°k, as in the preceding period. Again, the highest temperature (302.0°K) was associated with B-1; the lowest (299.7°K) with B-5. For bands 2,3, and 4, $d\overline{T} \leq 0.5$°K, with B-2 having the highest of the three, viz., $\overline{T} = 301.2$°K.

For each band, the average temperature was higher than the air temperature, 299.3°K; and differences, which ranged from 0.4°K to 2.7°K, were smaller than in the preceding three observation periods. This may have been a consequence of the very light winds which may have minimized the near-surface vertical temperature gradient because of reduced mechanical mixing.

MONOCHROMATIC RADIANCE, R_λ, AND EFFECTIVE TEMPERATURE, T

Date/Time: 780726/15:10 GMT Observation No. 332

Air Temperature, 299.3°K; Wind, 265° 03 km/h; Relative Humidity, 54%

Ground Cover, 30%; Maturity Stage, beginning to ripen; PLHT, 8.1 dm

Field Maturity, dry.

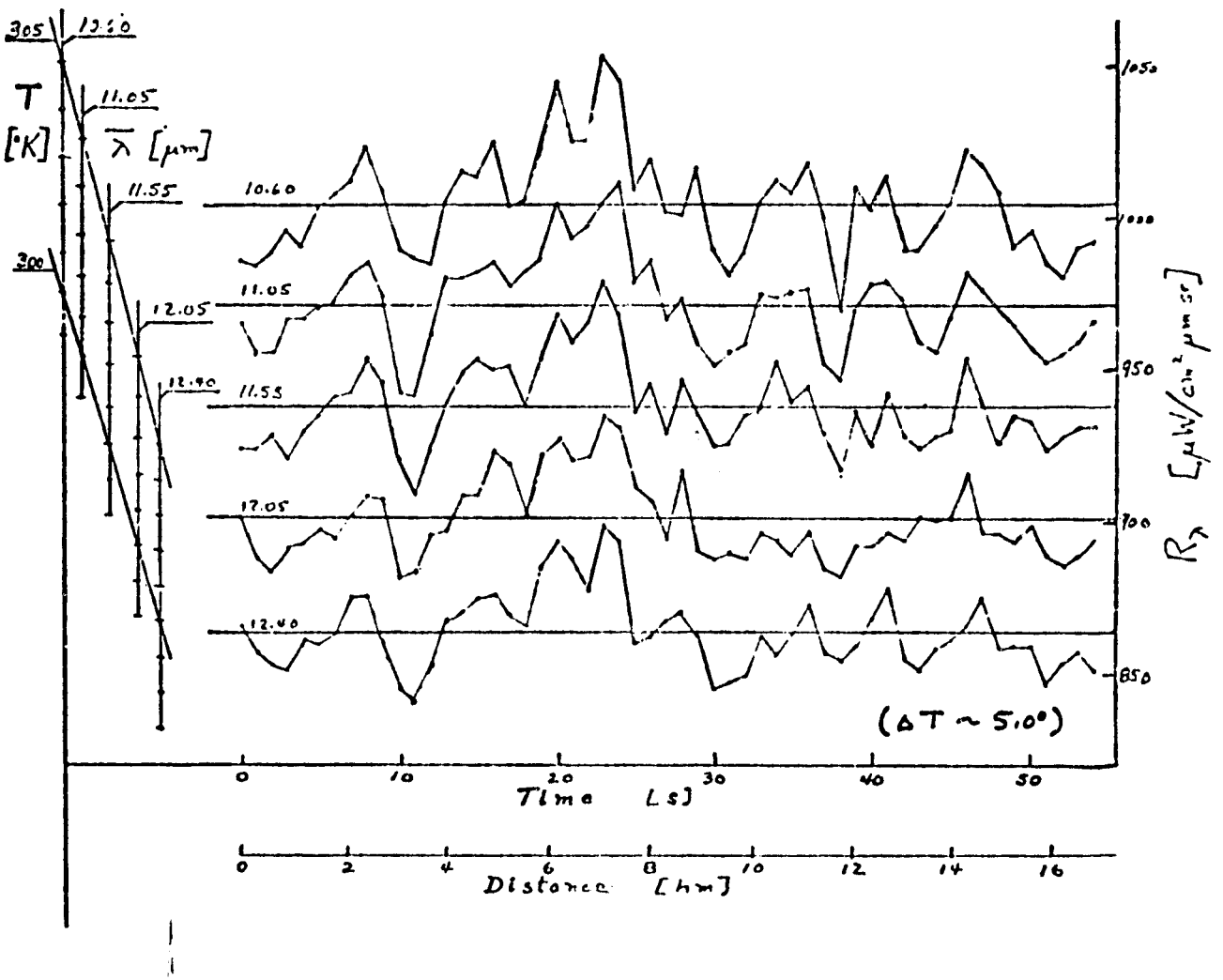

e. Observation number 423, 780816, 15:11 GMT

At this time, 112 days after planting, the wheat crop had been harvested, and the remaining stubble was 0.25 m high, having a ground cover of 10%. The field was damp and weedless, but very likely had some scattered remains of the harvested plants. Wind was moderate and southerly, sky was clear, and the relative humidity was 45%.

Except for minor deviations, the variations of radiance values in all bands were in phase, and showed the smallest ranges, viz., 22 SU to 45 SU, of all the periods in the crop year. The associated temperature ranges were 1.9°k for B-4, and 3.1°K for B-1, respectively. The average ΔT for all bands, as well as for B-5, was 2.5°K, which was the smallest of all periods.

The maximum interband difference of average temperature, between B-1 ($\bar{T}$ = 296.9°K) and B-5 ($\bar{T}$ = 295.3°K) was 1.6°K, and consequently the smallest of all periods. For bands 2,3, and 4, $d\bar{T} \leq 0.3$°K. This value compares favorably with the 0.2°K associated with the period before the crop emerged when the field was sparsely covered with weeds, i.e., OBNO 014.

Unlike all other cases, the average effective temperature of the surface, associated with all bands, was lower than the temperature of the air, which was 298.2°K. Differences ranged from 1.3°K with B-1 to 2.9°K with B-5. Since the soil was damp, we might surmise that this may have been due to evaporative cooling associated with the moderate southerly wind.

MONOCHROMATIC RADIANCE, R_λ, AND EFFECTIVE TEMPERATURE, T

Date/Time: 780816/15:11 GMT Observation No. 423

Air Temperature, 298.2°K; Wind, 190° 18 km/h; Relative Humidity. 45%

Ground Cover, 10%; Maturity Stage, harvested; Plant Height. 2.5 dm

Field Moisture, damp.

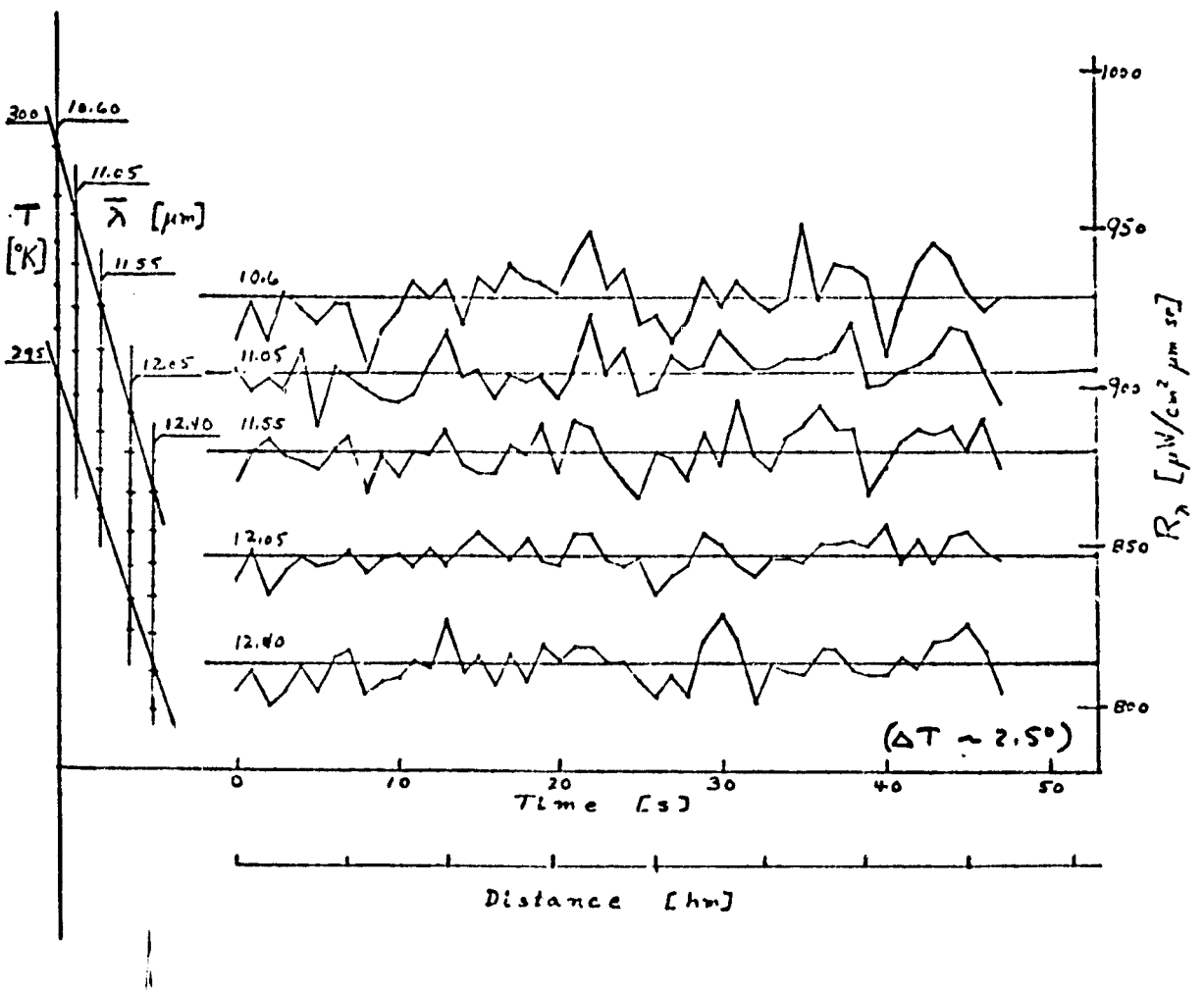

8. Summary

Pertinent details of this data diagnosis are summarized in the following figures, in which data for each observation period are aligned vertically. Fig. A presents field moisture and agronomic features, i.e., ground cover and plant height as a function of the number of days after planting. Fig. B shows temperatures of surface (only the extreme values) and air, as well as ΔT and maximum $d\bar{T}$ values as a function of time of day. The last, Fig. C, presents atmospheric data, i.e., relative humidity and wind (numbers near the plotted wind speed points represent direction in degrees), plotted versus date. Since the characteristics previously discussed are evident if the figures, no further comments are needed.

Acknowledgements. I extend my appreciative thanks to Dr. David E. Pitts, Chief, Radiation Characteristics Section, SAB/ERRD, and to his colleagues Dr. Gautam Badhwar, Kieth E. Henderson, and Melissa Wise (Coop Student, University of TN, Knoxville) for stimulating discussions, freely given help in obtaining data, and for extending much needed assistance on the computors. In addition, I am grateful for the NASA-ASEE Summer Faculty Fellowship Program, and to all members of the managerial staff for the opportunity to participate in a well conducted venture.

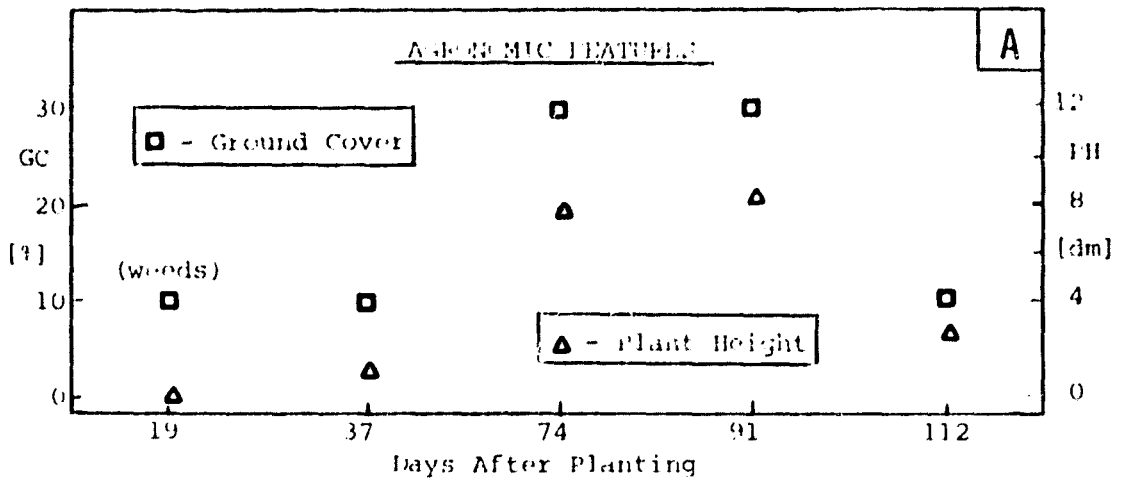

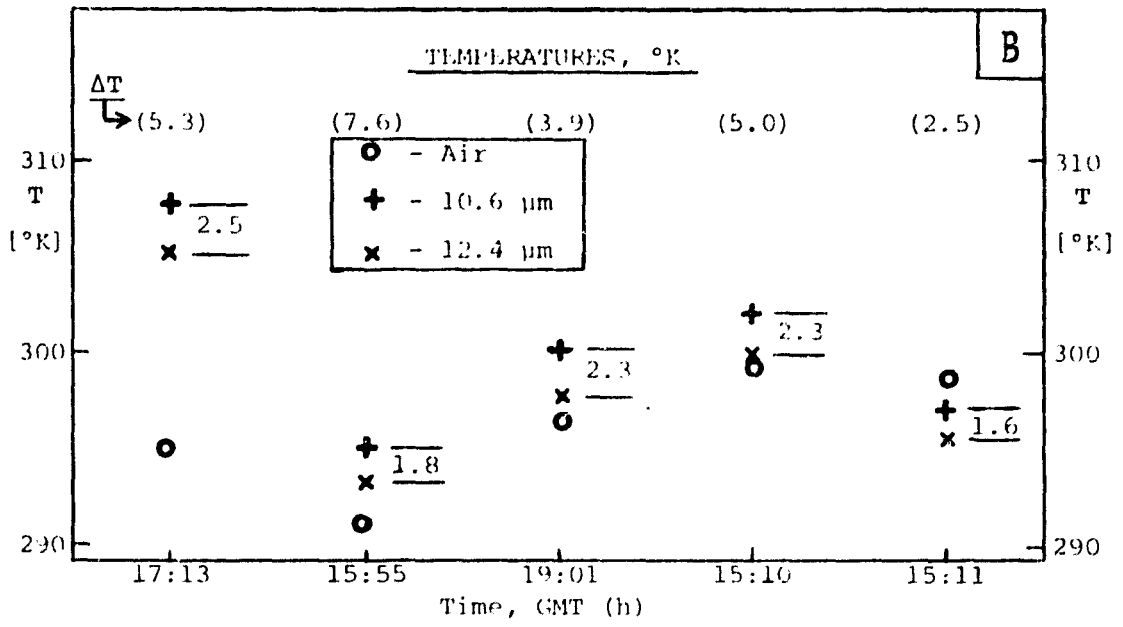

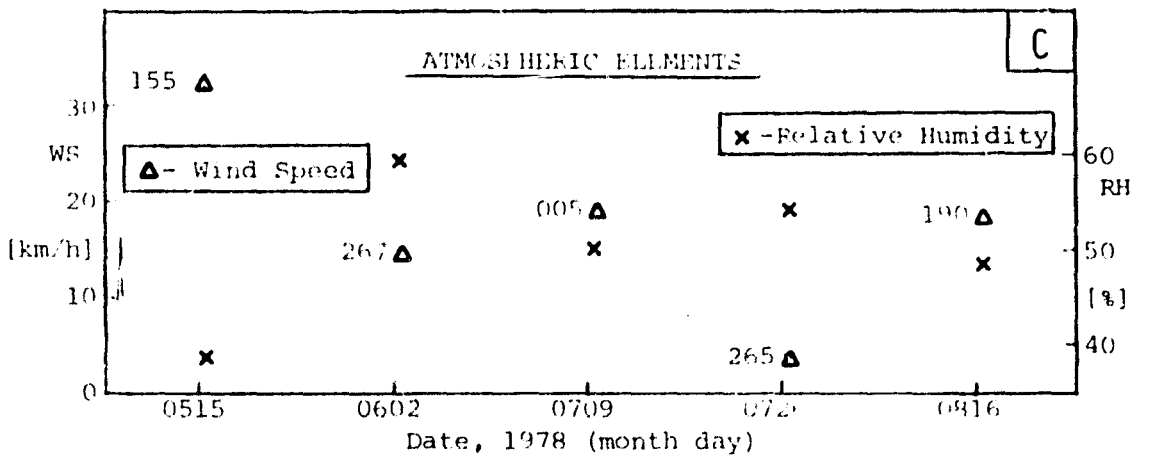

A GRADIENT MODEL OF VEGETATION AND CLIMATE UTILIZING NOAA SATELLITE IMAGERY

PHASE I: TEXAS TRANSECT

PRINCIPAL INVESTIGATORS

David H. Greegor, Jr.[1], and Jim Norwine[2]

APPROVED BY:

Project Manager, SR
Supporting Research
AgRISTARS Program

Earth Resources Applications Division
Space and Life Sciences Directorate
NATIONAL AERONAUTICS AND SPACE ADMINISTRATION
Lyndon B. Johnson Space Center
Houston, Texas
August 1981

---

[1]Biology Dept., Nebraska Wesleyan Univ., Lincoln, NE 68504 (On leave 81-82 to Alaska Pacific U., Anchorage, AK 99504.

[2]Dept. Geography and Geology, Texas A & I Univ., Kingsville, TX 78363.

FIGURE CAPTIONS

1. Sponge moisture variable.

2. Texas sponge values: 1980 (Appendix)
   Normal annual Texas sponge values "

3. Texas sponge values: April, 1980 "
   Normal Texas sponge values: April "

4. Texas sponge values: July, 1980 "
   Normal Texas sponge values: July "

5. Texas sponge values: October, 1980 "
   Normal Texas sponge values: October "

6. Example of a band of 5 NOAA/AVHRR Scanlines and the 5x5 pixel sampling grids along the Texas transect.

7. The normalized difference (ND) regression for 3 sample dates in 1980 along Texas transect.

8. The mean normalized difference (ND) regression line for 3 dates in 1980 along Texas transect.

9. Long-term (1941-1970) sponge normal values and regression from 25 stations on Texas transect.

10. Normalized difference (ND) values vs. sponge indices for 12 sites (3 dates) along Texas transect.

11. Mean normalized difference (ND) regression (see Figure 8) vs. sponge line (see Figure 9) on the Texas transect.

12. Vegetation - Sponge Index (VSI) values along the Texas transect and suggested limits of the vegetation regions.

MAP CAPTIONS

1. 8-inch sponge normals for Texas: 1941-1970.[1]
   [1]Except as noted in Table 2 (Appendix).
2. Normal annual average of 8-inch sponge - State of Texas.
3. Normal January average of 8-inch sponge - State of Texas.
4. Normal average April 8-inch sponge - State of Texas.
5. Normal July average 8-inch sponge - State of Texas.
6. Normal October average 8-inch sponge - State of Texas.
7. 12 sample locations on Texas transect. Letters (A-D) refer to major vegetation regions along transect.[1]
   [1]Modified from Gould (1975).
8. Location of stations used to calculate sponge values along Texas transect.
9. Mean 8-inch sponge values along Texas transect: 1980

TABLE OF CONTENTS

I. OVERVIEW

Phase 1 of this investigation has several objectives: (1) to test a new experimental climatological model/variable termed the sponge for potential biogeographical, ecological, and climatological applications (the sponge is a measure of moisture availability based on daily temperature maxima and minima, and precipitation); (2) to investigate the feasibility of utilizing NOAA/AVHRR meteorological satellite data for vegetation classification; and (3) to initiate a vegetation gradient model that utilizes climatological (i.e., sponge), biological, and NOAA data that is ultimately applicable to global vegetation stratification and monitoring.

To accomplish the initial objective, mean monthly and annual sponge values are calculated for 75 Texas locations for the "normal" period of 1941-70. Similar values are also computed for approximately 25 stations along an east-west transect across Texas for 1979 and 1980. Results suggest that as a generalized climatic index, sponge's simplicity and sensitivity make it particularly appropriate for trans-regional biogeographic studies.

The latter two objectives were approached by acquiring vegetation, climatological (sponge), and AVHRR pixel data (channels 1 and 2) for 12 locations along the east-west Texas gradient. The normalized difference (ND) values for the AVHRR data when plotted against the vegetation characteristics (biomass, net productivity, leaf area) and the sponge values suggest that a multivariate gradient model incorporating AVHRR and sponge data may indeed be useful in global vegetation analysis.

II. THE SPONGE: A NEW ECO-CLIMATOLOGICAL VARIABLE

The planetary distribution of types of natural vegetation is largely a function of climate, most especially of spatial variations in energy and moisture budgets. As a general rule, climate is recognized as the pre-eminent control of natural vegetation at subcontinental-to global-scales. For small areas, geologic, pedologic and other local factors may dominate for long, even indefinite, periods of time.

Natural scientists such as ecologists and biogeographers have attempted to utilize climatic measures and indices in surveys, stratifications and classifications of natural vegetation. Typically, it is assumed that most major ecoregion and native vegetation-region "boundaries" actually represent climatic discontinuities or "breaks". This assumption, while not entirely valid, probably is reasonably accurate.

A key problem for such scholars has been the determination of a simple but accurate climatic "index" (or indices) which would reflect the primary spatial variations in moisture and energy balances and, hence, could be applied to the classification of native vegetation. Climate itself, a complexly synergistic synthesis of many variables, does not readily succumb to quantitative classification. [For example, what is the "real" boundary between a desert and a (semi-arid) steppe? In fact, of course, there is no abrupt statistical limit but rather a gradual transition from one type into another.]

Identifying and quantifying climatic factors which explain the distribution of natural vegetation is even more challenging. Temperature and precipitation by themselves are poor descriptions of climate and, hence, explainers of vegetation distributions (Mather and Yoshioka, 1968).

It is therefore essential to select and/or develop climatic indices which influence vegetation growth and development. Most recent approaches to this problem emphasize the importance of moisture availability (e.g., surpluses versus deficits) and, more specifically, evapotranspiration. Unfortunately, evapotranspiration is measured at very few places, and even evaporation

itself is not widely monitored. Numerous models have been developed which estimate evaporation from measurements of air temperature, average wind speed, and net radiation (Penman, 1948; Jensen et al, 1970), but their usefulness is constrained by the sparcity of stations which record solar radiation and wind speed.

Simpler evapotranspiration schemes which require only air temperature and precipitation -- both commonly measured around the world -- have been devised (e.g., Thornthwaite, 1948; Griffiths, 1964; Moe, 1965; Trenchard, 1976). Thornthwaite's classification made use of mean monthly temperature and precipitation values to generate a moisture index. Because of its relative simplicity and accuracy, Thornthwaite's approach has been widely adopted (e.g., it is used to calculate the USDA's Crop Moisture Index). However, its use of average monthly temperatures somewhat limits its sensitivity to variations in continentality and altitude.

An alternate method of relating climate to vegetation is that of multivariate discriminant analysis of climatic variables to determine their relative influence in a particular ecoregion (e.g., Biogeoclimatic Units of Vancouver Island, Klinka and Nuszdorfer, 1979). While very accurate for detailed, site-specific studies, the resulting multiple regression equations tend to be (a) cumbersome and lengthy, and (b) less applicable to regional and global-scale vegetation classifications.

Thus climatologists, geographers, and ecologists interested in large-area comparisons have found themselves forced to choose between an approach which stratifies climate somewhat too broadly (e.g., Thornthwaite's) and another which "hides the forest for the trees", viz., too much emphasis on detail (e.g., Klinka and Nuszdorfer).

Recently, Trenchard and Artley (1981) developed a new climatological/meteorological variable whose simple form, minimal data requirements and accuracy make it an ideal candidate for application to meso- and macroscale biogeographical, agroclimatological, and ecological investigations.

This hypothetical medium is termed the sponge (see Figure 1). Sponge's rationale is summarized as follows (Trenchard and Artley):

> We desired a simple moisture variable with a sound physical basis that used common meteorological variables, was suitable over a broad range of climates, and applicable to a single station. The result was named sponge.
>
> Sponge is described as a simple medium with 8 inches of water holding capacity which is initialized half-full of water on 1 January.* Each day, in accordance with the hydrologic cycle, water is added to the medium from precipitation and lost through evaporation. Precipitation (both liquid and frozen) is added at the full amount until the layer is saturated. It is this sponge like behavior which gives the variable its name. Any additional precipitation is assumed to be lost as run-off or drainage. Evaporation occurs at a fraction of the Class A Pan rate, the exact proportion being the ration of the current contents to the total capacity of the sponge. Either actual or estimated evaporation pan values may be used. The daily contents of the sponge are defined as:

$$S_i = S_{i-1} + P_i - (E_i * S_{i-1}/CAP)$$

Where:

S_i = Sponge contents on day i, in inches.

P_i = Precipitation on day i, in inches.

E = Actual or estimated pan evaporation in inches on day i.

CAP = Sponge capacity in inches

and $0 \leq S_i \leq CAP$

When evaporation pan measurements are not available, they may be estimated with a divisor of 30 days to convert the evaporation function to a daily value.

$$S_i = S_{i-1} + P_{i-}(EP(TX_i, TN_i)*S_{i-1}/CAP*30)$$

*Alternatively, the final value of the previous year may be used as an initial value, and the capacity may be varied for a particular region.

SPONGE MOISTURE VARIABLE

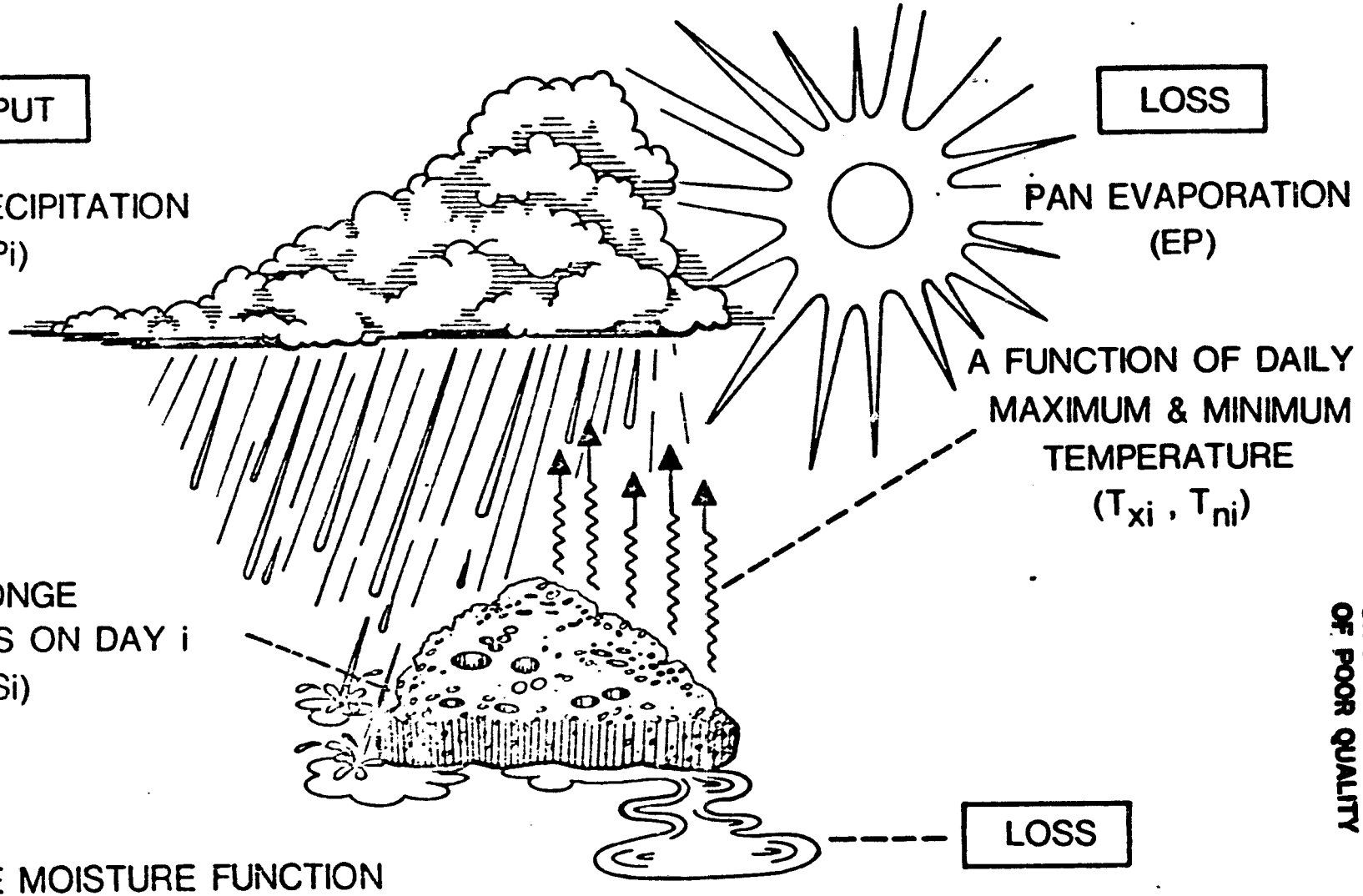

SPONGE MOISTURE FUNCTION

$$S_i = S_i\text{-}1 + P_i - EP(T_{xi}, T_{ni}) * S_i\text{-}1/CAP$$

WHERE $0 \leq Si \leq CAP$

Figure 1.

Where:

SP = Pan evaporation function

TX_i = Maximum temperature on day i.

TN_i = Minimum temperature on day i.

Because of its simple data requirements (daily precipitation and evaporation estimated form maximum and minimum temperatures), the sponge can be calculated at any temperature precipitation observation station.

Long-term (1941-1970) sponge "normals" (average values) were recently calculated for all first-order meteorological stations in the counterminous USA (Trenchard, 1981). Some representative values are presented in Table 1. It is interesting to note that mean annual sponge values were found to range between Yuma, Arizona (0.20") and Mt. Washington, New Hampshire (8.00", or absolute sponge capacity).

Sponge is concluded to present a meaningful measure of areal "environmental moistness". As a generalized climatic index, sponge's simplicity and sensitivity make it particularly appropriate for transregional biogeographical studies (e.g., a large-area vegetation classification).

Station	Latitude (°N)	Longitude (°W)	Mean January Sponge Value (")	Mean July Sponge Value (")	Mean Annual Sponge Value (")
Mt. Washington, N.H.	44.27	71.30	8.00	8.00	8.00
Stampede Pass, Wash.	47.28	121.33	8.00	6.78	7.49
Caribou, ME.	46.87	68.02	8.00	5.47	6.89
Duluth, Minn.	46.83	92.18	7.97	6.01	6.73
Pensacola, Fla.	30.47	87.20	6.98	6.11	6.41
Seattle, Wash.	47.45	122.30	8.00	2.98	5.67
Cincinnati, Ohio	39.05	84.67	6.89	4.00	5.24
Chicago, Ill.	41.98	87.90	5.85	4.32	5.04
Key West, Fla.	24.55	81.75	3.77	4.66	4.50
Houston, TX.	29.97	95.35	5.56	3.39	4.27
San Francisco, Cal.	37.62	122.38	6.17	1.24	3.35
Dallas, TX.	32.90	97.03	3.26	2.13	3.06
Walla Walla, Wash.	46.03	118.33	4.65	1.14	2.79
Salt Lake City, UT.	40.78	111.95	3.03	0.99	2.14
Goodland, Kan.	39.37	101.70	1.24	2.15	1.60
San Diego, Cal.	32.73	117.17	2.29	0.60	1.37
El Paso, TX.	31.80	106.40	0.76	0.67	0.64
Yuma, Ariz.	32.67	114.60	0.42	0.04	0.20

Table 1. Selected USA 8-Inch Sponge Normals: 1941-1970.[1]

[1] Calculations by W. Tegenhard (Lockheed), NASA-JSC, Houston, TX, July 1991

III. THE SPONGE VARIABLE AS APPLIED TO MOISTURE AND VEGETATION GRADIENTS IN TEXAS

There exists in Texas the most pronounced continuous, non-orgraphic, intrastate climatological gradient found anywhere in the United States. At least four distinct, first-order climatic types occur within the state (humid subtropical, tropical steppe, tropical desert, and mid-latitude steppe), with many more important subtypes (e.g., subtropical subhumid). In particular, there is an extraordinarily steep east-west moisture gradient, ranging from very humid in southeastern Texas (mean annual precipitation $\geq$ 50") to true desert in far western Texas (average yearly precipitation $<$ 8.0"). This gradient strongly influences ecological patterns, and virtually controls the regional distribution of natural vegetation.

Texas is, then, an excellent natural "laboratory" to test the responsiveness and usefulness of the sponge variable (e.g., with respect to the classification of natural vegetation utilizing satellite data). With this in mind, mean sponge values were calculated for various Texas locations in order to address these questions:

1. Does use of the sponge portray the distribution of climates (especially moisture regions) in Texas better than, say, precipitation alone?
2. If sponge accurately reflects the climates of Texas, can these values be meaningfully correlated with vegetation-index ("greenness") values as measured from space by NOAA meteorological satellites (see the discussion of these indices later in this report)?
3. If the answer to question (2) is affirmative, can a combination of sponge and satellite-derived greenness indices be used to classify the major natural vegetation regions/types of the state? If so, it might well prove feasible to utilize this methodology for other large-area and even global-scale vegetation surveys and classifications.

Climatic Strata And Gradients in Texas Using The Sponge: Long-Term "Normals".

In order to assess sponge's potential usefulness as a climatic index in Texas, long-term annual and monthly sponge "normal" (1941-1970 mean) values were computed for 75 locations widely distributed throughout the state (see Map 1). Sponge values were obtained by utilizing (1) the formula presented in section 1 of this report, and (2) mean monthly temperature maxima and minima, and precipitation, as compiled by th U.S. National Weather Service (NOAA)*.

The results of these computations are illustrated in Maps 2-6, while Tables 2a-2e (Appendix) present average normal (1941-70) monthly and annual precipitation and sponge values for each of the 75 locations. They are largely self-evident, but several of the more intriguing aspects should be briefly addressed.

Mean annual sponge values are greatest in the southeast (e.g., 5.2" at Beaumont) and decrease continuously to lows in the westernmost quadrant (0.49") at Presidio in the Chihuahuan Desert). This is virtually identical to the pattern of average annual precipitation. However, sponge appears to more accurately portray (1) seasonal moisture changes across the state, and (2) the magnitude of differences in the relative moistness of the varous parts of Texas than does either precipitation or potential evapotranspiration (estimated by Thornthwaite's method; see Table 3).

With respect to season, Figures 2-5 (Appendix) and Tables 2 (Appendix) and 3 clearly indicate that, for vegetative activity, winter and spring are the wet seasons in East Texas while summer and fall are the moistest periods in West Texas -- quite unlike the seasonal distribution of precipitation alone, which is greatest in the summer throughout the state. (Thornthwaite's "Index of Moisture" would also reveal this aspect but, because of its reliance on mean monthly temperatures, with less spatial sensitivity than sponge; Carter and Mather, 1966).

*Daily data were simulated from monthly mean temperature maxima, minima, and precipitation for each station for 1941-70 using a series of harmonic transformations. For 1979 and 1980, actual daily data were used.

Map 1.

8-INCH SPONGE NORMALS FOR TEXAS
(PERIOD 1941-70, EXCEPT AS NOTED IN TABLE 2)

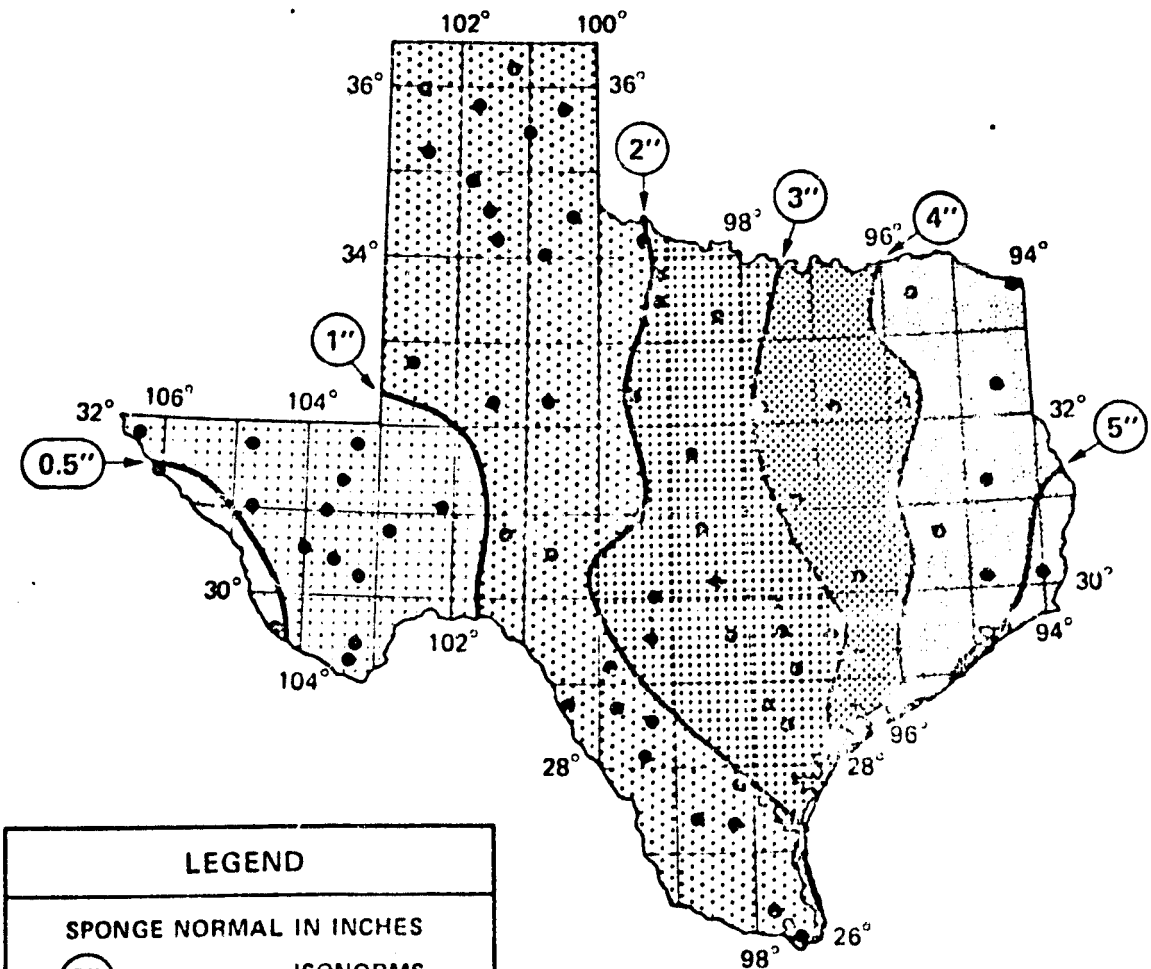

LEGEND

SPONGE NORMAL IN INCHES

5" ISONORMS

≤ 0.5"	3-4"
0.5-1"	4-5"
1-2"	≥ 5.0"
2-3"	

● STATIONS FOR WHICH NOAA CLIMATIC DATA WERE USED TO CALCULATE SPONGE "NORMALS" (i.e. MEANS, 1940-70)

Map 2.

NORMAL ANNUAL AVERAGE OF 8-INCH SPONGE - STATE OF TEXAS (PERIOD 1941-70, EXCEPT AS NOTED IN TABLE 2)

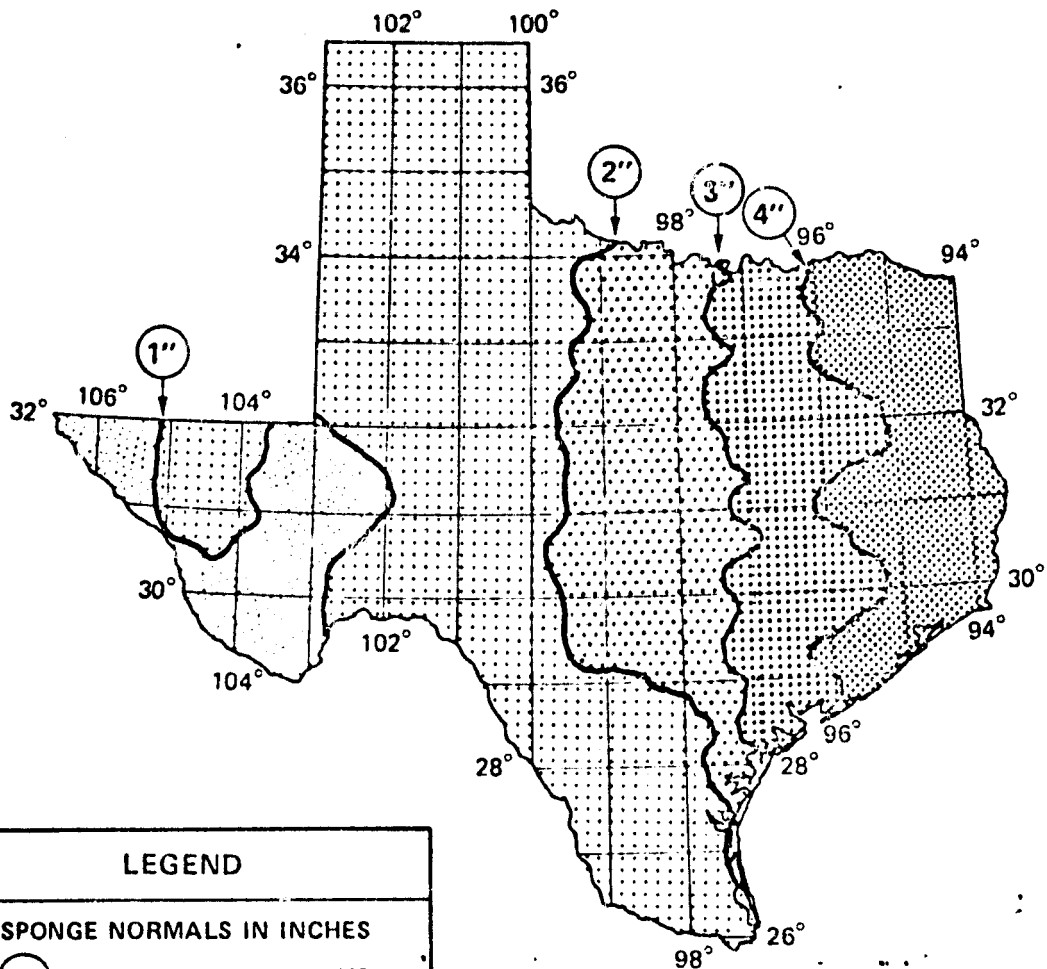

LEGEND

SPONGE NORMALS IN INCHES

5" ISONORMS

≤ 1"	3-4"
1-2"	≥ 4"
2-3"	

NOTE:

MAPS 2 – 6 ARE BASED ON COMPUTER-GENERATED GRAY-SCALE PLOTS –– VALUES SHOWN ARE GENERALIZED (1° x 1° AVERAGES).

Map 3.

NORMAL JANUARY AVERAGE 8-INCH SPONGE - STATE OF TEXAS (PERIOD 1941-70, EXCEPT AS NOTED IN TABLE 2)

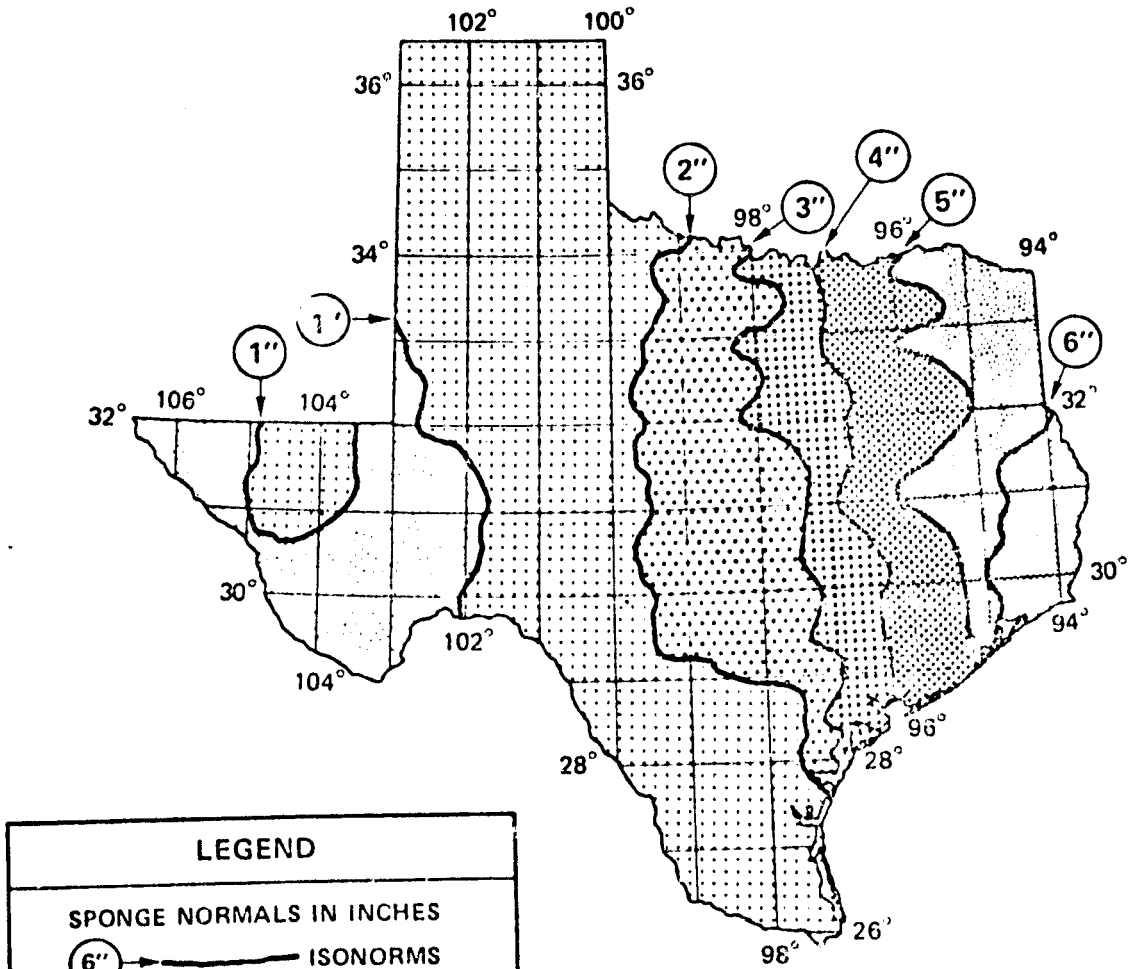

LEGEND

SPONGE NORMALS IN INCHES

6" → ISONORMS

≤ 1"	4-5"
1-2"	5-6"
2-3"	≥ 6"
3-4"	

Map 4.

NORMAL AVERAGE APRIL 8-INCH SPONGE - STATE OF TEXAS (PERIOD 1941-70, EXCEPT AS NOTED IN TABLE 2)

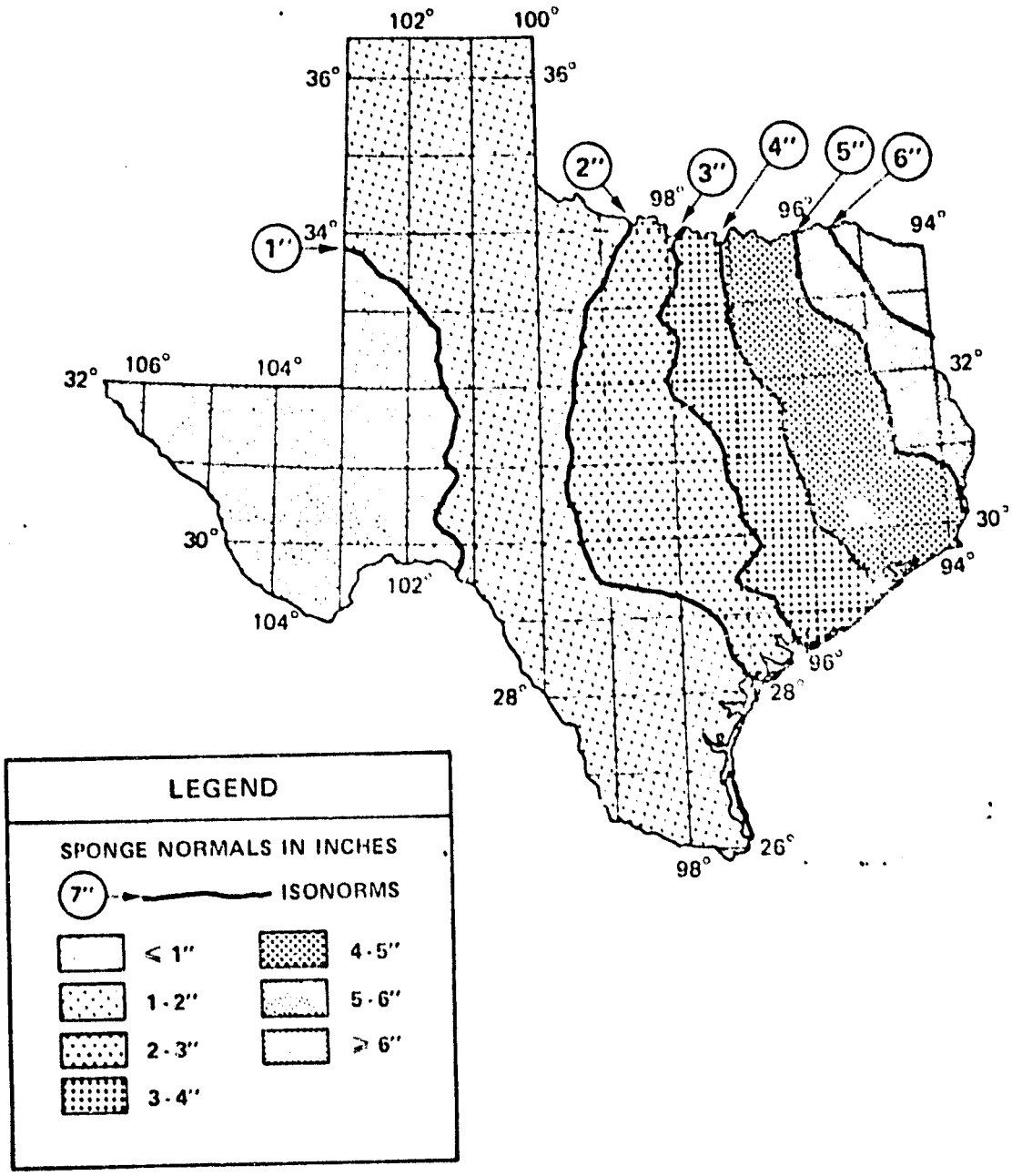

Map 5.

NORMAL JULY AVERAGE 8-INCH SPONGE - STATE OF TEXAS
(PERIOD 1941-70, EXCEPT AS NOTED IN TABLE 2)

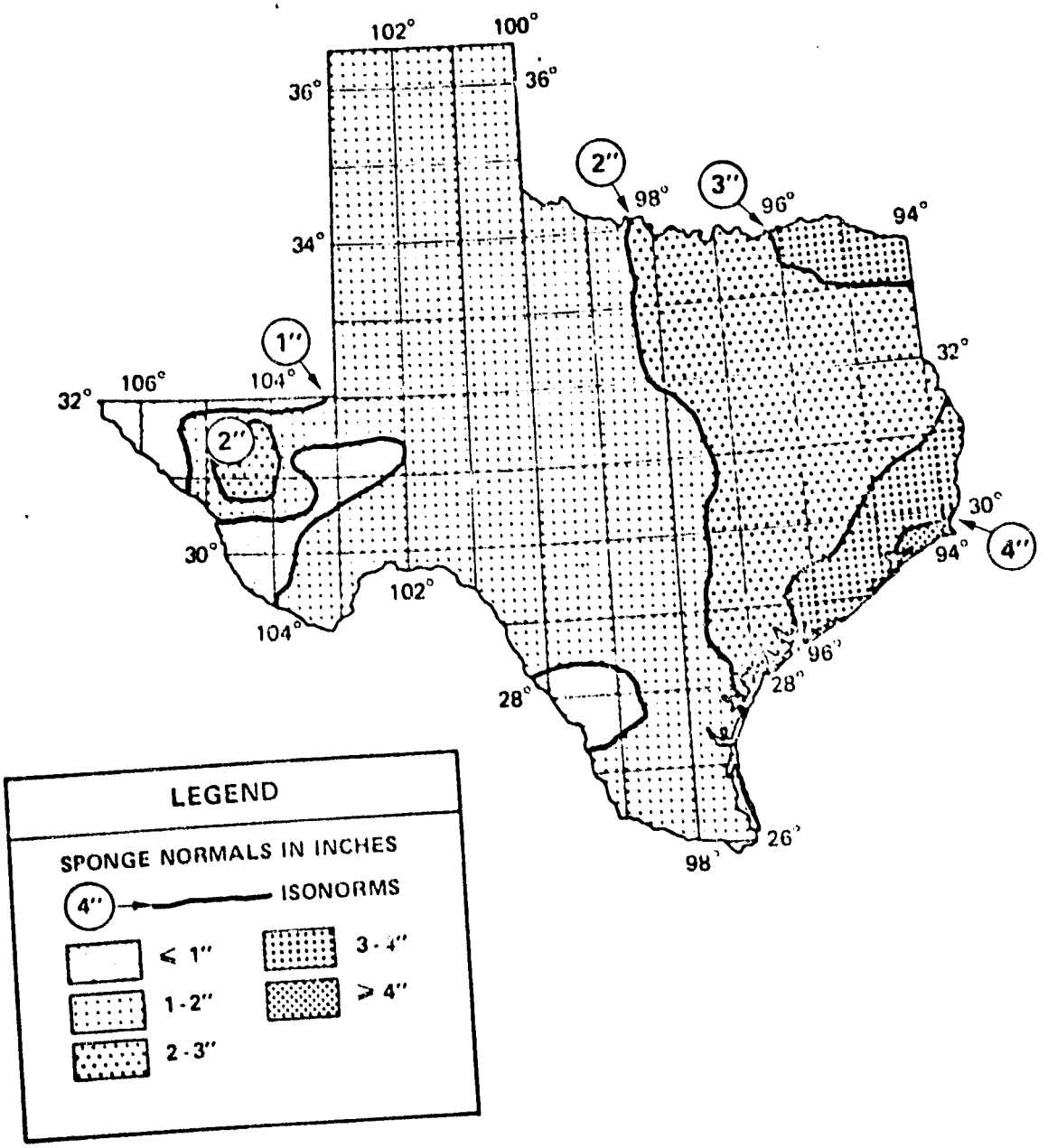

Map 6.

NORMAL OCTOBER AVERAGE 8-INCH SPONGE - STATE OF TEXAS (PERIOD 1941-70, EXCEPT AS NOTED IN TABLE 2)

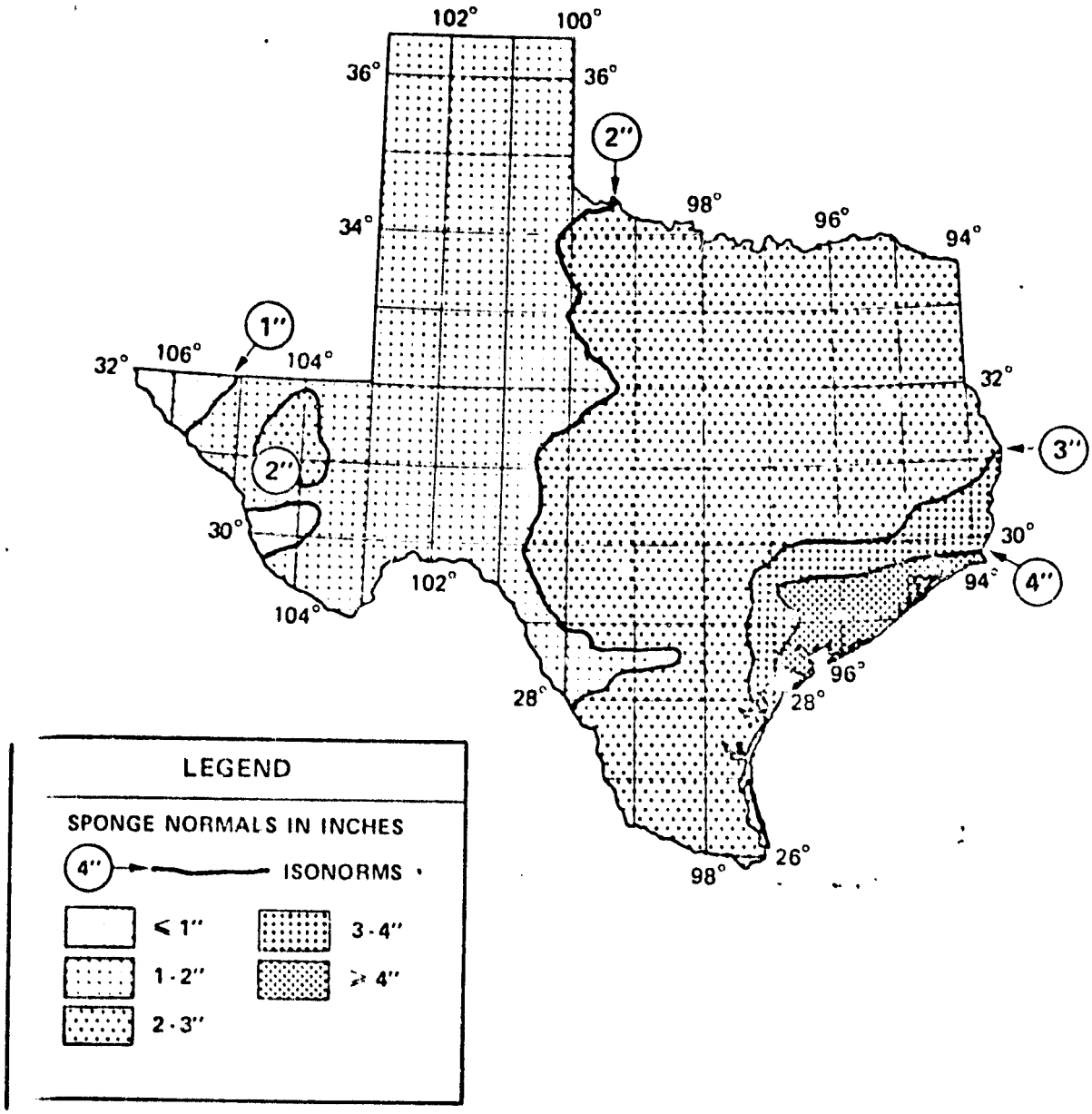

Station	Period	Precipitation	Potential Evapotranspiration	Actual Evapotranspiration	Sponge
l Paso/La Tuna	Annual	8.06	38.40	8.72	0.59
l Paso/La Tuna	January	0.41	0.4[illegible]	0.44	0.71
l Paso/La Tuna	April	0.15	2.72	0.32	0.35
l Paso/La Tuna	July	1.61	6.96	1.76	0.66
l Paso/La Tuna	October	0.70	2.60	0.84	0.73
lcCamey	Annual	12.75	42.72	14.28	0.94
lcCamey	January	0.64	0.32	0.32	0.98
lcCamey	April	0.77	3.24	0.88	0.61
lcCamey	July	1.64	7.48	1.60	0.99
lcCamey	October	1.39	3.04	1.20	1.14
Temple	Annual	33.87	41.20	33.68	3.08
Ier P	January	2.35	0.44	0.44	4.08
Temple	April	3.67	2.92	2.92	3.50
Temple	July	1.96	7.40	5.20	2.03
Temple	October	2.73	2.92	2.92	2.24
ort Arthur/Beaumont	Annual	54.77	43.44	42.44	5.20
Port Arthur/Beaumont	January	4.57	0.76	0.76	7.00
Port Arthur/Beaumont	April	4.43	3.12	3.12	5.33
Port Arthur/Beaumont	July	5.71	7.20	7.08	4.30
Port Arthur/Beaumont	October	3.19	3.40	3.36	3.85

Table 3. Comparison of Normal Average Sponge, Potential Evapotranspiration[1], Actual Evapotranspiration[1], and Precipitation at Four Texas Stations.[2]

[1]P. E. and A. E. values extracted from: Average Climatic Water Balance Data of the Continen Pa VII, United States, 1964, C. W. Thornthwaite Assoc Laboratory of Climatology, Pub. Cl. A Vol. 17, No.3, Centerton, N. J.

[2]All values in inches.

Regarding differences in the absolute magnitude of available moisture from place to place (i.e., how much wetter is site "x" than site "Y"?), sponge also proves highly effective. For example, note that Beaumont's mean precipitation is 6.4 times that of Presidio annually and, in April, Beaumont's average rainfall is 21 times that of Presidio. Sponge shows that the moisture gradient between these locations is actually much steeper: Beaumont's mean annual sponge value is 10.5 times greater than that of Presidio and, in April, Presidio's average sponge value of 0.15" is only 3% of Beaumont (5.33"), a difference of 35.5X. In other words, West Texas is nearly twice as dry -- compared with the humid eastern part of the state -- as precipitation averages alone would suggest. Considering that moisture availability is the primary limiting factor with respect to ecoregions and natural vegetation communities in Texas, it may be concluded that the sponge variable is an effective tool for analyzing climate-vegetation relationships.

Recent Sponge Conditions in Texas: 1979 and 1980. Mean monthly and annual sponge values for the 75 test stations, as well as an additional number of locations along the "Texas Transect" (see next section) were calculated for 1979 and 1980 to assess sponge's responsiveness to inter-annual moisture variability. (Only briefly examined here, these variations, and their associations with satellite-measured vegetative index values, will be more intensively studied in a later phase of this research effort.) Refer to Tables 2 and 4 (Appendix; also Figures 2-5 (Appendix).

It is evident that 1979 was wetter than normal in East Texas (e.g., 1979 $\overline{X}_{Sp}$ at Liberty - 5.31" compared with normal annual $\overline{X}_{Sp}$ of 4.41"), while it was dry in central Texas (e.g., at Brady, in 1979 $\overline{X}_{Sp}$ = 2.09"; $\overline{X}_{Sp}$normal = 1.96") and near-normal in West Texas (e.g., at Balmorhea, 1979, $\overline{X}_{Sp}$ = 0.87"; $\overline{X}_{Sp}$normal - 0.81").

Intrastate moisture conditions in 1980 were quite different than those of 1979. East Texas was unusually dry in 1980: For example, Huntsville's mean annual sponge was 2.57", only 61% of the long-term normal value. The difference was especially pronounced in mid-summer, when this area experienced drought conditions (see Figure 4 Appendix).

By contrast, 1980 was a relatively moist year in West Texas: Pecos and Balmorhea, for instance, had annual sponge values nearly 100% above their 30-year normals (see Table 4, Appendix).

Preliminary Assessment of Sponge

Based on these early results, it may be concluded that the sponge is a useful new climatic variable for purposes of identifying and interpreting trans-regional moisture (and, therefore, ecological) gradients and strata. In fact, it may well prove to be, on balance, the best such measure yet devised for practical large-area analysis. Accordingly, sponge is utilized in the following sections of this report as a generalized climatic index, one which is correlated with vegetative indices derived from NOAA meteorological satellite imagery, as part of a gradient study of natural vegetation along a hypothetical east-west "Texas Transect".

IV. THE VEGETATION GRADIENT UTILIZING NOAA SATELLITE IMAGERY

Historically, two broadly conceived research methods have evolved to allow stratification and abstraction of plan communities, classification and gradient analysis (Kessell, 1979). Classification involves grouping samples together on the basis of shared characteristics into an abstract class of plant communities. Such a grouping of communities by any definition of shared characteristics is referred to as a community-type (Whittaker, 1975 b). The second method, gradient analysis, deals not with discontinuous classes but with continuity and gradient relationships. When the arrangement is along a predetermined environmental gradient, i.e. moisture, the method is termed direct gradient analysis. Indirect gradient analysis is the arrangement of samples along abstract axes that may or may not correspond to environmental gradients. The process of arranging samples along one or more environmental gradients is called ordination (Goodall, 1954 cited in Kessell, 1979). Since vegetation varies continuously along a moisture gradient, samples can indeed be ordinated.

Frequently, the development of a useful classification system requires the use of ordination methods. Discontinuities in the natural vegetation are sought for the purpose of determining the boundaries of the community types recognized. These are often best determined objectively by employing the methods of gradient analysis and ordination. The development of a Montana habitat-type system (Phister, et al. 1977 cited in Kessell, 1979) is a good example of the successful use of ordination in developing a classification system.

Gradient modeling has been the first extensive application of gradient analysis to the needs of resource management information systems (Kessell, 1979). Gradient modeling involves the linkage of a multidimensional gradient analysis with a remote site-specific inventory and appropriate computer software. Once the gradient model is complete, it can provide quantitative community inferences (i.e., biomass, cover) if the location of each site within the gradient matrix is known (geographic coordinates, elevation, aspect, etc.).

The initial step is to obtain information about the vegetation. Data on the vegetation can be obtained by field samples ("ground truth" studies) and remote methods (aerial photography and satellite imagery). Most systems use both. Detailed ground truth data are used to derive community-types, whereas aerial photographs and imagery are generally used to infer the vegetation of unsampled areas.

To date, a considerable number of vegetation investigations have been carried out using Landsat MSS imagery but very little has been attempted with the meteorological satellite systems, particularly the NOAA/AVHRR. Gray and McCrary (1980, cited in Gray and McCrary, 1981) obtained a high correlation for detection of vegetation greenness between the NOAA-6 AVHRR Large Area Coverage (LAC) data sets and Landsat MSS data within identical target areas. This finding led Gray and McCrary (1981) to suggest the NOAA satellite systems should be used for monitoring global vegetation. One major advantage of NOAA over Landsat is the tremendous increase in frequency of data collection. Gray and McCrary (1981) anticipated that variations in the AVHRR responses will provide information about reactions of vegetation to moisture availability and thermal effects. They have demonstrated this for croplands in southern Texas before and after Hurricane Allen in April 1980. Since vegetation, particularly in regions arid and semi-arid is very responsive to moisture patterns, it is well worthwhile to investigate temporal changes in natural vegetation and how closely these relate to shifts in the AVHRP vegetation index.

Quite likely, we shall ultimately discover that the success of stratifying different vegetation types from AVHRR vegetation indices will depend not on spatial distinctions but on temporal distinctions, i.e., the rate and magnitude of the spectral shift during a single season. Eventually, vegetation indices can be ordinated (indirect gradient analysis) and correlated to ground truth vegetation and climatological gradients (direct gradient analysis). The ultimate gradient model, incorporating both field and satellite data, may permit vegetation classification and monitoring of changes with minimal ground truthing.

Data Acquisition and Processing

The vegetation gradient model initially necessitated establishing a sample series along an environmental gradient. At NASA/JSC, we were geographically sitting at the eastern edge of perhaps one of the best natural east-west gradients in North America: Trans-Texas, along approximately 30 (^{o}N) latitude. As one moves from Beaumont to El Paso, Texas, one passes through four major natural vegetation regions: (a) mixed pine-hardwood forest, (b) savannah, (c) shrubland, and (d) desert/desert scrub (Map 7). Precipitation exhibits a continuum that has an annual mean > 50" (east Texas) to < 8" (west Texas). The elevation is 0.0' at the Gulf, 5000' just east of El Paso. It would be difficult to identify a better east-west continuum anywhere that changes gradually, yet dramatically and without any obvious disjunctures over a distance of approximately 750 miles. While the soil and geology definitely change across Texas, we do not intend to include a discussion of those variables at this time.

Our main objective has been to design a model that may ultimately allow vegetation classification on a global scale utilizing satellite imagery. We initially expected to use Landsat data. By a stroke of good fortune, we discovered that NOAA/AVHRR "Metsat" data was not only being archived locally by NOAA personnel (T. Gray, D. McCrary) in a readily useable form but it fit our specifications perfectly. The appropriate software had been written by Lockheed, Inc., to be able to retrieve raw pixel data for AVHRR - channels 1 and 2 along specific scanlines or bands of scarlines across the entire state of Texas. In addition, the software provided geographic coordinates for each pixel. In order to obtain a specific scanline, it was really only necessary to provide the specific coordinates at the beginning and end of our trans-Texas transect. Since the NOAA - n series of satellites orbit is near-polar, sun-syncromous, and twice daily, it crosses a given longitude at an angle and at varying places. Consequently, since scanlines are perpendicular to the orbit, it was impossible to select scanlines that remained "isolatitude" or were exactly superimposed from one date to the next. It is also important to remember that NOAA scenes cover such an expanse that related angles to each pixel vary greatly. To permit comparisons, the pixel radiance values have been normalized to an overhead sun.

Map 7.

12 SAMPLE LOCATIONS ON TEXAS TRANSECT

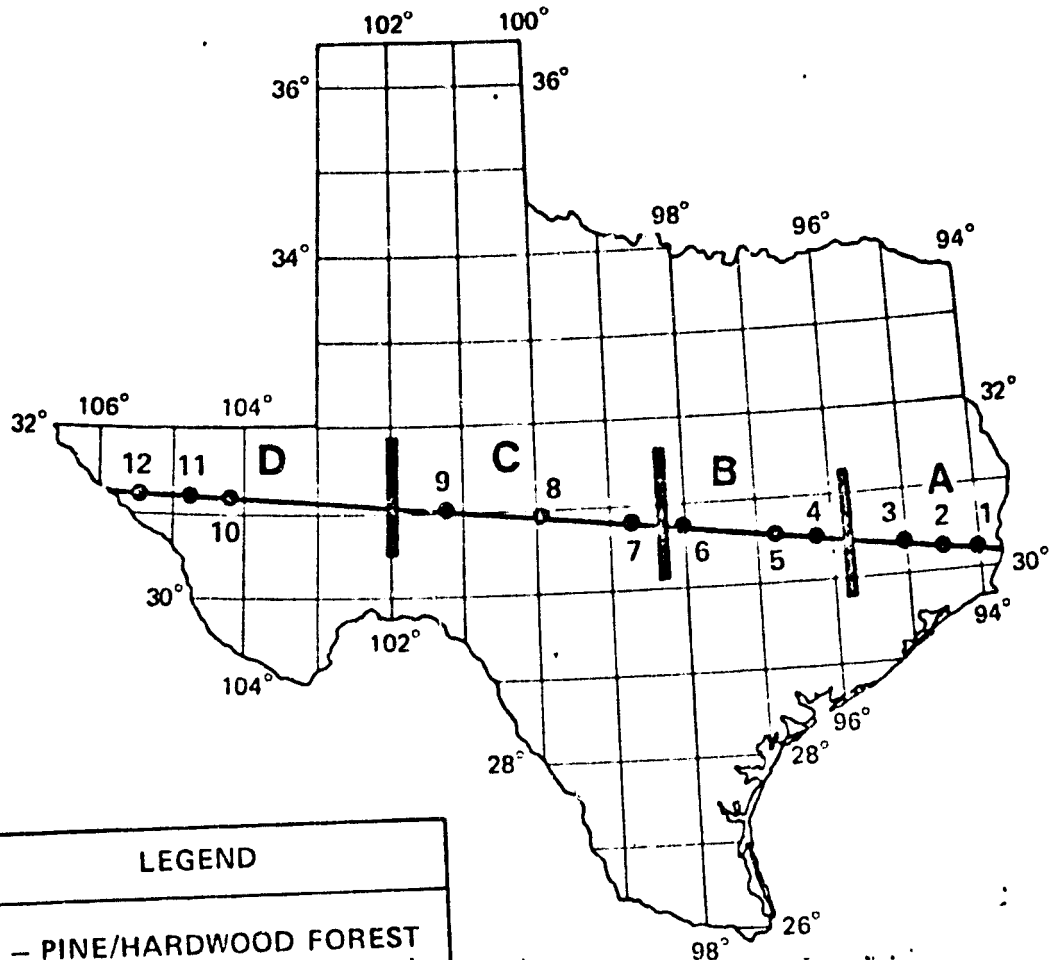

LEGEND
A – PINE/HARDWOOD FOREST
B – SAVANNAH
C – SHRUBLAND
D – DESERT/DESERT SCRUB

It has been our intention to acquire scanlines for four cloud-free days during 1980 - one from each season. At this point we have only been able to process 3 dates (April 19, July 10, October 9); winter has been excluded for lack of data. We requested and received bands of 5 adjacent scanlines, extending essentially from El Paso to Beaumont (Figure 6). At predetermined locations which corresponded to our ground truth sites along the strip, we sampled a 25 pixel grid (5 x 5), obtaining an average grid value of pixel counts for each two channels. The selection of the 25 pixel sample grids was somewhat difficult because it was not possible to accurately ground-truth the transect line. The intention has been to select 12 sites, approximately 3 sites in each of the four major vegetation regions bisected (Map 7). Using Texas vegetation-type maps (Texas Parks and Wildlife Department - based on Landsat data), original Landsat MSS scenes, aerial photos, Aeronautical Navigation maps (1:1,000,000), and selected vegetation references (Gould, 1975; see Smeins, 1978), an effort was made to choose "homogeneous" natural vegetation sites, devoid of water, urbanization, and cultivation. The site locations were shifted slightly between sampling dates because the scanlines could not be superimposed.

It was difficult deciding just how to initially treat the satellite data. Gray and McCrary (1981) have devised their own vegetation index, that they now rather appropriately call the Gray-McCrary Index (GMI). The GMI is simply the difference between the solar-zenith corrected albedo value for the two channels. At least initially, we are using the Landsat-derived normalized difference (ND) equation of Rouse, et al. (1973) and Deering, et al. (1975) where:

$$ND = \frac{\text{Channel 2 - Channel 1}}{\text{Channel 2 + Channel 1}}$$

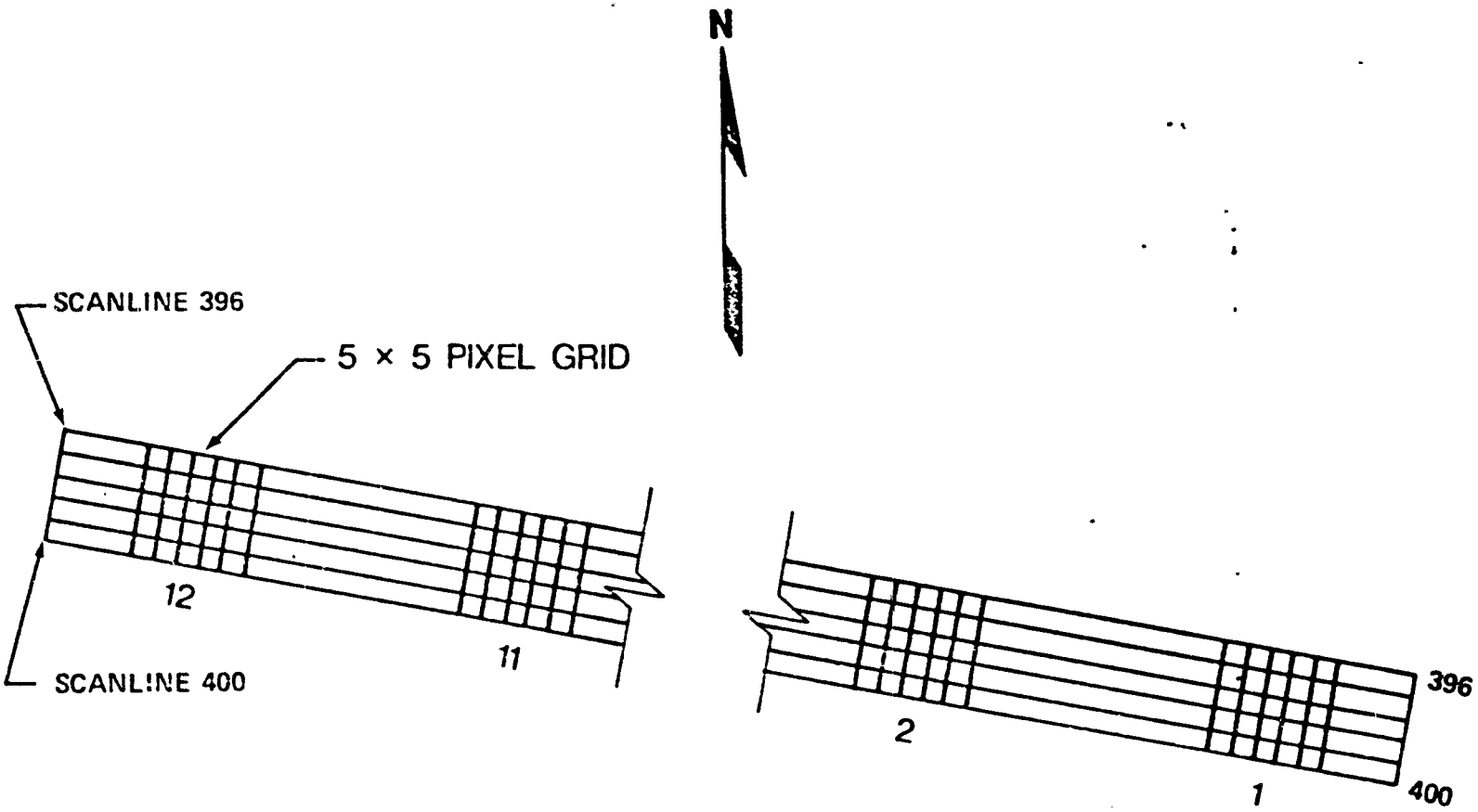

FIGURE 6.

Normalized difference values were obtained for each of the twelve (12) sites on the three (3) dates. The next step was to decide how to best statistically treat the ND values. At this stage we have simply been able to do some preliminary analysis of variance. Normalized difference values were plotted as a function of longitude, sponge and certain vegetation characteristics (i.e., biomass, net productivity, leaf area).

Vegetation Regions on the Texas Transect

The Texas transect selected for our model essentially runs from Beaumont (94^{o}W) to El Paso (106^{o}) and the 12 sample sites have been numbered east to west (see Map 7). Since it was not feasible to visit the transect for optimal site selection, it was necessary to utilize vegetation maps. At this level of our investigation, the ground-truth precision was not terribly critical since our initial concern has been to get a general feeling for the potential of NOAA imagery for global vegetation stratification.

Gould's (1975) vegetation map and discussion of the vegetation regions of the state is large-scale but is the best complete map available. The Texas Parks and Wildlife Department is in the process of completing a state-wide series of land-use classification maps based on Landsat data. Utilizing primarily those two sources, it appears as though our transect bisects four major vegetation regions. Table 5 enumerates those four regions from east to west, their approximate longitudinal boundaries on the transect, and document vegetation. For a more complete vegetation description, see Gould (1975), Texas Parks and Wildlife vegetation-type maps, and Smeins (1978).

VEGETATION REGION	GOULD (1975) NOMENCLATURE	LONGITUDE(^{o}W) LIMITS	DOMINANT VEGETATION
Pine-Hardwood Forest	Pineywoods	93.45^{o}-95.45^{o}	loblolly pine, slash pine, sweetgum, oak, elm, pecan, blackgum
Savannah	Post oak savannah, Blackland prairies	95.45^{o}-98.30^{o}	grasses, oak, elm, hackberry, (cropland)
Shrubland	Edwards Plateau	98.30^{o}-102^{o}	oaks, ash, juniper, mesquite, (rangeland)
Desert/Desert-scrub	Trans Pecos Mountains & basins	102^{o}-106^{o}	creosote, tarbush, yucca, (rangeland)

TABLE 5. The vegetation regions, their approximate longitudinal boundaries, and dominant vegetation along the Texas transect.

Results and Discussion

1. Normalized difference (ND) as a function of longitude. As previously mentioned it was impossible to insure superimposition of pixel sampling locations between dates because the satellite orbit fluctuates. For example, while still in pine-hardwood forest, site 1 on April 19 is not geographically identical to site 1 on October 9. The tabular and graphic summaries when the three sample dates were individually plotted as a function of longitude are presented below (Table 6, Figures 7, 8).

There is generally a high correlation between ND and longitude (mean r^2 = .756); ND decreases from east to west.

The sample size of 12 is not sufficiently large enough to merit serious discussion as to significant differences among the three sampling periods. Neither can we eliminate the real possibility of cloud cover affecting reflectance values. We definitely know that there was some cloud cover in West Texas on October 9. What the regressions do suggest is what one would expect knowing the phenological nature of the vegetation regions on the transect. April and July values are high in the mixed forest because the deciduous trees have leafed out. By October, they have dropped their leaves, reducing their "greenness". Progressing westward across the state, a greater percentage of the perennials are non-deciduous but the vegetation becomes less dense and more dependent on infrequent precipitation. In addition, the amount of exposed ground in the desert scrub poses problems of separating soil spectra from vegetation spectroreflectance (Miller, Lee D., pers. comm).

The variation between seasons appears to diminish going from east to west. The mean regression for all three dates (Figure 8) indicates not only that the greater between-date variation is in the pine-hardwood forest but also that April, and to a lesser extent July are well above the line for the three dates. We would have expected much higher values during the annual blooms in April in the Trans-Pecos but more extensive sampling may clarify this.

Site	April 19	July 10	October 9	Combined
1.	.258	.238	.161	
2.	.289	.229	.171	
3.	.286	.231	.215	
4.	.259	.136	.147	
5.	.224	.205	.151	
6.	.126	.137	.090	
7.	.138	.125	.033	
8.	.062	.141	.101	
9.	.038	.159	.112	
10.	.044	.029	.051	
11.	.046	.005	.044	
12.	.035	.001	.063	
$\bar{X}$	.150	.128	.112	.130
$\hat{Y}$	2.526 - .024X	2.268 - .022X	1.23 - .011X	2.00 - .019X
r^2	.752	.934	.636	.756

TABLE 6. Indidivudal normalized difference (ND) values, means, regression equations, and r^2 for 3 dates in 1980 along Texas transect.

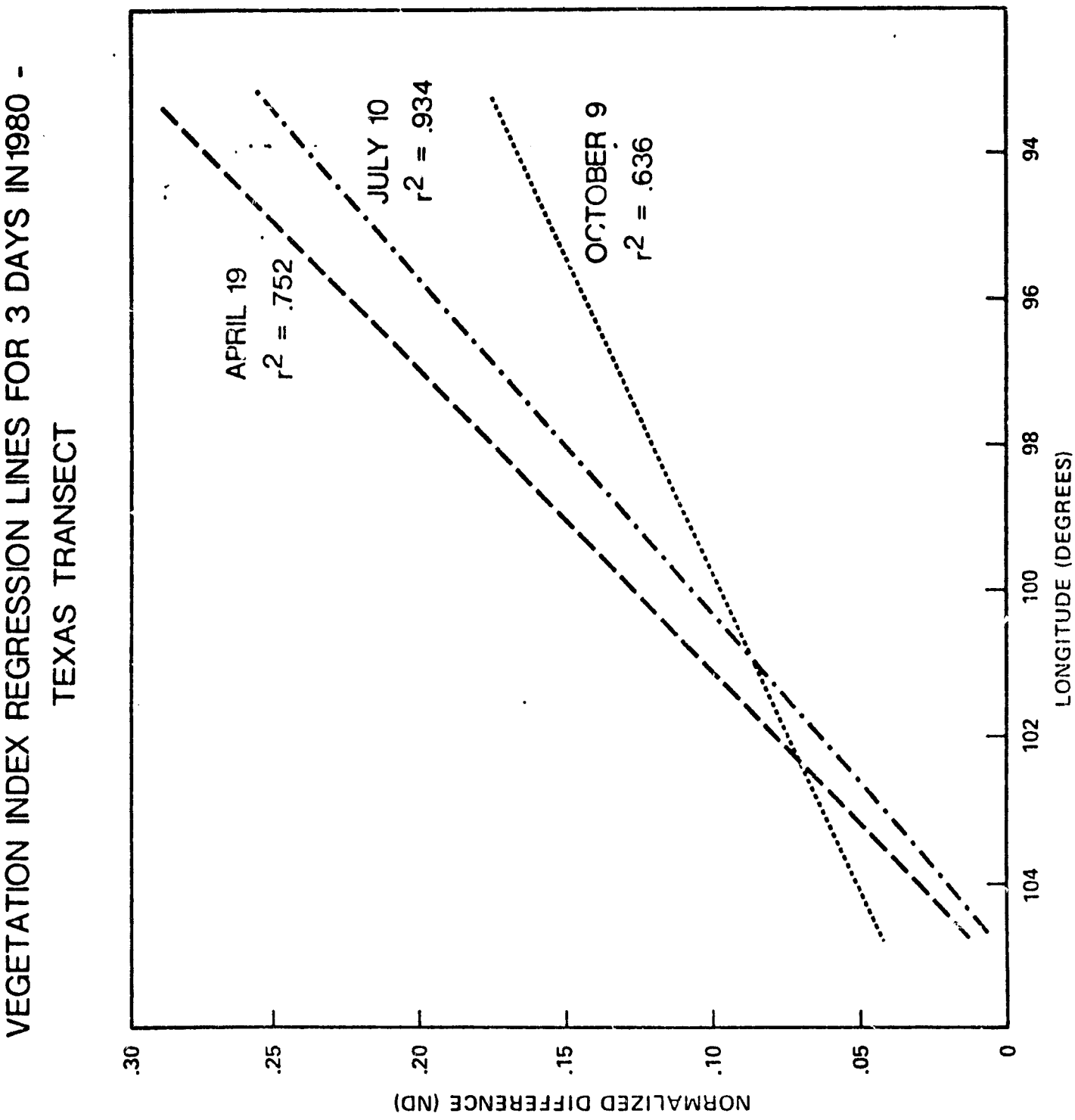

Figure 7.

FOLDOUT FRAME

1980 VEGETATION INDICES AND MEAN REGRESSION

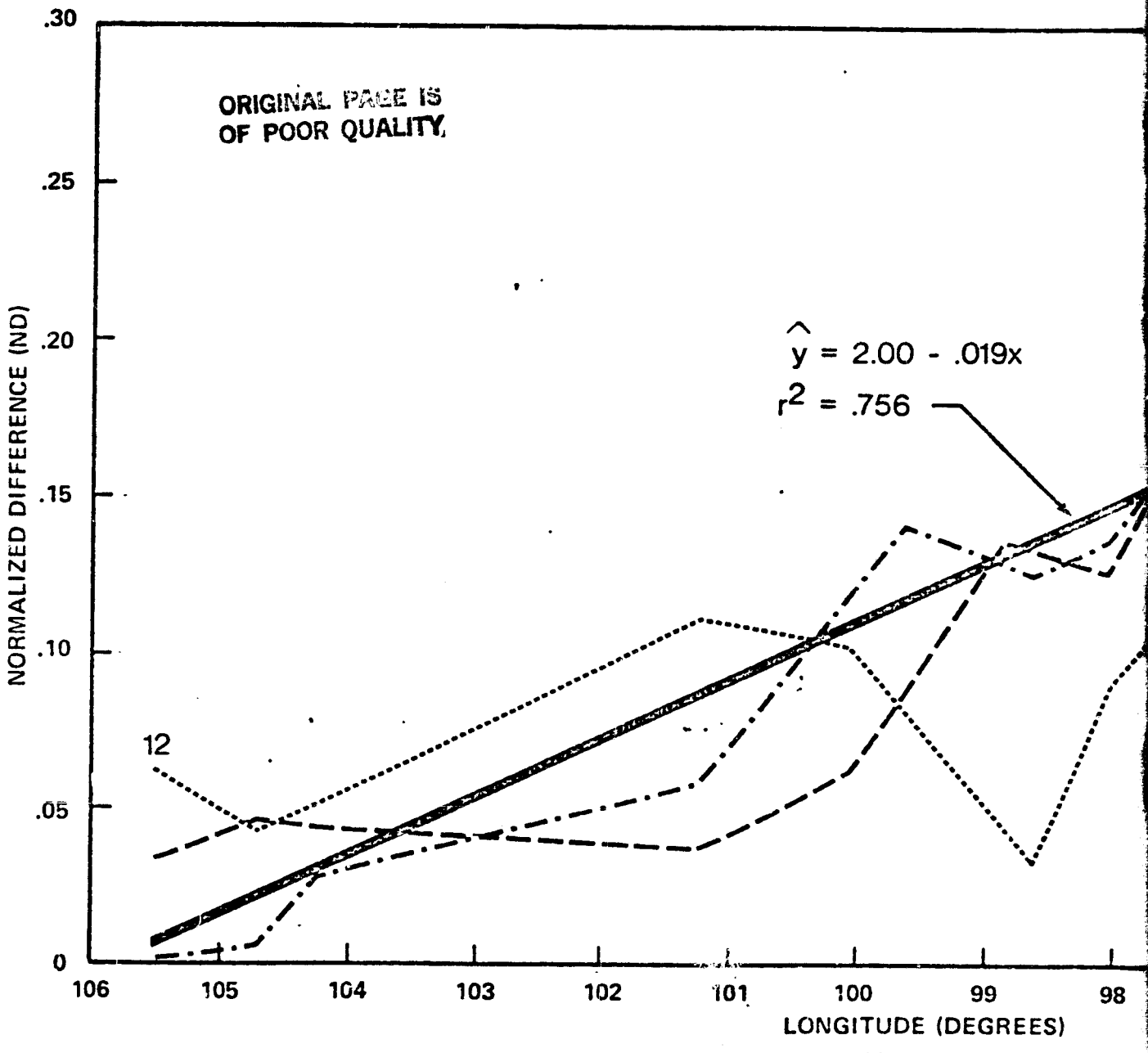

Figure 8.

MEAN REGRESSION LINE - TEXAS TRANSECT

FOLDOUT FRAME

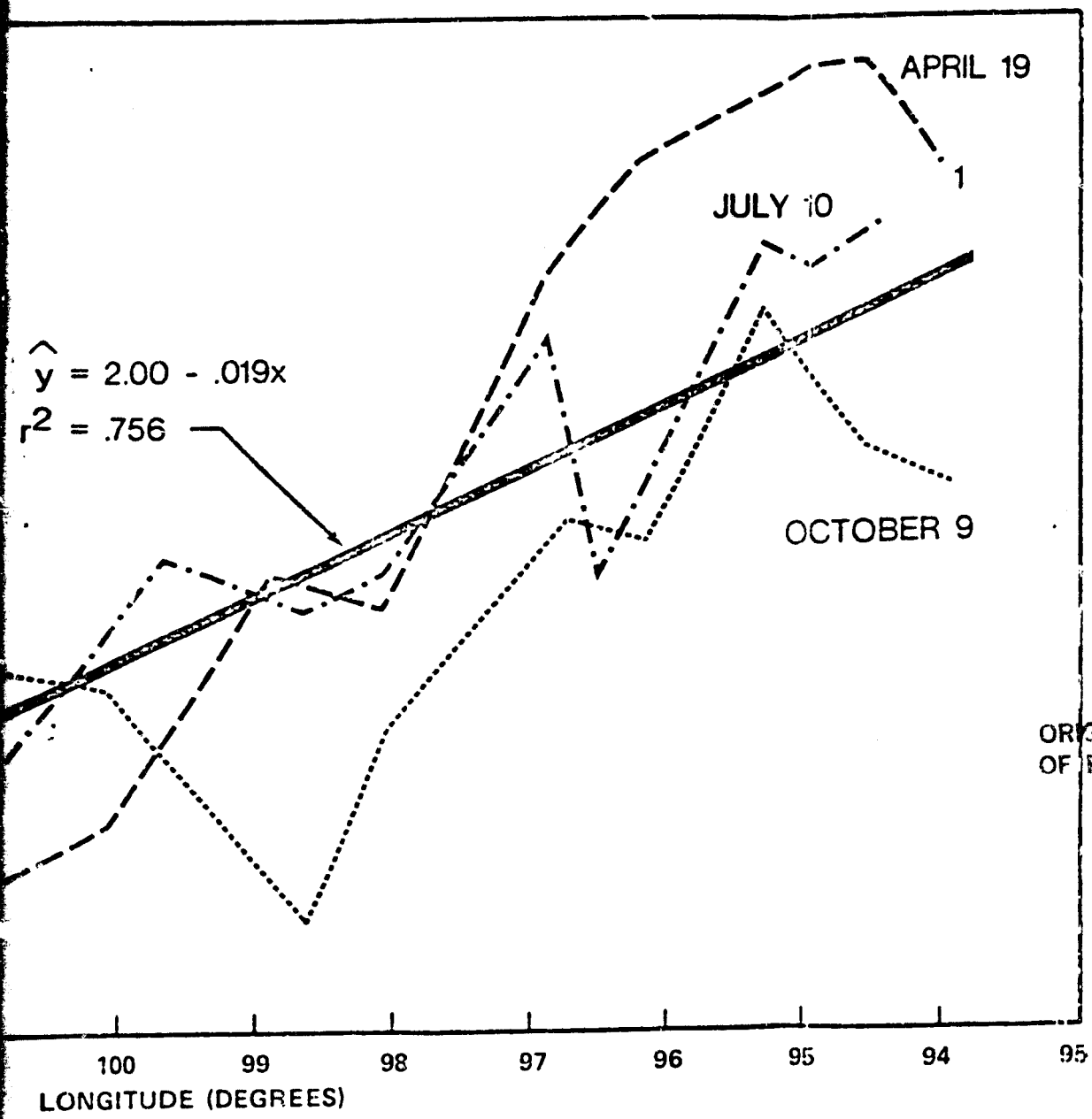

Figure 8.

2. Sponge index as a function of longitude. For a discussion of a new moisture variable, the sponge, we refer you to earlier sections II, III of this report. Long-term annual "normals" (1941-70) were calculated for 26 stations along or near the Texas transect. These values were plotted as a function of longitude (Figure 9). The results indicate an extremely high correlation (r^2 = .911) between sponge and longitude; sponge increases (as does precipitation) from west to east.

3. Normalized difference (ND) as function of sponge. Since both the vegetation index, ND, and sponge showed similar positive correlation with geographic position on the transect, it seemed appropriate to interpolate sponge values from the 26 stations (see Table 4 in Appendix; Maps 8,9) along the transect for each of 36 ND values (3 values for each of the 12 sites). When ND was plotted against sponge, there was a good correlation (r^2 = .777) (Figure 10). Regressing the two regressions, (ND (Figure 8) vs. Sponge (Figure 9), the result is a very please (r^2 - 1.001) but transect-limited, prediction model that permits estimating longitude, sponge index, and ND value, requiring input of only one of the 3 variables (Figure 11). This model serves to illustrate the very high correlation between the vegetation index and the sponge. To further establish this correlation, if one plots the highest ND value of the three dates at each 12 stations against the long-term sponge value for that particular month, r^2 = .946.

4. Normalized difference (ND) as a function of vegetation. As earlier mentioned, it was not feasible to actually ground truth the transect to verify and quantify the vegetation. No doubt this should be done at some later stage. In lieu of a better alternative, biomass, net productivity, and leaf area estimates from Whittaker and Likens (1973) were used (see Table 7). Since the predominant vegetation limiting factor along the Texas gradient is moisture, these vegetation parameters predictably decline from east to west. It has been previously demonstrated that all of these parameters have been correlated with spectral data (see introduction to Tucker, et al. 1981 for literature review). While general, when ND means for each site are plotted against biomass, net productivity, and leaf area mean values, the results are prophetic as to which vegetation characteristic has the highest correlation with the satellite data (Table 8).

	NET PRODUCTIVITY $gm/M^2/Yr$	BIOMASS Kg/M^2	LAI M^2/M^2
Temperate Evergreen/Deciduous Forest	1250	32.5	8.5
Savannah	900	4.0	4.0
Shrubland	700	6.0	4.0
Desert/Desert	90	0.7	1.0

TABLE 7. Mean values for world-wide estimates of net productivity biomass and leaf area index (Whittaker and Likens, 1973).

	r^2
Net primary productivity (g/m^2yr)	.895
Leaf area (M^2/M^2)	.815
Biomass (Kg/M^2)	.650

TABLE 3. Coefficients of determination (r^2) when mean ND values for the 12 Texas transect sites are plotted against net productivity, leaf area, and biomass.

LONG TERM (1941-70) SPONGE NORMALS FROM 26 STATIONS - TEXAS TRANSECT

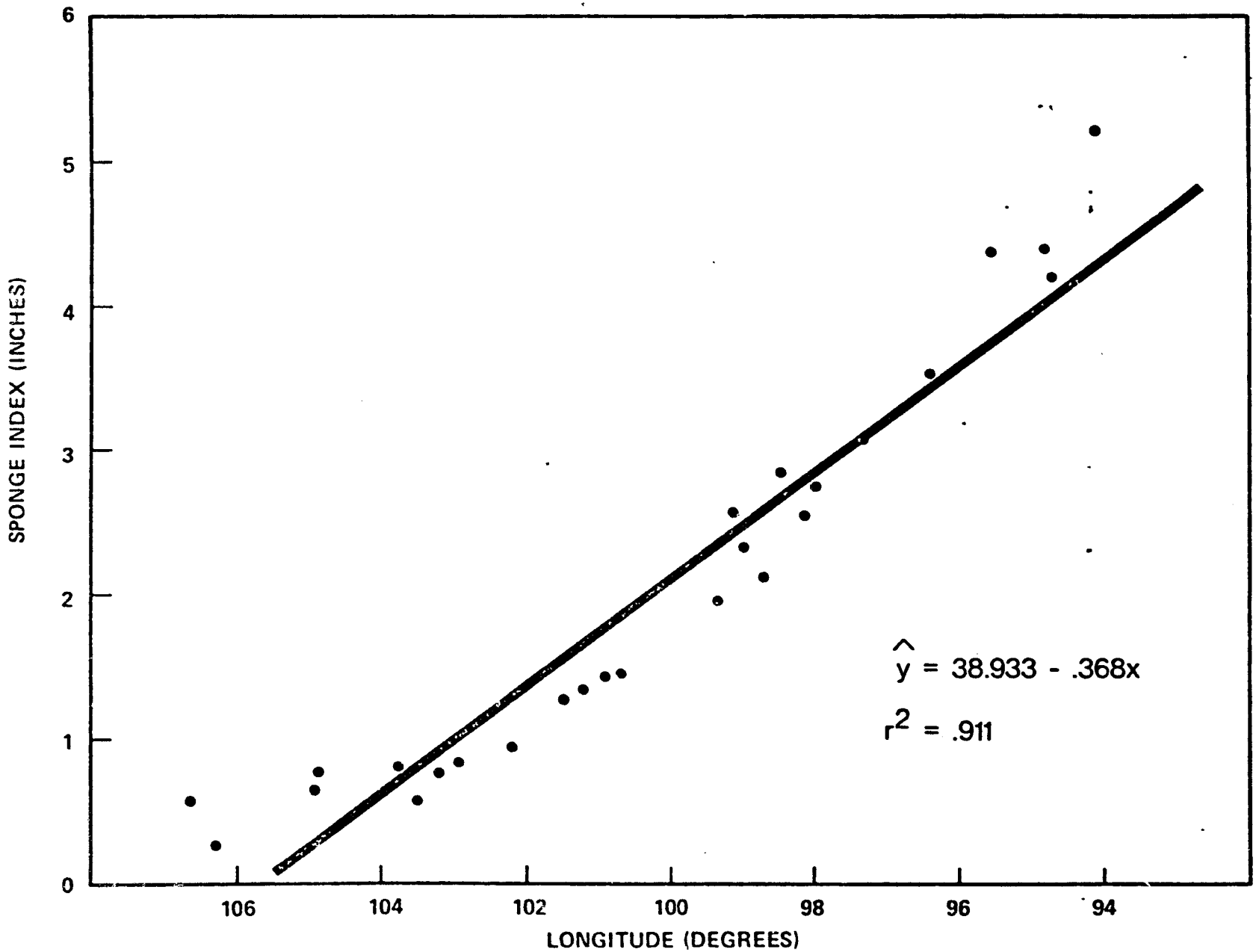

Figure 9.

VEGETATION AND SPONGE INDICES FROM 12 SITES (3 DATES) - TEXAS TRANSECT

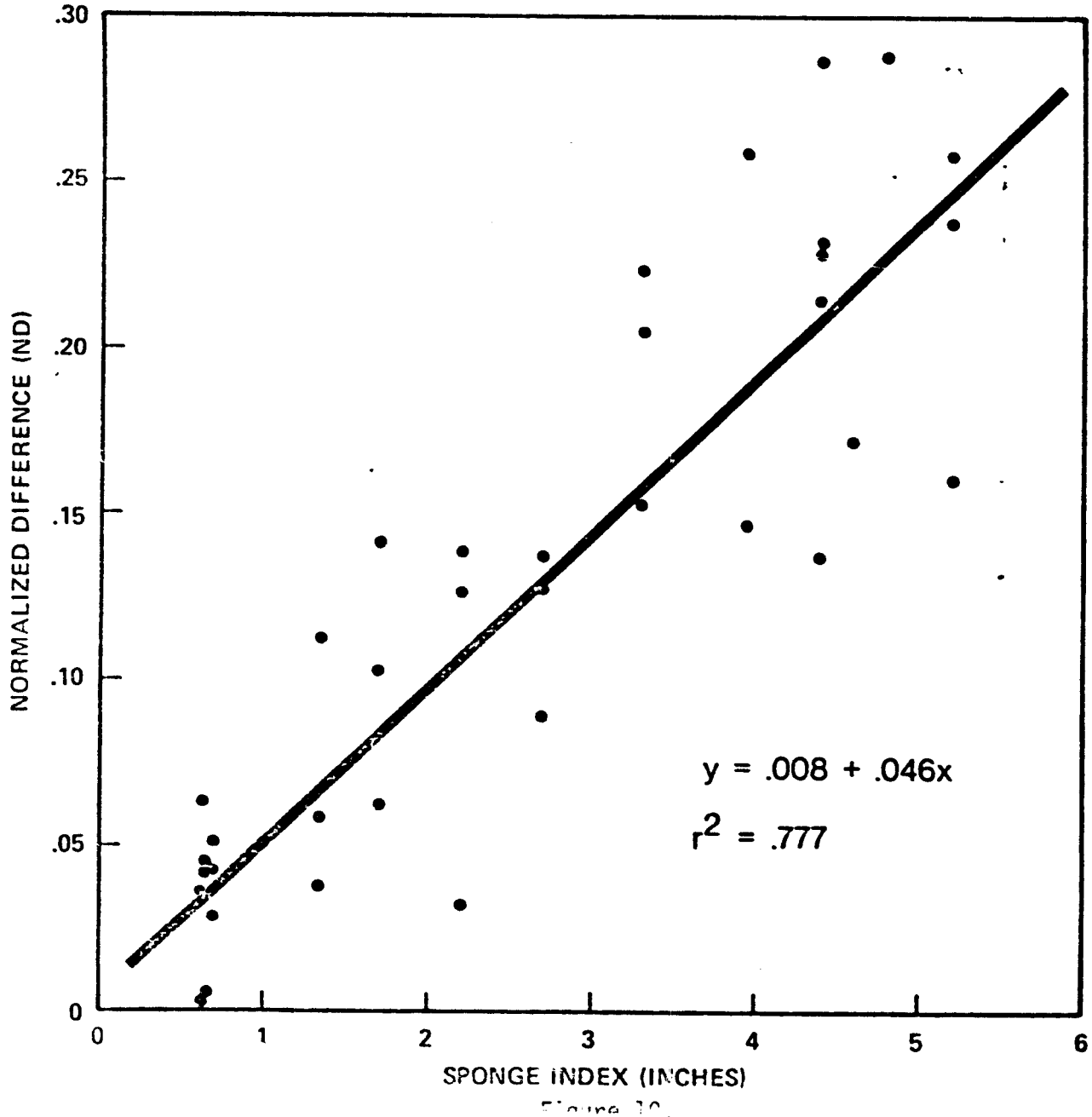

Figure 10.

VEGETATION-SPONGE PREDICTION MODEL - TEXAS TRANSECT

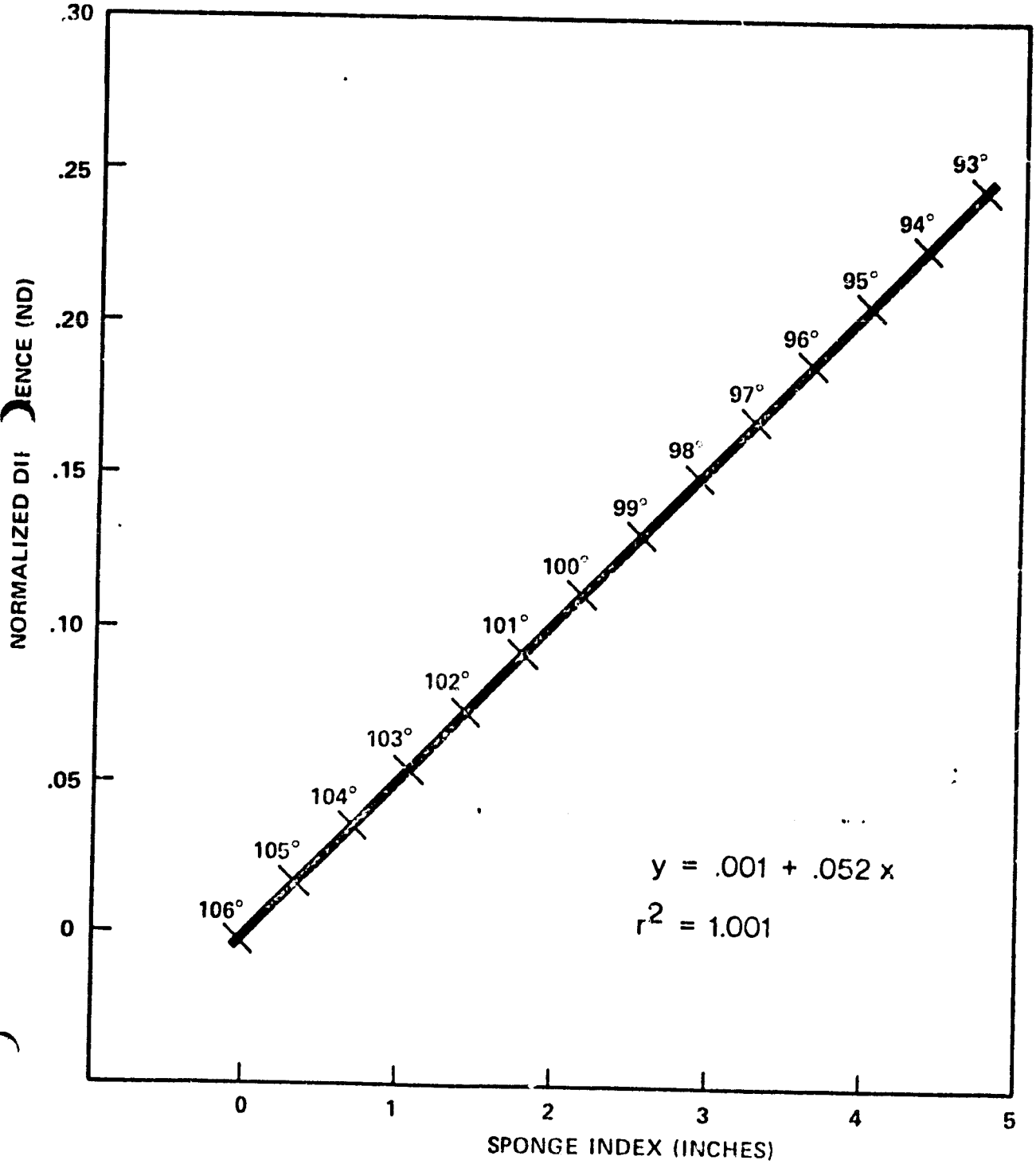

Figure 11.

STATION LOCATIONS FOR SPONGE CALCULATIONS ALONG TEXAS TRANSECT (PERIOD 1941-70 AND 1980, EXCEPT AS NOTED IN TABLE 2)

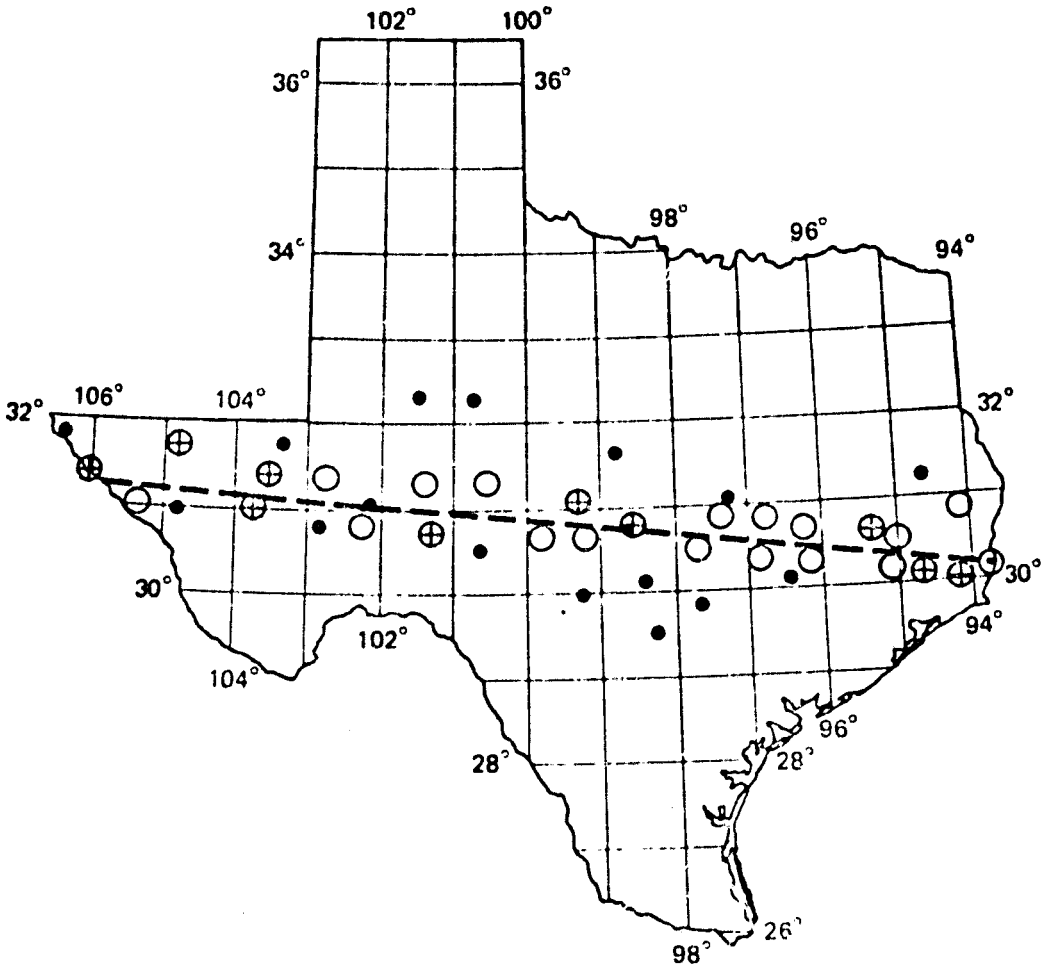

LEGEND

- ○ – STATIONS (17) USED TO CALCULATE MEAN SPONGE VALUE ALONG TRANSECT IN 1980
- ⊕ – STATIONS (10) USED FOR BOTH 1980 AND 1941-70 TRANSECT SPONGE NORMALS
- • – STATIONS (16) USED TO CALCULATE 1941-70 TRANSECT SPONGE NORMALS
- — — – APPROXIMATE TRANSECT PATH

Map 8.

MEAN 8-INCH SPONGE VALUES ALONG TEXAS TRANSECT (1980)

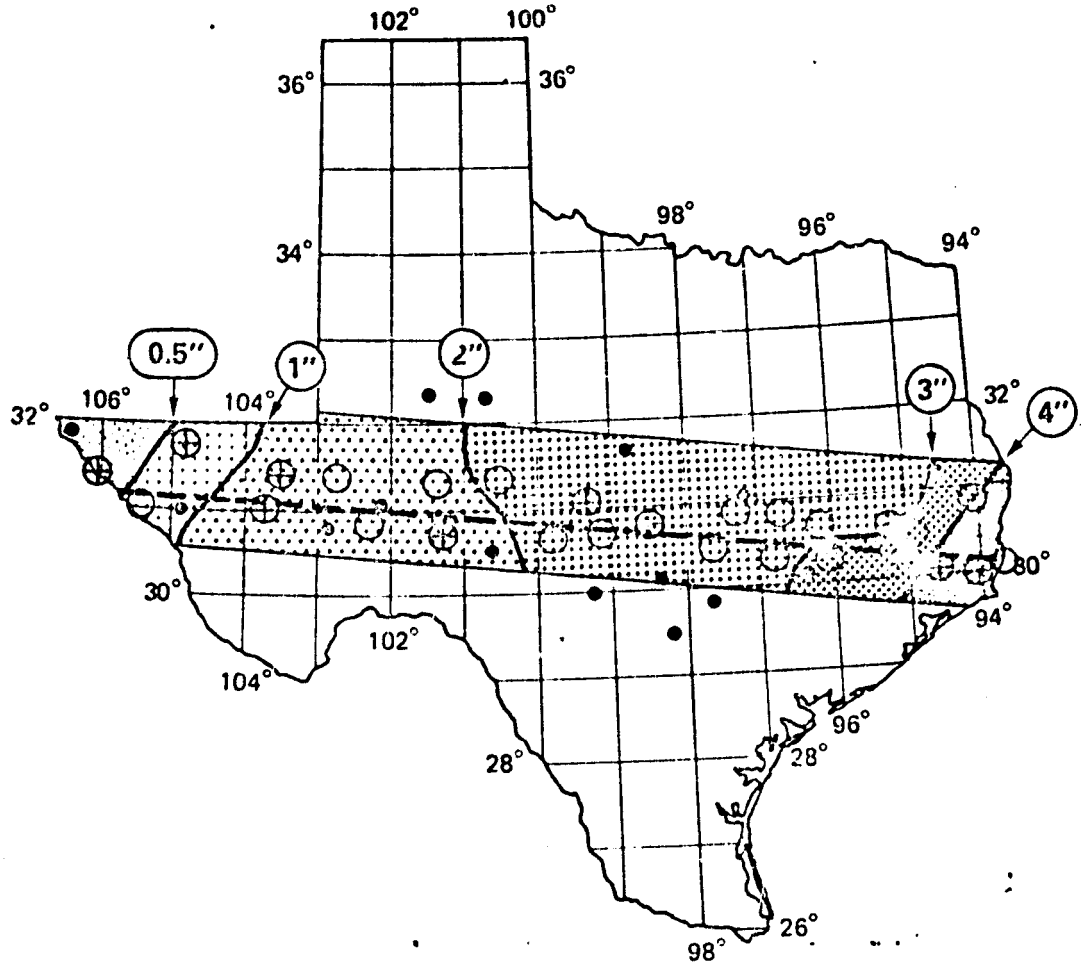

LEGEND

SPONGE NORMALS IN INCHES

4" ISONORMS

≤ 0.5" | 2-3"

0.5-1" | 3-4"

1-2" | ≥ 4"

○ – STATIONS USED TO CALCULATE MEAN SPONGE VALUES ALONG TRANSECT IN 1980

⊕ – STATIONS USED IN BOTH 1980 AND 1941-70 TRANSECT SPONGE NORMALS

• – STATIONS USED TO CALCULATE 1941-70 TRANSECT SPONGE NORMALS

– – – APPROXIMATE TRANSECT PATH

Map 9. C-4

The inference is that net productivity has the highest correlation to the vegetation index, biomass the lowest. Several studies have recently shown that currently used remote sensing techniques are not sensitive to non-green-leaf components of the phytomass. However, there appears to be a high correlation of spectral data with green-leaf area (biomass) and net production of certain vegetation types (see Introduction, Tucker, et al. 1981). Our selection of ND as a vegetation index was largely founded on Deering and Haas' (1977) high correlation between Landsat-derived ND and rangeland biomass.

In Table 7, it is noted that of the three parameters of vegetation, biomass is the only one that doesn't consistently decline from east to west along the transect. Shrubland, consisting largely of woody perennials, does not produce the annual net production that a savannah, containing more herbaceous annuals would, but its accumulative biomass would be greater. The ND does not respond to the increase in biomass from savannah to shrubland because much of that biomass is tied up in non-green components in shrubland which is not as true in the savannah. Because net productivity and leaf area more closely reflect the actual spectral component of those vegetation regions on our transect, we would anticipate their previously higher correlation with ND.

5. Vegetation-Sponge Index (VSI). Having previously established a high correlation between ND and sponge, we would like to propose a new index that represents the multiplicative of the two variables: the Vegetation - Sponge Index (VSI).

$$ND \times SPONGE = VSI$$

The mean VSI values for the 12 sample sites are presented below in tabular and graphic form (Table 9, Figure 12).

SITE	VEGETATION REGIONS	SPONGE	ND	VEGETATION-SPONGE INDEX (VIS)
1.	Pine-hardwood forest	5.20	.2192	1.13
2.	"	4.61	.2298	1.06
3.	"	4.40	.2440	1.07
4.	Savannah/cropland	4.10	.1806	0.74
5.	"	3.31	.1935	0.64
6.	Shrubland	2.70	.1176	0.32
7.	"	2.12	.0989	0.21
8.	"	1.71	.1012	0.17
9.	"	1.36	.0695	0.10
10.	Desert/desert scrub	0.70	.0414	0.03
11.	"	0.67	.0315	0.02
12.	"	0.63	.0333	0.02

TABLE 9. Sponge, normalized difference (ND), and Vegetation-Sponge Index (VSI) mean values for three dates in 1980 (April 19, July 10, October 9) for 12 sites along Texas transect.

FOLDOUT FRAME

VEGETATION-SPONGE INDEX (VSI)- TEXAS TRA

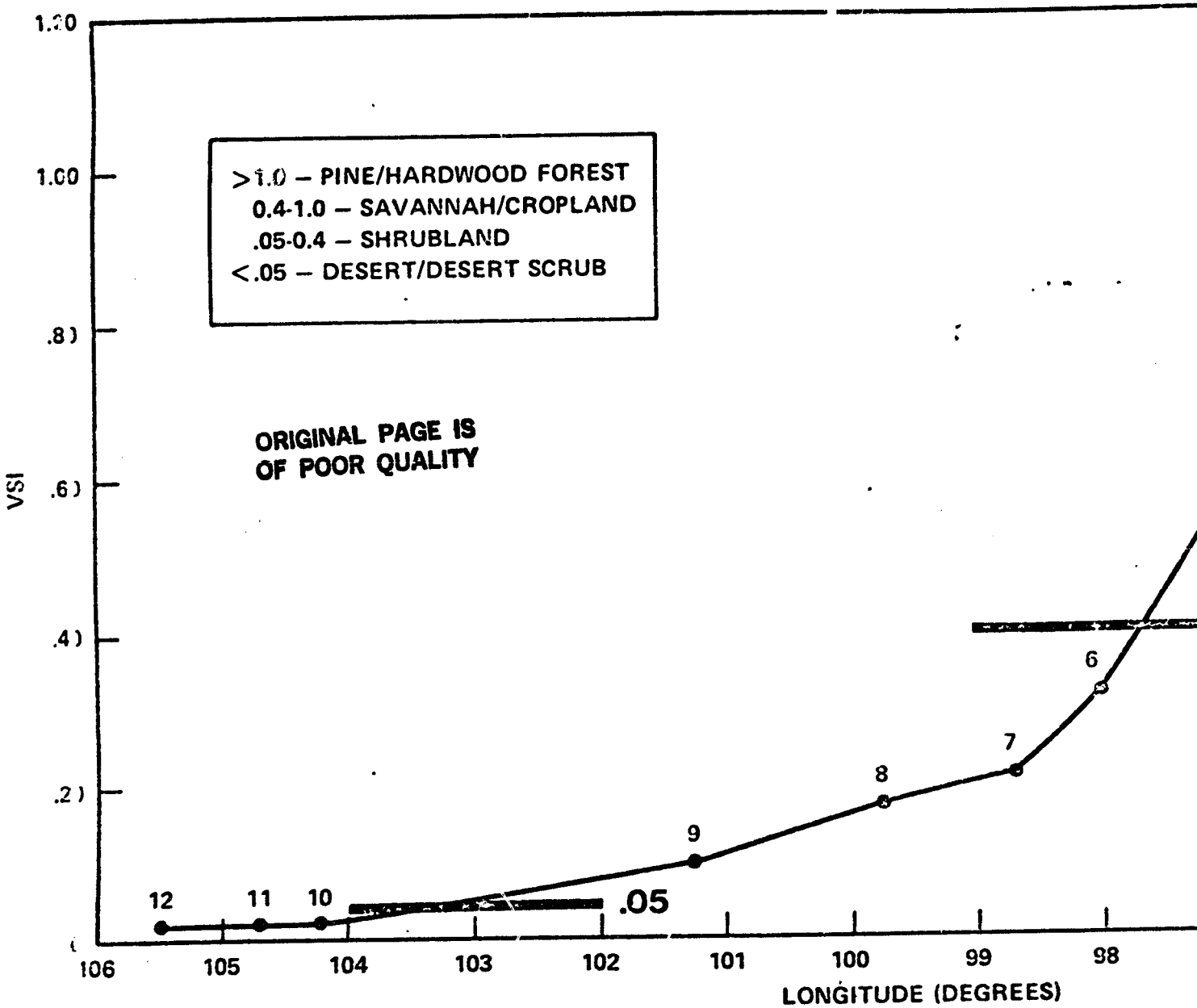

Figure 12.

ONGE INDEX (VSI_f)- TEXAS TRANSECT

FOLDOUT FRAME 2

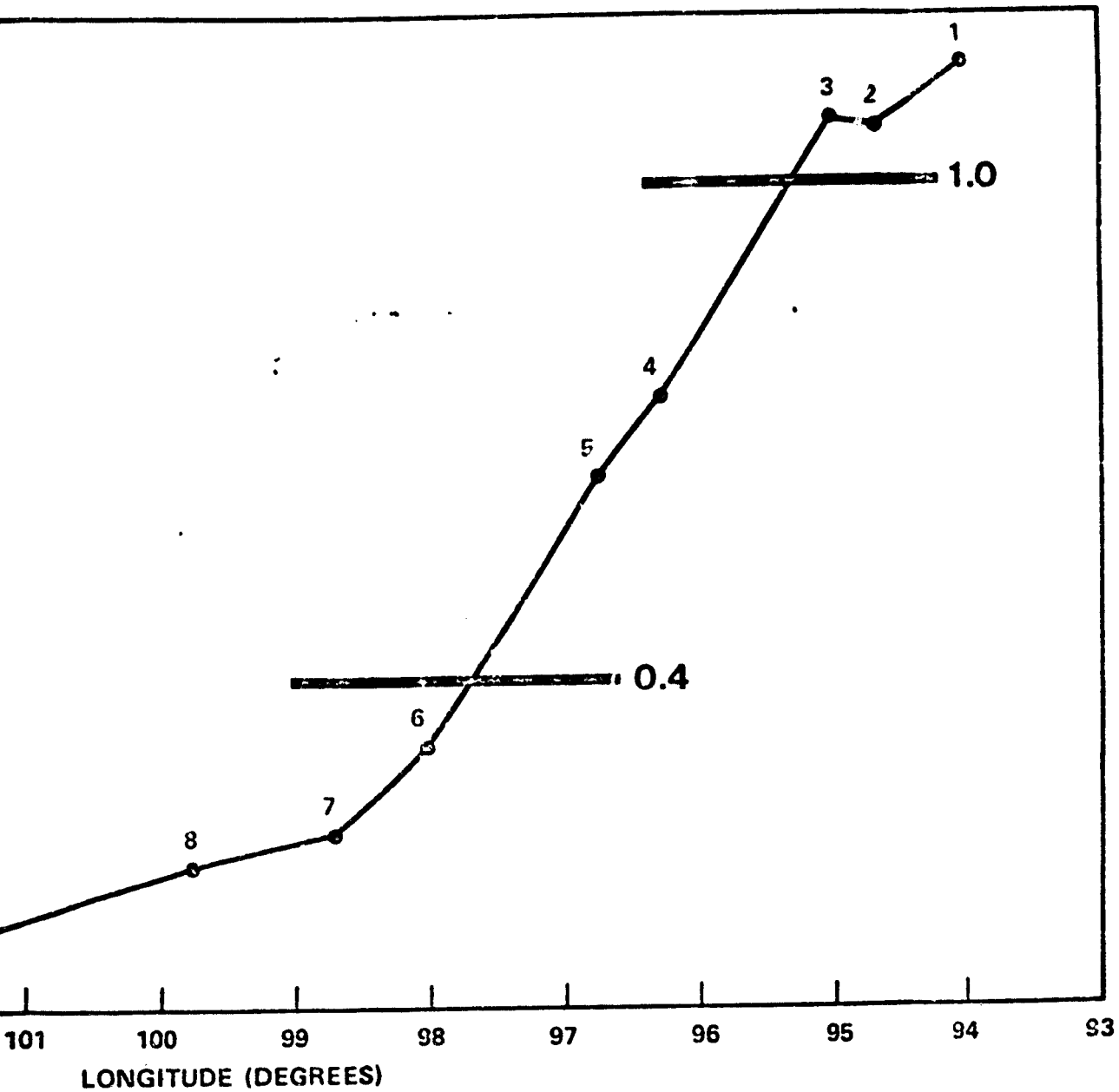

Figure 12.

When VSI is plotted as a function of longitude, the separation of the four major vegetation regions becomes much more apparent (Figure 12). It is ever possible to suggest boundaries for the four classes:

>1.0	pine-hardwood forest
0.4-1.0	savannah/cropland
.05-0.4	shrubland
<.05	desert/desert scrub

Using these suggested limits, it becomes readily apparent that the least within-class variation occurs in desert and forest; the greatest variation is in the shrubland and savannah/cropland classes. This seems consistent with what we would expect. The desert and mixed forest would be more homogeneous in the sense that desert has extensive bare soil during much of the year while the forest would have relatively little. The shrubland and savannah would be considerably more heterogeneous.

V. THE TEXAS MODEL: CONCLUSIONS AND PROJECTIONS

It has been demonstrated that the sponge variable is a superior tool for the analysis of climate/vegetation relationships. Furthermore, NOAA/AVHRR satellite data proved useful for vegetation stratification. Finally, a preliminary multivariate model of vegetation distribution, the VSI, was developed based on an experimental east-west Texas gradient. The next stage of this research effort will involve a more extensive analysis of the application of the model to the Texas transect (e.g., increasing the sample size), to be followed later by refinement of the model which will then be tested against other natural vegetation regions across North America. It is anticipated that ultimately such a model may be utilized for global vegetation surveys, and as a means of remotely monitoring vegetation region dynamics (e.g., desertification).

VI. ACKNOWLEDGEMENTS:

That this report was carried forth to completion owes in large measure to the assistance of certain key individuals. The authors are particularly indebted to K. Demel and R. Hill (NASA) for support, encouragement and substantive suggestions; M. Helfert (NOAA), M. Trenchard, and Ken Oney (Lockheed) were also quite helpful. Special appreciation is extended to Jimmy Gilbert (NASA) and Tom Gray and Dee McCrary (NOAA) for essential data-acquisition and -analysis. The manuscript was expertly prepared by C. M. Graham, M. B. Wiggins, and N. Maxey; graphics and publication were handled by S. B. Allbritton and R. Eason. Finally, the support of the ASEE/NASA Summer Faculty Fellowship Program is greatly acknowledged. Any remaining errors and shortcomings in this report are, of course, solely the responsibility of the authors, to whom they should be reported.

VII. REFERENCES AND NOTES

Carter, D. B. and J. R. Mather, 1966. Climatic Classification for Environmental Biology, Vol. 19 (4): 395 pp. C. W. Thornthwaite Assoc. Lab. of Climat., Pub. in Climatol., Elmer, N. J.

Deering, D. W., Rouse, J. W., Haas, R. H., and J. A. Schell. 1975. Measuring forage production of graging units from Landsat MSS data. Proc. Tenth Int. Symp. Remote Sens. Environ., ERIM, Ann Arbor, MI, pp. 1169-1178.

Deering, D. W. and R. H. Haas, 1977. Using Landsat Digital Data for Estimating Green Biomass Symp. on Rangeland Remote Sensing, Soc. for Range Mgmt., Portland, Oregon, 21 pp.

Gould, F. W. 1975. Texas Plants: A Checklist and Ecological Summary. Tex. Agr. Exp. Sta. Misc. Publ. 585/revised. 121p.

Gray, T. I., and D. G. McCrary, 1981. The Environmental Vegetation Index, a Tool Potentially Useful for Arid Land Management. AgRISTARS Report No. EW-N1-04076; JSC-17132.

Griffiths, J. F., 1964. Another Evaporation Formula. Proc. Sixth Nat'l. Conf. on Agr. Meteor., Lincoln, Nebraska

Jensen, M. E.; Robb, C. N.; and Franzoy, C. E., 1970. Scheduling Irrigation Using Climate - Crop Soil Data. Jour. Irrig. Drainage Div. Amer. Soc. Civil Eng., Vol. 96: 25-38.

Kessell, S. R., 1979. Gradient Modeling Resource and Fire Management. Springer-Verlag, New York. 432 p.

Klinka, K. and F. C. Nuszdorfer, 1979.. Biogeoclimatic Units of Central and Southern Vancouver Island, Province of British Columbia, Ministry of Forestry, Victoria, B. C. V8W 3E7. 120 pp.

Mather, J. R. and Yoshioka, G. A., 1968. The Role of Climate in the Distribution of Vegetation. Annual Assoc. Amer. Geo. V. 58 (1): 29-41.

Moe, K. D., 1965. A New Evaporation Formula for Texas. M. S. Thesis. Department of Meteor., Texas A&M University, College Station, TX.

Penman, H. L., 1948. National Evaporation from Open Water, Bare Soil, and Grass. Proc. Royal Soc. A, Vol. 193: 120-145. Cited in Rosenberg, N. J., 1974. Microclimate: The Biological Environment. New York: John Wiley and Sons. 315 pp.

Rouse, J. W., Haas, R. H., Schell, J. A., and D. W. Deering. 1973 Monitoring Vegetation Systems in the Great Plains with ERTS. Thus NASA ERTS Symposium, NASA SP-351 I:309-317.

Smeins, F. E., 1978. Natural Vegetation of Texas and Adjacent Areas, 1675-1975: A Bibliography. Texas Agr. Exp. Sta. No. 2M-12-78. 36 p.

Trenchard, M. C., 1981, Calculations of Sponge Normals for All First-Order Meteorological Stations in the Conterminous USA. Personal Communication with Authors, July, 1981. Lockheed Corporation, NASA, JSC, Houston, TX.

Trenchard, M. C. and J. A. Artley, 1981 (in press). The Application of a Thermal Model for Pan Evaporation to the Hydrology of Defined Medium, the Sponge. AgRISTARS Tech. Memo, Johnson Space Center, NASA, Houston, TX 77058.

Trenchard, M. H., 1976. A Simple, Time-Dependent Formula for Estimating Evaporation Rates in Texas. M.S. Thesis. Department of Meteor., Texas A&M University, College Station, TX.

Tucker, C. J., and B. N. Holben, 1981. Remote Sensing of Total Dry Matter Accumulation in Winter Wheat. Remote Sens. Environ., p. 171-189.

Whittaker, R. H., and G. E. Likens, Editors. 1973. The Primary Production of the Biosphere. Human Ecology 1(4) 299-369.

Whittaker, R. H. 1975b. Communities and Ecosystems. (2nd ed.) MacMillan, New York, 385 p.

Average Climatic Water Balance Data of the Continents, Part VII, United States, 1964. C. W. Thornthwaite Assoc. Lab of Climatol., Pub. in Climat., Vol. 17, No. 3., Centerton, N. J.

Climatological Summaries for Various Texas Stations, Climatography of the United States No. 20-41 (approx. 1970). NOAA, U.S. Department of Commerce. U.S. National Climatic Center, Asheville, N.C.

VIII. APPENDIX

FOLDOUT FRAME

ORIGINAL PAGE IS OF POOR QUALITY

Table 2(a). Mean Precipitation and 8-Inch Sponge Normal Va

STATION	(°N) LATITUDE	(°W) LONGITUDE	JAN		FEB.		MARCH		APRIL		MAY		JUNE		JULY	
			P	Sp	P	Sp	P	Sp	P	Sp	P	Sp	P	Sp	P	Sp
Canadian[1]	35.92	100.37	0.53	1.43	0.72	1.37	0.83	1.41	1.45	1.33	3.94	2.30	3.07	2.73	2.30	1.88
Canyon[11]	34.98	101.92	0.57	1.38	0.51	1.20	0.67	1.07	1.41	1.16	2.60	1.65	3.38	2.19	2.97	2.15
Childress[1]	34.43	100.28	0.80	1.75	0.87	1.74	0.94	1.65	2.00	1.72	3.53	2.39	3.08	2.56	1.79	1.69
Dalhart[4]	36.02	102.55	0.38	0.95	0.51	0.90	0.74	1.07	0.89	1.01	2.69	1.63	2.27	1.88	3.32	1.97
Dumas[7]	35.87	101.97	0.60	1.37	0.61	1.35	0.93	1.45	1.22	1.43	2.56	1.80	2.88	2.09	3.56	2.23
Matador[2]	34.02	100.83	0.67	1.48	0.64	1.36	0.71	1.25	1.56	1.25	3.20	1.94	3.05	2.27	2.67	1.95
Pampa[6]	35.57	100.97	0.52	1.49	0.70	1.45	0.81	1.49	1.31	1.45	3.35	2.16	3.34	2.79	2.33	2.17
Plainview[1]	34.18	101.70	0.76	1.40	0.65	1.37	0.62	1.21	1.40	1.16	3.04	1.83	3.11	2.19	2.67	1.97
Quanah[6]	34.25	99.68	0.79	1.94	0.96	1.87	1.33	1.90	2.31	2.02	3.87	2.68	3.10	2.62	1.98	1.68
Seminole[1]	32.72	102.67	0.55	0.90	0.58	0.89	0.58	0.86	1.08	0.82	2.25	1.29	1.67	1.27	2.30	1.25
Seymour[11]	33.58	99.27	1.16	2.16	1.25	2.21	1.32	2.10	2.40	2.05	3.95	2.66	3.49	2.69	2.63	1.94
Spearman	36.18	101.20	0.67	1.67	0.81	1.64	1.18	1.78	1.59	1.79	3.47	2.38	3.28	2.67	3.17	2.20
Tulia[24]	34.53	101.77	0.53	1.12	0.37	1.02	0.54	0.88	1.16	0.98	2.49	1.49	3.68	2.23	2.46	2.10
Vega[7]	35.25	102.43	0.58	1.55	0.66	1.46	0.80	1.43	1.25	1.38	2.62	1.79	3.04	2.20	2.99	2.08
Vernon[9]	34.17	99.30	0.99	2.03	1.31	2.08	1.29	2.04	2.43	1.97	4.63	2.83	3.33	2.81	1.84	1.64

[illegible]pt [illegible] noted. All values in inches. Data from Climatological Summaries for Texas, Natio

FOLDOUT FRAME

and 8-Inch Sponge Normal Valu 1941-1970*. North Texas Group. 2

MAY		JUNE		JULY		AUG.		SEPT.		OCT.		NOV.		DEC.		YEAR	
P	Sp	P	Sp	P	Sp	P	Sp	P	Sp	P	Sp	P	Sp	P	Sp	P	Sp
.94	2.30	3.07	2.73	2.30	1.88	2.32	1.54	2.04	1.55	1.75	1.70	0.64	1.54	0.71	1.39	20 30	1.67
.60	1.65	3.38	2.19	2.97	2.15	2.74	2.03	1.82	1.73	2.00	1.78	0.61	1.62	0.79	1.39	20 07	1.61
.53	2.39	3.08	2.56	1.79	1.69	2.07	1.29	2.21	1.48	2.07	1.86	0.78	1.77	0.89	1.64	21.03	1.79
.69	1.63	2.27	1.88	3.32	1.97	2.19	1.91	1.35	1.43	1.14	1.30	0.35	1.09	0.42	0.92	16.25	1.33
.56	1.80	2.88	2.09	3.56	2.23	2.45	2.02	1.57	1.55	1.34	1.45	0.48	1.29	0.75	1.20	18.95	1.60
.20	1.94	3.05	2.27	2.67	1.95	2.04	1.54	2.03	1.43	2.10	1.78	0.77	1.69	0.78	1.47	20.22	1.62
.35	2.16	3.34	2.79	2.33	2.17	2.51	1.85	1.91	1.76	1.88	1.92	0.54	1.78	0.60	1.49	19.80	1.82
.04	1.83	3.11	2.19	2.67	1.97	1.86	1.55	1.97	1.43	1.62	1.61	0.55	1.37	0.76	1.24	19.01	1.63
.87	2.68	3.10	2.62	1.98	1.68	2.08	1.23	3.06	1.69	2.57	2.27	1.13	2.17	0.93	1.98	24.11	2.00
.25	1.29	1.67	1.27	.30	1.25	2.05	1.34	2.07	1.38	1.64	1.52	0.50	1.25	0.37	0.92	15.64	1.14
.95	2.66	3.49	2.69	2.63	1.94	2.16	1.34	2.77	1.51	2.50	1.97	1.37	1.99	1.21	2.01	26.21	2.05
47	2.38	3.28	2.67	3.17	2.20	2.76	1.93	1.96	1.67	1.79	1.70	0.84	1.68	0.76	1.59	22.29	1.89
49	1.49	3.68	2.23	2.46	2.10	1.70	1.46	1.77	1.35	1.50	1.47	0.53	1.29	0.51	1.10	17.24	1.37
62	1.79	3.04	2.20	2.99	2.08	2.84	2.04	1.74	0.75	1.59	1.65	0.67	1.55	0.79	1.48	19.53	1.70
63	2.83	3.33	2.81	1.84	1.64	1.74	1.09	2.51	1.32	2.90	2.09	1.28	2.15	1.08	1.98	25.33	2.00

l Summaries for Texas, National Weather Service, NOAA.

FOLDOUT FRAME

STATION	(°N) LATITUDE	(°W) LONGITUDE	JAN. P	JAN. Sp	FEB. P	FEB. Sp	MARCH P	MARCH Sp	APRIL P	APRIL Sp	MAY P	MAY Sp	JUNE P	JUNE Sp	P
Albany[5]	32.73	99.30	1.17	2.03	1.38	2.13	1.18	1.95	2.79	1.99	4.21	2.85	2.71	2.53	2.4
Big Spring[5]	32.25	101.45	0.63	1.30	0.57	1.16	0.72	1.10	1.08	0.96	2.68	1.55	1.67	1.54	1.9
Blanco	30.10	98.42	2.12	3.23	3.00	3.76	2.10	3.59	3.54	3.22	3.98	3.47	2.92	2.78	1.9
Brady[1]	31.12	99.35	1.52	2.16	1.41	2.35	1.10	2.00	2.58	1.98	3.50	2.64	2.32	2.34	1.3
Brownwood[1]	31.72	98.98	1.72	2.63	1.77	2.88	1.46	2.59	3.03	2.53	4.22	3.18	3.40	3.02	1.8
Colorado City	32.38	100.87	0.82	1.46	0.78	1.32	0.86	1.17	1.82	1.20	3.19	1.86	2.17	1.77	2.1
Jacksboro[1]	33.23	98.15	1.48	2.68	1.39	2.63	1.70	2.39	3.88	2.84	4.34	3.57	3.16	3.01	2.4
Kerrville[2]	30.05	99.15	1.86	2.86	2.16	3.06	1.93	2.93	2.95	2.71	4.60	3.20	2.86	2.83	2.1
Llano	30.75	98.68	1.37	2.16	1.92	2.46	1.47	2.37	3.16	2.42	3.80	3.04	2.14	2.37	1.2
New Braunfels[1]	29.70	98.12	1.88	2.92	2.66	3.23	1.92	2.90	3.24	2.65	3.73	2.94	3.32	2.67	1.8
Ozona[3]	30.72	101.20	0.81	1.21	1.19	1.47	0.69	1.34	1.65	1.24	2.20	1.52	2.45	1.68	1.3
San Marcos[10]	29.88	97.95	2.05	3.08	2.85	3.58	1.86	3.21	3.28	2.88	3.27	2.90	3.86	2.77	1.8
Sonora[2,7]	30.57	100.65	0.82	1.28	1.19	1.41	0.75	1.26	2.07	1.31	2.95	1.95	2.19	1.88	1.6
Temple[1]	31.10	97.35	2.35	4.08	2.62	4.35	2.01	3.88	3.67	3.50	4.65	3.98	3.17	3.32	1.9
Weatherford[1]	32.75	97.80	1.89	3.40	2.35	3.85	1.97	3.71	4.12	3.76	5.07	4.54	3.10	3.70	2.0

*Except as noted. All values in inches. Data from Climatological Summaries for Texas, N

...ge Normal Values: 1941-1970*. Central Texas Group.

FOLDOUT FRAME

APRIL		MAY		JUNE		JULY		AUG.		SEPT.		OCT.		NOV.		DEC.		YEAR	
P	Sp	P	Sp	P	Sp	P	Sp	P	Sp	P	Sp	P	Sp	P	Sp	P	Sp	P	Sp
79	1.99	4.21	2.85	2.71	2.53	2.41	1.70	2.27	1.33	2.96	1.61	2.52	2.03	1.49	2.03	1.16	1.99	26.25	2.0
08	0.96	2.68	1.55	1.67	1.54	1.97	1.28	1.64	1.22	1.82	1.27	1.45	1.43	0.78	1.35	0.71	1.27	15.72	1.28
54	3.22	3.98	3.47	2.92	2.78	1.98	1.79	2.21	1.30	4.65	2.25	3.60	3.12	2.90	2.89	2.20	3.01	34.39	2.8
58	1.98	3.50	2.64	2.32	2.34	1.34	1.41	1.61	0.99	3.05	1.63	2.28	2.12	1.36	2.00	1.20	1.95	23.27	1.9
03	2.53	4.22	3.18	3.40	3.02	1.85	1.92	1.46	1.11	2.60	1.39	2.66	2.07	1.51	2.22	1.52	2.30	27.20	2.32
82	1.20	3.19	1.86	2.17	1.77	2.14	1.39	1.76	1.19	2.24	1.32	1.96	1.62	1.11	1.56	0.95	1.48	19.30	1.44
88	2.84	4.34	3.57	3.16	3.01	2.43	2.04	1.96	1.37	3.05	1.67	2.96	2.35	2.03	2.61	1.43	2.65	29.31	2.48
95	2.71	4.00	3.20	2.86	2.83	2.10	1.96	1.92	1.34	4.27	2.14	3.12	2.88	1.63	2.57	1.95	2.61	30.75	2.59
16	2.42	3.80	3.04	2.14	2.37	1.20	1.22	1.87	0.93	3.79	1.85	2.57	2.41	1.50	2.15	1.37	2.12	26.16	2.12
24	2.65	3.73	2.94	3.32	2.67	1.83	1.78	2.40	1.34	3.75	2.00	3.43	2.67	2.30	2.73	2.15	2.87	33.61	2.56
65	1.24	2.20	1.52	2.45	1.68	1.30	1.19	1.62	0.90	2.17	1.22	2.06	1.64	0.91	1.60	0.54	1.30	17.59	1.36
28	2.88	3.27	2.90	3.86	2.77	1.89	2.04	2.24	1.32	4.57	2.27	3.53	2.97	2.36	2.88	2.09	3.02	33.86	2.74
07	1.31	2.95	1.95	2.19	1.88	1.61	1.33	1.47	1.02	2.23	1.25	2.33	1.81	0.95	1.71	0.72	1.38	19.28	1.46
67	3.50	4.65	3.98	3.17	3.32	1.96	2.03	1.97	1.32	3.15	1.73	2.73	2.24	2.93	2.82	2.66	3.07	33.87	3.08
12	3.76	5.07	4.54	3.10	3.70	2.06	2.10	1.88	1.35	2.92	1.55	2.88	2.27	1.99	2.67	1.82	3.03	23.05	3.00

tological Summaries for Texas, National Weather Service, NOAA.

FOLDOUT FRAME

ORIGINAL PAGE IS OF POOR QUALITY

Table 2(C). Mean Texas Precipitation and 8-Inch Sponge Norma

STATION	(°N) LATITUDE	(°W) LONGITUDE	JAN. P	JAN. Sp	FEB. P	FEB. Sp	MARCH P	MARCH Sp	APRIL P	APRIL Sp	MAY P	MAY Sp	JUNE P	JUNE Sp	JULY P	JULY S
Athens[6]	32.20	95.85	2.51	4.80	3.30	5.10	2.58	4.78	4.64	4.51	5.17	4.81	3.14	3.77	1.41	1.
Beaumont	30.08	94.10	4.57	7.00	4.38	7.47	2.82	6.41	4.43	5.33	4.79	5.10	4.75	4.33	5.71	4.
Brenham	30.15	96.40	2.78	4.84	3.12	5.06	2.46	4.53	3.71	3.97	4.43	4.01	3.24	3.29	1.90	2.
Cuero[16]	29.08	97.25	2.03	2.88	2.41	3.18	1.41	2.71	2.95	2.41	3.79	2.91	3.18	2.64	2.22	1.
Freeport	28.98	95.38	3.41	6.08	3.48	6.31	2.28	5.55	3.25	4.68	3.29	4.36	4.17	3.99	5.46	4.
Hallettsville[16]	29.45	96.93	2.25	3.36	2.70	3.58	2.08	3.29	3.01	2.86	4.65	3.39	3.53	3.18	2.22	2.
Huntsville	30.72	95.57	3.80	6.25	3.76	6.65	2.98	5.85	4.34	5.13	4.35	4.70	4.57	3.97	3.28	3.
Liberty[8]	30.05	94.82	4.21	6.21	4.18	6.58	2.77	5.67	4.16	4.73	4.50	4.51	4.33	3.82	4.65	3.
Lufkin[7]	31.23	94.75	4.29	6.32	3.83	6.70	3.49	5.96	4.38	5.16	4.81	4.73	3.48	3.75	2.83	2.
Marshall[7]	32.53	94.35	4.40	7.06	3.85	7.62	4.08	7.14	5.02	6.42	4.78	5.52	3.45	3.94	2.97	2.
Palacios[9]	28.63	96.63	2.10	3.70	2.96	4.10	1.61	3.69	2.80	3.29	3.21	3.23	5.34	3.90	1.85	3.
Paris[15]	33.67	95.57	2.59	5.49	3.52	6.04	3.49	6.12	5.59	6.19	5.42	6.27	4.46	5.01	3.76	3.
Seguin[9]	29.57	97.95	1.72	2.67	2.34	3.00	1.75	2.71	3.27	2.67	3.18	2.87	3.17	2.53	1.89	1.
Texarkana[10]	33.30	94.17	4.09	6.51	4.05	7.43	4.04	7.33	5.91	7.15	4.81	6.24	3.54	4.35	3.16	3.
Waxahachie	32.38	96.85	2.19	4.04	2.98	4.59	2.19	4.34	4.51	4.09	4.87	4.57	3.60	3.87	2.21	2.

* Except as noted. All values in inches. Data from Climatological Summaries for Texas, Nat

ation and 8-Inch Sponge Normal Values· 1941-1970.* East Texas Group.

FOLDOUT FRAME 2

	MAY		JUNE		JULY		AUG.		SEPT.		OCT.		NOV.		DEC.		YEAR	
	P	Sp	P	Sp	P	Sp	P	Sp	P	Sp	P	Sp	P	Sp	P	Sp	P	Sp
51	5.17	4.81	3.14	3.77	1.41	1.96	2.04	1.24	3.82	2.02	3.45	2.88	3.38	3.48	3.26	4.43	33.70	3.54
33	4.79	5.10	4.75	4.33	5.71	4.30	5.34	4.23	5.30	4.35	3.19	3.85	4.54	4.19	4.95	5.93	51.77	5.20
97	4.43	4.01	3.24	3.29	1.90	2.01	3.09	1.68	3.97	2.43	3.17	2.79	3.72	3.38	3.37	4.41	38.96	3.53
41	3.79	2.91	3.18	2.64	2.22	1.89	2.75	1.52	4.69	2.44	3.27	2.88	2.35	2.64	2.12	2.77	33.17	2.57
68	3.29	4.36	4.17	3.99	5.46	4.53	4.98	4.57	6.56	5.21	3.78	5.08	4.10	4.78	4.07	5.64	43.83	5.06
86	4.65	3.39	3.53	3.18	2.22	2.09	3.08	1.68	4.37	2.48	2.72	2.61	2.71	2.58	2.60	3.13	38.92	2.35
13	4.35	4.70	4.57	3.97	3.28	3.10	3.05	2.23	4.05	2.62	3.27	2.94	4.39	3.89	4.11	5.44	44.95	4.39
73	4.50	4.51	4.33	3.82	4.65	3.49	3.90	3.04	4.23	2.99	3.69	3.13	4.07	3.82	4.92	5.15	48.61	4.41
16	4.81	4.73	3.48	3.75	2.83	2.63	2.81	1.96	3.22	2.18	2.97	2.40	4.60	3.63	4.22	5.26	44.93	4.22
42	4.78	5.52	3.45	3.94	2.97	2.67	2.81	2.05	3.09	2.18	2.86	2.44	4.20	3.62	4.41	5.50	41.92	4.68
29	3.21	3.23	5.34	3.90	1.85	3.05	4.16	2.48	5.60	3.77	3.94	4.15	2.42	3.64	2.59	3.70	38.56	3.56
19	5.42	6.27	4.46	5.01	3.76	3.63	3.05	2.53	3.68	2.57	3.10	2.93	2.62	3.68	3.06	4.96	45.32	4.61
67	3.18	2.87	3.17	2.53	1.89	1.85	1.98	1.27	3.80	1.97	3.35	2.73	2.05	2.69	1.73	2.68	30.23	2.49
15	4.81	6.24	3.54	4.35	3.16	3.03	2.71	2.16	4.03	2.66	2.75	2.99	3.53	3.47	3.88	5.02	46.50	4.86
09	4.87	4.57	3.60	3.87	2.21	2.44	2.03	1.55	3.05	1.78	2.90	2.39	2.73	2.94	2.47	3.69	35.73	3.36

ogical Summaries for Texas, National Weather Service, NOAA.

FOLDOUT FRAME 1 ... Mean Texas Precipitation and 8-inch Storage Normal

STATION	(°N) LATITUDE	(°W) LONGITUDE	JAN. P	JAN. Sp	FEB. P	FEB. Sp	MARCH P	MARCH Sp	APRIL P	APRIL Sp	MAY P	MAY Sp	JUNE P	JUNE Sp	JULY P	JULY S
Alpine	30.37	103.65	0.85	1.18	0.36	1.12	0.26	0.76	0.47	0.56	1.24	0.70	2.56	1.31	2.73	1.
Balmorhea	30.98	103.75	0.64	0.86	0.49	0.79	0.44	0.64	0.59	0.48	1.50	0.71	1.48	0.85	1.56	0.
Chisos Basin	29.27	103.30	0.76	1.20	0.40	1.08	0.29	0.79	0.65	0.60	1.68	0.97	1.96	1.29	3.07	1.
Fort Stockton	30.87	102.92	0.83	0.98	0.52	0.97	0.42	0.73	0.52	0.54	1.67	0.80	1.78	1.05	1.44	0.
La Tuna	31.97	106.60	0.41	0.71	0.36	0.64	0.33	0.55	0.15	0.35	0.28	0.22	0.71	0.30	1.61	0.
McCamey	31.13	102.20	0.64	0.98	0.51	0.90	0.48	0.76	0.77	0.61	1.91	0.98	1.49	1.09	1.64	0.
Marathon	30.20	103.23	0.51	0.75	0.41	0.70	0.36	0.57	0.65	0.49	1.36	0.74	1.70	0.96	1.78	1.
Mount Locke	30.67	104.00	0.83	1.82	0.48	1.68	0.46	1.37	0.46	1.08	1.49	1.08	2.48	1.59	3.87	2.
Panther Junction	29.32	103.22	0.58	0.89	0.53	0.84	0.39	0.70	0.50	0.46	1.49	0.72	1.43	0.89	1.70	1.
Pecos	31.42	103.50	0.34	0.57	0.31	0.51	0.32	0.43	0.60	0.39	1.07	0.56	1.07	0.57	1.35	0.
Presidio	29.55	104.35	0.41	0.49	0.21	0.41	0.15	0.24	0.21	0.15	0.61	0.23	1.26	0.46	1.35	0.
Salt Flat	31.78	104.90	0.30	0.65	0.19	0.55	0.20	0.41	0.33	0.35	0.34	0.27	1.03	0.45	1.48	0.
Van Horn	31.05	104.83	0.54	0.89	0.29	0.77	0.24	0.54	0.35	0.38	0.59	0.39	0.92	0.45	1.75	0.
Wink	31.78	103.20	0.59	0.79	0.31	0.72	0.31	0.55	0.75	0.52	1.44	0.79	1.26	0.83	1.64	0.
Valentine	31.70	106.32	0.40	0.56	0.38	0.57	0.30	0.50	0.17	0.32	0.20	0.19	0.57	0.22	1.39	0.

*Except as noted. All values in inches. Data from Climatological Summaries for Texas, Nati

...ipitation and s...ge Normal Values (1941-1970*. West Texas Group.

	APRIL		MAY		JUNE		JULY		AUG.		SEPT.		OCT.		NOV.		DEC.		YEAR	
	P	Sp	P	Sp	P	Sp	P	Sp	P	Sp	P	Sp	P	Sp	P	Sp	P	Sp	P	Sp
37	0.56	1.24	0.70	2.56	1.31	2.73	1.85	2.43	1.95	1.99	1.86	1.36	1.68	0.41	1.30	0.55	1.01	15.21	1.27
59	0.48	1.50	0.71	1.48	0.85	1.56	0.86	1.41	0.86	1.69	0.99	1.28	1.09	0.55	0.91	0.54	0.78	12.12	0.81
55	0.60	1.68	0.97	1.96	1.29	3.07	1.88	2.28	2.13	1.85	1.90	1.26	1.73	0.46	1.33	0.58	1.09	15.24	1.33
62	0.54	1.67	0.80	1.78	1.05	1.44	0.95	1.27	0.82	1.29	0.83	1.29	0.99	0.51	0.91	0.59	0.78	12.23	0.85
15	0.35	0.28	0.22	0.71	0.30	1.61	0.66	1.66	0.98	1.04	0.88	0.70	0.73	0.29	0.57	0.52	0.59	8.06	0.59
77	0.61	1.91	0.98	1.49	1.09	1.64	0.99	1.42	0.95	1.39	0.94	1.39	1.14	0.53	1.05	0.58	0.89	12.75	0.94
65	0.49	1.36	0.74	1.70	0.96	1.78	1.14	1.72	1.12	2.51	1.52	1.02	1.43	0.56	0.98	0.41	0.81	12.99	0.[illegible]
46	1.08	1.49	1.08	2.48	1.59	3.87	2.56	3.42	3.20	2.75	3.22	1.51	2.94	0.56	2.29	0.56	1.82	18.87	2.05
50	0.46	1.49	0.72	1.43	0.89	1.70	1.01	1.46	1.02	2.17	1.31	1.35	1.46	0.56	1.14	0.45	0.91	12.61	0.95
60	0.39	1.07	0.56	1.07	0.57	1.35	0.66	0.90	0.56	1.37	0.68	0.96	0.82	0.39	0.66	0.37	0.57	9.05	0.5[illegible]
21	0.15	0.61	0.23	1.26	0.46	1.35	0.63	1.23	0.63	1.51	0.78	0.99	0.81	0.35	0.60	0.33	0.47	8.67	0.49
33	0.35	0.34	0.27	1.03	0.45	1.48	0.74	1.98	1.13	1.11	1.09	0.86	0.92	0.30	0.75	0.39	0.65	8.51	0.66
35	0.38	0.59	0.39	0.92	0.45	1.75	0.80	1.82	1.09	1.71	1.20	0.97	1.11	0.54	0.91	0.51	0.85	10.23	0.73
75	0.52	1.44	0.79	1.26	0.83	1.64	0.86	1.52	0.96	1.19	0.86	1.41	1.04	0.30	0.93	0.39	0.66	11.11	0.79
17	0.32	0.20	0.19	0.57	0.22	1.39	0.56	1.36	0.80	0.94	0.72	0.55	0.58	0.26	0.45	0.38	0.46	6.90	0.49

...atological Summaries for Texas, National Weather Service, NOAA.

FOLDOUT FRAME 2

ORIGINAL PAGE IS OF POOR QUALITY

Table 2(e). Mea[illegible]as Precipitation and 8-Inch Sponge Normal

STATION	(ON) LATI-TUDE	(CW) LONGI-TUDE	JAN. P	JAN. Sp	FEB. P	FEB. Sp	MARCH P	MARCH Sp	APRIL P	APRIL Sp	MAY P	MAY Sp	JUNE P	JUNE Sp	JULY P	JULY Sp
Alice	27.73	98.07	1.37	2.00	1.48	1.98	1.10	1.68	1.80	1.45	2.93	1.91	2.96	2.11	1.96	1.7
Aransas County	28.27	96.80	2.18	3.86	2.45	3.88	1.61	3.40	2.43	2.97	3.17	3.16	3.52	3.40	2.26	2.8
Beeville	28.45	97.70	1.61	2.32	2.06	2.58	1.37	2.34	2.38	2.06	3.35	2.54	2.69	2.40	2.14	1.8
Cotulla	28.45	99.22	0.74	1.42	1.34	1.50	0.60	1.27	1.74	1.13	2.56	1.59	2.06	1.55	0.81	0.8
Crystal City	28.68	99.83	0.79	1.32	1.28	1.41	0.75	1.28	1.59	1.09	3.23	1.77	2.27	1.88	1.37	1.1
Eagle Pass	28.70	100.48	0.94	1.23	1.03	1.31	0.76	1.12	1.90	1.10	3.24	1.83	1.63	1.54	1.61	0.9
Encinal	28.08	99.37	0.92	1.42	1.29	1.51	0.72	1.25	1.88	1.12	3.14	1.73	2.29	1.69	1.21	0.9
Falfurrias	27.22	98.15	1.41	1.73	1.42	1.82	0.87	1.47	1.65	1.23	3.00	1.75	2.68	1.95	1.19	1.2
Harlingen	26.22	97.68	1.43	1.96	1.22	1.80	0.95	1.47	1.47	1.22	3.18	1.83	2.49	2.07	1.71	1.5
Hebbronville	27.30	98.67	1.15	1.32	1.44	1.74	0.55	1.39	1.55	1.14	1.64	1.21	2.13	1.29	0.64	0.9
Hondo	29.35	99.13	1.72	2.32	2.22	2.73	1.46	2.50	2.77	2.26	3.67	2.73	2.72	2.42	1.65	1.4
Kenedy	28.82	97.85	1.54	2.34	2.39	2.64	0.99	2.19	2.70	1.93	3.50	2.52	2.98	2.38	1.48	1.4
Kingsville	27.53	97.88	1.43	1.68	1.64	1.86	0.84	1.57	1.26	1.13	3.40	1.87	2.69	2.29	1.21	1.4
San Benito	26.13	97.63	1.01	1.62	1.38	1.63	0.65	1.32	1.49	1.15	2.34	1.54	2.58	1.86	1.39	1.4
Uvalde	29.22	99.77	1.20	1.54	1.55	1.79	1.15	1.66	2.06	1.54	2.96	1.96	2.53	1.95	1.63	1.3

FOLDOUT FRAME

[illegible] as noted. All values [illegible] inches. Data from Climatological Summaries for Texas, Nati

ecipitation and 8-Inch Snonge Normal Va : 1941-1970*. South Texas Group.

APRIL		MAY		JUNE		JULY		AUG.		SEPT.		OCT.		NOV.		DEC.		YEAR	
	Sp	P	Sp	P	Sp	P	Sp	P	Sp	P	Sp	P	Sp	P	Sp	P	Sp	P	Sp
.80	1.45	2.93	1.91	2.96	2.11	1.96	1.70	2.28	1.28	4.90	2.41	2.69	2.77	1.41	2.03	1.55	1.97	6.43	1.94
.43	2.97	3.17	3.16	3.52	3.40	2.26	2.80	4.49	2.89	5.82	4.19	3.97	4.54	2.11	3.72	2.80	3.67	5.81	3.54
.38	2.06	3.35	2.54	2.69	2.40	2.14	1.81	2.58	1.53	4.68	2.51	2.94	2.95	1.70	2.41	1.59	2.28	9.09	2.31
.74	1.13	2.56	1.59	2.06	1.55	0.81	0.87	1.53	0.70	2.94	1.42	2.44	1.99	1.26	1.81	1.03	1.64	9.05	1.46
.59	1.09	3.23	1.77	2.27	1.88	1.37	1.14	2.23	1.14	2.69	1.57	2.51	2.03	0.87	1.79	0.82	1.42	0.40	1.48
.90	1.10	3.24	1.83	1.63	1.54	1.61	0.98	2.01	1.00	2.96	1.52	1.96	1.78	0.70	1.37	0.78	1.13	9.52	.32
.88	1.12	3.14	1.73	2.29	1.69	1.21	0.98	2.03	0.89	3.11	1.52	2.38	1.89	1.13	1.62	1.06	1.47	1.16	. .
.65	1.23	3.00	1.75	2.68	1.95	1.19	1.26	2.38	1.05	4.83	2.35	2.38	2.56	1.10	1.77	1.24	1.60	4.15	1.71
.47	1.22	3.18	1.83	2.49	2.07	1.71	1.52	3.04	1.54	4.80	2.68	2.56	2.77	1.43	2.03	1.57	1.89	5.35	1.89
.55	1.14	1.64	1.21	2.13	1.29	0.64	0.90	1.54	0.62	4.05	1.88	2.11	2.23	1.20	1.68	0.66	1.37	8.66	1.39
.77	2.26	3.67	2.73	2.72	2.42	1.65	1.49	2.43	1.24	3.89	2.01	3.00	2.60	1.41	2.27	1.50	2.12	28.46	2.22
.70	1.93	3.50	2.52	2.98	2.38	1.48	1.49	2.28	1.16	3.64	1.86	3.03	2.35	2.19	2.31	1.83	2.47	28.55	2.13
.26	1.13	3.40	1.87	2.69	2.29	1.21	1.49	2.76	1.36	5.01	2.70	2.63	2.88	1.21	2.01	1.19	1.69	5.27	1.87
.49	1.15	2.34	1.54	2.58	1.86	1.39	1.46	3.08	1.53	4.97	2.78	3.09	3.08	1.43	2.33	1.14	1.91	4.55	1.84
.06	1.54	2.96	1.96	2.53	1.95	1.63	1.32	2.30	1.19	3.10	1.68	2.89	2.20	0.98	1.57	0.92	1.47	3.22	1.67

atological Summaries for Texas, National Weather Service, NOAA.

FOLDOUT FRAME 2

[1]1931 - 1969

[2]1931 - 1970

[3]1932 - 1969

[4]1933 - 1967

[5]1933 - 1968

[6]19?? - 1969

[7]193? 1966

[8]1937 - 1969

[9]1938 - 1967

[10]1939 - 1968

[11]1939 - 1969

[12]1940 - 1966

[13]1940 - 1969

[14]1941 - 1967

[15]1941 - 1968

[16]1942 - 1971

[17]1943 - 1970

[18]1947 - 1966

[19]1947 - 1970

[20]1948 - 1967

[21]1948 - 1969

[22]1948 - 1970

[23]1949 - 1966

[24]1949 - 1967

[25]1949 - 1968

[26]1949 - 1969

[27]1949 - 1970

[28]1950 - 1969

[29]1950 - 1971

[30]1951 - 1966

[31]1951 - 1967

[32]1953 - 1970

[33]1956 - 1970

[34]1959 - 1971

Periods of Record Other Than 1941-1970: Tables 2(a) - 2(e).

Station	Sta. No.	Period	Latitude (°N)	Longitude (°W)	January Precip	January Snowge	July Precip.	July Snowge	Year Precip.	Year Snow
umont	0613	1941-70	30.08	94.10	4.57	7.00	5.71	4.30	54.77	5.2
umont	0613	1980	30.08	94.10	5.84	5.04	0.95	1.34	57.59	4.7
umont	0613	1979	30.08	94.10	7.91	7.43	15.50	3.93	79.56	5.9
kin	4524	1941-70	31.23	94.75	4.29	6.32	2.83	2.63	44.93	4.2
erty	5196	1941-70	30.05	94.82	4.21	6.21	4.65	3.49	49.61	4.4
erty	5196	1980	30.05	94.82	0.40	3.99	0.36	2.65	56.77	4.3
erty	5196	1979	30.05	94.82	8.91	7.49	7.61	4.08	70.11	5.3
tsville	4382	1941-70	30.72	95.57	3.80	6.25	3.28	3.10	45.95	4.1
tsville	4382	1980	30.72	95.57	0.94	2.61	0.05	0.78	28.30	2.6
tsville	4382	1979	30.72	95.57	7.65	7.64	5.90	3.20	64.07	5.1
nham	1048	1941-70	30.15	96.40	2.78	4.84	1.90	2.01	38.96	3.5
ple	8910	1941-70	31.10	97.35	2.35	4.08	1.96	1.97	33.87	3.4
Marcos	7983	1941-70	29.88	97.95	2.06	3.08	1.89	2.04	33.86	2.7
Braunfels	0832	1941-70	30.10	98.42	2.12	3.23	1.98	1.79	34.39	2.8
nco	6276	1941-70	29.70	98.12	1.88	2.92	1.83	1.78	32.61	2.5
no	5272	1941-70	30.75	98.68	1.37	2.16	1.20	1.22	26.16	2.1
w od	1138	1941-70	31.72	98.98	1.72	2.63	1.85	1.92	27.20	2.3
rville	4782	1941-70	30.05	99.15	1.86	2.36	2.10	1.96	30.73	2.5
dy	1017	1941-70	31.12	99.35	1.52	2.16	1.34	1.41	23.27	1.9
dy	1017	1980	31.12	99.35	1.18	2.42	0.00	0.44	24.21	2.1
dy	1017	1979	31.12	99.35	1.14	2.98	1.96	1.33	23.47	2.6
ora	8449	1941-70	30.57	100.65	0.82	1.28	1.61	1.33	19.28	1.4
orado City	4974	1941-70	32.38	100.87	0.82	1.46	2.14	1.39	19.80	1.4
na	6734	1941-70	30.72	101.20	0.81	1.21	1.30	1.19	17.59	1.3
na	6734	1980	30.72	101.20	0.08	2.52	0.00	0.87	17.10	1.6
Spring	0786	1941-70	32.25	101.45	0.63	1.30	1.97	1.28	15.72	1.2
amey	5707	1941-70	31.13	102.20	0.64	0.98	1.64	1.42	12.75	0.9
amey	5707	1979	31.13	102.20	0.08	0.67	1.01	0.58	8.29	0.7
t Stockton	3278	1941-70	30.87	102.92	0.83	0.98	1.44	0.95	12.23	0.8
k	9829	1941-70	31.78	103.20	0.59	0.79	1.64	0.86	11.11	0.7
os	6892	1941-70	31.42	103.50	0.34	0.57	1.35	0.66	9.05	0.6
os	6892	1980	31.42	103.50	0.04	1.46	0.09	1.44	15.78	1.1
[illegible]	6892	1979	31.42	103.50	0.75	1.10	0.94	0.40	8.19	0.6
lmorhea	0498	1941-70	30.98	103.75	0.64	0.86	1.56	0.86	12.12	0.8
lmorhea	0498	1980	30.98	103.75	0.26	1.27	0.00	0.14	18.15	1.4
lmorhea	0498	1979	30.98	103.75	1.43	1.51	1.89	0.68	12.78	0.8
n Horn	9311	1941-70	31.05	104.83	0.54	0.89	1.75	0.80	10.23	0.7

amey	5707	1941-70	31.13	102.20	0.64	[illegible]	1.64	[illegible]	[illegible]
amey	5707	1979	31.13	102.20	0.08	0.67	1.01	0.58	8.29
t Stockton	3278	1941-70	30.87	102.92	0.83	0.98	1.44	0.95	12.23
k	9829	1941-70	31.78	103.20	0.59	0.79	1.64	0.86	11.11
os	6892	1941-70	31.42	103.50	0.34	0.57	1.35	0.66	9.05
os	6892	1980	31.42	103.50	0.04	1.46	0.09	1.44	15.78
[illegible]	6892	1979	31.42	103.50	0.75	1.10	0.94	0.40	8.19
lmorhea	0498	1941-70	30.98	103.75	0.64	0.86	1.56	0.86	12.12
lmorhea	0498	1980	30.98	103.75	0.26	1.27	0.00	0.14	18.15
lmorhea	0498	1979	30.98	103.75	1.43	1.51	1.89	0.68	12.78
n Horn	9311	1941-70	31.05	104.83	0.54	0.89	1.75	0.80	10.23
t Flat	7920	1941-70	31.78	104.90	0.30	0.65	1.48	0.74	9.51
lt Flat	7920	1980	31.78	104.90	0.11	0.56	0.16	0.10	7.08
lt Flat	7920	1979	31.78	104.90	0.88	0.88	2.65	0.79	9.47
leta	9966	1941-70	31.70	106.32	0.40	0.56	1.64	0.86	11.11
[illegible]	9966	1980	31.70	106.32	0.96	1.38	0.00	0.03	9.30
leta	9966	1979	31.70	106.32	0.80	0.51	1.37	0.49	8.17
[illegible]	4931	1941-70	31.97	106.60	0.41	0.71	1.61	0.66	8.06

Table 4. Precipitation and 8-inch Sponge Values at Selected Stations Along an East-West [illegible]

[illegible] precipitation and sponge values in inches. Data from National Climatic Center, NOAA, Asheville, N.C.

Figure 2

Texas Sponge Values: 1980[1]

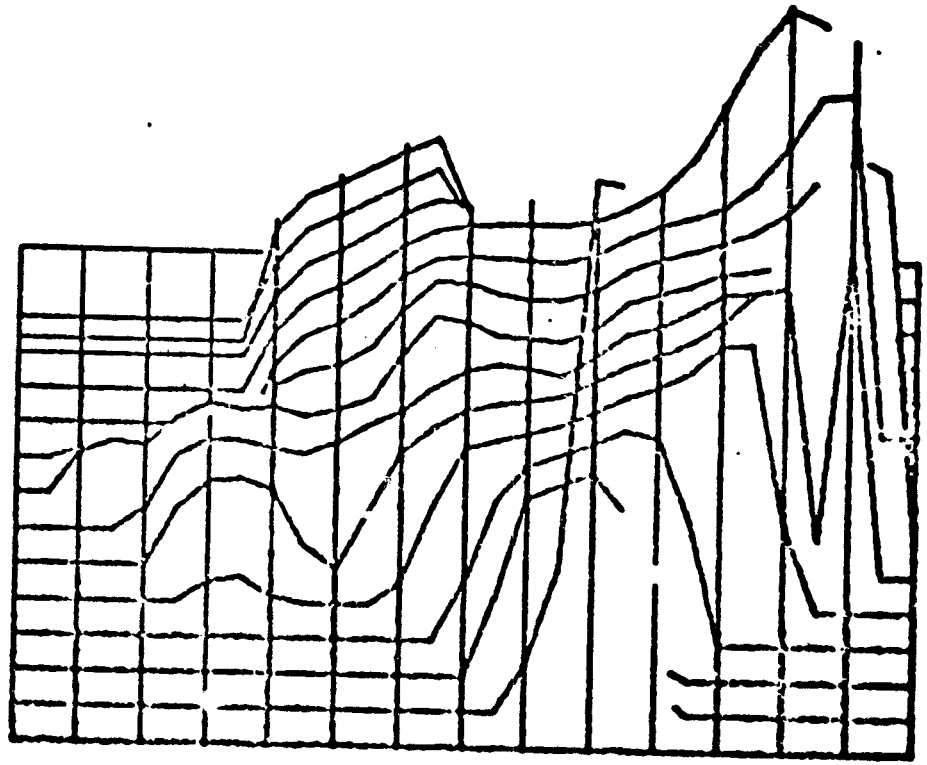

West

East

Normal Annual Texas Sponge Values[2]

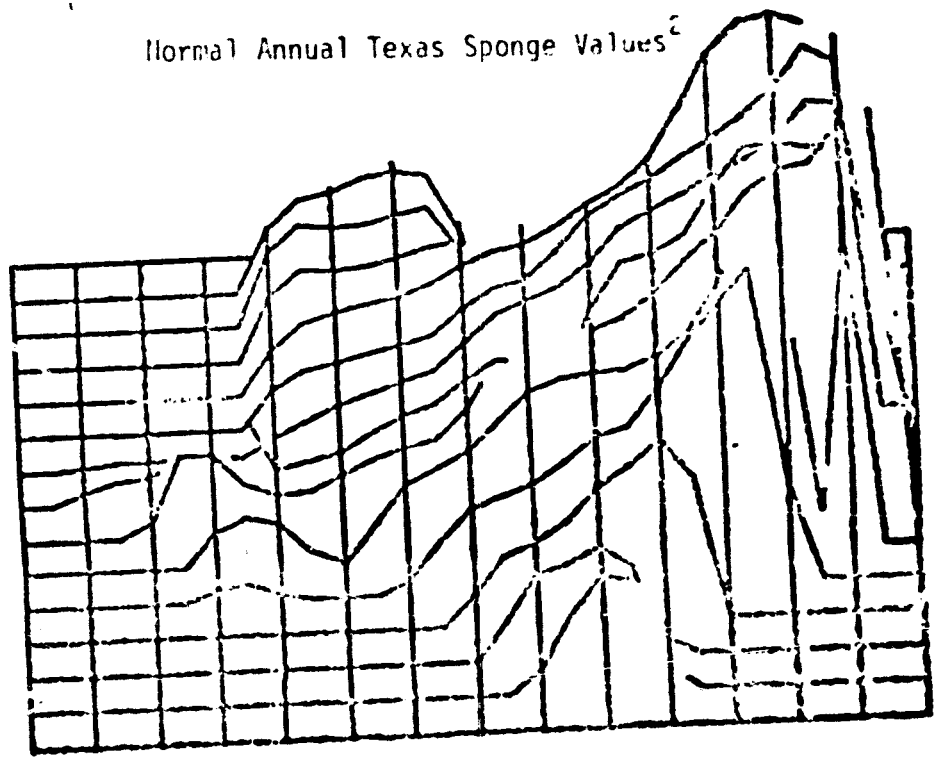

West

East

[1]Based on 28 stations along E-W "Texas Transect" from Beaumont to La Tuna

[2]1941-1970; 75 stations throughout Texas.

Note: 20x vertical exaggeration on all plots.

Figure 3

Texas Sponge Values: April, 1980[1]

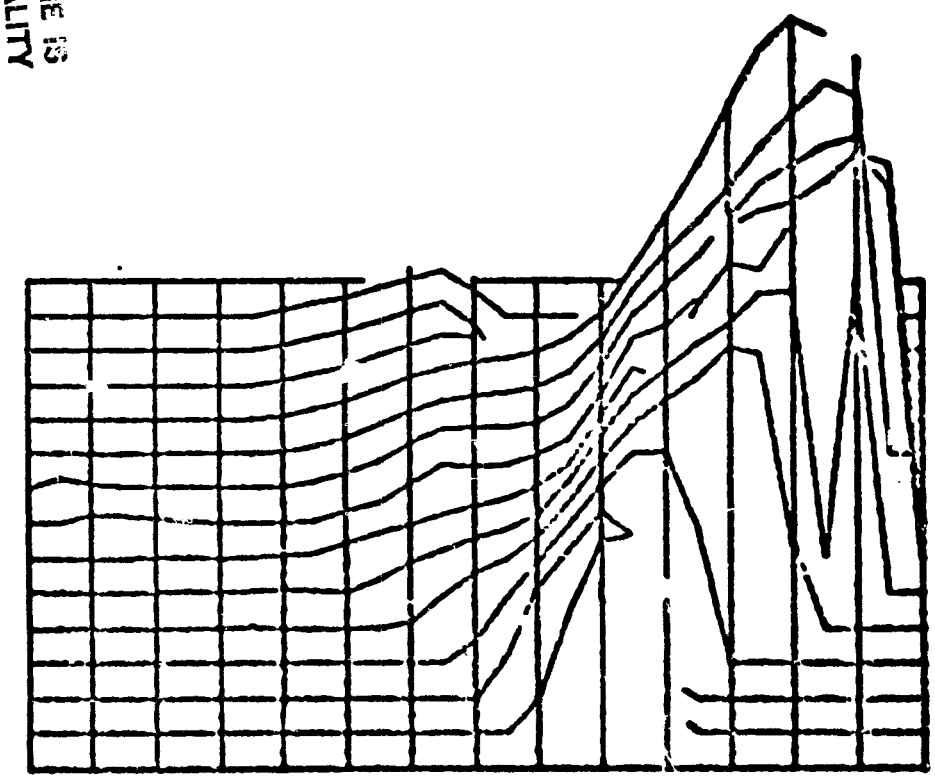

Normal Texas Sponge Values: April[2]

Normal Texas Sponge Values: April[2]

West

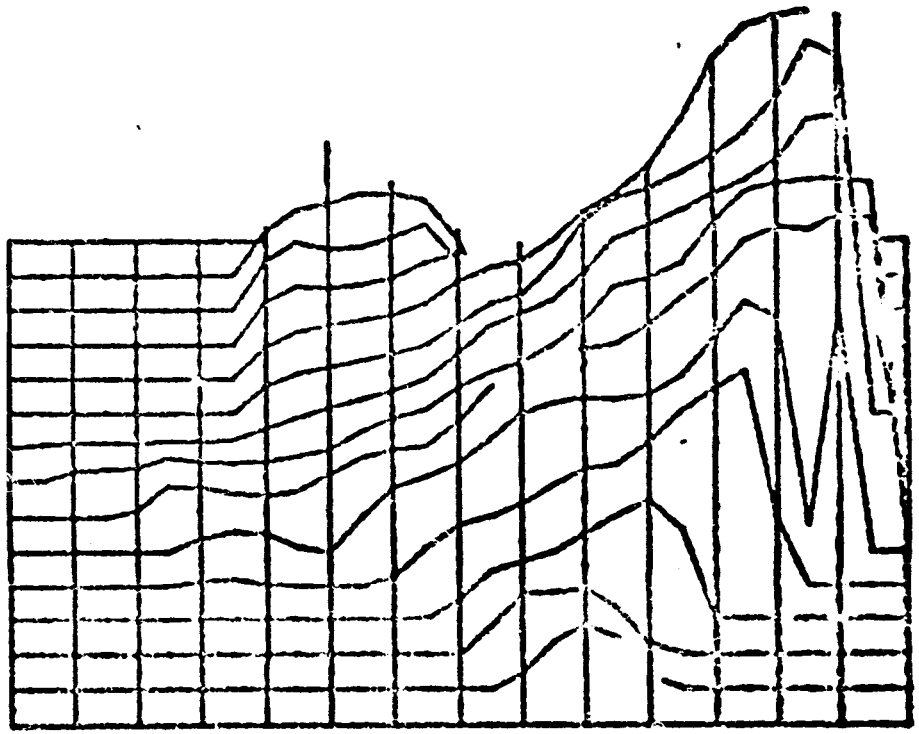

East

[1]Based on 28 stations along E-W "Texas Transect" from Beaumont to La Tuna.

[2]1941-1970; 75 stations throughout Texas.

NOTE: [illegible] suggestion on all plots.

FOLDOUT FRAME 2

Figure 4

Texas Sponge Values: July, 1930[1]

West

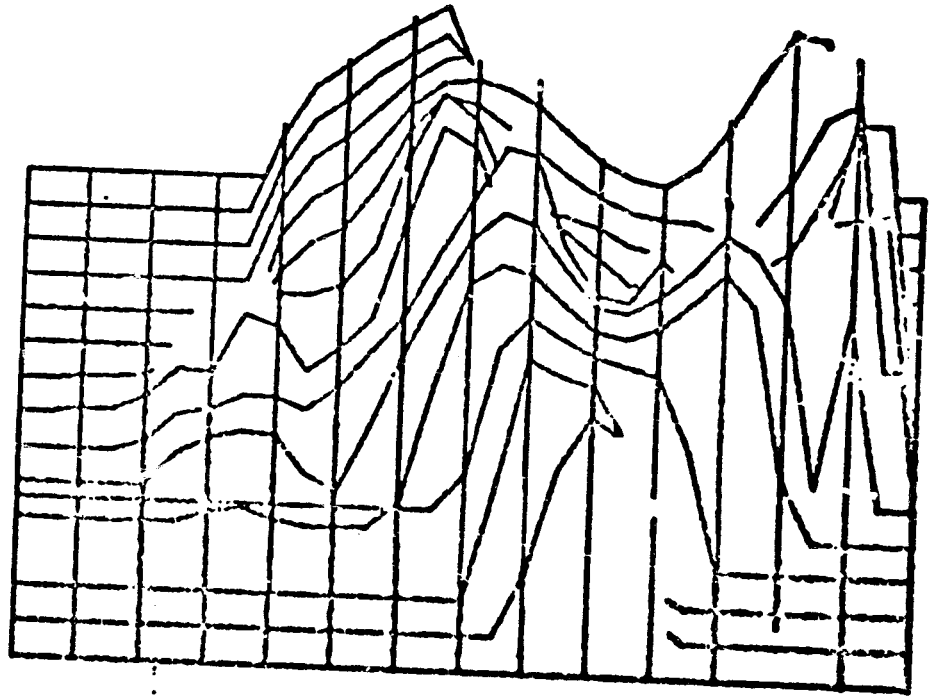

East

Normal Texas Sponge Values: July[2]

Normal Texas Sponge Values: July[2]

West

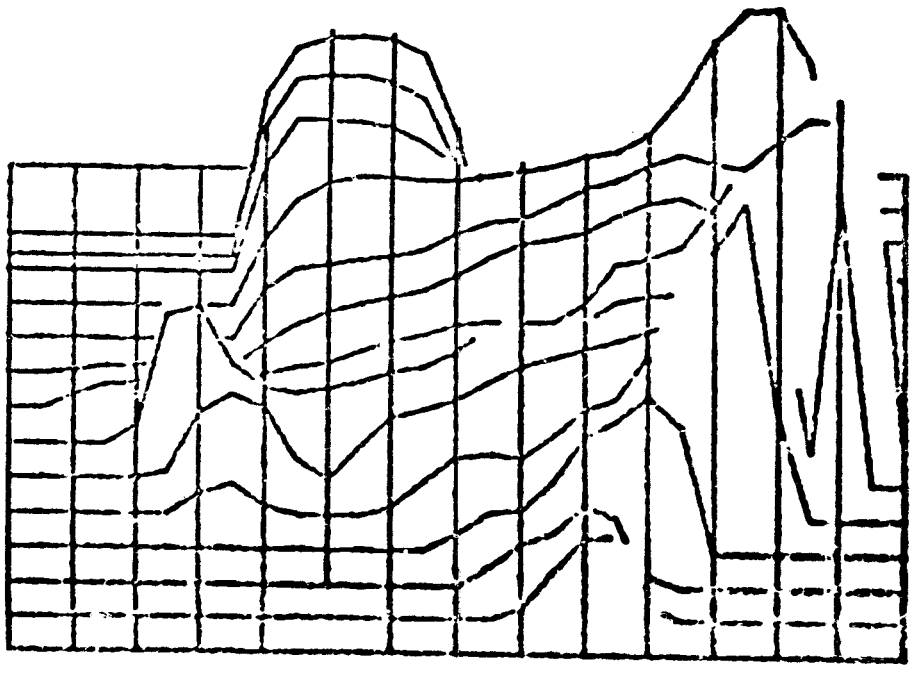

East

[1]Based on 28 stations along E-W "Texas Transect" from Beaumont to La Tuna.

[2]1941-1970; 75 stations throughout Texas.

Note: 25% Vertical Exaggeration on all plots.

Figure 5

Texas Sponge Values: October, 1980[1]

West

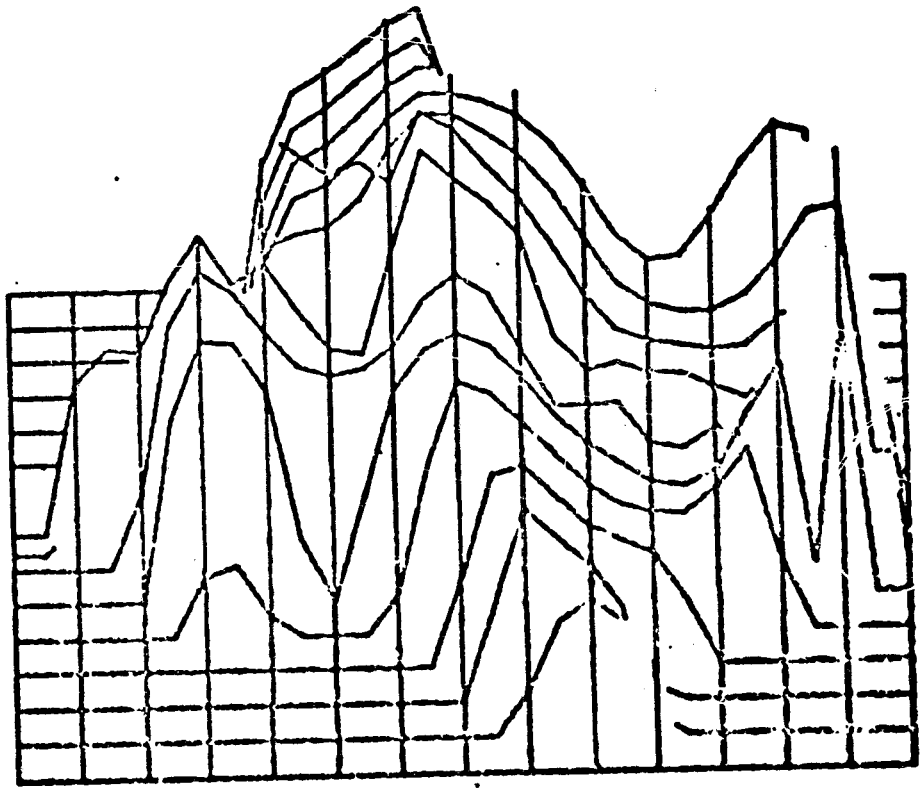

East

Normal Texas Sponge Values: October[2]

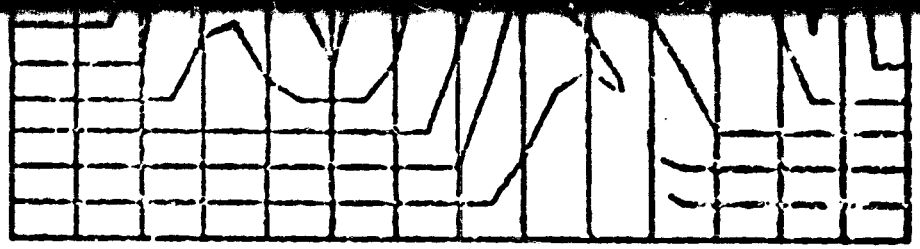

Normal Texas Sponge Values: October[2]

West

East

[1]Based on 28 stations along E-W "Texas Transect" from Beaumont to La Tuna.

[2]1941-1970; 75 stations throughout Texas.

Note: 25% Vertical Exaggeration on all plots.

ORBITER FUEL CELL IMPROVEMENT ASSESSMENT

Richard E. Johnson, Ph. D.
Le Tourneau College, Longview, Texas
1981 NASA-ASEE Summer Faculty Fellow

Supervisor:
Hoyt McBryar
Power Generation Branch
Propulsion and Power Division

Abstract - The history of fuel cells and the theory of fuel cells is given. Expressions for thermodynamic and electrical efficiencies are developed. The voltage losses due to electrode activation, ohmic resistance and ionic diffusion are discussed. Present limitations of the Orbiter Fuel cell are given as well as proposed enhancements These enhancements are then evaluated and recommendations are given for fuel cell enhancement both for short-range as well as long-range performance improvement. Estimates of reliability and cost savings are given for enhancements where possible

NATIONAL AERONAUTICS AND SPACE ADMINISTRATION
LYNDON B. JOHNSON SPACE CENTER
HOUSTON, TEXAS
JULY 17, 1981

I. DEFINITION OF A FUEL CELL

A fuel cell is a device for converting chemical energy directly into electrical energy where the reacting materials are supplied from reservoirs external to the electrochemical cell.

II. HISTORY OF THE FUEL CELL[1]

In 1839, Sir William Grove of England constructed the first known fuel cell. In 1842 he built a "gaseous-voltaic battery" (Figure 1) with 50 H_2 - O_2 cells in series. Fifty years later the name "fuel-cell" was given to the bank of cells built by Mond and Langer which operated with a 50% efficiency and produced 1½ watts. However, it wasn't until the early 1930's that Sir Frances Bacon in England built a 5 kilowatt fuel cell using nickel electrodes of dual porosity, H_2 and O_2, and KOH electrolyte. This cell operated at 205°C and 600 psi. Industry (e.g., Allis Chalmers) began developing fuel cells in the 1950's for terrestrial use and then NASA gave impetus to the technology in the 1960's with funding to companies such as GE and Pratt and Whitney who developed fuel cells for the Gemini and Apollo programs respectively. The advantages of fuel cells were seen to be high efficiency compared to heat engines, operation independent of environmental conditions, and potable water as a by-product for use by crew (for hydrogen-oxygen fuel cell).

III. THEORY OF THE FUEL CELL

Since the fuel cell is a voltaic cell in concept then there is an oxidizable material (fuel) and an oxidizing material (oxidant). Some fuels that have been used include hydrogen, hydrazine, methane and methanol; oxidizers have commonly been oxygen or air.[2] The main fuel cell development thus far has been on the hydrogen-oxygen system and thus

FIGURE 1 FUEL CELLS AS SHOWN BY GROVE

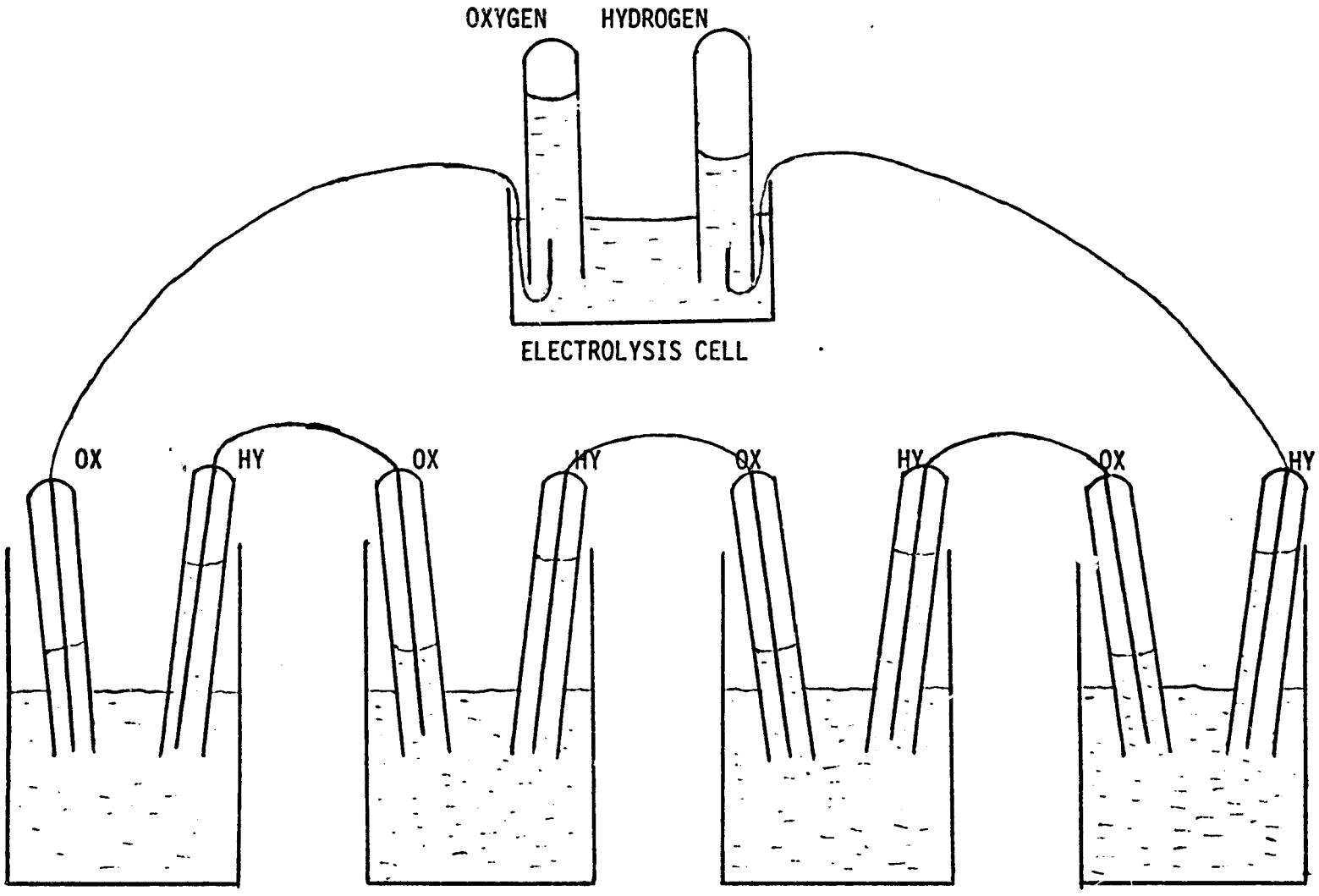

the remainder of this report will deal with this system utilizing an alkaline (KOH) electrolyte. In Figure 2, a schematic of the fuel cell is shown. In contrast to a conventional battery, note that in a fuel cell, the electrode materials do not react chemically but they provide reaction sites for the fuel, oxidizer and electrolyte as well as a conduction path for electrons through an external circuit. Between the electrodes in the cell is the electrolyte which is shown as an alkaline solution such as potassium hydroxide in water. The electrolyte could be an acidic solution also with appropriate cell materials. Through the electrolyte the electrical circuit is completed by ion transport between the electrodes. One advantage of the fuel cell is obvious from the diagram since the use of several external storage tanks or a rechargeable tank system allows for continuous operation of the cell without interrupting the external electrical circuit. By contrast, the circuit would have to be interrupted to recharge secondary batteries or to replace primary batteries.

In order to understand the fuel cell operation consider the basic reaction:

$$H_2(g) + \tfrac{1}{2}O(g) \rightarrow H_2O(l) + \text{Energy}$$

Figure 3 illustrates how the energy released is utilized in a heat engine-generator system and in a fuel-cell. The heat engine must operate at high temperatures to get reasonable efficiencies but, then other components still bring down the overall efficiency to near 30%. The fuel cell has a much higher overall efficiency at ordinary temperatures. For example the fuel cells on STS-1 were operating at about 64% efficiency based on data given in Rockwell Internal letter (PG-MWF-81-027).

FIGURE 2 SCHEMATIC OF HYDROGEN-OXYGEN FUEL CELL

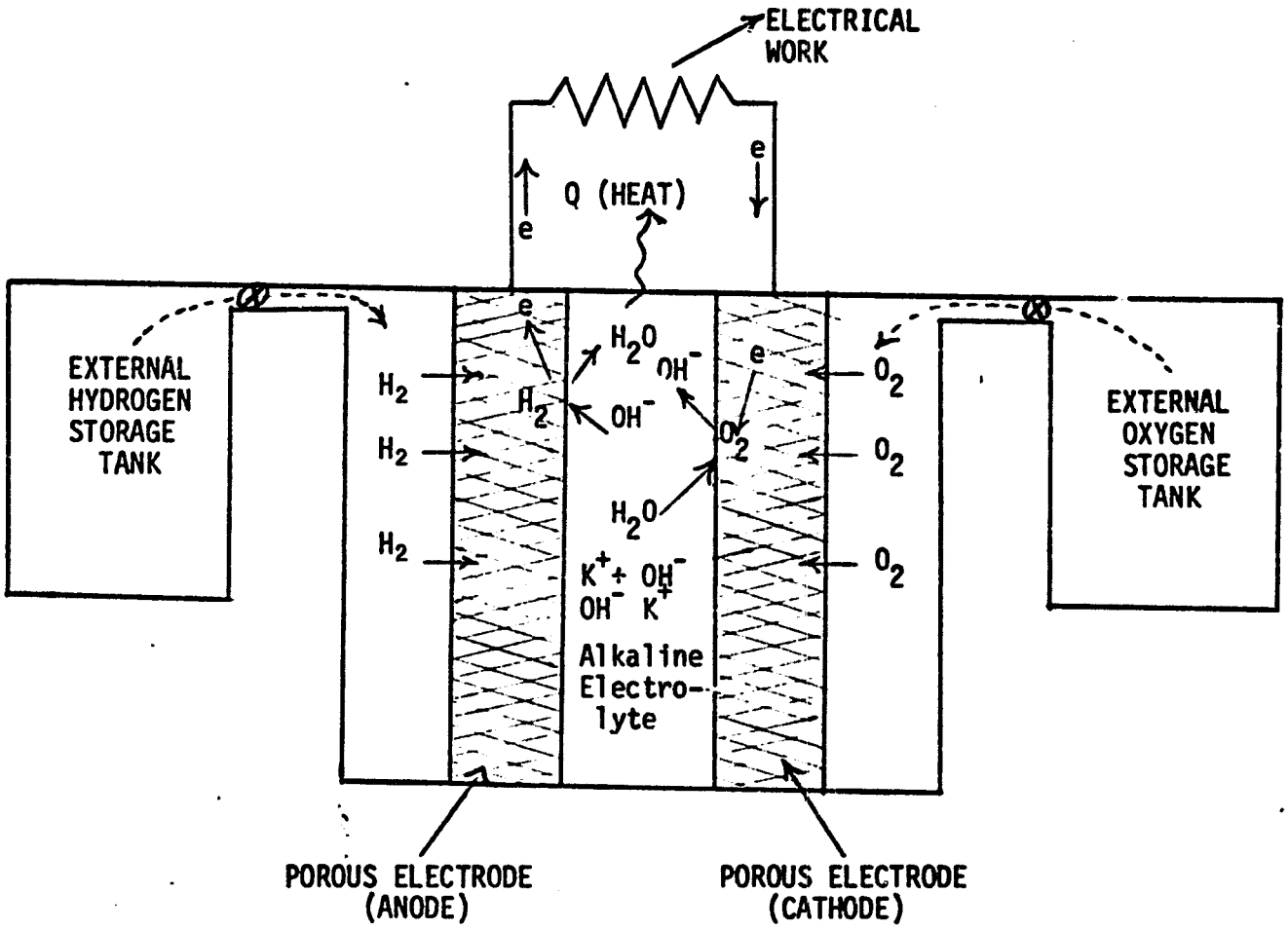

Anode Reaction

$H_2 + 2OH^- \rightarrow 2H_2O + 2e$

Cathode reaction

$\frac{1}{2}O_2 + H_2O + 2e \rightarrow 2OH^-$

OVERALL REACTION

$H_2 + \frac{1}{2}O_2 \rightarrow H_2O$ + Electrical work + Heat

FIGURE 3 BLOCK DIAGRAM OF HEAT ENGINE-GENERATOR VS. FUEL CELL SYSTEM

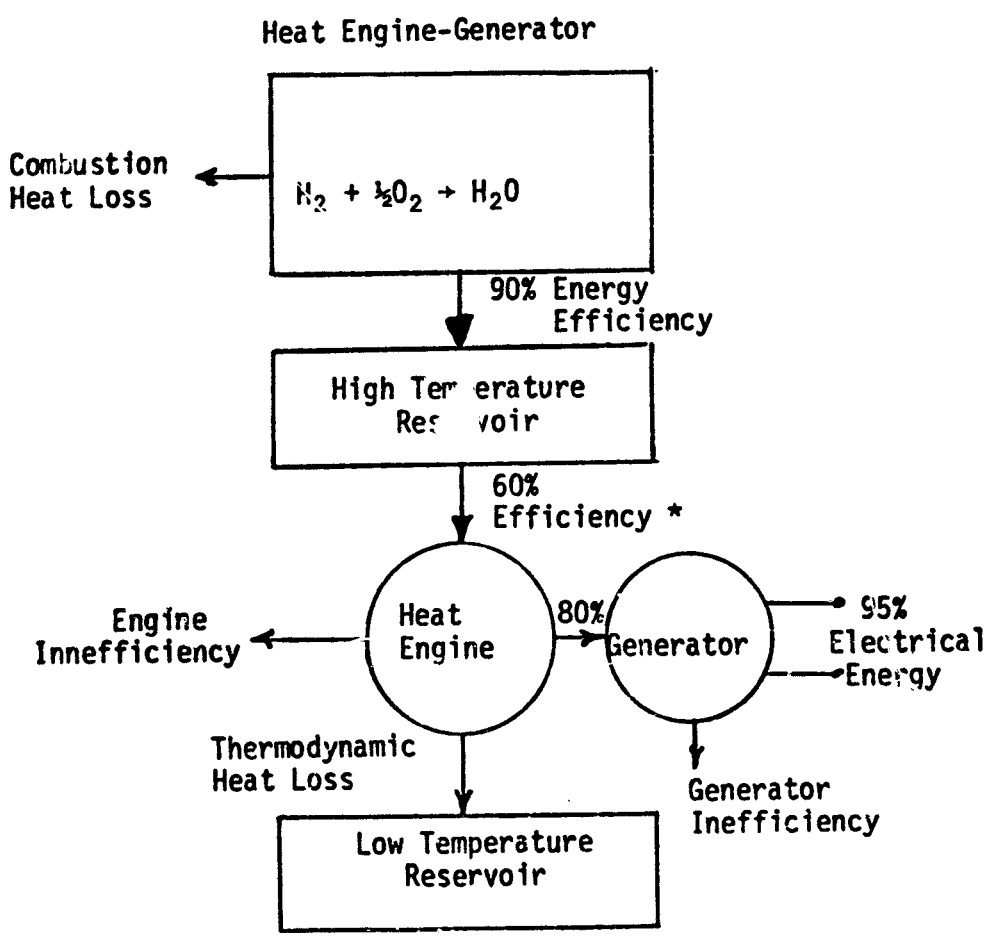

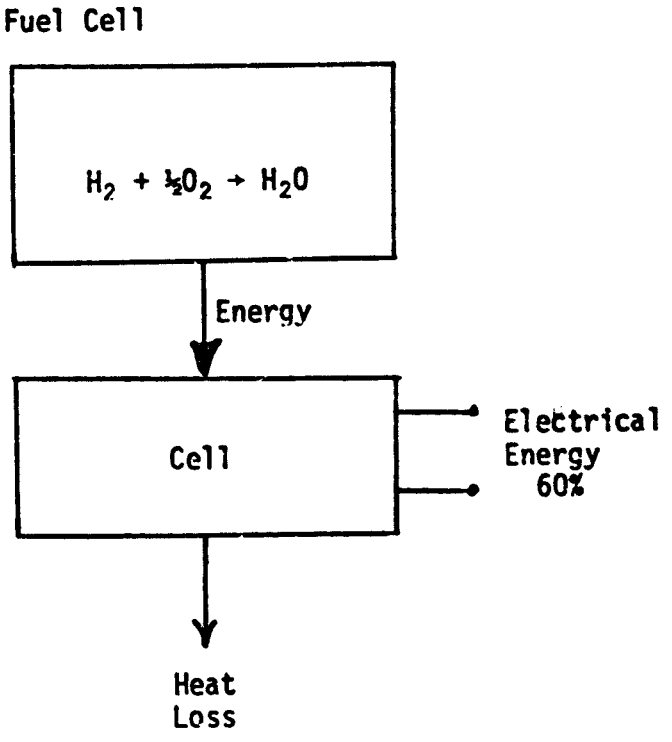

Thermodynamic Heat Loss, $T\Delta S$ = 10%

Current and Voltage Inefficiency loss = 30%

Total Heat Loss = 40%

Approximate Overall Efficiency 60%

* Carnot efficiency for heat engine operating between 900°F and 70°F.

Approximate overall efficiency 0.90 x 0.60 x 0.80 x 0.95 = 0.41 or 41%

The energy given off when hydrogen and oxygen are burned to form liquid water at constant pressure is called enthalpy, ΔH, of this reaction and for 1g-mole (18g) of the liquid water formed, $\Delta H = -68.317$ kcal. The negative sign means that the reaction is exothermic (heat is liberated). That would be the maximum heat available to operate a heat engine. The efficiency of that engine would be $\eta = \frac{(\text{work out})\ 100}{68.317\ \text{kcal}}$ (on the basis of one g-mole H_2O liquid formed).

The maximum efficiency of a heat engine is limited by the Carnot cycle and is given by

$$\eta_c = \frac{T_2 - T_1}{T_2} \times 100$$ where T_2 is Absolute Temperature of high Temperature Reservoir. T_1 is Absolute Temperature of low Temperature Reservoir.

In Figure 3, $t_2 = 900^\circ F$

$T_2 = 1359^\circ R$

$t_1 = 70^\circ F$

$T_1 = 529^\circ R$

Therefore $\eta_c = \frac{(1359 - 529)100}{1359} = 61\%$

Other energy losses due to boiler inefficiency, friction and electrical loss reduce the efficiency of heat engine-generator system to about 40% and in actual practice it would be less than this.

For the fuel cell operating at a fixed temperature and pressure, the energy available for conversion to electricity is not equal to ΔH but is given by the Gibbs free energy ΔG, where

$$\Delta G = \Delta H - T\Delta S$$

and ΔS for $H_2(g) + \frac{1}{2}O_2(g) \rightarrow H_2O(l)$ is $-0.039\ \frac{\text{kcal}}{\text{mole K}}$

Therefore at 25°C

$$\Delta G = -\quad 17 + 298(0.0390) = -56.69\ \frac{\text{kcal}}{\text{g-mole}}\ H_2O(\ell)$$

ΔG is the energy available for external work in a system other than P-V work and the only work we are considering is electrical work so

$$\Delta G = -nFE$$

where E is voltage of fuel cell, F is Faraday's constant and is equal to 23.060 $\frac{kcal}{volt}$ and n equals the number of moles of electrons involved in the reaction. To find n, the reaction can be broken down into an oxidation half and a reduction half where by definition oxidation occurs at the anode of a cell and reduction occurs at the cathode of a cell. The overall reaction can be divided as follows:

Oxidation (Anode)	$H_2(g) + 2OH^- \rightarrow 2H_2O(1) + 2e$
Reduction (Cathode)	$\frac{1}{2}O_2(g) + H_2O(1) + 2e \rightarrow 2OH^-$
Overall Reaction	$H_2 + \frac{1}{2}O_2 \rightarrow H_2O$

From the half reactions n=2, since 2 moles of electrons are transferred through an external electrical load for each mole of water produced.

Since $\Delta G = -nFE$

then $$E = \frac{-56.69 \frac{kcal}{mole}}{-(2 \text{ moles}) \left(23.060 \frac{kcal}{V}\right)} = 1.229V.$$

This is the maximum voltage obtainable from H_2 - O_2 fuel cell in basic solution at 25°C. However, to compare on an equivalent basis to the heat engine the theoretical efficiency of a fuel cell should be given by

$$\eta_T = \frac{\Delta G \times 100}{\Delta H} = \frac{-56.69 \times 100}{-68.32} = 83.0\%$$

or in terms of the voltage ratio, it would be

$$\eta_T = \frac{\frac{1.229 \times 100}{68.32}}{2 \times 23.060} = \frac{1.229 \times 100}{1.481} = 83.0\%$$

This is the maximum thermal efficiency of the fuel cell at 25°C and 1 atmosphere pressure.

The actual thermal efficiency of the fuel cell is

$$\eta_{T_a} = \frac{E \times 100}{1.481} = 67.52E(\%)$$ where E is the measured voltage output of the cell. If the electrical efficiency of the fuel cell is of interest then $$\eta_e = \frac{E \times 100}{1.229} = 81.37E(\%)$$ where E is the actual voltage and 1.229 is the maximum theoretical voltage of the cell at 25°C and 1 atmosphere.

The electrical efficiency should contain a factor for current inefficiencies, however current efficiencies are normally > 95% unless there are mechanical problems with the cell such as cell shorting, diffusion of reactants to opposite electrode to react directly, or leakage of reactants out of the cell. The voltage inefficiency has been a major concern of developmental work in the fuel cell. The factors involved that result in the cell voltage being less than the theoretical voltage of 1.229V can be summarized into three categories:

(1) Electrode Activation

(2) Ohmic Losses

(3) Diffusion Losses

The first effect of electrode activation can be understood from the fact that almost every reaction has an activation energy as shown in Figure 4. Even though the products are more stable (lower energy) than reactants, there is a certain energy barrier that the reactants must overcome in order to react and form products. This energy barrier is the activation energy. For example, the reaction of $H_2(g) + \frac{1}{2}O_2(g) \rightarrow H_2O(l)$ is very exothermic (-68.3 kcal/mole H_2O), and yet a mixture of $H_2(g)$ and $O_2(g)$ is stable almost indefinitely because of a high activation energy for this reaction. Heat or a spark added to this mixture would then cause an explosive reaction with the formation of $H_2O(l)$.

FIGURE 4 ENERGY RELATIONSHIPS IN A CHEMICAL REACTION

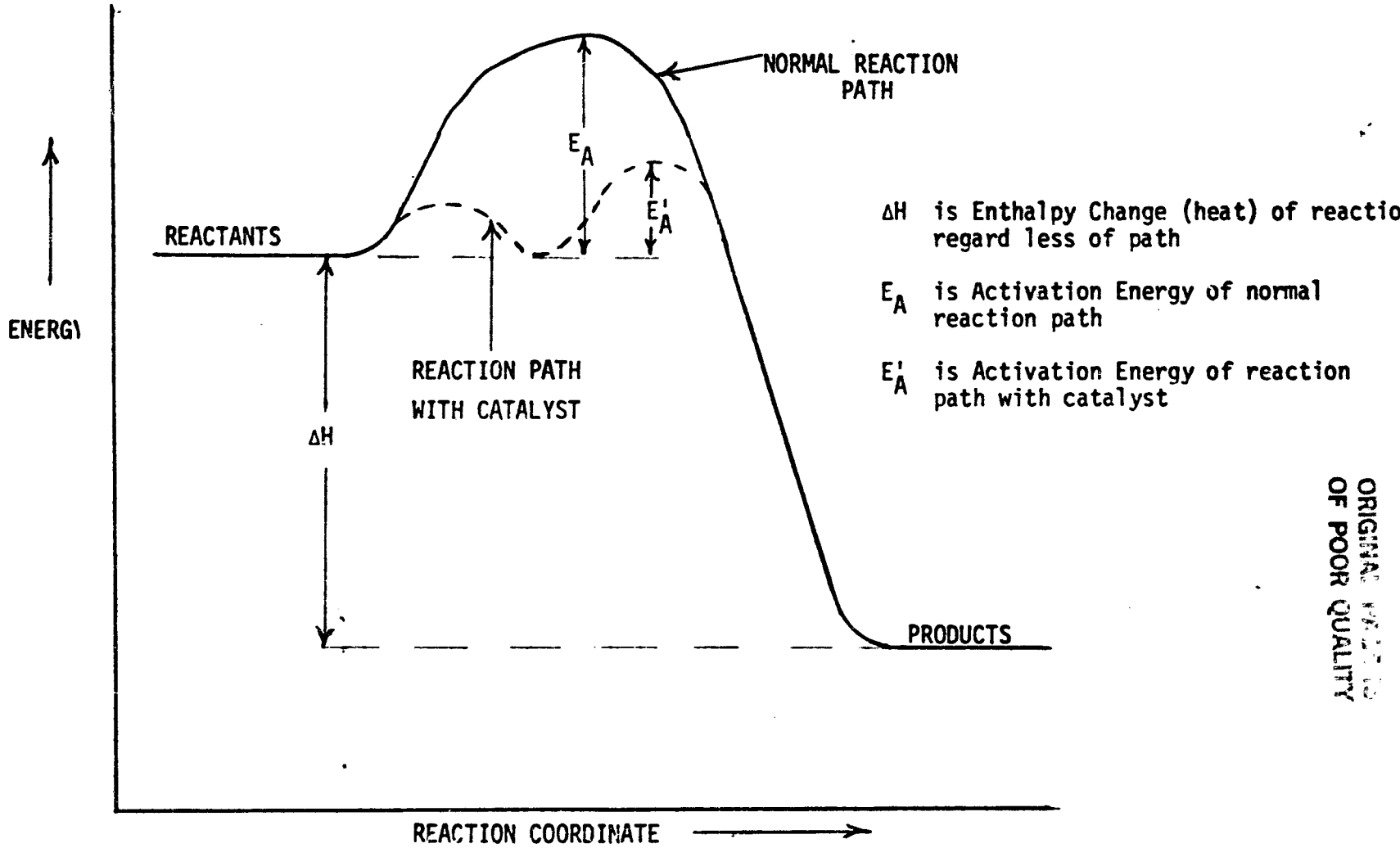

Another alternative to going over the high activation energy barrier is to provide another reaction mechanism by means of a catalyst. A catalyst is a substance that alters the activation energy and thus the rate of the reaction but is not used up itself in the reaction. Most catalysts lower the activation energy and speed up the reaction, but there are cases when "negative" catalysts or inhibitors are desirable.

Thus in Figure 4 the reaction path with a catalyst has a much lower activation energy than the normal path and the reaction will proceed faster. Increasing the temperature will increase the thermal energy of the reactants and will also increase the rate of the reaction since the reactants will have more energy to go over the activation energy barrier.

In the fuel cell there are two half reactions and each one must be catalyzed separately and each one has a separate effect on reducing the voltage output of the cell due to its activation. At the anode of the cell the following reaction takes place:

$$H_2 + 2OH^- \rightarrow 2H_2O + 2e$$

Many of the transition metals, Ruthenium, Indium, Platinum, Paladium, Osmium, Gold, Rhenium, Tungsten, and Nickel catalyze this reaction. For practical use Platinum-Palladium mixtures have been found to be the best for catalytic activity and long life. However, carbon monoxide and chloride ions have had a detrimental effect on the catalytic activity of Pt-Pd mixtures. The catalyzed reaction appears to be a 2-step mechanism as illustrated below. . . (1), physical adsorption of hydrogen on the metal surface followed by (2), dissociation into chemi-sorbed hydrogen atoms which are chemically reactive.

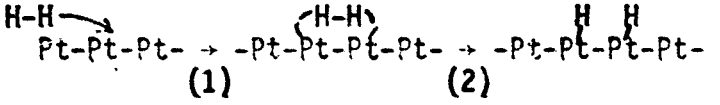

The anode reaction takes place on a catalytic electrode with very little voltage loss and usually it is not a problem in the fuel cell operation. At the cathode of the cell the other half of the reaction is as follows:

$$\tfrac{1}{2}O_2 + 2e + H_2O \rightarrow 2OH^-$$

This reaction is also catalyzed by many transition metals but best results have been achieved with a Gold-Platinum alloy catalyst. This reaction is more complicated than the anode reaction and has several steps in the mechanism. One postulated mechanism is as follows:[3]

$$O_2 + Pt \rightarrow Pt(O_2)$$
$$Pt(O_2) + e + H_2O \rightarrow Pt(HO_2) + OH^-$$
$$Pt(HO_2) + e \rightarrow Pt(HO_2^-)$$
$$Pt(HO_2^-) + 2e + H_2O \rightarrow Pt + 3OH^-$$

The cathode exhibits the greatest voltage loss due to activation. If the perhydroxyl ions do not break down in the last step, the voltage loss is very high. Gold seems to be a very effective catalyst in the decomposition of perhydroxyl ions and therefore, it is used in combination with platinum on the cathode to reduce this activation loss. In general, activation losses can be reduced by better catalysts, more surface area of catalyst exposed for reaction, increasing temperature of system, and increasing the pressure of the reactants.

The second type of voltage loss in fuel cells is the ohmic loss. This is due to the electrical resistance internal to the cell (usually called internal resistance of a battery). This generally depends upon the cell electrolyte, electrode geometry (area and distance between electrodes) and the temperature of the system. The use of an alkaline cell meant that some type of hydroxide must be used and potassium hydroxide (KOH) was chosen because it has a high electrical conductivity. Within limits,

the more concentrated solution of electrolyte also is more conductive, but viscosity and phase change effects rule out very concentrated solutions except at higher temperatures. For cell operation at approximately 180°F, KOH concentrations of about 30% have been satisfactory. Design considerations determine the electrode area for required performance.

The last type of voltage loss is that due to diffusion effects. Both electrodes involve reactions with ionic species. For the reaction to proceed it is necessary that the active catalyst be in contact with reacting gas and dissolved ionic species. At very high current flow the diffusion of ionic species into or away from reacting sites becomes a current-limiting factor.

The diffusion-limited region can be extended by increasing temperature, increasing electrolyte concentration and by electrode design, but eventually current will become diffusion-limited. The three effects are summarized in Figure 5.[4] This figure summarizes many of the concepts for the hydrogen-oxygen fuel cell. It gives the total heat energy possible and thus a scale for the thermal efficiency, η_T and also it gives the maximum free energy which determines the maximum voltage of a cell and the associated electrical efficiency based on that value, η_e. The activation loss is evident at low currents. There is a diagnostic test called the Taffel plot in which voltage is plotted as a function of the log of current in the low current region. The slope of this plot compared with a norm established from other cells determines the quality of activation for the electrodes. The ohmic loss is a linear function of current, but finally the current reaches a limiting value due to diffusion of ionic species in the electrolyte. The linear region of the graph is the range

FIGURE 5 HYPOTHETICAL HYDROGEN-OXYGEN FUEL CELL PERFORMANCE NEAR ROOM TEMPERATURE

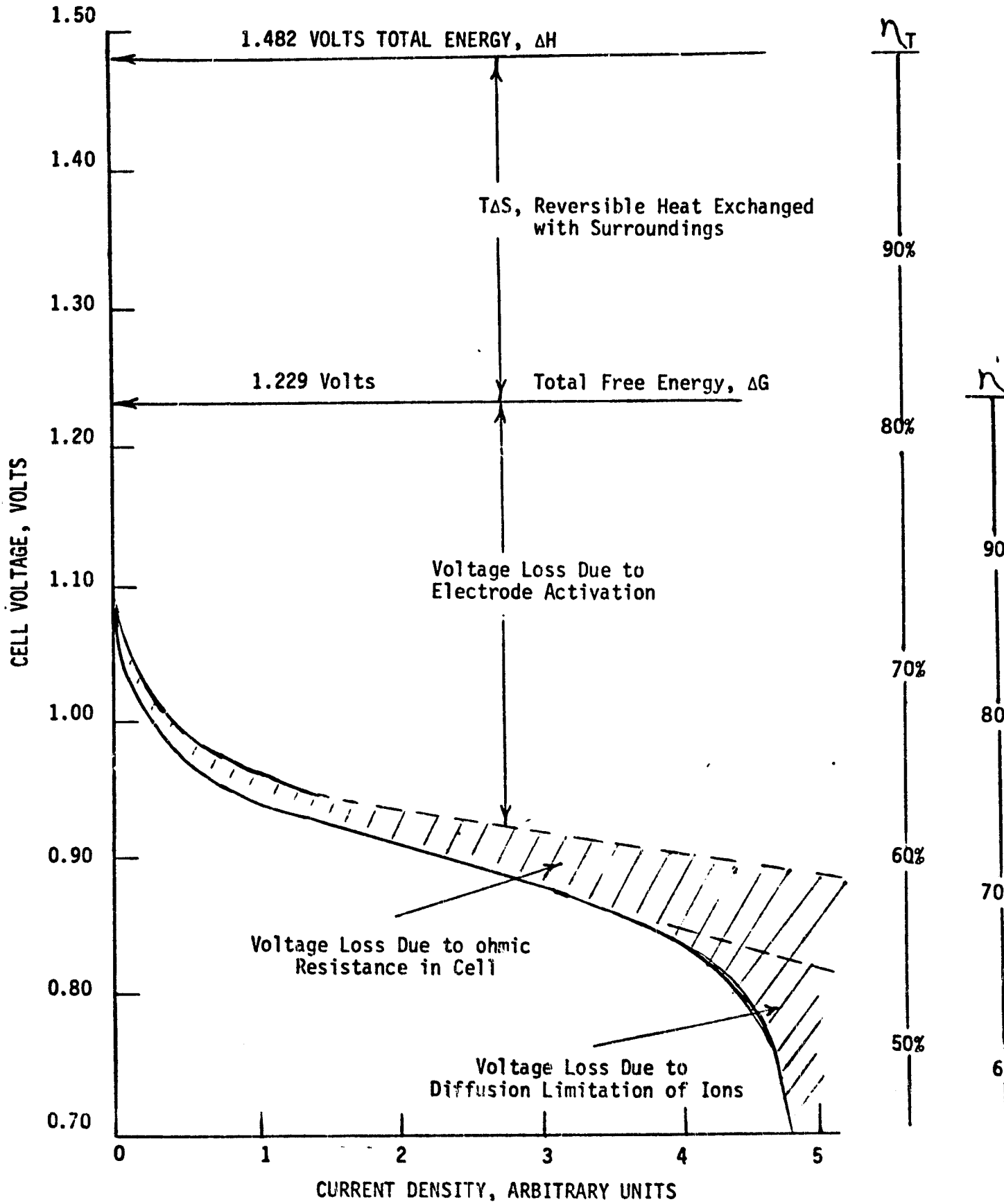

of performance utilized in the design of a fuel cell for a specific application.

IV. ORBITER FUEL CELL

With this background of fuel cells, the Orbiter fuel cell will be considered in regard to its components, present status and future improvements.

A. CELL COMPONENTS

Figure 6 illustrates a single fuel cell in a schematic as well as configurational diagram.[5] In actual use 32 of those cells are connected in series and then two of these stacks are connected in parallel to form the power section of the Fuel Cell Powerplant. This provides 27.5 - 32.5 VDC with a 2 - 12 kw output. In Figure 7 this power section is shown with auxiliary equipment such as reactant gas regulators, water condensing equipment, coolant system and associated valves and pumps.[5] This schematically represents the fuel cell powerplant. However, this report deals with the fuel cell itself and referring back to Figure 6, the componen are as follows:

1. Oxygen Electrode (Cathode) - Nickel screen plated with gold and then 20-25 mg/cm^2 Gold-Platinum alloy with 20% TFE deposited on screen and sintered at 590^{0}F (TFE is tetrafluorethylene and acts as a wet-proofing agent which prevents electrode flooding while providing more interfacial area between catalyst, gas and electrolyte).
2. Electrolyte- Potassium Hydroxide in water with an allowable concentrati range of 25 - 45%.
3. Matrix - Porous asbestos mat to contain electrolyte. RAM refers to reconstituted asbestos matrix devleoped as a process by H. McBryar at JSC to produce a more uniform matrix with high bubble pressure

FIGURE 6

ALKALINE ELECTROLYTE FUEL CELL

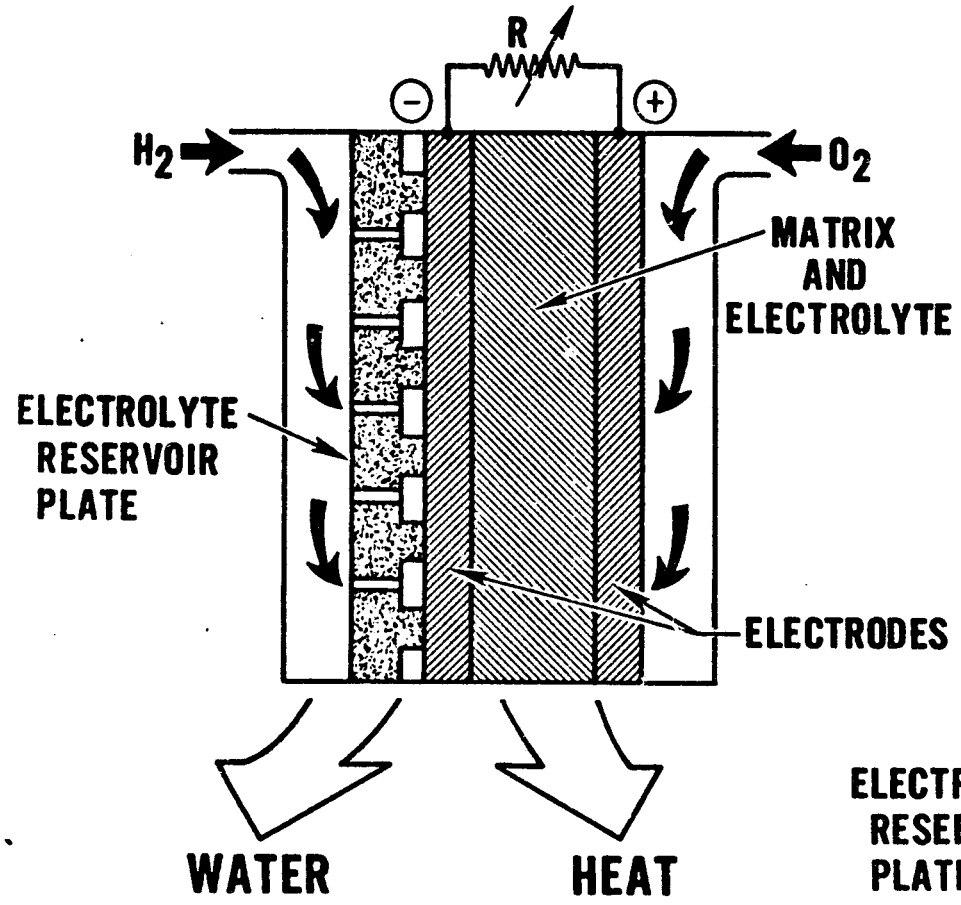

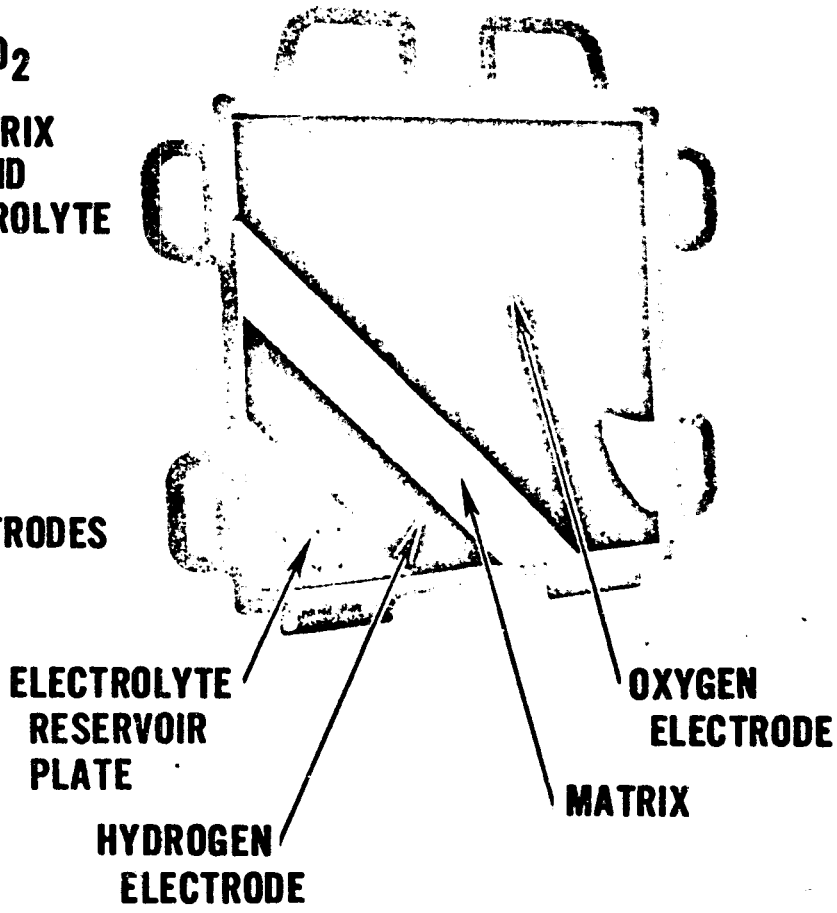

FIGURE 7

TYPICAL POWER PLANT SCHEMATIC

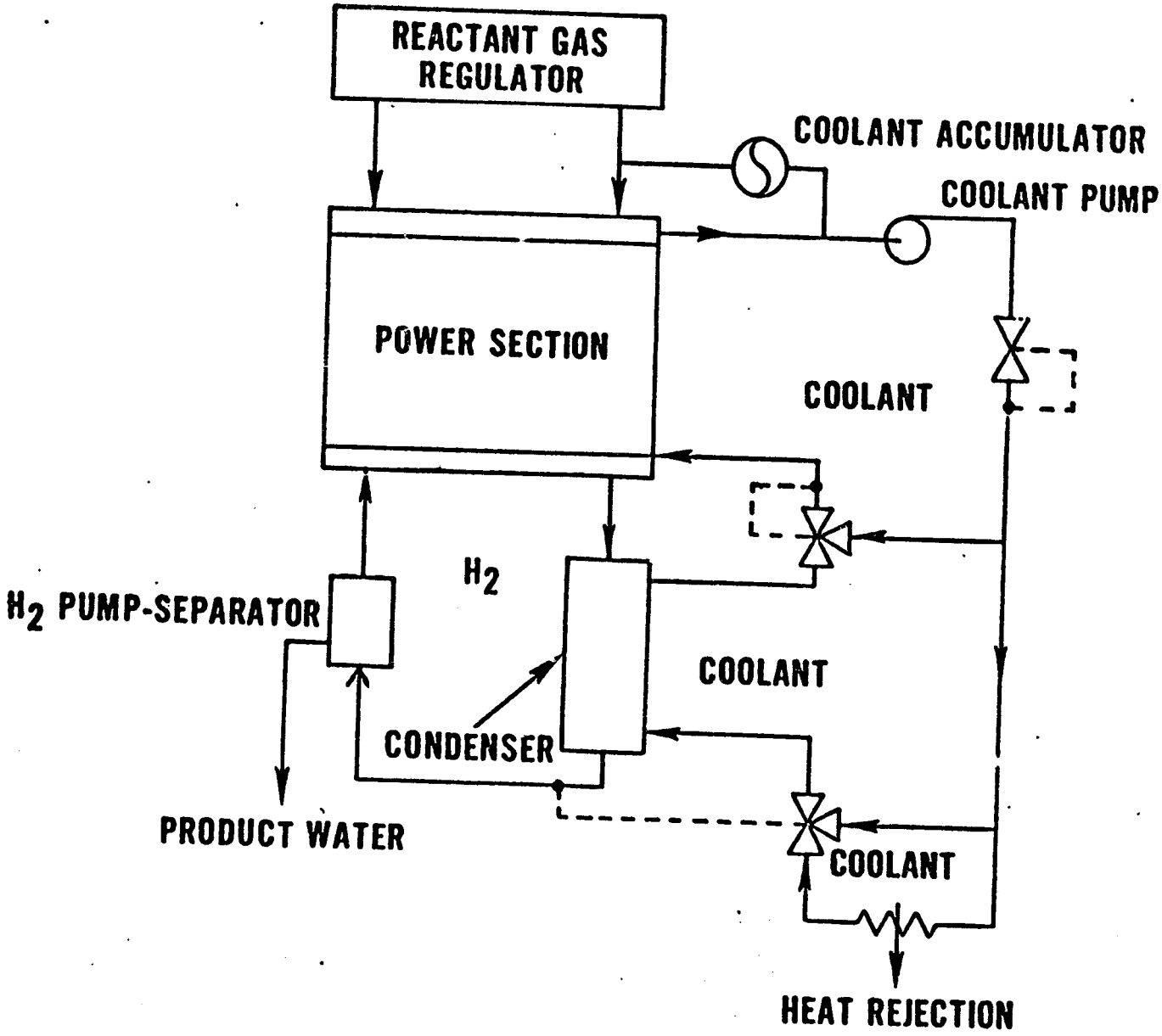

(prevents crossover reactions of one gas to the other electrodes). Also a side benefit is that some contaminating material has been leached out.

4. Hydrogen Electrode - (Anode) - Nickel screen with gold plating and then 10 mg/cm^2 of Platinum-palladium with 30% TFE is deposited on screen and sintered at 590°F.
5. Electrolyte Reservoir Plate (ERP) - Porous Nickel plate is present to provide additional inventory of electrolyte and to accomodate volume changes of the electrolyte during use. This plate is perforated in order to permit passage of hydrogen to the reactive electrode surface.
6. Separator Plates - between series cells are gold-plated magnesium separator plates grooved for reactant gas flow or coolant flow as specified by power plant design.
7. Frame - Cells are separated with fiberglass-epoxy material and sealed against fluid leakage with rubber rings seated into grooves around the periphery of the cell plates.

B. STATUS OF ORBITER FUEL CELL

A shuttle prototype stack of 32 cells referred to as DM2A fuel cell was evaluated by the Thermochemical Test Branch at JSC and the following comments were made concerning cell performance:[6]

1. The fuel cell experienced a high performance degradation rate for the first 100 hours of operation; the degradation rate then tapered to a normal value.
2. The Phase I performance loss was attributed to a change in catalyst activity.
3. Approximately half the performance loss experienced during Phase I testing was regained upon startup for Phase II testing.

4. The performance recovery was attributed to regeneration of the degraded catalyst activity.

5. Fuel cell performance during Phase II testing was erratic and unpredictabl

6. The erratic performance complicated the definition of the fuel cell degradation rate; however, the average degradation rate during Phase II testing was approximately 0.168 millivolts per hour.

7. If the cause of the high initial performance degradation rate could be determined and alleviated, the fuel cell stack useful lifetime could be extended considerably.

8. High continuous loads (150 amperes) resulted in accelerated degradation as much as 16.2 times that of moderate current loads.

9. Less than half the degradation associated with high current loads was due to a change in catalyst effectiveness; the majority of the loss was due to increased internal resistance or increased electrode diffusion loss.

10. The fuel cell required as much as two hours to achieve voltage stability following a step load change.

11. The stack and individual cell voltages exhibited high amplitude damped oscillations with "instantaneous" load increases followed by typical exponential decay to the voltage value commensurate with the new load.

12. Purge gas flow blockage in specific cells precluded normal boot-strap startups following inerting after a total on load operating time of 3818 hours.

13. Oxygen dual feed mode operation after an ET of 2954 hours considerably extended the allowable oxygen purge interval compared to single feed mode; the single feed mode resulted in rapid inert buildup in select cells.

14. Stack voltage performance degradation between on-load elpased times of 1920 hours and 5150 hours primarily resulted from increased electrode diffusion losses, with some catalyst degradation also apparent.

Previous work reported cell performance degradation due to anode flooding which seemed to be caused by a gray deposit containing silicon on the anode. Other work had shown that CO or CO_2 contamination of reactant gases result in the formation of carbonates in the electrolyte replacing the hydroxide ions.[8] This is detrimental to cell performance since the resistance of the cell increases due to a decrease in ionic conductivity as hydroxide ions are replaced by carbonate ions. The decrease in cell perforamnce was evident in electrode and electrolyte degradation. However, the source of degradation was found to be contaminants in reactant gases, matrix degradation and frame corrosion.

C. POTENTIAL IMPROVEMENTS IN THE ORBITER FUEL CELL

Goals for the orbiter fuel cell enhancement program recommended by Power Systems Division of United Technologies Corporation are to decrease weight, increase operating life to 10,000 hours, increase power output from 12 kW to 20 kW and reduce cost. Proposed areas of work to meet these goals are as follows:

1. Floccing electrode process
2. Superior Matrix
3. New Frame Material
4. Graphite Electrolyte Reservoir Plate
5. Platinum-on-carbon anode
6. Bonded cell construction

D. BACKGROUND INFORMATION TO THESE PROPOSED CHANGES

1. Floccing Electrode Process

The standard process for electrode manufacture involves filtering a suspension of Teflon and catalyst particles onto a teflon sheet, transferring to the electrode screen, wash catalyst mixutre, dry, and sinter.

This process has produced electrodes with undesirable variations in performance.

An improved process involves the addition of a proprietary flocculating agent to the suspension before filtering.[9] These flocced electrodes when compared to standard electrodes have a finer and more uniform grain structure. This is the result of a more uniform distribution of Teflon and catalyst particles. These flocced electrodes have less variation in production runs than the standard electrode reducing the rejection rate of electrodes from 10% to almost zero.

Test data on flocculating have shown that with few exceptions improved cell performance resulted with flocced electrodes. For example data from Navy Power Plant tests indicated that fuel cells with flocced electrodes averaged 10 mv higher than standard electrodes which translated to an increase of 0.4V on a 32 cell stack. Also, after 500 hour test at about 175 amperes, flocced cells lost 6.7 mv per cell on the average while the standard cells lost 9.9 mv per cell on the average.[10]

2. Matrix Materials

Asbestos was one of the earliest matrix materials used in fuel cells and is still the best one. Other materials have been tried but are not used for various reasons. Some of those are discussed below:[7]

a) Brucite (Magnesium Hydroxide) - Not available in quantity.

b) Litofol-S-asbestos - dissolved too rapidly in hot alkali.

c) Silicon nitride - also dissolved in hot alkali.

d) Polybenzimidazole (PBI) - This material had excellent resistance to alkaline solution but NASA-Lewis research indicated that this material poisoned the catalyst.

e) Fybex (Potassium Titanate) (PKT) - This material had excellent resistance to alkali solution and tests in fuel cells with Fybex matrix indicated after 14 hours that the carbonate production was only 50% of that in standard asbestos matrix cell. However this material is not available. It was reported by a phone conversation with Johns Manville representative that Fybex was a rapid tumor producing agent.

Since asbestos is the best material, an improved matrix may be obtained by washing or leaching the asbestos matrix with alkaline solution or possibly EDTA before use in cell. This has resulted in a 50% reduction in carbonate formation when compared to the standard asbestos matrix cell over 1400 hours of operation.(5)

3. Frame Materials

This is definitely a problem area as the fiberglass-epoxy frames presently used in fuel cell corrode in hot alkali electrolyte solution. Of the other frame materials tried such as polyphenylene sulfide, polysulfone, and Celanese epoxy Novolac; the polysulfone had a very low corrosion rate in KOH solution. It is not easily molded however, and would best be used as a hybrid with fiberglass where contact with the electrolyte is limited to the polysulfone material (Figure 8). Test by UTC reported a 44% lower carbonate level in the electrolyt after 5000 hours in cell with hybrid polysulfone-fiberglass compared to standard epoxy-fiberglass frame cell.(5)

4. Graphite ERP - This change compared to Nickel ERP is proposed to effect a weight reduction in a 32 cell stack of 8.3 lbs or about 13%

FIGURE 8

CELL EDGE FRAME CONSTRUCTION

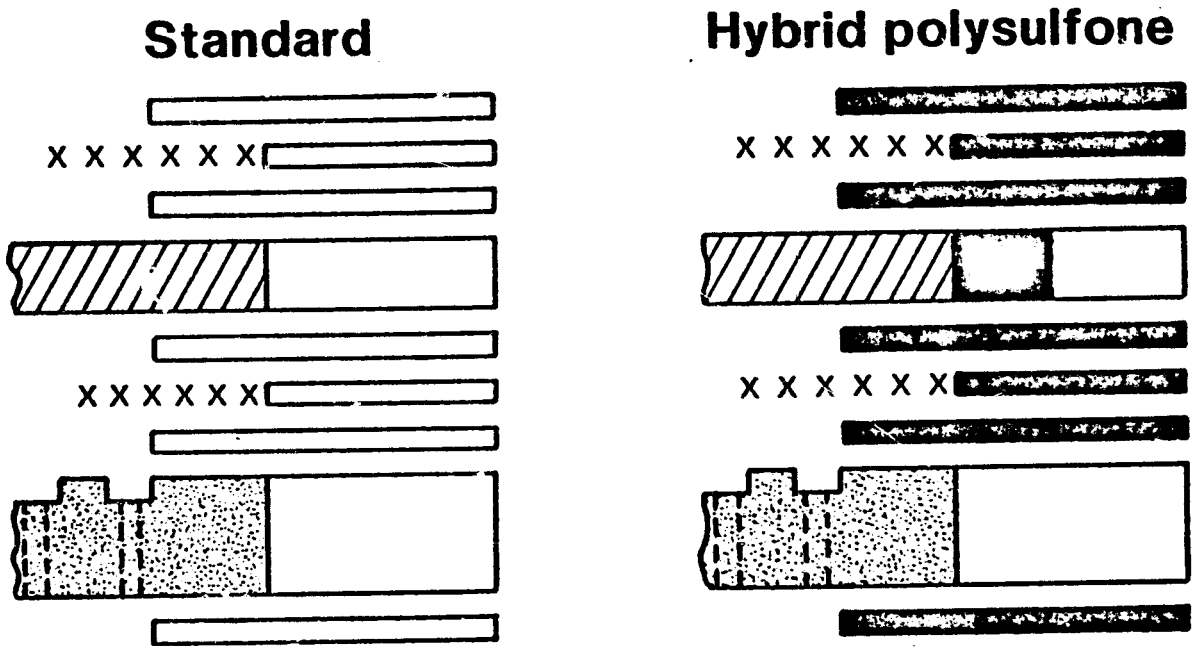

weight reduction in the fuel cell stack. Graphite was used in early fuel cells as electrode material but they were not long-life cells. The graphite ERP is in a reducing atmosphere and therefore no adverse effects on performance would be expected.

5. Platinum on Carbon as an anode has been tested and preliminary studies show good long-term stability (6000 hours). The platinum on carbon electrode has more voltage loss initially but seems stable and possibly improves with time although the data are sketchy.[9]

6. The bonded cell (Figure 9) is a technique to completely encapsulat each cell in its reactant housing with thermo-setting plastic bond material.[11] This technique provides a good seal to contain the electrolyte and also provides a significant weight reduction, 16.2 lbs. per 32 cell stack which is about a 25% reduction in stack weight. However, the fabrication technique has produced some problems in the cell, and further work is needed in this area. Also since new materials are used, these could present unforseen problems in cell operation. Thus a thorough screening and selection activity must be an integral part of a new cell construction approach.

E. RECOMMENDATIONS

Based on the past, present and anticipated future needs of the orbiter fuel cell, the following recommendations are made with regard to future fuel cell enhancement. These recommendations are based on the presumption that for the immediate future, fuel cell operating life is more important than weight reduction.

FIGURE 9

BONDED CELL CONFIGURATION

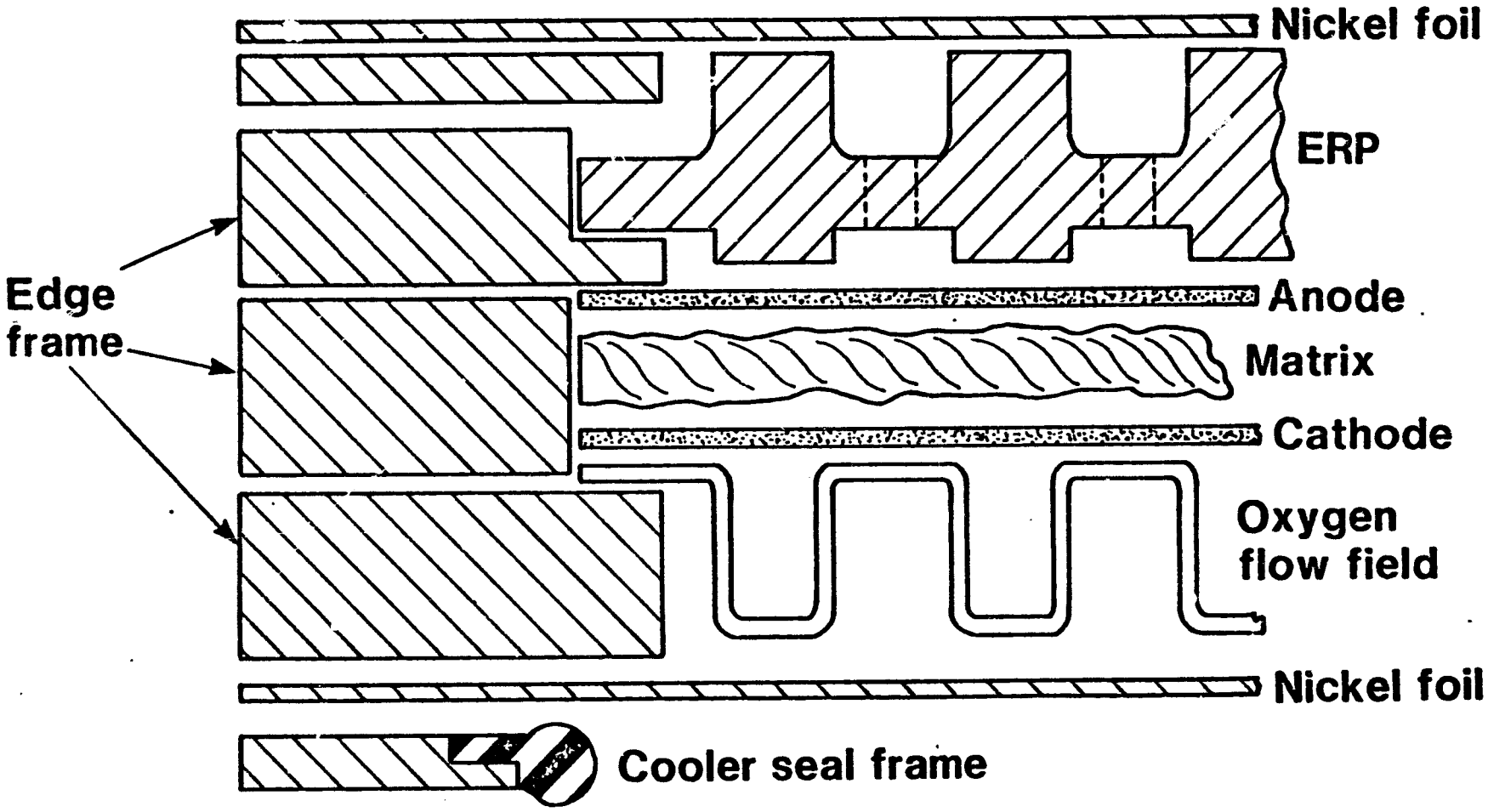

1. Short-Range Enhancements

The following items can be considered for the Orbiter Fuel-Cell Program in the time range from immediate use to a one-year testing and acceptance program.

a. Electrode Floccing - This procedure is ready for immediate incorporation and involves no major changes in materials or processes. The major effect would be a more uniform, consistant-performing electrode. This appears to be almost a 0% risk of decreasing performance contrasted to a 90% possibility of improving performance. Standard production results in a 10% rejection of electrodes whereas flocced electrodes have a 0% rejection so far. For 15 power plants (the present orbiter order) containing 96 cells at $1500 x 96 x 15 x 10% = $ 216,000. It is difficult to give a dollar value for the improved performance, but this will proivde a higher voltage per cell and a longer life before falling below the minimum voltage specification.

b. Matrix Leaching - This procedure is ready for immediate incorporation into the Orbiter Fuel-Cell Program. This procedure provides a more uniform composition of the matrix by leaching out detrimental impurities that are present in variable amounts. It is particularly effective in removing calcium carbonate and this has been identified as a problem in the deterioration of the cell electrolyte. The leaching agent is a solution of ethylenediaminetetraacetic acid (EDTA) and is known to complex divalent metal ions such as calcium and iron. Data presented by Ben Gitlow from United Technology

Corporation in a March 3, 1981 presentation at JSC indicated that a leached matrix fuel cell had only 50% of the carbonate build-up in the electrolyte after 1390 hours compared to a standard production cell. This could double the life of the fuel cell since carbonate build-up is the principal degradation mode.

Based on a presentation by Fulton Plauche' of the Power Generation Branch, JSC dated June, 1981 the following data are used for cost estimates. The 3-substack BOM fuel cell is estimated to have a 4000 hour life and for four orbiter vehicles requiring 20,000 hours of fuel cell life each, the estimated cost is $ 127.6 million. Flocced electrodes and leached matrix enhancements have a good possibility (80% my estimate) of achieving a 10,000 hour fuel cell. This would eliminate the refurbishments and rebuilds in this total program as well as two fuel cell changeouts for a savings of $ 42.1 million or a 33% cost savings in the fuel cell program.

Therefore, I strongly recommend immediate incorporation of these two enhancements described above.

c. New Frame Material - The present fiberglass-epoxy frame is subjected to long-term degradation in the hot alkaline solution in the fuel cell. If a satisfactory material could be found, then my estimate would be that with flocced electrodes, leached matrix and improved frame material the probability of a 10,000 hour fuel cell is close to 100%.

The most promising frame material to be incorporated in the fuel cell in the near future would be a hybrid structure of polysulfone and fiberglass. Polysulfone has been shown to have a very low corrosion rate (weight loss) in alkaline solution and also in a 5000 hour test in fuel-cells. It exhibited a 50% reduction in the carbonate produced compared to the standard cells with fiberglass-epoxy frames.

Therefore I recommend that effort be put forth to develop manufacturing procedures for this hybrid frame and concurrently do long term testing of this frame in short stack test cells.

The possible savings of $ 42.1 million has already been mentioned for the Orbiter Fuel-Cell Program by developing a 10,000 hour cell and these three short-range enhancements have the potential to provide that life.

2. Long-Range Enhancements

There are several areas of investigation that could improve fuel cell stability and life or reduce weight and these are recommended for longer range study (one - three years).

a. A graphite electrolyte reservoir plate (ERP) would provide a significant weight reduction (13%) over the standard gold-plated nickel ERP. Fabrication, assembly and long-term testing would be required before new materials could safely be used in the cells. At the present time, extended cell life is more important than weight reduction and thus this enhancement is assigned to longer term study.

b. The platinum-on-carbon anode has been proposed for a long-time fuel cell. Preliminary testing on this electrode has shown a good stability for 5000 hours although the initial performance was about 15 mv lower than the standard cell.[5] This modification involves new material introduced into the cell, new electrode design and long term testing and evaluation of this modification.

c. Finally, the bonded cell approach has the potential to reduce the weight of the fuel cell (25% reduction in stack weight). However, the techniques of bonding a new frame material and all the associated problems of leakage, thermal expansion and corrosion problems would require long-range investigations.

The problem in evaluating these long-range enhancements is to determine their cost effectiveness. If it were possible to extend the life of the fuel cell stack to 20,000 hours is this as effective as extending it from 5000 hours to 10,000 hours? The answer is probably "no" since the accessory section components are designed for 10,000 hours and will require servicing at that interval. Thus it becomes uneconomical to overdesign one part of the fuel cell power plant compared to the other.

It seems reasonable to continue some long-range improvement work since beyond the first four orbiter vehicles is the possibility of an on-going effort for other orbiter vehicles and even other applications unknown at the present time.

However, I feel that the short-range enhancements have the potential to produce a 10,000 hour fuel cell and a major program decision must be made concerning the effort to develop the fuel cell life beyond this.

F. POTENTIAL PROBLEM AREAS

1. One of the contaminants identified in the degradation of fuel cells is carbonate which is believed to come mainly from the matrix and the frame materials. There is the possibility, however of almost any organic material in the presence of oxygen, catalyst and alkaline solution to be oxidized to carbon dioxide and then converted to carbonates. This means that any organic solvents used in washing of electrodes or matrix materials must be thoroughly washed away. Experimental work has shown that platinum and many other catalytic metals bond very tightly to organic molecules so that heating above the normal boiling point will not remove the organic material. In some cases very high temperatures (400 - 500^{o}C) and a high vacuum are necessary to remove contaminating materials from a catalyst surface. This heat conditioning in vacuum or in other gas atmospheres is called "activating" the catalyst. After activation the catalyst is handled very carefully to avoid contamination before it is used. Therefore the use of organic solvents or other organic additives in processing the fuel cells needs to be carefully evaluated to determine possible contributions to accelerated fuel cell degradation or to reduced activation of the electrodes.

2. Another potential problem area is the introduction of new materials, graphite electrodes, and graphite ERP. Poor activation of electrodes or degradation of the cell performance could be due to trace amounts of materials present in these materials. For example sulfur-containing substances are notoriously bad catalyst poisons (i.e. reduce activity of catalyst) and polysulfone which is a good frame material contains sulfur. Other contaminants in graphite or even the products of a slow oxidation could produce contaminants in the cell. Therefore, poor electrode activity or cell performance degradation should not be dismissed as just a statistical probability but careful analysis of data and materials used as well as chemical analysis of electrodes and electrolyte should be performed to identify other (if any) contaminating materials.

G. OTHER POSSIBLE ENHANCEMENTS FOR CONSIDERATION

In the course of reading and preparing this study two possible enhancements were identified for consideration.

1. Electrode activation is more serious at the cathode than at the anode. Early fuel cell work indicated that a radioactive electrode lowered the activation potential resulting in increased cell voltage.[12] It seems possible then, to incorporate a weak β source into the oxygen electrode to reduce the activation potential and improve the voltage efficiency of the fuel cell.

2. If graphite electrodes are reconsidered, then the use of an acid electrolyte is possible. The asbestos matrix and fiberglass-epoxy frame would be less subject to corrosion in the acid medium. Also,

carbonate formation would not be a problem in acidic solution so that carbonate-forming contaminants in reactant gases as well as from other materials would not be as critical.

This report is not an exhaustive review of the fuel cell work to date nor are all factors considered in regard to cost savings or reliability. Production costs of changeover to new processes are unknown and could not be considered.

It was my intent to evaluate certain proposed enhancements and make a judgement in my opinion as to the most promising enhancements to be incorporated into the orbiter fuel cell and to provide an estimate of the cost savings and/or reliability factor.

BIBLIOGRAPHY

1. Fuel Cells, B. J. Crowe, NASA, Washington, D. C., 1973.

2. Fuel Cell Systems, G. J. Young and H. R. Lindon ed., American Chemical Society, Washington D. C., 1965.

3. Fuel Cells, Review, L. G. Austin, NASA, SP-120, Washington, D. C., 1967.

4. Transient Thermodynamic Analysis of a Fuel-Cell System, W. E. Simon, NASA TND-4601, NASA, Washington, D. C., June 1968.

5. Orbiter Cell Improvement Program, Presentation to NASA-JSC by B. Gitlow, UTC, March 3, 1981.

6. Internal Note for Performance and Degradation Evaluation of the Shuttle Prototype DM2A Fuel Cell, David Saucier, JSC-12543, NASA-JSC, June 24, 1977.

7. Development of Advnaced Fuel Cell System, Phase III, L. M. Handley, A. P. Meyer, and W. F. Bell, NASA CR-134818, Pratt and Whitney Aircraft, January 30, 1975.

8. Effects of Carbon Dioxide on Trapped Electrolyte - Hydrogen - Oxygen, Alkaline Fuel Cells, L. H. Thaller, R. E. Post, and R. W. Easter, NASA TMX-52812, NASA-LeRC, September, 1970.

9. Final Report - Advanced Technology Light Weight Fuel Cell Program, R. E. Martin, United Technologies Corporation (PSD), NASA CR-159653, September 28, 1979.

10. Presentation to Johnson Space Center, Ben Gitlow, United Technologies Corporation, July 9, 1981.

11. Development of Advanced Fuel Cell System, Phase IV, A. P. Meyer and W. F. Bell, United Technologies Corporation (PSD), NASA CR-135030, January 31, 1976.

12. Fuel Cells II, G. J. Young, Reinhold Publishing Company, New York, 1963.

OTHER REFERENCES

A) Fuel Cells I, G. J. Young, Reinhold Publishing Company, New York, 1960.

B. Fuel Cell Systems II, Advances in Chemistry Series (90), B. S. Baker, American Chemical Society, Wahsington, D. C., 1969.